UNIVERSITAT POLITÈCNICA
DE CATALUNYA
BARCELONATECH

PhD program in Electronic Engineering

Textile UHF-RFID Antenna Sensors Based on Material Features, Interfaces and Application Scenarios

Doctoral thesis by:

Chengyang Luo

Thesis advisor:

Raúl Fernández García (Supervisor)

Ignacio Gil (Co-supervisor)

Department of Electronics Engineering

Barcelona, March 2022

ACKNOWLEDGEMENT

I would like to firstly thank my supervisor Prof. Raúl Fernández García for giving great help to my Ph.D research work. I appreciate our meeting conversations from fundamental physics to more potential topics. Thanks that he gave me adequate support in scientific research experience, funds and facilities.

I am grateful to my co-supervisor Prof. Ignacio Gil. He is very kind and knowledgeable. I appreciate his support in research knowledge and paper writing. For each of my published articles, he helped me review them very carefully.

From my middle school to my first university, I am always studying hard in order to reduce the financial burden of my parents by obtaining scholarships. Three years ago, my country was willing to give me a national scholarship for my Ph.D. education, therefore, I would like to thank my home country for the fund.

In our lab, I would like to thank my friend Marc for his daily concern and guidance on the research equipment. As an international Ph.D. student, he introduced the unique culture and language of Spain. And then I visited some famous places and took some small trips around Barcelona. I really like the local cultures, friendly people and unique buildings after the introduction from my friend Marc.

Another very nice friend I need to keep in heat forever is Mariam. She accompanied me almost throughout my Ph.D study period. She helped me in daily communication when I could understand native language, accompanied me to many places and was willing to be a lab assistant. Thanks sincerely.

Thanks to my parents for their support and understanding. Because of the epidemic situation, they are always worried about my safety in a foreign country and I feel sorry that I can go back to visit them for three years. Hope they can keep healthy and happy.

Thanks to Dr. Fang WenXiao for building my fundamental research habits. I am glad that I learned more from him and obtained the chance for the Ph.D. experience by his recommendation.

Finally, I would like to thank my girlfriend for waiting three years. From her, I learned how to keep patience on whatever I am doing. Persistence is indeed an essential quality as a researcher.

ABSTRACT

Textile radio-frequency identification operating in ultra-high frequency (UHF-RFID) antenna sensors are a promising technology for developing new applications in the healthcare field and the Internet of things (IOT) since textiles are widely used for everyone and due to the maturity of embroidery techniques. The textile UHF-RFID technique started to be applied in combination with the textile technique and the textile sensors arose about 15 years ago. However, up to now there have not been enough research achievements applied for current production and living, which also means the huge development prospect is worth paying attention to.

Through the analysis of the current research status, there are several novel research orientations worth exploring. The first is to explore novel sensing functions for textile UHF-RFID antenna sensors; the second is to find a connection/interface solution between textile antennas and integrated circuit (IC) chips; the third is to reduce the cost of textile UHF-RFID antenna sensors to promote future commercial applications.

This thesis is aimed at improving the research on textile UHF-RFID antenna sensors based on the above three novel orientations as the main objectives. In order to explain the work, some essential principles and methods are given, including the operating principle of textile UHF-RFID antenna sensors, the impedance measurement method, the conjugate matching principle and several electro-textile embroidery methods. For achieving the first objective, the textile UHF-RFID tag with two sensing positions (‘radiation parts’ and ‘loop part’) are proposed for sucrose solution measurements. The two sensing positions with the different sensing features show good performance and can give two choices for future complete applications. In addition, three progressive designs of textile UHF-RFID antennas on surgical masks are developed due to the current worldwide epidemic situation. Related reliability tests prove that the designs with the function-extensible chip can be used for healthcare applications. For achieving the second objective, three electro-textile interfaces integrated with the corresponding textile UHF-RFID antennas are proposed and the chip-textile connection solutions are provided(by sewing, snap buttons and inserting). It is worth noting that the mixed-use feasibility of the proposed electro-textile interfaces and textile UHF-RFID antennas can be proved, thus reducing the cost in the design procedure. For the third objective, apart from the mixed-use feasibility of the interfaces, the mentioned electro-textile UHF-RFID antenna with the corresponding electro-textile interface is proposed and evaluated as a compression sensor for two application scenarios. The antenna sensor tested in two healthcare application scenarios, bending on a knee and respiration frequency, shows good sensing performance.

As a result of the research carried out in this thesis, five articles indexed in the Journal Citation Report have been written, which are located in the first, second and third chapters. Four of them are published and one is pending acceptance, which are included as an annex in this thesis.

Keywords – Textil**e**, Ultra-high Frequency (UHF), Radio-frequency Identification (RFID), Antenna Sensor, Integrated Circuit (IC) Chip, Healthcare Applications, Electro-textile Interfaces, Read Range

RESUMEN

La identificación por radiofrecuencia de ultra alta frecuencia (UHF-RFID) con capacidad de sensado basada en substratos textiles ha recibido especial interés por parte de la comunidad científica para el desarrollo de aplicaciones en el campo de la salud y el internet de las cosas (IOT) gracias a la masiva utilización de los textiles por parte el ser humano. La tecnología UHF-RFID comenzó a aplicarse en combinación con los substratos textil y posteriormente con sensores textiles hace unos 15 años. Sin embargo, hasta la fecha, no ha habido suficientes logros en el campo de la investigación que haya permitido extender esta tecnología al ámbito de la producción y/o de la salud, por lo que vale la pena prestar atención a la enorme perspectiva de desarrollo de la misma.

Tras el análisis del estado actual de la investigación de la tecnología, se han detectado diferentes puntos débiles en la madurez de dicha tecnología que vale la pena explorar y fijan los objetivos de la presente tesis: El primero, el desarrollo de funciones de detección novedosas para sensores de antena UHF-RFID textiles; en segundo lugar, encontrar una solución de conexión entre antenas textiles y chips de circuitos integrados (IC) convencionales y en tercer lugar la reducción del coste desarrollo de dicha tecnología para para facilitar la expansión de futuras aplicaciones comerciales de la tecnología de sensado basada en UHF-RFID con substratos textiles.

Para contextualizar la tesis, se detallan los principios y métodos esenciales de la misma, incluyendo el principio de funcionamiento de los sensores de antena UHF-RFID textiles, el método de medición de impedancia, el principio de impedancia conjugada y adaptación de impedancia, así como los métodos tecnológicos textiles utilizados. Para el primer objetivo, propongo un TAG UHF-RFID textil con dos posiciones de detección ('partes de radiación' y 'parte de bucle') para mediciones de solución de sacarosa. Las dos posiciones de detección con las diferentes características de detección muestran un buen rendimiento y pueden ofrecer dos opciones para futuras aplicaciones completas. Además, debido a la situación epidémica mundial durante el desarrollo de la tesis, se presentan tres diseños progresivos de antenas textiles UHF-RFID sobre mascarillas quirúrgicas. Las pruebas de fiabilidad demuestran que los diseños propuestos se pueden usar para aplicaciones del cuidado de la salud. Para el segundo objetivo, propongo y analizo tres interfaces electro-textiles integradas con las antenas UHF-RFID textiles correspondientes: Costura, botones a presión e inserción. Se presenta un modelo eléctrico para dicha interfaz y se analiza la viabilidad de uso mixto de las interfaces electro-textiles propuestas y las antenas UHF-RFID textiles, reduciendo así el coste en el procedimiento de diseño.Para el tercer objetivo, además de la viabilidad de uso mixto de las interfaces, propongo y evalúo una antena sensor de compresión de utilidad para dos escenarios de aplicación del ámbito de la salud distintos, como son la caracterización del ángulo de flexión de la articulación de la rodilla y el análisis de la frecuencia respiratoria.

Fruto del resultado de la investigación desarrollada en la presente tesis se han escrito 5 artículos indexados en el Journal Citation Report situados en el primer y segundo cuartil, cuatro de ellos publicados y uno pendiente de aceptación y que se incluyen como anexo en la presente thesis.

Palabras clave - Textil, Frecuencia ultra alta (UHF), Identificación por radiofrecuencia (RFID), Sensor de antena, Chip de circuito integrado (IC), Aplicaciones para el cuidado de la salud, Interfaces electrotextiles, Ragne de lectura

CONTENT

LIST of FIGURES

LIST of TABLES

LIST of ABBREVIATIONS

ASIC	Application Specific Integrated Circuit
CNN	Convolutional Neural Network
FPCB	Flexible Printed Circuit Board
HF	High Frequency
IOT	Internet Of Things
LF	Lowe Frequency
OOK	On–Off Keying
PVC	Polyvinyl Alcohol
RCS	Radar Cross-Section
RFID	Radio-Frequency Identification
RSSI	Received Signal Strength Indicator
UHF	Ultra-High Frequency

Publications

This part shows the list of papers of international journals and conferences that were published in the scope of this thesis.

Journal papers

[1] **C. Luo,** I. Gil and R. Fernández-García, "Wearable textile UHF-RFID sensors: A systematic review." *Materials,* 2020. (Published)

[2] **C. Luo,** I. Gil and R. Fernández-García, "Textile UHF-RFID antenna sensor for measurements of sucrose solutions in different levels of concentration." *Meas Sci Technol,* 2021. (Published)

[3] **C. Luo,** I. Gil and R. Fernández-García, "Textile UHF-RFID Antenna Embroidered on Surgical Masks for Future Textile Sensing Applications," *IEEE Trans. Antennas Propag.*, 2022. (Published)

[4] **C. Luo,** I. Gil and R. Fernández-García, "Experimental Comparison of Three Electro-textile Interfaces for Textile UHF-RFID Tags on Clothes," *Int. J. Electron. Commun.*2022. (Published)

[5] **C. Luo,** I. Gil and R. Fernández-García, "Electro-textile UHF-RFID Compression Sensor for Healthcare Applications," *IEEE Sens. J.* 2022 (Under Review)

Conference paper

[6] **C. Luo,** I. Gil and R. Fernández-García, "Embroidered Textile Capacitive Sensor for Sucrose Solutions Measurement," 2020 IEEE International Conference on Flexible and Printable Sensors and Systems (FLEPS), 2020. (Published)

Chapter 1
Introduction

* Ref. A: **C. Luo,** I. Gil and R. Fernández-García, "Wearable textile UHF-RFID sensors: A systematic review." *Materials*, 2020. (Published)

1.1 Motivation and objectives

Textile radio-frequency identification operating in ultra-high frequency (UHF-RFID) antenna sensors are a promising technology for developing new applications in the healthcare field and the Internet of things (IOT) since textiles are widely used for everyone and due to the maturity of embroidery techniques. [1][2]. Different from conventional RFID sensors based on common materials such as rigid and flexible PCBs as substrates and copper as RFID antennas, textile materials for UHF-RFID antenna sensors have great potential based on some special features such as ductility, hygroscopicity, light weight and comfort. Since 2012, related research on textile UHF-RFID antenna sensors has been mainly focused on tag-only or ductility-based applications such as exercise tracking [3] and strain capacity [4] but applications based on other features are expected to be explored. Therefore, one objective of the thesis is to explore useful textile UHF-RFID antenna sensors with novel functions.

For conventional RFID tags based on PCBs and copper, the welding technique is a popular and simple way to connect RFID antennas and integrated circuit (IC) chips [5]. However, this popular technique is not suitable for most textile RFID devices on clothes due to the high temperature intolerance (< 200°C) of the common knit yarns and fabrics [6][7][8]. To avoid this connection problem, some works are exploring free welding methods such as fixing with glue [9], non-conducting yarns or copper plates [10]. The mentioned methods are foreseen to have difficulties such as chip pads rust due to textile washing and the detachment of the chip-welded board in textile devices. Therefore, one objective of the thesis is to develop some new connection methods for the electro-textile interfaces.

From the early 21st century, the standards and theory of RFID have been improving [11][12][13] while the cost of RFID tags has been decreasing gradually. Cost is a key parameter for industrial products. Common RFID antennas working at any frequency band need to be designed for application specific integrated circuit (ASIC) chips due to their different complex impedance. In addition, most researches on UHF-RFID sensors focus on one design for one type of sensing function. Based on the above two cases, one objective of my work is to reduce related costs. There are two methods to address this issue . One is to explore the feasibility of one electro-textile interface with a chip for several designed textile UHF-RFID antennas. The other is to develop a textile UHF-RFID antenna sensor with multi functions.

For all of the research situations and reasons presented above, the main objectives of my work in this thesis are:

- Explore useful textile UHF-RFID antenna sensors with novel functions

- Develop some new connection methods for the electro-textile interfaces
- Reduce related cost by two methods:
    - One electro-textile interface with a chip for several designed textile UHF-RFID antennas
    - Develop a multi-function textile UHF-RFID antenna sensor

1.2 State of the art

1.2.1 Development of textile UHF-RFID sensors

Since the standard EPC Gen2 was first published in 2004, the physical and logical requirements for UHF RFID tags and readers have been defined, which give researchers a basic framework to design a UHF-RFID system integrating many kinds of sensors for different applications. At the beginning, in the textile industrial field, the UHF-RFID technique was mainly applied for identification purposes for applications such as clothing manufacturing, inventory control, warehousing, distribution, logistics and automatic object tracking. Currently, UHF-RFID tags are gradually used for daily living applications with sensing capabilities.

As shown in Figure 1.1, a brief history of textile UHF-RFID and sensing technologies preceding current UHF-RFID sensors is provided. From 2007 to 2010, the textile UHF-RFID technique was not yet mature and it was mainly focused on feasibility and simple applications with just tags, such as size-optimizing exploration for the textile UHF-RFID antenna as shown in Figure 1.1 (a), accessories trace and production process monitor in Figure 1.1 (b) and exploration for the relation between conductivity and different sewing methods in Figure 1.1 (c) and (d). Then from 2010 to 2015, the textile UHF-RFID technique was gradually applied for simply sensing uses with just the UHF-RFID antennas and ICs, such as the textile UHF-RFID strain sensors for monitoring human bodily functions and movements, as shown in Figure 1.1 (e) and (f), textile UHF-RFID tag for performance exploration in Figure 1.1 (g), RSSI-based passive UHF-RFID for indoor localization applications in Figure 1.1 (h) and textile UHF-RFID with broad

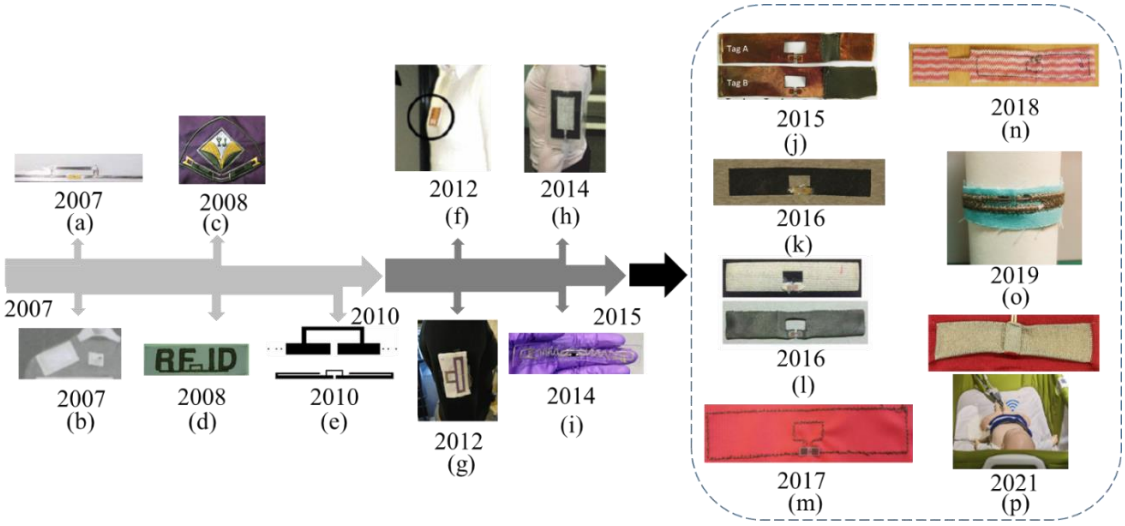

Figure 1.1. Brief history of textile UHF-RFID and sensing technologies adapted from ref. (a) [14], (b) [15]. (c) [16]. (d) [17]. (e) [4]. (f) [18]. (g) [19]. (h) [20]. (i) [21]. (j) [22]. (k) [23]. (l) [24]. (m) [25]. (n) [26]. (o) [27]. (p) [28].

Table 1.1 Achievements of the researches as shown in Figure 1.1

Label	Achievements	Ref.
(a)	Flexible electro-thread UHF-RFID tag antenna designed using the T-matching method, with a read range of about 2.4 m	[14]
(b)	Textile UHF-RFID tag for accessories trace and production process monitor, attached on a garment	[15]
(c)	Fabricated 'YJ' symbol type textile UHF-RFID tag for exploring different shapes of embroidery tag antenna	[16]
(d)	Fabricated 'RFID' symbol textile UHF-RFID tag for analysing the changes of conductivity for different sewing methods	[17]
(e)	Textile UHF-RFID strain sensor for human bodily functions and movement monitoring, fabricated by screen printing the ink on stretchable PVC and on fabric substrates	[4]
(f)	Textile UHF-RFID strain sensor for human movement monitoring and feasibility of effective data interaction	[18]
(g)	Textile UHF-RFID tag for performance exploration, mainly validated by the read range	[19]
(h)	Textile UHF-RFID tag for positioning and localization through recording and analysing on-body readability and Received Signal Strength (RSSI) in an office environment	[20]
(i)	E-fiber UHF-RFID broadband tag for tie health information monitor, fabricated on conductive textiles and embedded into polymer	[21]
(j)	Textile UHF-RFID strain sensor for exploring the relation between the antenna elongation and its backscatter strength, based on a stretchable antenna made of conductive fabrics	[22]
(k)	Graphene-based UHF-RFID tag on a fabric substrate for exploring feasibility and reliability of the low-cost and eco-friendly graphene tag	[23]
(l)	Health-care-based UHF-RFID sweat sensor for sweat rate measurements in exercise, by comparing the silver plated sample and the graphene-printed sample	[24]
(m)	Health-care-based textile UHF-RFID moisture sensor for body moisture sensing	[25]
(n)	Environment-based textile UHF-RFID moisture sensor for humility detection, with a sensor part and an antenna part	[26]
(o)	Textile UHF-RFID tag for exploring the impact from geometrical variations and deformations	[27]
(p)	Textile UHF-RFID compression sensor for on-body breath monitoring, by obtaining the relationship between the RSSI and respiratory periods	[28]

impedance bandwidth for tire performance monitoring inFigure 1.1 (i). Up to now, textile UHF-RFID systems integrated with textile sensors have been deployed, and many novel textile materials on different kinds of sensing fields have been tested. There are some typical applications, such as UHF-RFID strain sensors with copper-coated fabric, as shown in Figure 1.1 (j), graphene-based UHF-RFID sensors for moisture monitoring in Figure 1.1 (k) and sweat sensing in Figure 1.1 (l), silver-plated thread UHF-RFID sensors for environment humidity monitoring in Figure 1.1 (m) and (n), deformation-based UHF-RFID compression sensors for on-body breath monitoring in Figure 1.1 (p), and equally important, reliability

exploration (deformation sensitivity) in Figure 1.1 (o). The related achievements of these researches are listed in Table 1.1.

1.2.2 State of the art of textile UHF-RFID sensors applications

In modern society, electronic devices are always closely relevant to specific application fields. The rule is also suitable for current researches on textile UHF-RFID sensors. The textile UHF-RFID technique started to be applied in combination with the textile technique and then textile sensors about 15 years ago. However, up to now there have not been enough research achievements applied for current production and living, which also means the huge development prospect is worth paying attention to.

A medical-based UHF-RFID body-worn sensor was fabricated and tested for monitoring fluid accumulation in the lungs, which was integrated as part of the garment on various locations such as front, back and shoulders, as shown in Figure 1.2 (a) [29]. In this work, textiles made by e-fabrics (conductive polymer fibres) were evaluated with a microstrip transmission line structure, which demonstrates the e-fiber transmission line surface had electrical equivalence to metallic but inflexible surfaces of copper transmission lines. Note that some useful fabrication methods were adopted, such as bundled fibers for

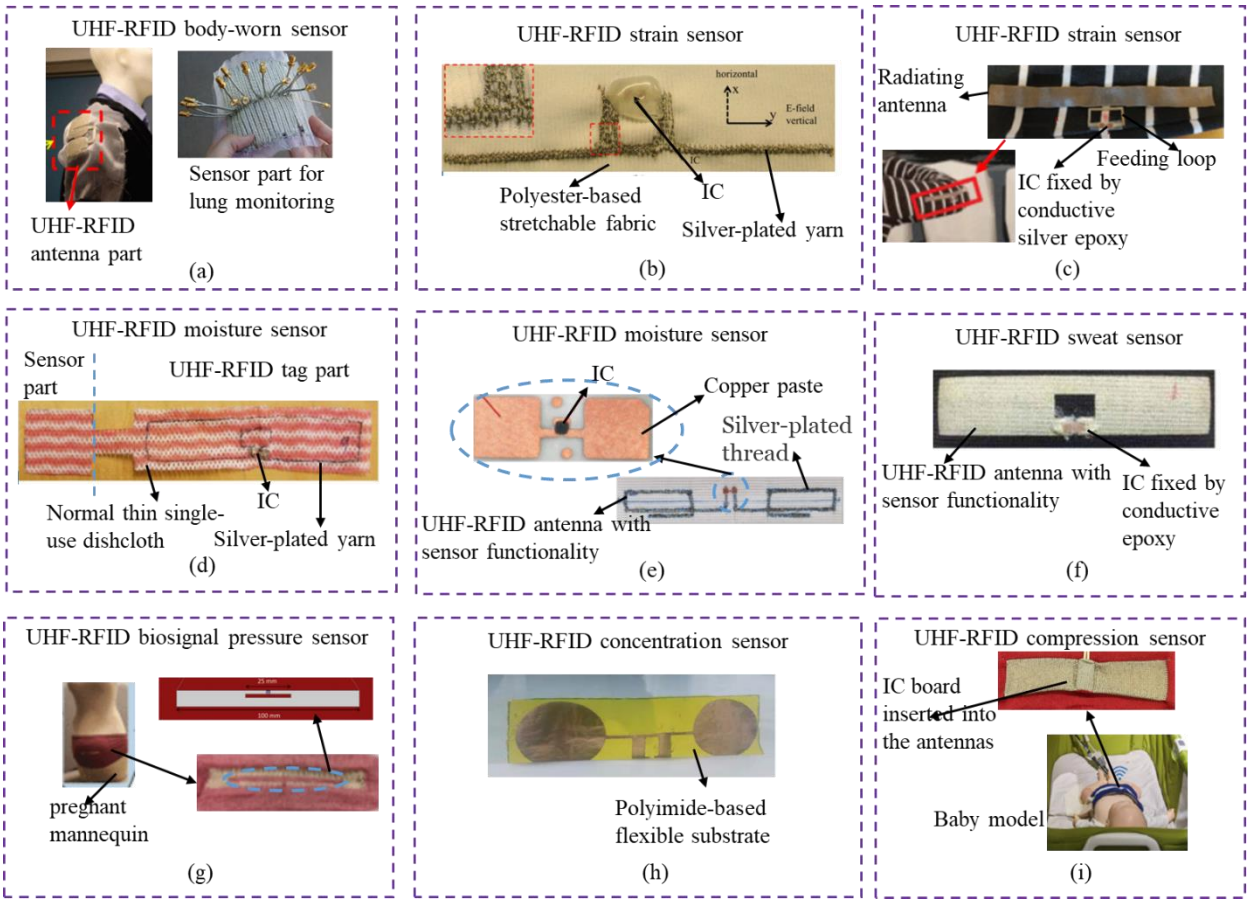

Figure 1.2. Typical textile UHF-RFID sensor applications adapted from ref. (a) [29]; (b) [30]; (c) [31]; (d) [26]; (e) [32]; (f) [24]; (g) [33][34]; (h) [35]; (i) [28].

improving conductivity and assistant yarn for avoiding abrasion damage of the silver coatings on the e-fiber's polymer core. The important achievement was to use the same e-fibres to fabricate the medical-

based UHF-RFID body-worn sensor for lung monitoring. In addition, textile versions were found to be nearly equivalent to the metal one even after being repetitively flexed, washed, and dried. This work gave a pioneering application for textile sensors for lung monitoring in medical-based fields.

For the flexible feature of textiles, a deformation-monitoring-based UHF-RFID strain sensor was proposed for structural health monitoring applications, as shown in Figure 1.2 (b) [30]. In this work, a novel dual-interrogation mode was applied for the design of the textile UHF-RFID strain sensor, which provided a large identification coding capacity for the UHF-RFID sensor. The dual-interrogation mode consisted of reading range extraction mode for the threshold-power-required chip-enabled approach and RCS-based (radar cross section) sensing mode for the chipless approach. In fact, the range extraction mode relied on the read range changing with the applied strain, while the RCS-based sensing mode was directly linked to the frequency shift depending on the strain changing. Note that here the strain was related to the electrical length of embroidered UHF-RFID sensor structures. This work proved the feasibility of double modes for the design of textile UHF-RFID strain sensors and it is worth considering in future research, but certainly, some important validation measurements such as bending, environment impacts and washing for the performance and reliability need to be considered.

In another example of the textile UHF-RFID strain sensor, as shown in Figure 1.2 (c) [31], a notable evaluation for the elongation from an attached object was implemented, compared to the last example in Figure 1.2 (b). This textile UHF-RFID strain sensor was based on silver-plated material fabricated by plain knitting and designed into two separate parts, the feeding loop and the radiating antenna. This design makes the radiating antenna part fully stretchable while the IC attached to the feeding loop could be non-stretchable, which avoids the reliability challenges caused by mechanical stresses from clothing-integrated electronics. In this work, this textile UHF-RFID strain sensor was integrated on the shirt, the performance of which was examined on-body by means of backscattered signal power measurements under strain and in unloaded conditions. The results revealed that the strain sensitivity was great and the achievements had the potential for future smart monitoring applications. However, for real applications such as a controller in an embodied game, as mentioned in the paper, some safety and reliability validation measurements were expected to be considered, such as the performance impact after washing or working in a high electromagnetic interference (EMI) area.

These above three current kinds of research actually make use of the flexible feature of textile UHF-RFID sensors, which also lead our way to do related research in this area. In addition to this feature, it is worth knowing that there are many potential features that push the researches on textile UHF-RFID sensors forward.

There is another example for textile UHF-RFID sensors that are sensitive to humidity as shown in Figure 1.2 (d) [26]. It is an environment-based textile UHF-RFID moisture sensor fabricated on a very common substrate, thin single-use dishcloth, which consists of a sensor part and UHF-RFID antenna part. In this work, the performance of the textile UHF-RFID moisture sensor was evaluated by 10 drops of water

from wet state to dry state and the evaluation parameter was the read range in office conditions after 5, 10, and 15 min. The result showed the small changes of the read range from 4.7 m in the dry state and 5.2 m in the wet state. From the result, this textile UHF-RFID moisture sensor had certain moisture detection ability, however the changes of the read range were small relative to the humility from 10 drops of water and the impact from impurities in water also needed to be considered. Thus, this kind of application research had the potential to be focused on in the future.

Compared with the textile UHF-RFID moisture sensor mentioned in Figure 1.2 (d), another example in a work [32] is only a textile UHF-RFID tag with moisture sensor functionality as shown in Figure 1.2 (e). In this work, textile UHF-RFID sensors could curve automatically and permanently after being dipped into the water due to the special material, polyvinyl alcohol (PVA). Note that in contrast to the example in Figure 1.2 (d), the test parameter in this work was the change in the backscattered power percentage, which could be measured and compared in order to detect and record the presence of moisture. The comparative measurements in this work proved the results reliable, which showed the potential of the textile UHF-RFID sensors to be applied in environment moisture detection.

In the health-care monitoring field, many kinds of common wearable UHF-RFID sensors on flexible substrates, such as the flexible printed circuit board (FPCB), have been proposed and applied for commercial health-care monitoring applications, whereas textile UHF-RFID sensors for this area are still in the early stages and most investigations for health-care application are at the stage of laboratory research. For example, a health-care-based textile UHF-RFID sweat sensor was proposed for sweat rate measurements as shown in Figure 1.2 (f) [24]. In this work, the textile UHF-RFID sweat sensor made by screen printing had a noticeable difference in the response of backscattered signal power. The paper explains that the response curve differences are caused by the conductive antenna impedance and material parameter of the textile substrate changing due to the absorbed sweat. This work indicates the high potential of textile UHF-RFID technology in perspiration sensing, but related sweat components were not analyzed, which were attractive and worth considering.

In another example of the health-care-based textile UHF-RFID biosignal pressure sensors, reliable and secure manner for real-time medical data collection was considered by a software framework, which fills the gap between data safety and textile UHF-RFID sensors for health-care monitoring Figure 1.2 (g) [33][34]. The textile UHF-RFID biosignal pressure sensor named bellyband sensor for infant heart monitoring in the paper was applied on a pregnant mannequin driven by proprietary software to simulate various behaviors. In addition, a modular software framework was developed to both interrogate sensor devices and to store that streaming data for live and post-processing. In this work, considering the missed tag reads, two impact factors were found. One was the delay caused by periodic frequency hopping and another one was the greater distance between the tag and the reader. These research achievements are helpful for future applications, but more other impact factors need to be tested such as the comfort and electromagnetic safety for pregnant women and infants.

A textile UHF-RFID concentration sensor for concentration detection is shown in Figure 1.2 (h) [35]. In this work, the UHF-RFID concentration sensor was printed on a special textile material, which is a polyimide flexible substrate, while the sensing antenna was made of copper. The proposed sample is sensitive to the frequency and the concentration of the NaCl solutions and sucrose solutions. Moreover, from the measurement results in the paper, the author proposed that the sensitivity increases with the increase in the percentages of the NaCl and sucrose in water. Although in the work there is no accurate application mentioned, it can give us a research orientation for using total textile UHF-RFID concentration sensors to detect elements in human body fluids.

In addition to textile UHF-RFID sweat sensors for sweat rate measurements and biosignal pressure sensors for infant heart monitoring, another health-care-based textile UHF-RFID compression sensor as shown in Figure 1.2 (i) was proposed for breath monitoring on a baby model [28]. In this work, the sensing device is used to measure the breathing activity of a programmable infant patient emulator mannequin (SimBaby). The antenna is highly sensitive to respiratory compression and relaxation. Fluctuations in the backscatter power level/Received Signal Strength Indicator (RSSI) in both cases range from 6 dB to 15 dB. Although in the work there is no description for the port interface, the related connection way in this work shows a pcb with the chip is inserted into the textile antenna sensor, therefore more reasearches on reliability of the interfaces need to be tested.

1.2.3 State of Art on Reliability of Textile UHF-RFID Sensors

For each technique and related application from start-ups to mature products, the reliability validation is a crucial and necessary step. Currently, for textile UHF-RFID sensors, related reliability researches are constantly advancing with the development of textile UHF-RFID sensors. The reliability researches mainly focus on the impacts from sensitive features of textile UHF-RFID sensors, such as the washing reliability [36][37][38], corrosion-resisting reliability, strain and bending reliability.

Washing reliability is an inevitable research point, which needs to be considered and tested before applied for real applications. The main damage factors for textile UHF-RFID sensors from washing are the mechanical and the chemical impacts. Some works prove that taken separately, neither mechanical constraints nor chemicals used have a significant impact on a silver-plated-nylon yarn on short terms (<30 wash cycles) but the coupling of aggressive chemicals and the mechanical rubbings inside the machine can have a dramatic impact [39]. Certainly, different textile materials for the designs have different degrees of ability to resist the impacts from washing cycles, while if washed for enough times, device damages are unavoidable and have a direct impact on the read range [40]. In order to keep the function of devices, protective coating materials are expected to be printed on the devices [41], however some textile glues as a fit conformal coating could not always provide good protection [42]. All in all, washing reliability is an important evaluation factor for a good textile UHF-RFID sensor, the impact of which can be reduced by reducing washing cycles or using better protective coating materials.

Corrosion-resisting reliability is another impact factor worth considering for the textile UHF-RFID sensors that are specially applied for sweat and other solution concentration monitoring. The impacts from chemicals involved in the washing process are proved small when there are no mechanical rubbings but complex and corrosive solution and body fluids are proved to have a certain influence on the resistance of textile materials and radiation efficiency of the UHF-RFID antenna in the work [43]. Especially for textile UHF-RFID sweat sensors, due to the complex elements in sweat, the measured data will be interfered with through continuous detection. Currently, painting with conductive paint [37] and developing machine learning techniques are some popular methods to reduce this kind of impact.

Strain and bending reliability is also an important factor on performance degradation of textile UHF-RFID sensors although some textile UHF-RFID strain sensors utilise this feature to achieve some health-care monitoring applications [33][34]. However, even for this kind of textile UHF-RFID sensor, the most vulnerable part is the connection of antenna and IC, which can cause total failure of systems when it gets damaged. The sewed and glued interconnections still show strain reliability issues that need to be considered and tested after fabrication [44]. However, when the textile UHF-RFID sensors are applied in harsh conditions, generally a suitable coating would be used to protect the antenna-IC interconnection from mechanical stress. In addition, graphene UHF-RFID on textile substrates is proved to have a remarkable and unique response to high reliability in harsh bending conditions [23], which is another potential choice to solve the problem.

In addition to the above three typical reliability problems, many other scenario-based reliability researches need to be explored combining actual situations and applications. Textile UHF-RFID sensors are expected to develop and grow more with the coming of the IOT society and increasing of the health-care concerns, meanwhile related safety and reliability of the devices always stay in the spotlight.

Considering the state of the art of the textile UHF-RFID sensor applications and related reliability mentioned above, there are still some researches that need to be done. Textile UHF-RFID sensors are expected to be deployed more on many kinds of fields such as the garment industry, healthcare service industry, sports equipment industry and so on [45]. Due to short development time, textile UHF-RFID sensors still have a long way to go on improving the performance and the futuristic, promising applications and enhancing reliability. Especially for the calling for varieties of IOT applications and the coming-of-age society, more attention needs to be paid to develop useful textile UHF-RFID sensors and close research gaps between laboratory researches and scenario-based textile UHF-RFID sensors.

In the future, the main research will focus on two aspects, one of which is to develop new designs of textile UHF-RFID tags and sensors with common or novel textile materials and manufacturing processes [46], and the other to explore novel application scenarios with certain commercial potential.

New designs with novel textile materials and manufacturing processes are always explored but further research on it is still needed. The novel textile materials such as special conductive yarns integrated with graphene as mentioned in [23] and conductive ink on textile substrates [4], are introduced to improve textile

UHF-RFID sensor performance and are expected to reduce their cost. Certainly, if the novel textile materials are applied for new designs, related manufacturing processes are needed such as the advanced screen printing technique especially for conductive ink on textile substrates. Compared with the traditional materials and manufacturing processes, the novel ones are still in development and they will require a notable research orientation.

Machine learning technology for textile UHF-RFID sensors is also a novel research direction [47]. As mentioned in [48], a classical machine learning algorithm is used, which is capable of generating probabilistic models using feature vectors extracted from segments. As a part of machine learning, deep neural networks [49] are useful for feature extraction and classifier building when the textile UHF-RFID sensors are applied in some complex conditions for numerous data analysis. Currently, the internet of things (IOT) is a hot topic, in which machine learning technology plays an important role pushing textile UHF-RFID sensor techniques to revolutionize traditional applications. Textile UHF-RFID sensor techniques integrated with the machine learning technology are expected to have a big application market in the future IOT era.

With regard to the scenario-based applications, textile UHF-RFID sensors have great development potential in many different fields of production and life. Currently, the main application researches focus on the fundamental functions of textile UHF-RFID sensors such as the ID-sensing, strain sensing [50], humidity sensing, sweat sensing and others. However, advanced functions are not covered. For example, there are exercise-based textile UHF-RFID sweat sensors just for sweat sensing without any elements analysing, on which further researches are worth implementing. Moreover, textile UHF-RFID sensors are more suitable for medical-based applications due to the various medical textiles used for patients or the elderly. Many kinds of medical parameters or body fluids can be detected and analysed by complete textile UHF-RFID sensing systems. The abundant scenarios can create numerous chances for designs and applications of novel textile UHF-RFID sensors in the future.

In addition, reliability is an unavoidable but crucial research direction especially for this kind of flexible and washing-needed component [52]. For example, after fabricating the designs on textile substrates, the performance of UHF-RFID antenna and sensors may decrease such as the resonant frequency shift and gain penalty due to conformal bending or on-body touching. Moreover, environmental factors such as the well-studied humidity and temperature and human factors such as washing and sweat corrosion can imply certain impacts on performance. In the future, the concomitant reliability researches still need to be considered.

1.3 Textile UHF-RFID sensing technology

In the last section, the state of the art of the textile UHF-RFID sensors was discussed. It was found that the typical sensing systems for textile UHF-RFID tags are based on the material features and the textile antenna properties. The material features include the hydrophilic and the ductility of the textile substrates. The textile antenna parameters include the impedance, read range and Received Signal Strength Indicator (RSSI). In this section, the sensing technology needs to be discussed.

1.3.1 Operating principle of popular textile UHF-RFID antennas

Energy supply principle

A common RFID system is based on RFID tags and base stations. There are two possible modes of energy transfer from base stations to tags by the remote power supply of the tags:

- Non-simultaneous: Energy transfer and communication in different phases
- Simultaneous: Energy and communication in one exchange

In the first case (Non-simultaneous), the energy storage mode integrated in the tag so as to provide a sufficient supply, is charged by the RF radiation propagated from the base station. After this power supply phase, the tag can receive commands from the base station and return data to it. In order to continue the communication between the both, the cycle is then repeated with more energy supplied to the tag.

In the second case (Simultaneous), the radiation from the base station can provide the energy supply and data exchange simultaneously during the exchange between the base station and the tag. In the current market, the second case is used for the majority of tags.

Load Modulation Principle

According to the current development of RFID devices in many applications, the main operating frequencies are at a low frequency band (120–150 kHz), high frequency band (13.56 MHz), ultra-high frequency band (865–868 MHz in Europe, 917–922 MHz in China and 902–928 MHz in North America) and microwave band (2.45–5.8 GHz and 3.1–10 GHz) [53]. The details are listed in Table 1.2.

Table 1.2 RFID operating bands

Band	Range	Regulations	Typical Use
120–150 kHz (LF)	10 cm	Unregulated	Animal identification, factory data collection
13.56 MHz (HF)	10 cm–1 m	ISM band worldwide	Smart cards
865–868 MHz (Europe) and 902–928 MHz (North America) (UHF)	1–12 m	ISM band	staff identification, logistic tracking
2.45–5.8 GHz (microwave band)	1–12 m	ISM band	802.11 WLAN, Bluetooth standards
3.1–10 GHz (microwave band)	Up to 200 m	Ultra wide band	Ultra wide band Active tags

In the thesis, the UHF band (Europe) is focused on, the operating principle of which is different from that at the low frequency band and high frequency band:

- ‘magnetic coupling’ at LF and HF;
- ‘retro-reflection’ or ‘re-radiation’ or back scattering of the incident radiation at UHF

A complete UHF-RFID tag is mainly composed of two parts, the tag antenna and the chip as shown in Figure 1.3. The antenna specifically designed for the UHF band is connected to the chip which is generally composed of several functional units and circuits. When the reader (base station) supplies a physical medium in the form of an unmodulated and constantly maintained ‘carrier’ frequency (called a ‘forward link’), the tag sends signals to the base station by modulating the electrical characteristics of this carrier based on the tag data (called a return link).

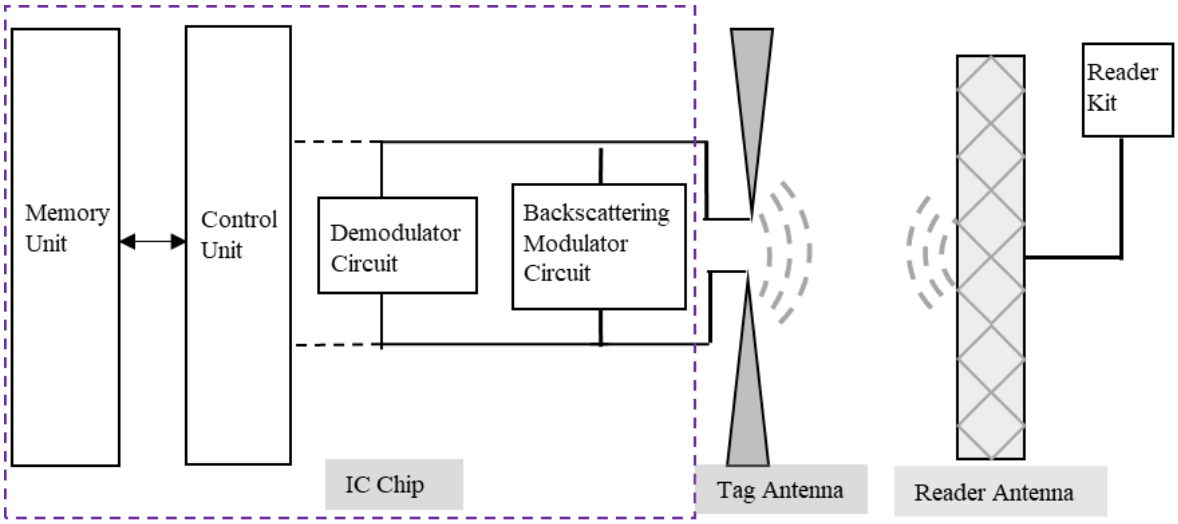

Figure 1.3. Fundamental and structure of an ultra-high frequency (UHF-RFID) tag system

Generally, the ‘load modulation technique’ is commonly used in most of the commercially available tags. As shown in Figure 1.4, the backscatter modulator circuit in the chip is composed of the chip load equivalent circuit and the load modulation circuit. In detail, a transistor as a switch, by on–off keying (OOK) according to a specific binary coding, controls whether a modulation load is connected into the chip

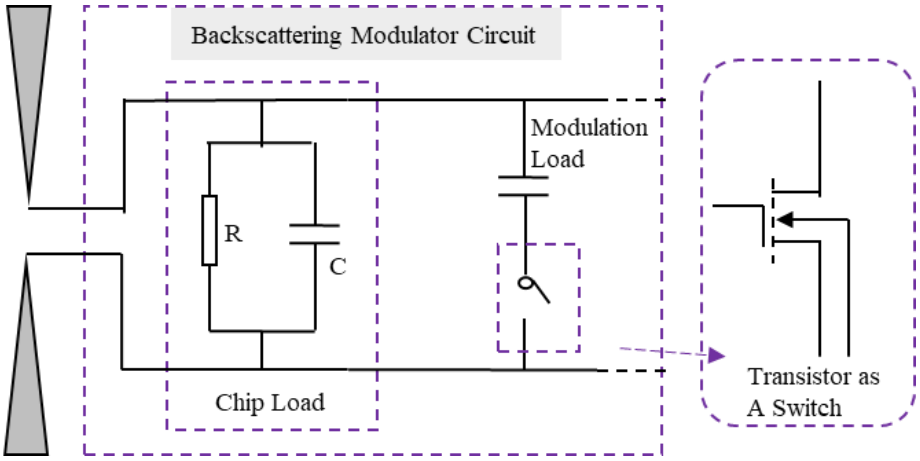

Figure 1.4. Backscattering Modulator Circuit

load circuit. At UHF band, the modulation of the load impedance of the tag antenna, in the case of propagating radiation, has the end result of modifying the proportion of radiation reflected (reradiated or backscattering) towards the reader (base station).

Back Scattering Principle

The back scattering is a type of the propagation characteristics of electromagnetic waves. In concrete physical terms, when an electromagnetic wave encounters an object, it sets up oscillating charges and currents in the surface of the object, thus creating local magnetic fields. This leads to produce power that the object can reradiate, thus appearing to scatter (reflect) part of the incident wave. Especially for back scattering mode, in this mode the directions of the relevant incident and scattered waves coincide, but are opposite to each other. In addition, in order to represent an object such as UHF-RFID tag antennas with back scattering properties, an 'equivalent' scattering area (called the radar cross-section (RCS)) can be considered as a simple way.

In general, the spatial distribution of the scattered energy can be affected by the dimension, structure (shape) and composition of the objects and the wave incidence, which is like the same scattering phenomenon in optics. Considering the ratio between the size of the object and the wavelength of the incident wave, there are three main cases to be explained.

- Size of the object $\ll$ incident wave length (λ): In this case, the phase of the signal changes slightly when striking the surface of the object, so the effective RCS of the object is very small and the wave seems to pass through the object.
- Size of the object $\approx$ incident wave length (λ): In this case, the incident wave tends to remain attached to the surface of the object which creates surface waves.
- Size of the object $\gg$ incident wave length (λ): In this case, the wave propagates as in optics, parts of which are absorbed, reflected or diffracted in all directions.

In UHF-RFID areas, tag antennas are generally developed in the second case (in the dimensions of the same order of λ). Therefore the surface waves are preponderant.

In addition, the values of the radar cross-section (RCS) depend on many parameters of the tags. There are some important ones as listed below,

- Shape and dimensions
- Material
- Wavelength and the polarisation of the transmitted wave
- Load impedance

1.3.2 Sensing principle of textile UHF-RFID antenna sensors

Currently, there are three popular parameters/ways for textile UHF-RFID antennas as sensors as below,

- Received signal strength information (RSSI) of tags
- Read range of tags
- Extended sensors connected to chips

The first and second case are relative to the tags, in which the change of the antenna state of the tags can make an impact on the values of the two indexes. For example, a textile UHF-RFID antenna is used as a strain sensor. When the tag is pulled by external force, the impedance of the antenna is expected to change, thus causing mismatch with the required conjugate impedance of the corresponding chip. In this case, the RSSI and read range are bound to be affected. The sensing ability can be confirmed after finding the relationship between the two indexes and the strain levels.

The third case depends on whether the used chip is extendable or not. In detail, the chips used for simple tags have only two pads for the RFID antennas. But if the chips tend to be extended by additional sensing devices, they are expected to be designed with more interfaces for the sensing devices.

RSSI

RSSI can be known as the strength of a wireless signal received by a receiving device, which is affected by many factors in the environment. The analysis can be done from its calculation equation as below,

$$RSSI = P_t + G_t + G_r - L_c - L_{bf} \quad 1.1$$

Where P_t (dBm)is the power from transmitting antennas, G_t (dBi) is the gain of transmitting antennas, G_r (dBi) is the gain of receiving antenna, L_C (dB) is the power loss of conductive lines and L_{bf} (dB) is the power loss in free space.

When the gain of the transmitting antennas is affected by the factors to be sensed, the relationship between the RSSI and the factors can be explored. Therefore, the transmitting antennas can operate as a sensor.

Electromagnetic waves will have a loss when they penetrate any medium, and there will be a certain energy loss when they propagate in the air. Therefore, RSSI is also easy to be affected by environmental factors due to the wave power loss in free space (L_{bf}). L_{bf} can be calculated by,

$$L_{bf} = 32.5 + 20\log f + 20\log D \quad 1.2$$

Where f is the wave frequency (MHz) and D is the transmission distance (km). Note that the equation 1.2 is obtained in the ideal case of one bar at 25 degrees.

Read range

Read range is an essential parameter for UHF-RFID tags. It can also be used as a sensing parameter. The reason can be explained by an equation derived from the famous Friis Transmission Equation. An

uncomplicated derivation from the Friis Transmission Equation to the popularly used read range calculation equation needs to be discussed,

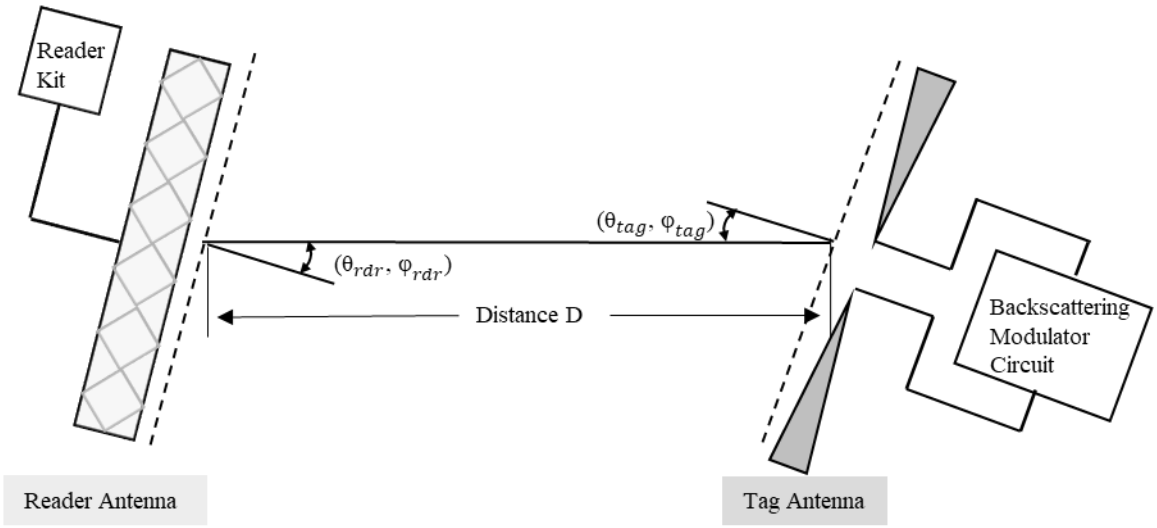

Figure 1.5. Geometrical orientation of reader and tag antennas for derivation.

As shown in Figure 1.5, the reader antenna and the tag antenna are positioned at different directions ($\theta_{rdr}\ and\ \varphi_{rdr}$ for the reader antenna, $\theta_{tag}\ and\ \varphi_{tag}$ for the tag antenna). If the reader antenna can be fed by input power P_{rdr}, its power density W_{rdr} at the distance D from the reader antenna in the direction $\theta_{rdr}\ and\ \varphi_{rdr}$ is

$$W_{rdr} = \frac{P_{rdr} G_{rdr}(\theta_{rdr},\ \varphi_{rdr})}{4\pi D^2} \tag{1.3}$$

Where G_{rdr} $(\theta_{rdr}, \varphi_{rdr})$ is the gain of the reader antenna in the direction $\theta_{rdr}\ and\ \varphi_{rdr}$. Since the effective area A_{tag} of the tag antenna is related to its gain G_{tag} $(\theta_{tag}, \varphi_{tag})$ by

$$A_{tag} = G_{tag}(\theta_{tag}, \varphi_{tag}) \frac{\lambda^2}{4\pi} \tag{1.4}$$

Based on the equations 1.3 and 1.4, the amount of the power P_{tag} collected by the tag antenna can be obtained as

$$P_{tag} = G_{tag}(\theta_{tag}, \varphi_{tag}) \frac{\lambda^2}{4\pi} \cdot W_{rdr} \tag{1.5}$$

Also,

$$\frac{P_{tag}}{P_{rdr}} = G_{tag}(\theta_{tag}, \varphi_{tag}) G_{rdr}(\theta_{rdr}, \varphi_{rdr}) \cdot \left(\frac{\lambda}{4\pi D}\right)^2 \tag{1.6}$$

Note that the power P_{tag} calculated by the equation 1.6 assumes that the reader antenna and tag antenna are matched to the components connected to their feed ports. If the matching situation changes, the equation 1.6 needs to be represented by

$$\frac{P_{tag}}{P_{rdr}} = (1 - |\Gamma_{rdr}|^2)(1 - |\Gamma_{tag}|^2)G_{tag}(\theta_{tag}, \varphi_{tag})G_{rdr}(\theta_{rdr}, \varphi_{rdr}) \cdot (\frac{\lambda}{4\pi D})^2 \quad 1.7$$

Where Γ_{rdr} and Γ_{tag} are the port reflection coefficients of the reader antenna and the tag antenna, respectively.

All above are the derivations of the Friis Transmission Equation 1.7. But considering the real situation of the reader kits and tag antennas, the Equation 1.7 can be simplified. First of all, the reader kit and reader antenna can be obtained from some commercial products, therefore the reader antenna can be considered to be matched to the connected cables. So,

$$(1 - |\Gamma_{rdr}|^2) \approx 1 \quad 1.8$$

Secondly, in common tests for the tag read ranges, the reader antenna and the tag antenna are positioned to be straight in the direction. Therefore, the $\theta_{tag}, \varphi_{tag}, \theta_{rdr}$ and φ_{rdr} can be considered as constant values and the Equation 1.7 can be simplified as,

$$\frac{P_{tag}}{P_{rdr}} = (1 - |\Gamma_{tag}|^2)G_{tag}G_{rdr} \cdot (\frac{\lambda}{4\pi D})^2 \quad 1.9$$

Finally, in order to calculate the read range of the tags, the standard equation can be written as,

$$D = \frac{\lambda}{4\pi}\sqrt{\frac{P_{rdr}G_{rdr}G_{tag} \cdot (1 - |\Gamma_{tag}|^2)}{P_{tag}}} \quad 1.10$$

Now, the read range as a sensing factor can be derived from the Equation 1.10. When impact factors or test variables such as applied force, liquid solution level or mechanical bending, are tested on a textile UHF-RFID tag, the impedance or radiation ability of the tag antenna are expected to change, thus causing the variation of the reflection coefficient Γ_{tag} or the gain G_{tag}. If the relationship between the impact factors and the sensing factor (read range) is demonstrated, the sensing ability of the textile UHF-RFID antenna can be proved.

1.3.3 Conjugate matching principle

Understanding the detailed principle is more important and essential than just showing the conjugate matching formula. A common method ‘T-Match network’ is used for many UHF-RFID antenna designs [51]. Some works use a ‘T-Match network’ as Balun circuits and some propose the antenna designs using a modification of a ‘T-match structure’ directly. All of them aim to achieve the conjugate match between

the chip and antennas.In order to explain the principle, the signal reflection principle including voltage reflection and power reflection is worth discussing.

Voltage reflection Coefficient

Signal reflection is directly related to the characteristic impedance of the interconnect lines. In fact, the main reason for the signal reflection is that the impedance of the interconnect lines changes suddenly. The signals are transmitted in the form of electromagnetic waves in mediums. As shown in Figure 1.6, a signal is transmitted in two mediums with different impedance, Z_1 for the medium 1 and Z_2 for the medium 2. The two mediums have an interface and the reflection generally happens at this part. Let us assume that the incident wave to the interface has the incident voltage V_{inc} and current I_{inc} at the medium 1, the reflected wave from the interface has the reflected voltage V_{ref} and current I_{ref} at the medium 1 and the transmitted wave through the interface has the transmitted voltage V_{trans} and current I_{trans} at the medium 2.

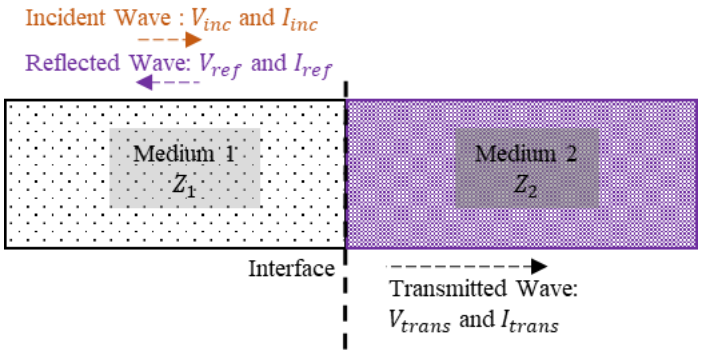

Figure 1.6. Diagram of the voltage and current waves in two mediums

Due to the equal values of the voltage on both side of the interface,

$$V_{inc} + V_{ref} = V_{trans} \tag{1.11}$$

Similarly,

$$I_{inc} - I_{ref} = I_{trans} \tag{1.12}$$

In addition, according to Ohm's law,

$$I_{inc} = \frac{V_{inc}}{Z_1}$$

$$I_{ref} = \frac{V_{ref}}{Z_1} \tag{1.13}$$

$$I_{trans} = \frac{V_{trans}}{Z_2}$$

By calculating the Equation 1.11, 1.12 and 1.13, the Equation 1.14 and 1.15 can be obtained as

$$\Gamma_V = \frac{V_{ref}}{V_{inc}} = \frac{Z_2 - Z_1}{Z_2 + Z_1} \quad 1.14$$

and,

$$T_V = \frac{V_{trans}}{V_{inc}} = \frac{2 * Z_2}{Z_2 + Z_1} \quad 1.15$$

where Γ_V is the voltage reflection coefficient and T_V is the voltage transmission coefficient. It is found from the Equation 1.14 that when Z_2 is equal to Z_1, there is no reflected wave which means the two mediums are matched due to both having equal characteristic impedance. All above in this section have discussed the typical and common (voltage) reflection coefficient in the electronic engineering field.

Power reflection coefficient

It is worth noting that the common voltage reflection coefficient mentioned in last section is not the first choice for RFID applications due to the complex impedance of chips. According to Equation 1.10, P_{tag} can be considered as the wake-up power of a chip, so the feed power from the corresponding RFID antenna should be as high as possible than the wake-up power. Therefore, pursuing maximum load power is the first target of the RFID tag designs.

In order to achieve this target, it is worth making it clear how the total power is distributed between the tag antenna and the chip.

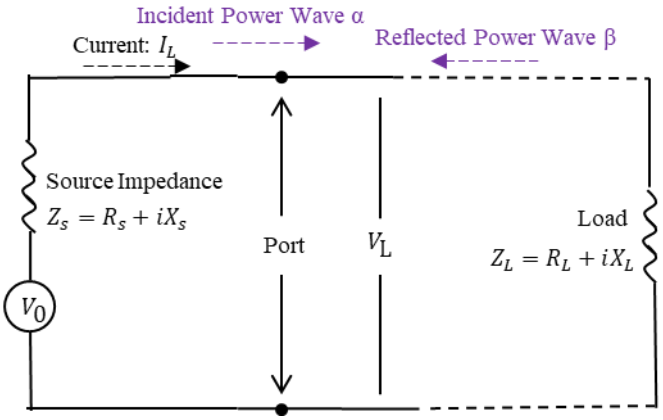

Figure 1.7. Simple equivalent circuit of a tag with a chip.

A simple equivalent circuit of a tag with a chip is shown in Figure 1.7. The Source can be seen as the RFID antenna with the complex impedance $Z_s = R_s + jX_s$ and the Load can be seen as the chip with its complex impedance $Z_L = R_L + jX_L$. In the source part, V_0 is the equivalent open circuit voltage caused by the tag antenna. Now, the active power P_L into the chip load can be given by

$$P_L = Re\,[V_L I_L^*] = Re\,[\frac{V_0(R_L + jX_L)}{(R_s + R_L) + i(X_s + X_L)} \frac{V_0}{(R_s + R_L) - i(X_s + X_L)}] \quad 1.16$$

simplified as

$$P_L = \frac{|V_0|^2 R_L}{(R_s + R_L)^2 + (X_s + X_L)^2} = \frac{|V_0|^2}{4R_s + \frac{(R_s - R_L)^2}{R_L} + \frac{(X_s + X_L)^2}{R_L}} \quad 1.17$$

Generally, the RFID antennas are always designed to have a positive real part of the complex impedance, therefore, R_s is positive and from Equation 1.17, the chip can obtain the maximum power P_{Lmax} when

$$R_s = R_L,\ X_s = -X_L \quad 1.18$$

and the maximum power P_{Lmax} is

$$P_{Lmax} = \frac{|V_0|^2}{4R_s} \quad 1.19$$

All above derivation can explain that for a specifical RFID chip with a certain complex impedance at a required resonance frequency, the corresponding RFID antenna should be designed with a conjugate impedance of the chip to obtain a maximum feed power. This is called conjugate matching.

However, conjugate matching is always a target, but in a real design procedure, it is not easy to achieve. Similar to the common voltage reflection coefficient equation, there is a special reflection coefficient for power used in many circuit simulation software such as the Electronic Design Automation Software (ADS) but it is not clearly explained in many textbooks or handbooks. Here, the related derivation is given.

The incident power wave α and reflected power wave β as shown in the Figure 1.7 can be defined by

$$\alpha = \frac{V_L + Z_s I_L}{2\sqrt{|Re\ Z_s|}} \quad 1.20$$

$$\beta = \frac{V_L - Z_s^* I_L}{2\sqrt{|Re\ Z_s|}} \quad 1.21$$

where V_L and I_L are the voltage and the current flowing into the chip load. 'Re Z_S' is the real part of the source antenna complex impedance which is positive as explained in the previous section. The relationship between the α, β and the active power to the chip load need to be validated.

The voltage at the port ($V_L = V_0 - Z_S I_L$) can be inserted into the Equation 1.20 and the square of the magnitude of the α is

$$|\alpha|^2 = \frac{|V_0|^2}{4R_s} \quad 1.22$$

Referring to the Equation 1.22, $|\alpha|^2$ can be identified as the maximum power that the RFID antenna can supply for the chip load. Then considering the Equation 1.20and 1.21, a new equation can be obtained as

$$|\alpha|^2 - |\beta|^2 = \alpha\alpha^* - \beta\beta^* = \frac{(V_L + Z_s I_L)(V_L^* + Z_s^* I_L^*) - (V_L - Z_s^* I_L)(V_L^* - Z_s I_L^*)}{4R_S} \quad 1.23$$

simplified as

$$\frac{(Z_s + Z_s^*)(V_L^* I_L + V_L I_L^*)}{4R_S} = (V_L^* I_L + V_L I_L^*) = Re\,[V_L I_L^*] \quad 1.24$$

Therefore, the active power P_L from the antenna to the chip load can be calculated by

$$P_L = |\alpha|^2 - |\beta|^2 \quad 1.25$$

Referring to the Equation 1.22 and 1.25, when the designed antenna is conjugate matched with the chip load, the active power P_L can reach the maximum value $|\alpha|^2$. However, when it is not matched, there is a reflected power $|\beta|^2$ and the active power P_L only has the value of $|\alpha|^2 - |\beta|^2$.

Similar with the voltage reflection coefficient, considering V_L=$Z_L I_L$there is a definition of power wave reflection coefficient as

$$\Gamma_P = \frac{\beta}{\alpha} = \frac{Z_L - Z_s^*}{Z_L + Z_s} \quad 1.26$$

and thus the power reflection coefficient is

$$|\Gamma_P|^2 = \frac{|\beta|^2}{|\alpha|^2} = |\frac{Z_L - Z_s^*}{Z_L + Z_s}|^2 \quad 1.27$$

Referring to the Equation 1.26 and 1.27, when the conjugate matching is satisfied, the power reflection coefficient can be obtained as zero which is expected.

Chapter 2
Materials and Methods

2.1 Modelling method of textile UHF-RFID sensor designs

Modelling is an elaborate research process, in which it is essential to obtain actual material parameters for simulation and use related research experience based on the design theories as discussed in previous sections. In order to obtain an accurate model in simulation software, there are the necessary steps in the research work:

- Measuring the properties of the used materials such as the dielectric constant (ε_r), loss tangent (tanD) and thickness of the textile substrates.
- Selecting a suitable type of antenna structures in terms of the application and other requirements such as the dimension and port interfaces.
- Obtaining the information of the used chips such as the dimension and impedance at a required resonance frequency point.
- Developing a model in EM simulation software and tuning the model parameters.

2.1.1 Material property

Measuring the electrical and physical properties of the used materials is necessary for simulation. In this thesis, considering different applications need different substrates, the textile materials are tested every time. The substrate parameter measurements are shown in Figure 2.1. The relative dielectric constant and loss tangent of the substrate in a dry situation can be measured by a Microwave Frequency Q-Meter as shown in Figure 2.1 (a). On the other hand, its thickness can be measured by an Electronics Outside Micrometer (132-01-040A) as shown in Figure 2.1 (b).

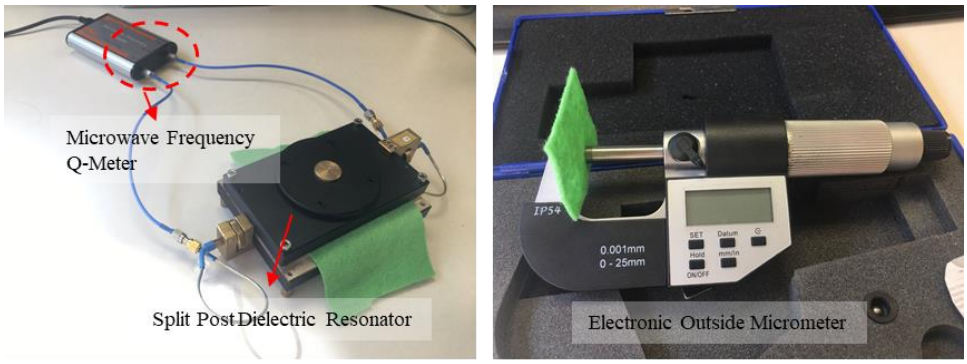

Figure 2.1. Substrate parameters measurements. (a) Permittivity and loss tangent measurements and (b) thickness measurement.

In this thesis, the polyester [54] is selected as one of the substrates due to its better hygroscopicity. Its relative dielectric constant and loss tangent in a dry situation are 1.24 (ε_r) and 0.00163 (tanD), respectively. Different from the polyester fibres adopted as the tag substrate, my research target for my first objective is the UHF-RFID tags on surgical masks, the material of which is different from the polyester fibres. Due to the non-rigid geometry of the surgical mask and its electrical parameters such as permittivity (ε_r = 1.1439) and loss tangent (tanD = 0.0001265), the surgical mask has an effect on the UHF-RFID antenna performance. Therefore, the property of the surgical masks is expected to be tested carefully for next simulation and tag designs. The details are discussed in the next chapter.

In addition, the textile material of the UHF-RFID antennas in my work is a commercial conductive twisted yarn (Shieldex 17/17 dtex 2-ply) made of 99% pure silver-plated Nylon. Note that in order to reduce the impact from the difference between pure silver and real silver-plated Nylon [55][56], the most closed bulk conductivity of the yarns is defined as 11500 siemens/m in the simulation software.

2.1.2 Simulation Methods

As explained at the beginning of this chapter, considering the size requirement and applications, a suitable simulation model can be designed after obtaining the parameters of the materials. Note that there are some important and easily overlooked different settings in different simulation software. They are :

- S-parameters calculation equation
- Port lumped element setting
- Port impedance setting
- Radiation boundary setting

For example, there are three popular simulation software, Ansys HFSS using the Finite Element Method (FEM), CST using the Finite Integration Time Domain Method (FITD) and ADS momentum using the Method of Moments (MoM). In the HFSS and CST full 3D EM simulation software, the S-parameters calculation equations are based on the voltage reflection coefficient. But they are different from the calculation equation in ADS 3D planar EM simulation software which is based on the power reflection coefficient. The voltage reflection coefficient and the power reflection coefficient are discussed in detail in the last chapter. Moreover, the complex impedance as the port is not available in CST EM Studio and UHF-RFID chips generally have the complex impedance, therefore the port needs to be set to a real number with some lumped elements (capacitors and inductors). But in HFSS and ADS momentum, the port can be set to the complex impedance. As for the radiation boundary setting, the HFSS has a conductive environment around the model. A radiation boundary (an ‘air box’) around the model is needed. Conversely, in the CST and ADS momentum, the environment around the model is insulated.

After obtaining the necessary parameters of the materials and understanding the difference between the simulation softwares, the model can be drawn and simulated. In order to reach the specifications such

as the resonance frequency, the model size can be automatically tuned by the software until the simulation results can be accepted.

2.2 Electro-Textile Embroidery Methods

After the simulation model is developed, the layout is digitized and embroidered with professional machines. There are two typical electro-textile embroidery methods. The fundamental process is illustrated in Figure 2.2. The conductive yarns are twisted by a proportional metal-plated thread as shown in Figure 2.2 (a). By this embroidery method, the conductive yarns can be embroidered on many kinds of common textile substrates by commercial embroidery machines [14]. Generally, the technological process begins from the design model simulated by means of an electromagnetic software solver to the model importation into embroidery machines and ending with the manufacturing process. Using this method for UHF-RFID products, the connection of electronic elements such as chips and textile structures can be implemented by commercial glue or needlework. There are some studies [57][58][59] on this method, proving its feasibility for electro-textile RFID or sensors with well ranked performance. In addition, as mentioned in the previous section, some non-ignorable problems still exist such as metal rust of chip pads after washing and poor contact by needlework. In this thesis, a contribution to this research on the interface between chips and textile materials was made.

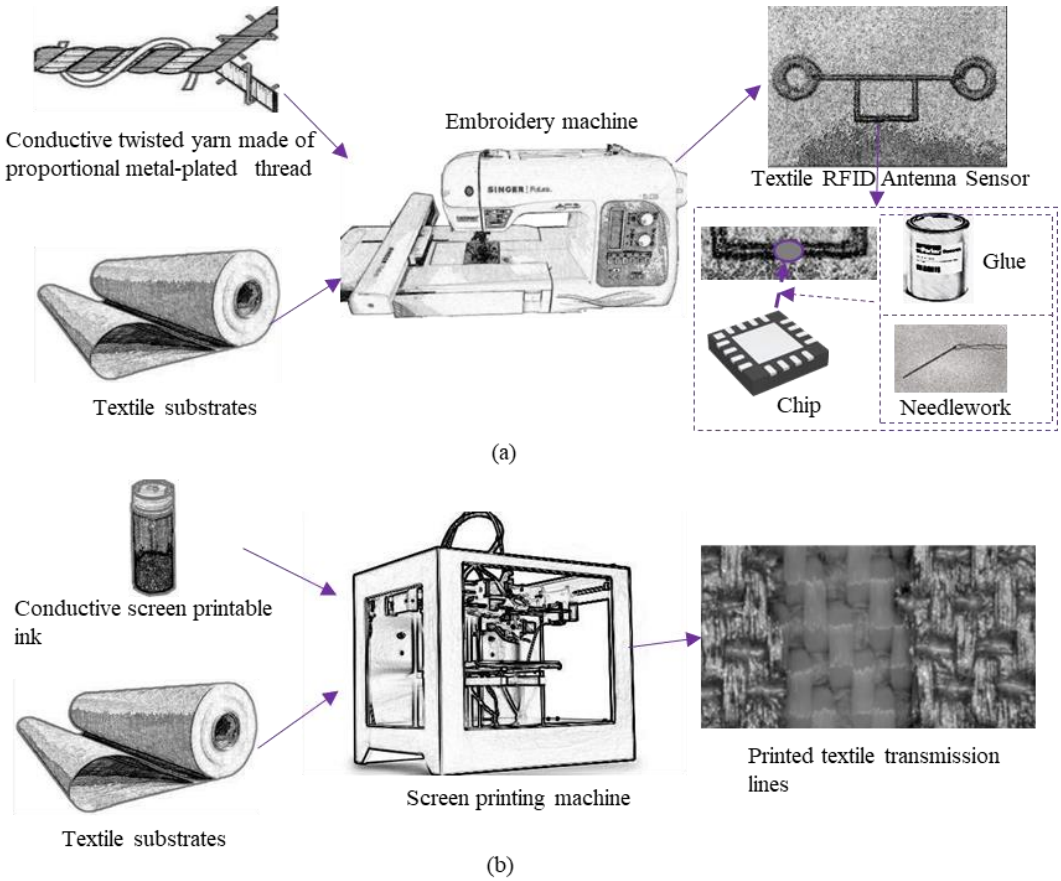

Figure 2.2. Two typical electro-textile embroidery methods. (a) Embroidery technique using conductive yarns, (b) screen printing technique using special conductive ink.

Compared with the embroidery method using conductive yarns, the screen printing technique using special conductive ink, as shown in Figure 2.2 (b), is another popular method for electro-textile applications but more complex due to its technological process [60]. The essential elements are the specially configured conductive ink and the complex screen printing machines. The general conductive ink is a metal-filled paste with a solid content of a certain percentage, for which the curing process under a required temperature by the screen machine is necessarily performed after the ink is pressed. Although the screen printing technique was originally invented in ancient China, this technique has been systematically developed in the last 20 years and is employed for the design of robust non-bendable chemical sensors [61], electrochromic materials [62], and non-bendable UHF-RFIDs [63]. As for textile applications, the invention of conductive compositions for textile printing, described by Ujiie in 2006 [64] that was further developed by Cie in 2015 [65] opens the door for utilisation of screen printing in flexible electronics. Considering the cost in my work, the first embroidery method is my main choice.

In the thesis, the first method is my first choice because of the lower cost and simple operation. In detail, the embroidery method to embroider the patterns on the substrate, a professional embroidery machine (Singer Futura XL-550) is used. For the embroidery procedure as shown in Figure 2.3, some details need attention:

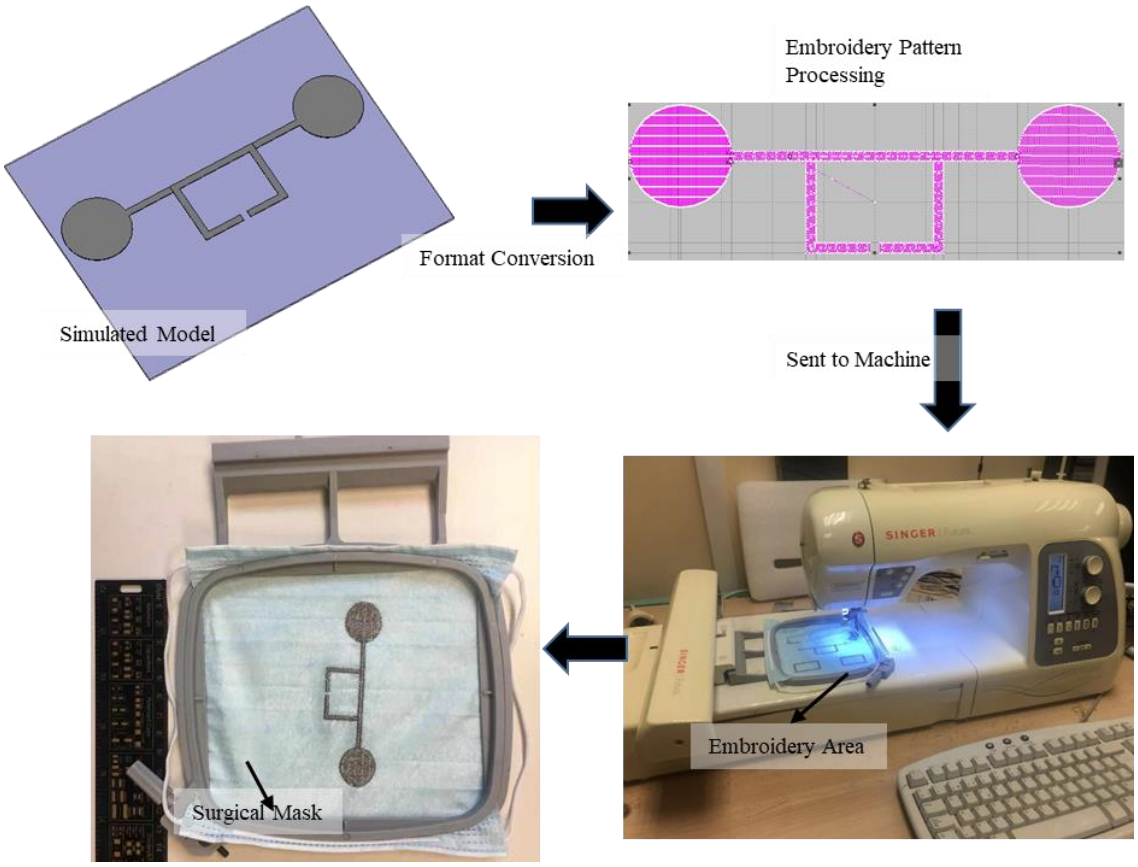

Figure 2.3. Embroidery procedure.

- First of all, after obtaining appropriate designs in simulation software (ADS momentum and CST), the simulated models need to be exported to a type of format which can be converted with the same size into the related embroidery software.

- Secondly, the knit pattern size and boundaries of the designs affected slightly by embroidery modes in the embroidery software (EasyDesign EX4.0) need to be adjusted carefully, which is a factor affecting real conductivity of the conductive yarns. For the proposed designs, the ‘satin fill’ mode in the embroidery software is adopted.
- Finally, in the manufacturing process, the proposed yarn is utilized in both sides of the substrate as the conductive yarn and support yarn for reducing the influence from other dielectric yarns.

2.3 Characterization methods of the textile UHF-RFID designs

2.3.1 Impedance measurements method

As shown in Figure 2.4, for symmetrical structures, a popular method validated in some works [66][67][68] for impedance measurements used in this research for differential input port antennas. It is achieved by combining the function (port extension [69]) of the Microwave Analyzer (N9916A) with the differential mode probes. The probes are made from two semi-rigid cables with ground shields soldered together.

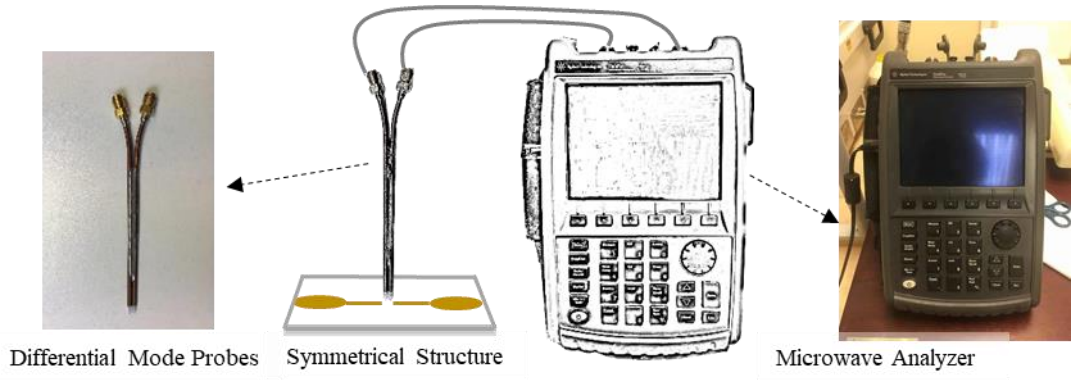

Figure 2.4. Calibration setup with the differential mode probes for impedance measurements method

Concerning the procedure,

- First of all, the Microwave Analyzer with two coaxial cables needs to be calibrated by a standard calibration kit.
- Secondly, after connecting the coaxial cables to the differential mode probes, the function (port extension) of the Microwave Analyzer needs to be adjusted in order to move the calibration plane from the ends of the coaxial cables to the ends of the differential mode probes.
- Meanwhile, the traces in Smith chart of the two ports should roughly converge to the open circuit position in the Microwave Analyzer.
- Next, the two tips of the differential mode probes are connected to the proposed textile UHF-RFID antennas or the feed port PCBs and the Z parameters in 50 ohms can be obtained. Note that the measured Z parameters using the differential mode probes are earth-referenced and need to be transferred for the differential reflection coefficient (ρ) of the symmetrical samples [70][71].

- Finally, the Z parameters of the tested samples in the complex conjugate impedance of the chip can be calculated using the Equation 2.1 as follows,

$$Z_{ant} = \frac{2Z_0(1 - S_{11}S_{22} + S_{12}S_{21} - S_{12} - S_{21})}{(1 - S_{11})(1 - S_{22}) - S_{12}S_{11}} \quad 2.1$$

Where Z_0 is the port impedance of the Microwave Analyzer (50 ohms in my work), S_{11}, S_{12}, S_{21} and S_{22} are the measured S parameters, Z_{ant} is the Z parameter of the symmetrical samples.

In this thesis, for the measurements of the impedance and reflection coefficients of the embroidered designs, the experimental setup is shown in Figure 2.5. As shown in Figure 2.5 (a) and (b), the measured differential S parameters can be obtained in the port of 50 Ohm and then the Z parameters can be calculated by Equation 2.1. In the next chapters, the impedance tests are implemented by the sample setup photos as shown in Figure 2.5 and the difference is only the different tested designs.

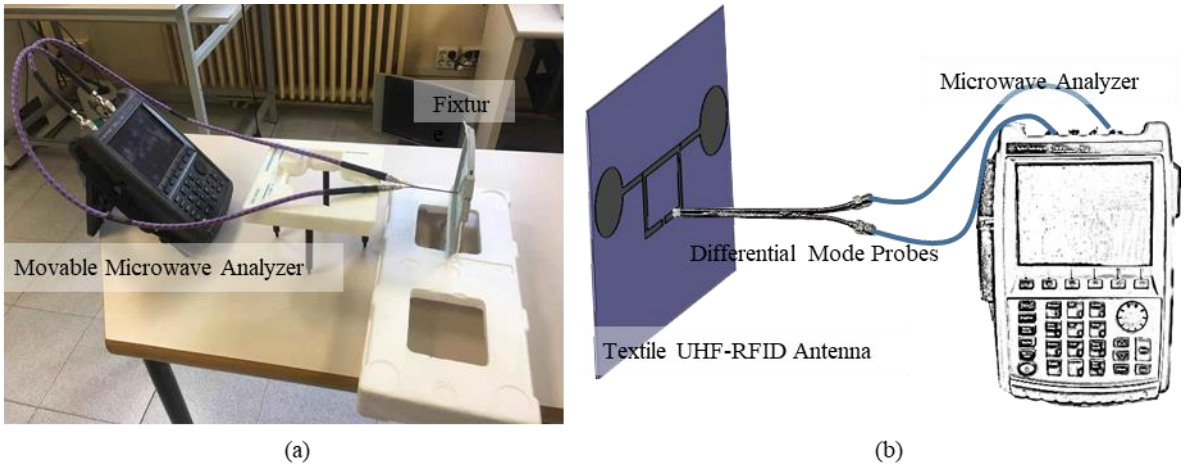

Figure 2.5. Measurement setup for the impedance and reflection coefficients of the embroidered designs. (a) Photograph of measurement setup, (b) Measurement setup configuration.

2.3.2 Read range measurements method

For read range measurement, a commercial RFID Reader is adopted in this thesis. The read range can be measured by a RFID reader with a reader antenna (MT-242 025/TRH/A/A) controlled by the M6E Kit and the measurement setup is shown in Figure 2.6. Note that considering the read range of some UHF-RFID antennas can be more than 5 m and the maximum input power from the M6E Kit is lower than the maximum required radiated power from regional regulatory authorities, the read range can be calculated by the mentioned Friis Equation 1.10.

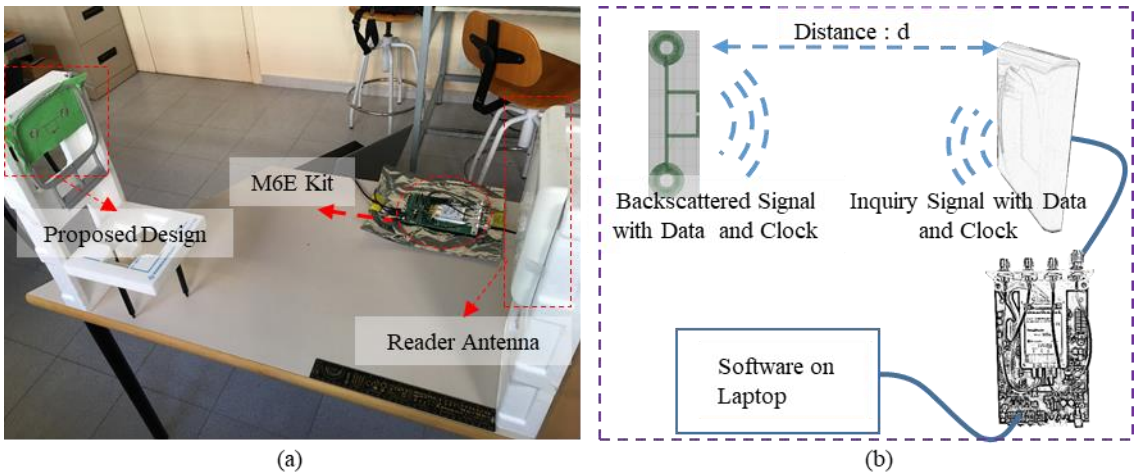

Figure 2.6. Measurement setup for the read ranges of the broidered designs. (a) Photograph of measurement setup and (b) measurement setup configuration.

The main steps are:

- Keep a certain distance d between the tested design and the reader antenna
- Decrease the reader antenna power until the reader can not detect the UHF-RFID designs
- Use the Equation 1.10 and the maximum required radiated power from regional regulatory authorities to calculate the maximum read range.

In addition, in order to meet the requirements of different application scenarios, the read range tests need to be implemented in some special places such as corridors or rooms. Therefore, in the next chapter, the read range measurement setup in special places is discussed especially.

Chapter 3
Results

3.1 Textile UHF-RFID Antenna Sensor for Measurements of Sucrose Solutions

***** Ref. B**: C. Luo,** I. Gil and R. Fernández-García, "Textile UHF-RFID antenna sensor for measurements of sucrose solutions in different levels of concentration." *Meas Sci Technol*, 2021. (Published)

3.1.1 Introduction

As mentioned in the previous chapter, textile materials are obtaining more attention due to their special features such as flexibility, hygroscopicity and comfort according to the aforementioned background. Current RFID antenna designs deployed on textile materials involve two main approaches, one of which is a copper-based RFID antenna printed on a textile substrate, another of which is the metal-plated yarns sewed on a textile substrate. Some of them focus on feasibility, reliability and common applications such as tracking. Especially for some designs based on a copper antenna and a polyimide substrate, they are applied for sensing solutions in the liquid through sensitivity (read power) of the RFID tag as the sensing parameter. It is a good idea for some RFID antenna sensor designs based on complete textile materials which offer the advantage of being more sensitive to liquids due to the conductive yarns in comparison with normal copper designs. In addition, compared with some studies using chemical sensors on a PCB for the target of wireless sweat-based monitoring, some textile materials with better hygroscopicity are expected to reach the same target by supporting conductive-yarns-plated UHF-RFID tags. Therefore one of the objectives in the thesis is to explore useful textile UHF-RFID antenna sensors with novel functions. In detail, a textile UHF-RFID antenna sensor for solutions concentration measurement is explored to replace or simplify some complex or expensive UHF-RFID sensors on standard PCBs.

In this section, a textile UHF-RFID tag with two sensing positions (‘radiation parts’ and ‘loop part’) is proposed for sucrose solution measurements. Considering the possibility of expanding future sensing applications, the function-extensible IC chip (ROCKY 100) is used in the proposed design. Before the tests on the proposed textile UHF-RFID sensor, a test board is developed in the preparation work for confirming the relative dielectric constants of the sensing substrate area in the real measurements. The fundamental resonance analysis for the simulated and the relative measurements is performed. In order to explore the relationship between variables of the proposed design and the sucrose solutions, two sensing positions are used to absorb the sucrose solutions with different levels of concentration. The read ranges of the design in different situations are tested by a RFID reader (M6e Kit) and analyzed combined with simulated results after obtaining the real relative dielectric constants of the sucrose solutions by the preparation work.

3.1.2 Test procedures of the whole work

In this work, a relatively novel approach is adopted to achieve the final sensing target of measurements of sucrose solutions in different levels of concentration by a proposed textile UHF-RFID antenna sensor. In order to make the approach clear, the test procedures of the whole work are divided into two main parts linked by the special 'medium' as shown in Figure 3.1.

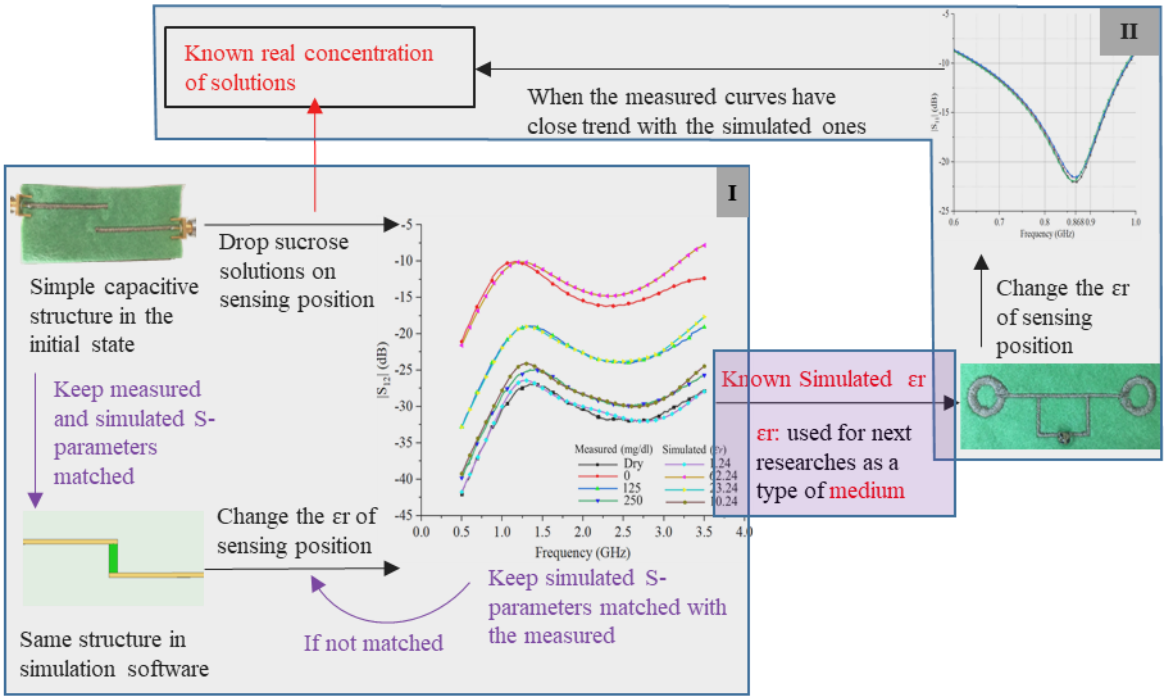

Figure 3.1. Test procedures of the whole work

The two parts can be generally summarised as:

- First part (I): The preparation work for the corresponding pairs of the concentration levels and the dielectric constant (ε_r) of the sensing position.
- Second part (II): The UHF-RFID antenna sensor test for the corresponding pairs of the dielectric constant (ε_r) and the read range values, thus obtaining the corresponding pairs of the concentration levels and the read range values

In detail, a simple capacitive structure is developed by means of simulation software and embroidered by the aforementioned embroidery machine. The S-parameter curves of the simulation and the real measurements are expected to be matched to obtain the corresponding values of ε_r as the fitting parameter. The obtained values ε_r related to the solution concentration are used in the UHF-RFID sensor simulation of the second part and then the simulated results are compared with the measured results to confirm the feasibility of the measurement method by the textile UHF-RFID sensors. Note that the ε_r is the bridge or medium to connect the first and second parts but make no effect on the corresponding pairs between the concentration levels and the read range values.

3.1.3 Preparation test

Considering the textile materials have the special feature (better hygroscopicity than PCBs), the solutions in different levels of concentration are expected to make an impact on substrate performance. In order to confirm the real relative dielectric constants of the sensing areas of the proposed design in different concentration levels of sucrose solutions, a preparation test is conducted in this section. As shown in Figure 3.2, the same textile-based test board is designed by a professional embroidery machine (Singer Futura XL-550) to measure the real relative dielectric constants of the sensing areas with the sucrose solutions in the different levels of concentration. Figure 3.2 (a) depicts the simulated test board model which is embroidered by the mentioned method in the previous section as shown in Figure 3.2 (b). In addition, the related size parameters are given in Table 3.1.

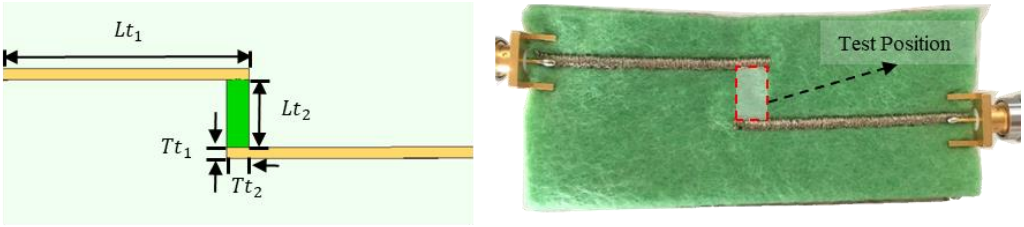

Figure 3.2. Geometry and configuration of the test board. (a) Simulated test board diagram, (b) photograph of the test board.

Table 3.1 Size parameters of the test board (unit: mm).

Parameter	Lt_1	Lt_2	Tt_1	Tt_2
Value	44	12	2	2

Moreover, the sucrose solutions are prepared by distilled water and sucrose (0, 125 mg•dl^{-1} and 250 mg•dl^{-1}). In order to obtain the sucrose solutions with different levels of concentration, accurate weighing is done for the sucrose by a precise balance (PCE-BS 300).

The measurement setup for the preparation test is shown in Figure 3.3 and the test procedure is listed as follows,

(a) Connect the two ports of the test board to the Microwave Analyzer N9916A as shown in Figure 3.3 (a), and save the reflection coefficients of the test board in dry conditions.

(b) Compare the saved data from the first step with the simulated curves of the test board model and confirm that both are matched.

(c) Drop the sucrose solutions in different levels of concentration (0, 125 mg•dl^{-1} and 250 mg•dl^{-1}) onto the sensing position of the test board, and save the reflection coefficients in each situation.

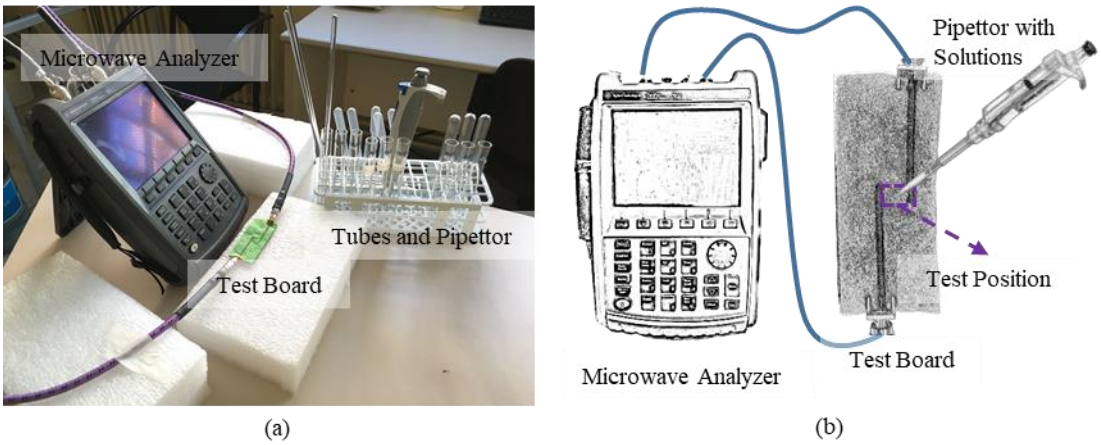

Figure 3.3. Measurement setup for the preparation test. (a) Photograph of measurement setup, (b) measurement setup configuration.

(d) Adjust the relative dielectric constants of the sensing area in the simulation software to find the matched curves with the measured curves. The corresponding relative dielectric constants are closed to the real relative dielectric constants of the sensing substrate area in the real measurements.

By the above test procedure, the test results are shown in Figure 3.4 and Figure 3.5. From the experimental results, the relative dielectric constants of the sensing substrate are tuned to 62.24, 23.24 and 10.24 for 0, 125 mg•dl^{-1} and 250 mg•dl^{-1}, respectively. Therefore, the obtained relative dielectric constants can be used for the proposed design in the next sensing tests.

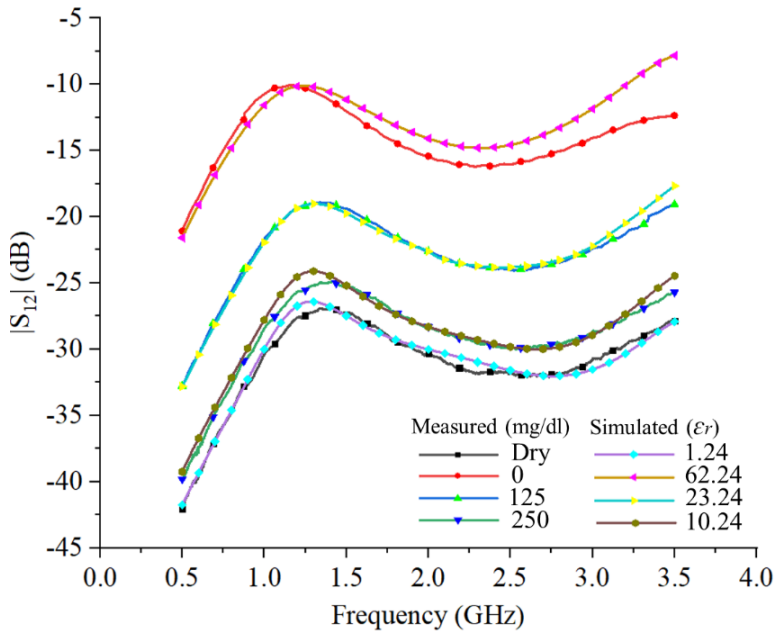

Figure 3.4. Simulated and measured $|S_{12}|$ of the test board for measuring the relative dielectric constant of the tested position with solutions.

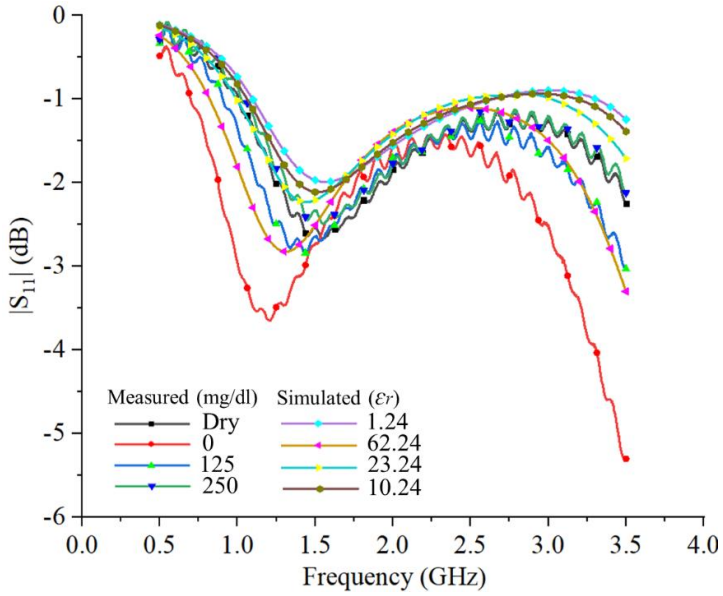

Figure 3.5. Simulated and measured $|S_{11}|$ of the test board for measuring the relative dielectric constant of the tested position with solutions.

3.1.4 UHF-RFID Antenna Sensor Details and Tests

Structure of the proposed textile UHF-RFID antenna

The geometry and configuration of the proposed textile UHF-RFID antenna sensor are shown in Figure 3.6. The design mainly consists of two parts which are the 'loop part' for impedance match and the 'radiation parts' for improving the transmiter/receiver ability as shown in Figure 3.6 (c). In Figure 3.6 (a), the simulated design is presented and its related size parameters are detailed in Table 3.2. Note that when the design is embroidered by specific machines, the embroidery pattern makes certain influence on the impedance of the textile UHF-RFID antenna due to roughness and small inhomogeneities. As a result, the proposed design is converted to an embroidery pattern by 'satin fill' mode as shown in Figure 3.6 (b).

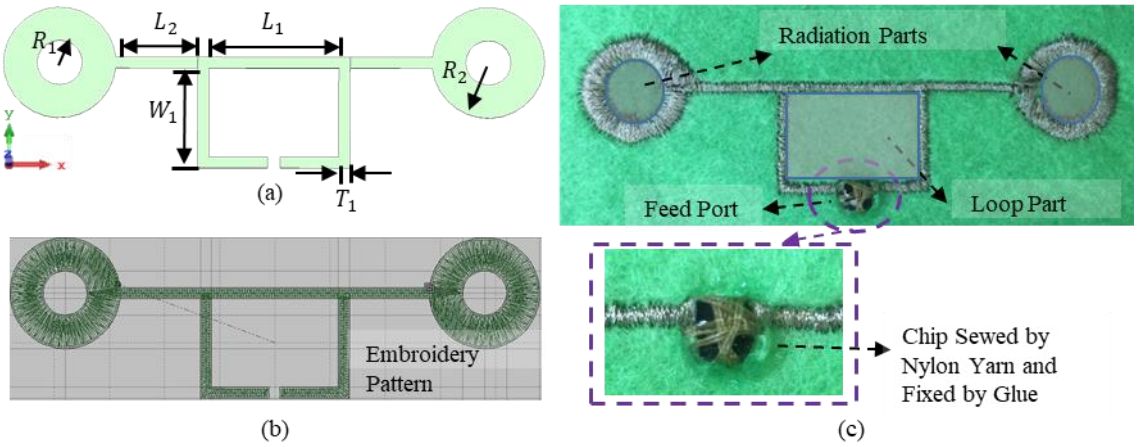

Figure 3.6. Geometry and configuration of the proposed design. (a) Simulated design diagram, (b) embroidered pattern diagram, and (c) photograph of the proposed design.

In addition, for the UHF-RFID integrated circuit (IC) chip, a ROCKY 100 is selected due to its function-extensible feature. Compared with some popular chips for textile RFID tags such as Monza R6, the ROCKY 100 can extend functions by connecting to various sensors. Certainly, in this paper, the

proposed textile UHF-RFID tag is explored to be an antenna sensor without sensor expansion. The complex impedance of the used chip (ROCKY 100) is 64−i469 ohm and the minimum wake-up power is −10 dB. For conjugate matching, the impedance of the design in simulation software needs to be tuned to be 64+i469 ohm.

Table 3.2 Size parameters of the design (unit: mm).

Parameter	L1	L2	W1	T1	R1	R2
Value	23	14.5	18	2	4	10

Sensing factors impacted by sucrose solutions in different levels of concentration

Considering the specific features of the proposed textile UHF-RFID tag such as the sensitive impedance change and the better substrate hygroscopicity than that of a common PCB,the sucrose solution for the proposed textile UHF-RFID tag is selected to explore the possibility as a sensor and the relationship between the concentration and the read ranges. For the proposed design, there are two positions selected as the sensing areas, the ‘radiation parts’ and the ‘loop part’ as shown in figure 1(c). The two positions are analyzed with respect to the Friis Transmission Formula as follows,

$$d_{max} = \frac{\lambda}{4\pi}\sqrt{\frac{P_t G_t G_{r3} \cdot \tau_3}{P_{thR}}} \qquad 3.1$$

where d_{max} is the maximum value of the read range, λ is the wave length at 868 MHz, P_t is the power fed into the reader antenna, G_t is the gain of the reader antenna (7 dBi), G_{r3} is the gain of the proposed antennas, τ_3 is the largest power transmission coefficient and P_{thR} is the minimum wake-up power of the chip (-10 dBm). In addition, the cable loss between the reader antenna and the reader is taken into account (0.8 dB).

From the Equation 3.1, the maximum value of the read range (d_{max}) can be affected by the gain of the proposed antenna gain (G_{r3}) and the largest power transmission coefficient (τ_3). Therefore, the ‘radiation parts’ and the ‘loop part’ related to the G_{r3} and τ_3 , respectively, are suitable choices. When the solutions with different levels of concentration are dropped on the sensing areas, the relative dielectric constants of the sensing areas are expected to change. The measured relative dielectric constants of the sensing area in different levels of concentration are confirmed in the preparation test above.

Tests and results at the ‘radiation parts’ position

The reflection coefficients ($|S_{11}|$) are simulated by sweeping the relative dielectric constant of the substrate at only the ‘radiation parts’ and the results at εr = 1.24 (dry), εr = 10.24 (250 mg•dl^{-1}), εr = 23.24 (125 mg•dl^{-1}) and εr = 62.24 (0 mg•dl^{-1}) are selected to compare with the real measurement results.

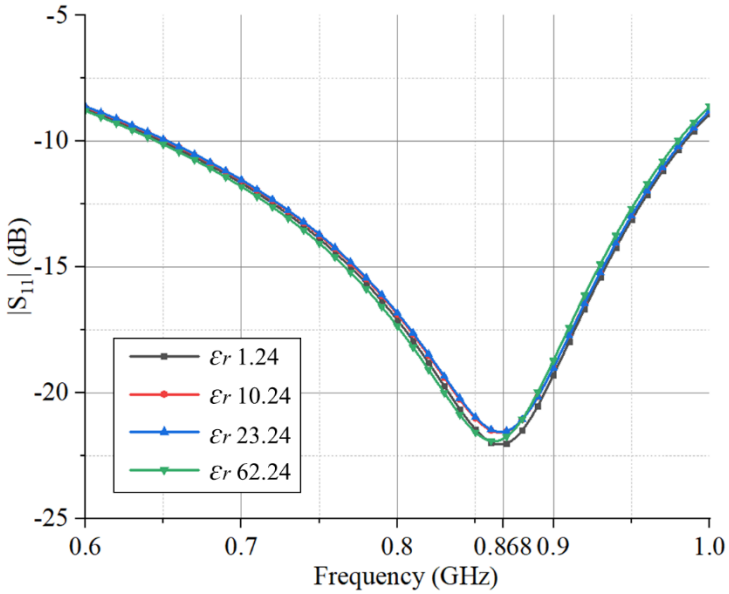

Figure 3.7. Simulated reflection coefficients of the proposed design with different relative dielectric constants at two 'radiation parts' positions.

As shown in Figure 3.7, all $|S_{11}|$ curves are close, which means when using 'radiation parts' to measure the sucrose solutions, the resonance frequency is expected to be stable. Meanwhile, as shown in Figure 3.8, the realized gain curve including all situations (ε_r: 10.24, 23.24 and 62.24) shows an increase in the target concentration range from 0 to 250 mg•dl^{-1}. In addition, the realized gain in a dry situation (ε_r: 1.24) reaches 0.9 dBi, which means compared to the results in wet situations the realized gain is expected to increase when sensing the solutions.

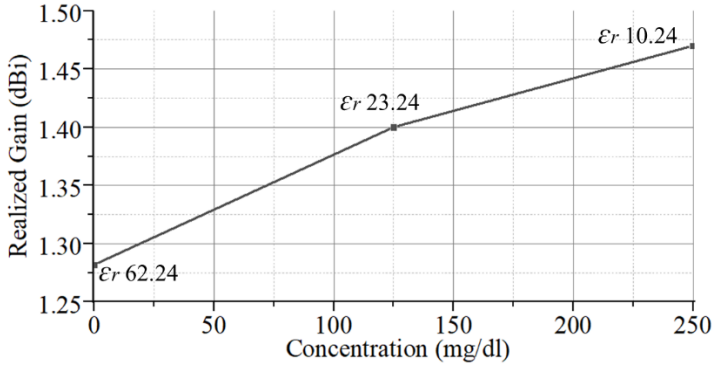

Figure 3.8. Simulated realized gain at 868 MHz of the proposed design with different relative dielectric constants at the two 'radiation parts' positions.

According to Equation 3.1, the maximum read range is related to the six factors including λ, P_t, G_t, Gr, τ and P_{thR}. There are four of them (λ, P_t, G_t and P_{thR}) which are determined by the resonance frequency (868 MHz in the work), EIRP (Europe, P_tG_t = 2 W), RFID IC chip (Rocky 100 in the work, P_{thR} = –10 dBm). However, the G_{r3}, τ_3 are determined by the UHF-RFID antenna.

When the match situations (τ) are close as shown in Figure 3.7, the simulated read range curve has a linear relationship with the square root of simulated realized gain (liner values not dB value) as Equation 3.2 shows,

$$d_{max} \propto \sqrt{G_{r3}} \qquad 3.2$$

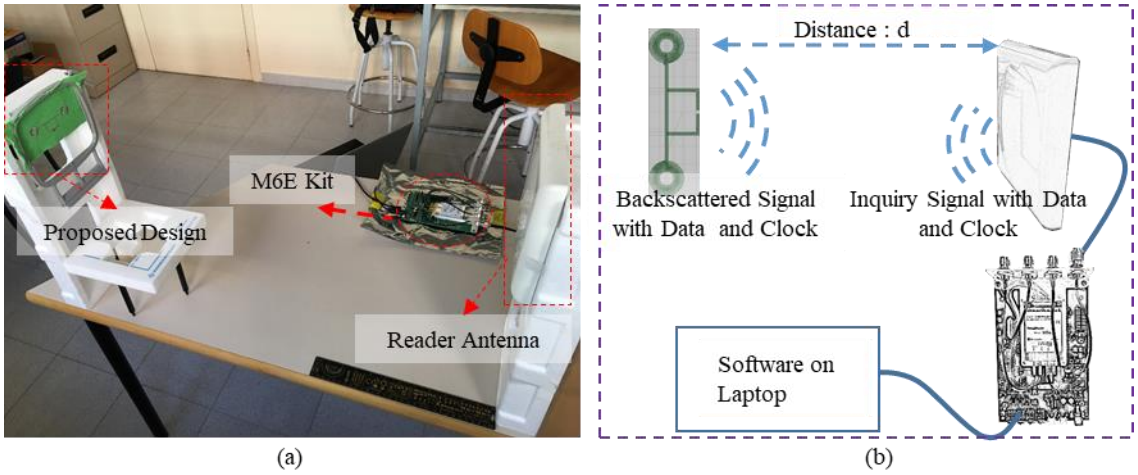

Figure 3.9. Measurement setup for the read ranges of them broidered designs when sensing solutions. (a) Photograph of measurement setup and (b) measurement setup configuration.

In order to validate the trend and explore the sensing ability, the real design embroidered by the same embroidery mode with the test board (‘satin fill’) is tested by sucrose solutions in different levels of concentration (0, 125 mg•dl^{-1} and 250 mg•dl^{-1}) at the ‘radiation parts’. The read range can be measured by a RFID reader with a reader antenna (MT-242 025/TRH/A/A) controlled by the M6E Kit as shown in Figure 3.9.

The tests on ‘radiation parts’ as shown in Figure 3.9 are conducted four times and final read powers are obtained by calculating average value as shown in Table 3.3. The validation points are used to confirm the reliability of the sensing characteristics obtained by the test points. Note that the distance between the design and the read antenna is set to 0.35 m and the read range can be calculated by using Equation 3.1.

To explore the trend of the real read range, the linear fit is adopted. In addition, in order to validate the trend of the measurement curve, the solutions in the concentration of 75 mg•dl^{-1} and 175 mg•dl^{-1} are detected. All the results are shown in Figure 3.10.

Table 3.3 Tests and validation results on 'radiation parts'.

/	Test points			Validation Points	
Concentration (mg•dl−1)	0	125	250	75	175
Read power 1st (dBm)	12.1	11	10.5	11.3	10.8
Read power 2nd (dBm)	12.1	10.9	10.6	11.4	10.8
Read power 3rd (dBm)	11.9	11.1	10.4	11.3	10.7
Read power 4th (dBm)	12	11	10.5	11.3	10.8
Average read power (dBm)	12	11	10.5	11.3	10.8
Read range (m)	1.926	2.161	2.289	2.087	2.211

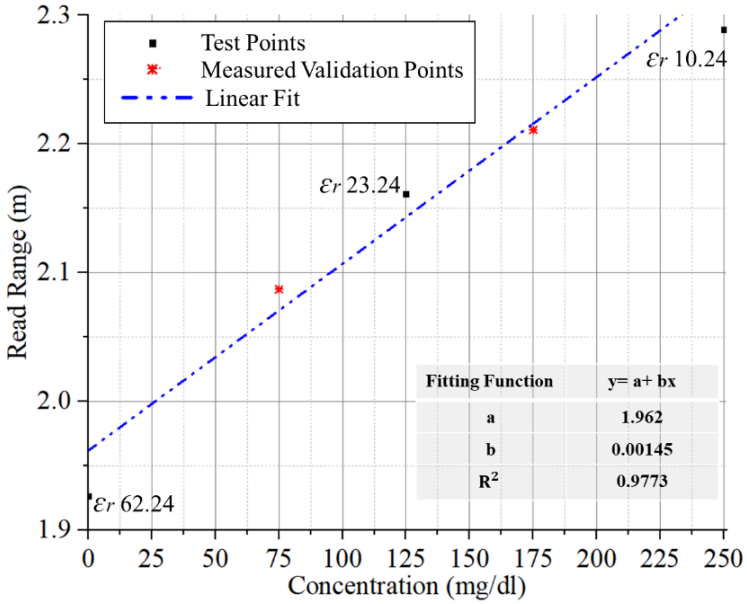

Figure 3.10. Measured read range at 868 MHz of the proposed design dropped by sucrose solutions at the 'radiation parts'.

The measured read range rises as the concentration goes up, but all the values in wet situations are higher than that when the sensing position is dry as shown in Figure 3.10,. Note that the permittivities of the sucrose solution decrease as the levels of concentration increase. The measured validation points are close to the fitting curve as shown in Table 3.4, which confirm the feasibility and availability of the measurement curves and method. In addition, by comparing the two figures, Figure 3.8 and Figure 3.10, the measured results have a trend that all the values in wet situations are higher than that in dry situations, which match with the linear trend of the simulated realized gain curve.

Table 3.4. Error between the measured validation points and the fitting curves.

Concentration (mg•dl^{-1})	75	175
	Read range (m)	
Validation points	2.087	2.211
Linear fit	2.071	2.216
|Error|	0.016	0.005

Tests and results at the 'loop part' position

The same tests are conducted on the 'loop part'. As shown in Figure 3.11, the resonance frequency shift left gradually as the permittivities (ε_r) increase continuously. However, only the curves whose (ε_r) is below 23.24 have the $|S_{11}|$ below −10 dB at 868 MHz. In other words, when using 'loop part' to measure

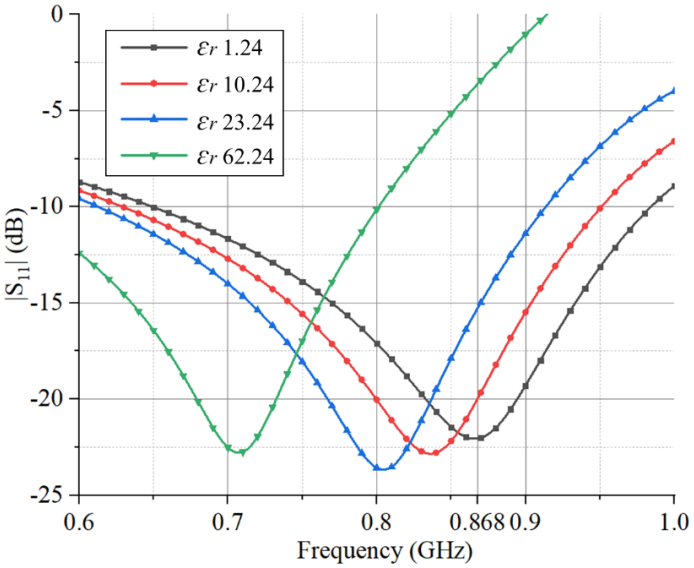

Figure 3.11. Simulated reflection coefficients of the proposed design with different relative dielectric constants at the 'loop part'.

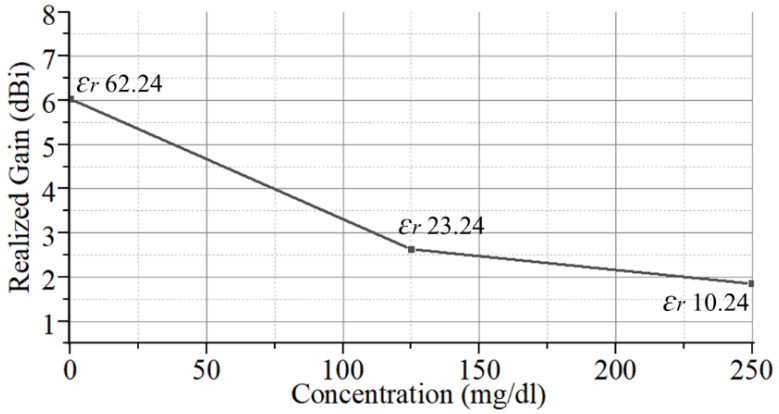

Figure 3.12. Simulated realized gain at 868 MHz of the proposed design with different relative dielectric constants at the 'loop part'.

the sucrose solutions, the performance of the textile UHF-RFID antenna sensor decreases as the levels of concentration are fairly low. Meanwhile, as shown in Figure 3.12, the realized gain curve including all situations (ε_r: 10.24, 23.24 and 62.24) shows a continuous decrease in the target concentration range from 0 to 250 mg•dl^{-1}. As aforementioned, the G_{r3}, τ_3 are determined by the UHF-RFID antenna, one of which in this situation, τ_3 , can be calculated by Equation 3.3,

$$\tau_3 = \frac{4R_{ant}R_{ic}}{(|Z_{ant} + Z_{ic}|)^2} \tag{3.3}$$

where R_{ant} is the resistant part of the antenna impedance, R_{ic} is the resistant part of the IC chip impedance, Z_{ant} is the antenna impedance and Z_{ic} is the IC chip impedance. When λ, P_t, G_t and P_{thR} are determined, the relationship between the maximum read range and the antenna is obtained as Equation Table 3.4 shows,

$$d_{max} \propto \sqrt{G_{r3} \cdot \tau_3} \tag{3.4}$$

By calculation, the results can be obtained as shown in the Table 3.5,

Table 3.5. Realized gain data and calculated results.

ε_{r3}	10.24	23.24	62.24
G_{r3} (dBi)	1.8472	2.6324	6.0251
G_{r3} (linear value)	1.5301	1.8333	4.0041
τ_3	0.8126	0.6354	0.2043
$\sqrt{G_{r3}} \cdot \sqrt{\tau_3}$	1.115	1.0793	0.9045

The read range of the real embroidered design is also tested by sucrose solutions in different levels of concentration (0, 125 mg•dl^{-1} and 250 mg•dl^{-1}) at the ‘loop part’ and measured by the RFID reader. As shown in Figure 3.13, the measured read range rises as the concentration goes up, but all the values in wet situations are lower than that when the sensing position is dry.

The tests on ‘loop part’ as shown in Figure 3.9 are conducted four times and final read powers are obtained by calculating the average value as shown in Table 3.6. Note that the certain distance between the design and the read antenna is set to 0.35 m and the read range can be calculated by using Equation 3.1.

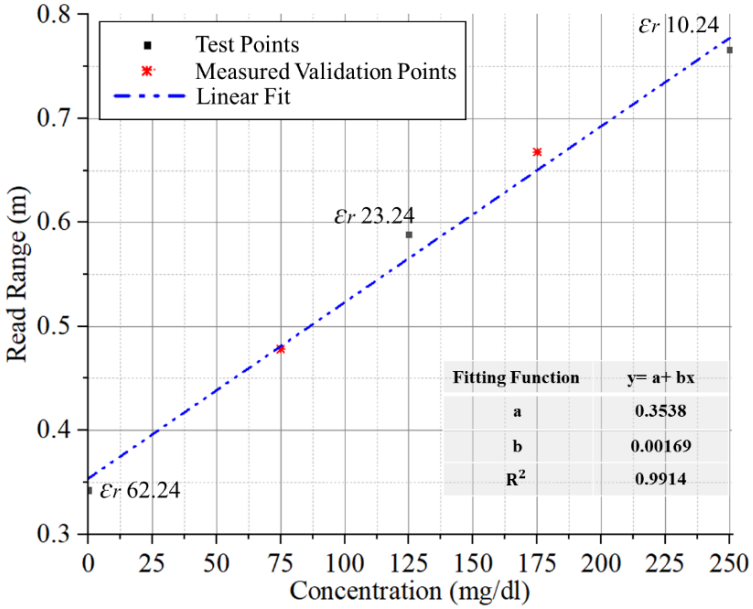

Figure 3.13. Measured read range at 868 MHz of the proposed design dropped by sucrose solutions at the 'loop part'.

Table 3.6. Tests and validation results on 'loop part'.

/	Test points			Validation Points	
Concentration (mg•dl−1)	0	125	250	75	175
Read power 1st (dBm)	27	22.3	20.1	24.1	21.3
Read power 2nd (dBm)	27.2	22.1	19.9	24	21.3
Read power 3rd (dBm)	27.1	22.4	19.8	24.2	21.1
Read power 4th (dBm)	26.8	22.3	20	24.1	21.2
Average read power (dBm)	27	22.3	20	24.1	21.2
Read range (m)	0.3424	0.5365	0.766	0.4782	0.6677

To explore the trend of the real read range, the linear fit is adopted. In addition, in order to validate the trend of the measurement curve, the solutions in the concentration of 75 mg•dl^{-1} and 175 mg•dl^{-1} are detected. All the results are shown in Figure 3.13. Moreover, the measured validation points are close to the fitting curve as shown in Table 3.7, which confirm the feasibility and availability of the measurement curves and method.

Table 3.7. Error between the measured validation points and the fitting curves.

Concentration (mg•dl^{-1})	75	175
	Read range (m)	
Validation points	0.4782	0.6677
Linear fit	0.4806	0.6496
|Error|	0.0024	0.0181

In addition, by comparing Table 3.5 and Figure 3.13, the measured results that all the values in wet situations are lower than that in dry situations match with the simulated results. The reason for the opposite trends of the realized gain curve and the read range curve is that the shifting resonance frequency (different match situations) presents a bigger influence on the read range than the affecting factor from the realized gain.

Moreover, by analyzing the curves with the relative dielectric constants (10.24, 23.24 and 62.24) in figures 10 and 14 compared with the measured read range results in Figure 3.10 and Figure 3.13, the trends in real measurements are matched with the simulated trends and the sensing feasibility of the proposed textile UHF-RFID antenna is confirmed.

The proposed textile UHF-RFID antenna sensor has the feasibility to be a wireless sensor for the concentration measurement of sucrose solutions. In addition, another novel point is that the proposed design has two sensing positions, the ‘radiation parts’ and the ‘loop part’. The two sensing positions have different advantages, one of which (‘radiation parts’) have a stable operation performance but sensing range is from 1.71 m (dry) to 2.3 m (current measured solutions), while another of which (‘loop part’) have a wide sensing range from 0.4 m (current measured solutions) to 1.71 m (dry) but a lower operation performance. The two choices can be adopted with respect to different applications.

3.1.5 Conclusion

In this section, a textile UHF-RFID antenna sensor with two sensing positions (‘radiation parts’ and ‘loop part’) is presented. To explore the possibility for textile UHF-RFID tag as a sensor and relationship between variables, the proposed design has been tested by sucrose solutions in different levels of concentration (0, 125 mg•dl^{-1} and 250 mg•dl^{-1}) compared with the dry situation. Before the tests on the proposed design, the test board is developed in the preparation work for confirming the relative dielectric constants of the sensing substrate area in the real measurements (62.24, 23.24 and 10.24 for 0, 125 mg•dl^{-1} and 250 mg•dl^{-1}, respectively). The simulated and measured resonance curves of the proposed designs both match well (−20 dB in the simulation and −15.8 dB in the measurement at 868 MHz) and the read range measured by the RFID reader (M6e kit) is 1.71 m in air. After simulation and real tests, the proposed design

used for sensing the sucrose solutions shows good feasibility by comparing the simulated and measured results. Moreover, its two sensing positions have different sensing features. The sensing 'radiation parts' shows a stable frequency operation performance but sensing range is from 1.71 m (dry) to 2.3 m (current measured solutions), while the sensing 'loop part' have a wide sensing range from 0.4 m (current measured solutions) to 1.71 m (dry) but a lower frequency operation performance. The sensing features provide future complete application for the two choices.

3.2 Textile UHF-RFID Antenna Embroidered on Surgical Masks

***** Ref. C**: C. Luo,** I. Gil and R. Fernández-García, "Textile UHF-RFID Antenna Embroidered on Surgical Masks for Future Textile Sensing Applications," *IEEE Trans. Antennas Propag.*, 2022. (Published)

3.2.1 Introduction

In current society, we are living in a constant epidemic situation which has a great effect on the researches on masks. Considering the growing concern about the UHF-RFID tags and sensors for healthcare monitoring and diagnosis, the UHF-RFID tag can be explored to be used on masks. Based on current popular application scenarios such as breath monitoring for pregnant women or babies, move tracking for patients and temperature monitoring, the UHF-RFID tags have the potential to be designed on masks and applied for these scenarios.

In addition, as mentioned in the last section, the function-extensible chips are useful for UHF-RFID tags with many other sensing functions. Some textile RFID tags and sensors are designed with two-pad IC chips which are small and more sensitive to wake up. However, these types of chips with two pads and low wake-up power are especially used as ID textile tags. The related sensing functions can be only explored by the features of textile materials, which limits the sensing applications. For example, the textile antenna (Bellyband antenna) designed with the IC chip Murata Magicstrap LXMS31ACNA-011 is used as a tag with a strain sensing function. In addition, there is no other interface for extensional sensing functions and on-body read range is only 0.6 m. As a result, exploring the possibility and reliability of the function-extensible IC chips is also a novel research orientation.

In this section, considering a general epidemic situation in which the surgical masks are frequently used for human beings protection, three progressive designs of textile UHF-RFID antennas on surgical masks is developed and the used IC chip (Rocky 100) is extensible for different sensors. Related preparatory work before simulation such as the permittivity, loss tangent, thickness measurements and detailed embroidery method is implemented and presented. The progress of the three designs through comparison between their simulated resonance and radiation performance is explained. For the measurements of the impedance and read range, the results to the electromagnetic simulations to validate their performance are compared. Finally, the selected sample is applied to validate the reliability by the tests under bending and skin contact situations. The basic use of the designs is the user identification, nevertheless, due to the function extensibility of the chips, various textile sensors can be considered under specific scenarios.

3.2.2 Progressive textile UHF-RFID designs

The textile UHF-RFID antennas are designed on surgical masks and the configuration of the proposed progressive designs are shown in Figure 3.14. Considering the used chip (Rocky 100) with a capacitive impedance of 64-i*469 ohm, the proposed antennas are expected to be designed with an inductive behavior. Note that for UHF-RFID chips with complex impedance, the corresponding antenna design way is different

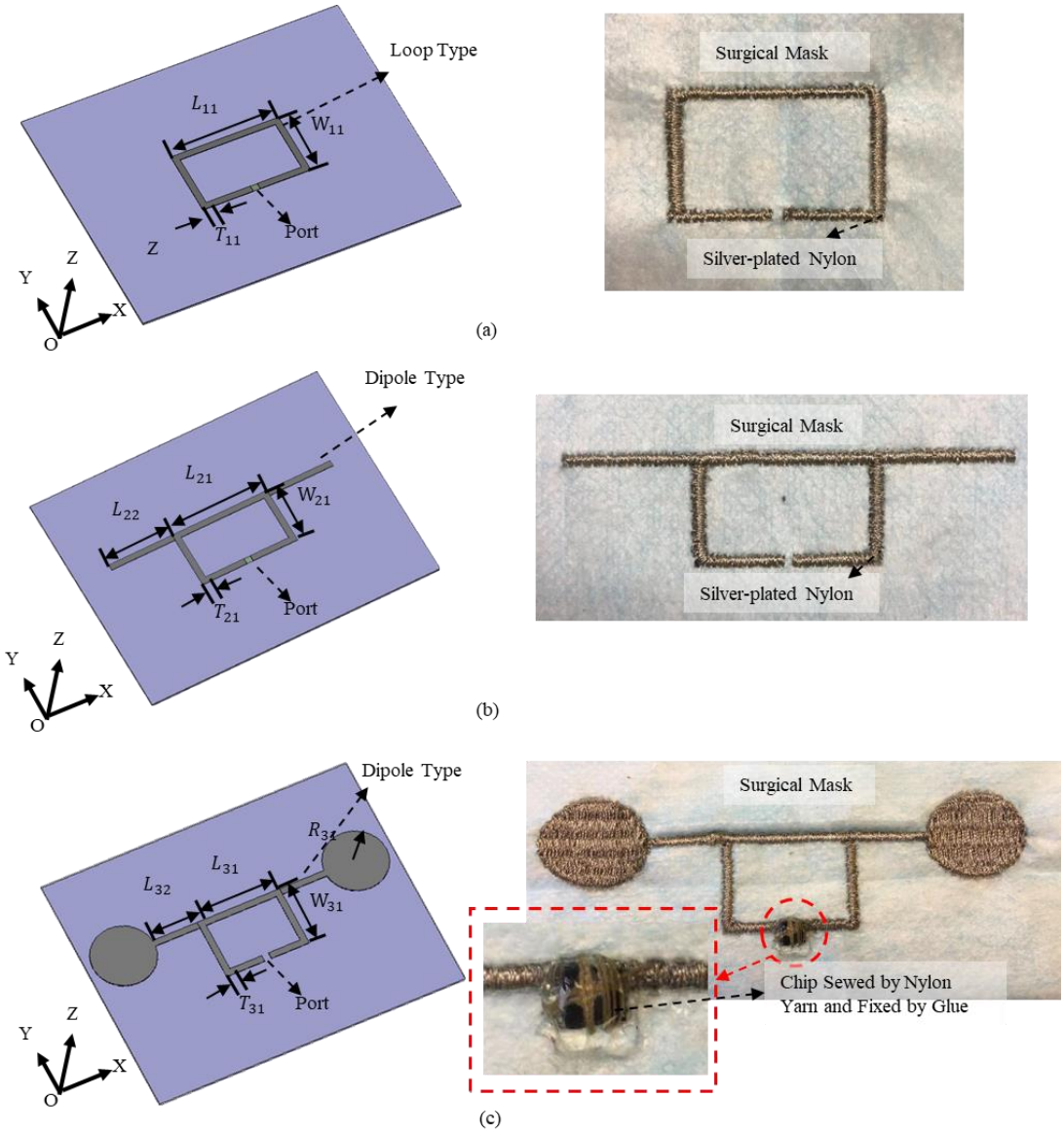

Figure 3.14. Configuration of the proposed progressive designs. (a)loop type, (b) dipole type with balanced 'arms', (c) dipole type with balanced 'circular end caps'.

from conventional antenna design experience (such as W_{11}<<L_{11} for a conventional folded dipole in Figure 3.14) with a feed port of 50 ohm. Therefore, a loop structure for matching as shown in Figure 3.14 (a) has been selected as a design strategy. Then through an electromagnetic field analysis as illustrated in next section and typical 'T-match' structure analysis, the progressive structures, Design 2 and 3 are developed as shown in Figure 3.14 (b) and (c), respectively. As a consequence, the Design 3 is derived from the simple 'T-match' structure with 'circular end caps' for increasing the radiation property (directivity and realized gain). The size parameters are detailed in Table 3.8. All of the designs are embroidered using

conductive yarns as antennas and surgical masks as substrates. The textile material of the antennas is a commercial conductive twisted yarn (Shieldex 117/17 dtex 2-ply) made of 99% pure silverp-lated Nylon (bulk conductivity: 11500 siemens/m). Moreover, as shown in Figure 3.14 (c), the UHF-RFID chip (Rocky 100) is sewed by Nylon yarn which is not conductive and fixed by a type of glue (G-15). The substrate is a type of common surgical mask made of staple fibres (short) and long fibres (continuous long).

In addition, note that the UHF-RFID chip (Rocky 100) is selected for the work, which is different from the chips used in most textile/knitted wearable UHF-RFID tags. The Rocky 100 chip is normally used for UHF-RFID sensors on PCB. In other words, this chip has several pads (16 pads) which can be used for sensor connection in active/passive situations for many different sensing applications. Compared with some popular chips such as Monza R6 with two pads, the Rocky 100 has a lower sensitivity (minimum wake-up power) of -10 dBm, while Monza R6 has higher sensitivity of about -20 dBm. As a result, the UHF-RFID antenna needs to be designed for higher gain and good conjugate impedance matching with the chip.

Table 3.8 Size parameters of the designs (unit: mm)

Type	L_{11}	W_{11}	T_{11}		
Design 1	34	21	2		
Type	L_{21}	L_{22}	W_{21}	T_{21}	
Design 2	33	22	20	2	
Type	L_{31}	L_{32}	W_{31}	T_{31}	R_{31}
Design 3	27	20	20	2	10

3.2.3 Simulation and Measurements

Considering that the complex impedance of the used chip (Rocky 100) is 64-i*469 ohm, the impedance of the designed antenna should be close to 64+i*469 ohm. Note that the chip has higher resistance and reactance than that of some two-pad UHF-RFID chips such as the Monza R6 with the complex impedance of 12-i*120 ohm. In some antenna designs, resistance and reactance curves for antennas present fast-changing slopes and larger tangent, which means that the resistance and reactance values change sensitively. Hence in order to reduce the effects on frequency bandwidth of antenna designs, it is more important that the designed antenna can have a good conjugate impedance match with the chip, which implies that the designed antennas need to have complex impedance with the conjugate impedance of the chip as close as possible. In addition, the differential reflection coefficient (ρ) of the work band should be lower than -10 dB.

In addition, as mentioned in the previous section, although the function-extensible feature of the chip (Rocky 100) is attractive, its lower sensitivity still needs to be considered. Therefore, the UHF-RFID antenna needs to be designed to achieve a realized gain as high as possible (at least higher than -3 dBi). For

the proposed three designs, one of the targets is to improve the gain but reduce the impact on the conjugate impedance match. As a result, the Design 1, 2 and 3 are optimized progressively. After being optimized, the three designs are shown in Figure 3.14 and the final size parameters are shown in Table 3.8.

Resonance Analysis

Figure 3.15 shows the simulated impedance for the three progressive designs, including the resistance and reactance curves. The three designs behave inductively at the resonance frequency (868 MHz), in which the closer two to the feed impedance are the Design 1 and 2 with impedance of 67+i*468 ohm and 74+i*466 ohm, respectively. The Design 2 can be developed by a size-optimized Design 1 with balanced 'arms'. By adding the circular end caps to the Design 2 and optimizing the size parameters, Design 3 has impedance of 119+i*421 ohm. Although the impedance matching seems to degrade from Design 1 to 3, the reflection coefficients of the three designs as shown in Figure 3.16 are still within acceptable limits. In addition, the 'arms' and the 'circular end caps' are expected to increase the antenna gain.

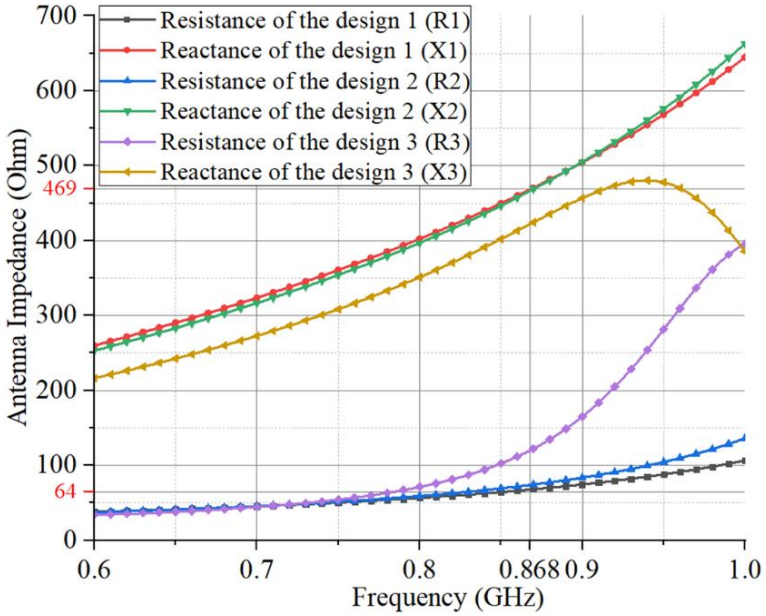

Figure 3.15. Simulated impedance for the three progressive designs (Dashed lines: required antenna complex impedance 64+i*469 ohm at 868 MHz).

In detail, the S parameters (reflection coefficients) of the three designs as shown in Figure 3.16 are all under the -10 dB at 868 MHz. At resonance point (868 MHz), the Design 1, 2 and 3 have reflection coefficients of -48 dB, -39 dB and -22 dB, respectively. The Design 1 and 2 present a bandwidth of at least 400 MHz (Design 1: 560 MHz and Design 2: 515 MHz), while Design 3 have a bandwidth of 370 MHz. In addition, transmission coefficients (τ) for the Design 1, 2 and 3 can be calculated as 0.9992, 0.9945 and 0.8519, respectively. Due to the basic features of general textile materials, environmental factors often make an influence on the resonance frequency of the textile UHF-RFID antennas. As a result, the bigger bandwidth can improve reliability when the resonance frequency shifts within a certain range.

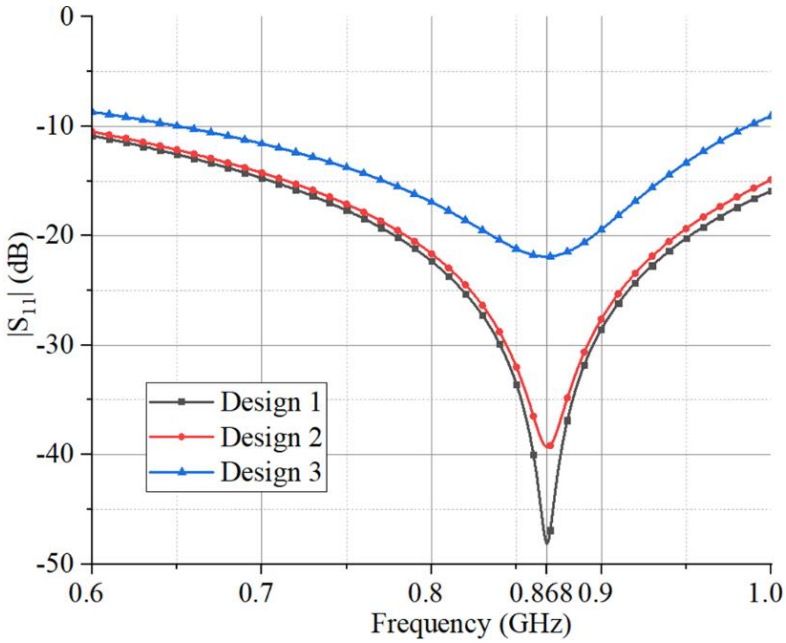

Figure 3.16. Simulated reflection coefficients for the three progressive designs.

Radiation Performance Comparison

The electric field, magnetic field and current distribution at 868 MHz are shown in Figure 3.17. It is found that from the Design 1 to the design 3, the electric fields and magnetic fields are raised and their distribution ranges are extended gradually after adding the ‘arms’ and ‘circular end caps’ and adjusting loop and ‘arms’ sizes. In addition, it is found that after adding arms and changing loop size, the overall fields and currents of the Design 1, 2 and 3 get stronger. From the aforementioned features, adjusting the loop and ‘arms’ can obtain the required frequency and changing the size of the ‘circular end caps’ can affect the radiation performance. Figure 3.18 shows the radiation patterns in the xoy cut for the three designs. The structure of the Design 1 is only a loop which means the radiation ability is weak. For increasing the radiation ability (realized gain), the ’arms’ can be added into the structure as the Design 2 which also makes an impact on the impedance. From the current distribution as shown in Figure 3.17, the realized gain of the Design 3 is expected to be higher than that of the previous designs. As shown in Fig. 7, the peak realized gain values of the three designs are -10.86 dBi, -7.87 dBi and 1.09 dBi, respectively. In addition, from the H-plane (yoz cut) as shown in Figure 3.18 (b), the proposed Design 3 has a dipole-like radiation pattern as expected.

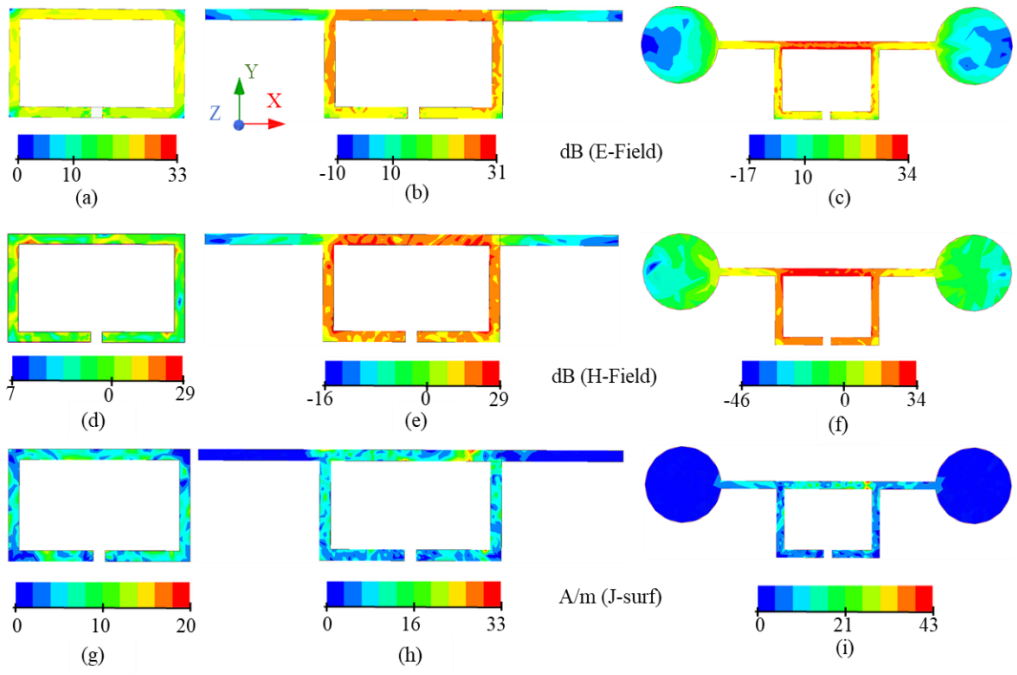

Figure 3.17. Electromagnetic fields and current distribution at 868 MHz. Design1: (a), (d) and (g). Design 2: (b), (e) and (h). Design 3: (c), (f) and (i).

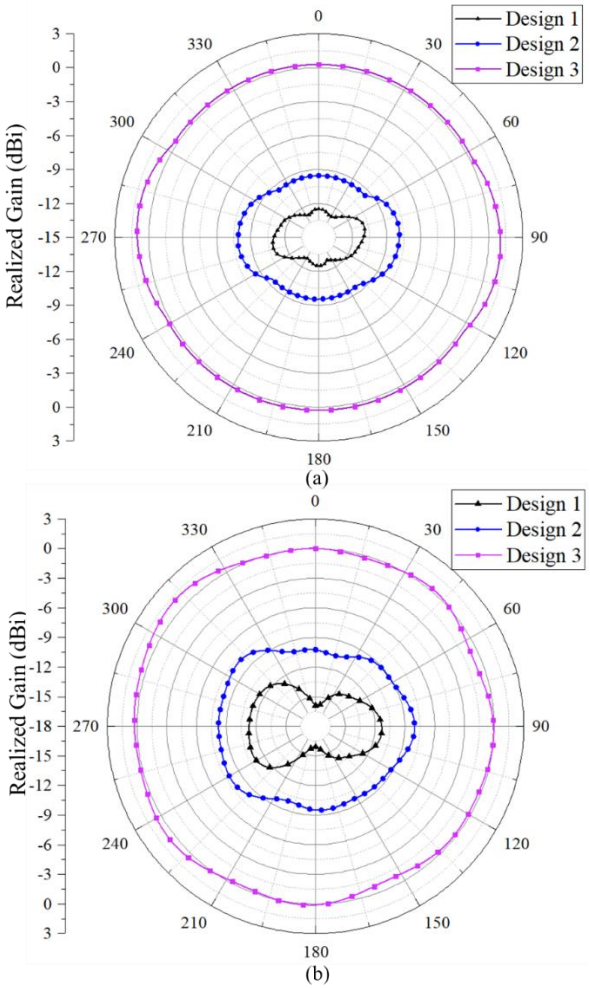

Figure 3.18. Simulated normalized radiation patterns (normalized realized gain) for the three progressive designs (a) xoy cut, (b) yoz cut.

3.2.4 Measurement and Test Results

Impedance Tests

As mentioned in the previous chapter, the differential mode probes are added at the end of the two ports and the related differential measurement method is used. Figure 3.19 shows the antenna impedance of the proposed simulated and measured designs, including the resistance part and the reactance part. Figure 3.19 (a) and (b) shows the good impedance match of the simulated and measured design 1 and 2 at the targeted resonance frequency (868 MHz) and the both impedance is fairly close to the target (64+i*469 ohm). The results of the simulated and measured design 3 are shown in Figure 3.19 (c). In this case, the resistance parts are higher than 64 ohm and reactance parts are lower than 469 ohm. Certainly, analyzing all of the results, the measured curves are very close to the simulated curves.

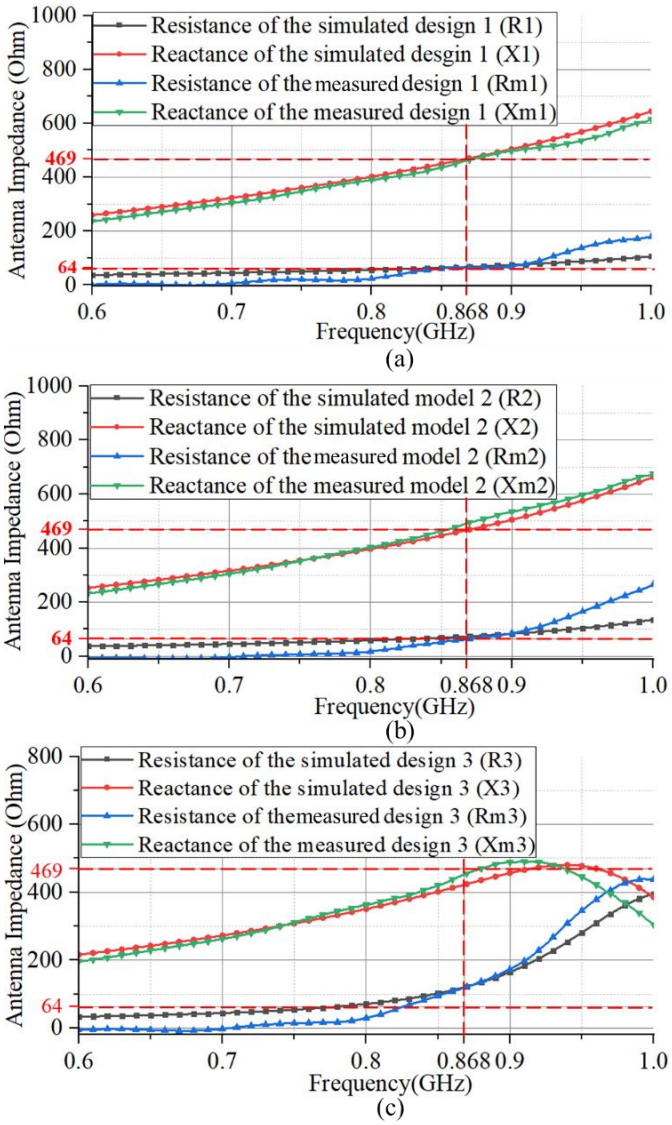

Figure 3.19. Simulated and measured impedance for the three embroidered designs (Dashed lines: required antenna complex impedance 64+i*469 ohm at 868 MHz). (a) Design 1, (b) Design 2, (b) Design 3.

Moreover, the reflection coefficient (S parameter) can be obtained as shown in Figure 3.20. It can be observed that the $|S_{11}|$ of the measured design 1 is -42 dB at 868MHz, which is close to the simulated |S11|

of -48 dB. Figure 3.19 (b) shows the measured design 2 has resonance frequency shift but the $|S_{11}|$ at 868 MHz still reaches -32.8 dB compared with that of -39 dB in simulation. Different from that of the design 1 and 2, the |S11| of the measured design 3 is -24 dB which is better than the simulated results at 868 MHz. Note that all the designs have slight differences in the resonance frequency shift degrees between the simulated and measured results (all below 10 MHz). In addition, all of the measured designs 1, 2 and 3 have narrower bandwidths of about 330 MHz, 280 MHz and 220 MHz, respectively, than that of the simulated designs.

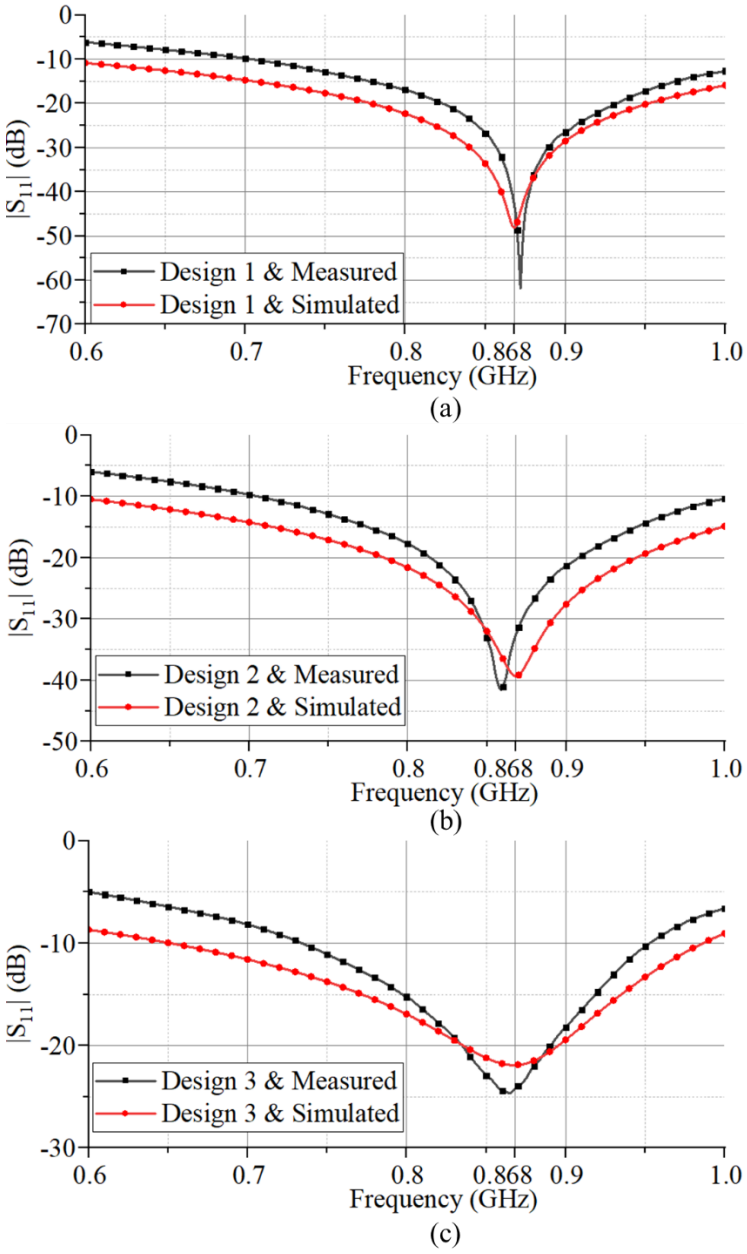

Figure 3.20. Simulated and measured reflection coefficients for the three embroidered designs. (a) Design 1, (b) Design 2, (b) Design 3.

Read Range Tests

Considering real scenario conditions of the proposed textile UHF-RFID tag on surgical masks such as in the hospital facilities and rooms, the read range measurement setup is shown in Figure 3.21. The reader

antenna (MT-242025/TRH/A/A) can be controlled by the M6E Kit which is connected to a laptop with control software. An inquiry signal with data and clock can be adjusted by the software and sent by the reader antenna. The proposed textile UHF-RFID antennas can send a backscattered signal with data and clock after receiving the inquiry signal. Note that backscattering coupling is a common mode in UHF RFID and Radar areas. In detail, when an electromagnetic wave encounters a space target, part of its energy is absorbed by the target, while the other part is scattered in various directions at different intensities. A portion of the scattered energy is reflected back to the transmitting antenna.

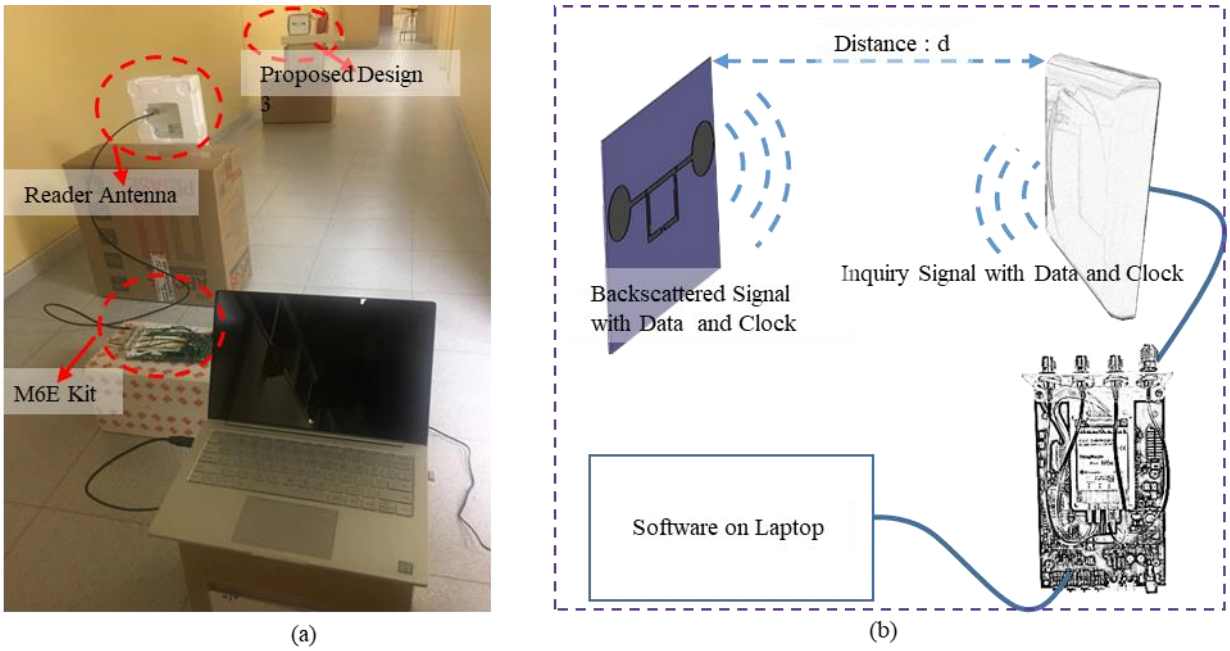

Figure 3.21. Measurement setup for the read ranges of the embroidered designs. (a) Photograph of measurement setup, (b) Measurement setup configuration.

When moving the proposed designs to a certain distance d as shown in Figure 3.21, the signal transmission is expected to be interrupted. This threshold distance is the maximum value of the read range. To avoid moving the design holders frequently, a certain distance is fixed (1 m) which is different from the distance (0.35 m) used in the last section and then adjust the reader power to obtain the read range. In addition, the simulated read range can be calculated by the Friis Transmission Formula as follows,

$$d_{max} = \frac{\lambda}{4\pi}\sqrt{\frac{P_t G_t G_{r4} \cdot \tau_4}{P_{thR}}} \qquad 3.5$$

where d_{max} is the maximum value of the read range, λ is the wave length at 868 MHz, P_t is the power fed into the reader antenna, G_t is the gain of the reader antenna (7 dBi), Gr_4 is the gain of the proposed antennas in this section, τ_4 is the largest power transmission coefficient and P_{thR} is the minimum wakeup power of the chip (-10 dBm). In addition, the cable between the reader antenna and the reader has a loss of 0.8 dB.

Table 3.9. Simulated and measured maximum read range of the designs (unit: m)

Type	Design 1	Design 2	Design 3
Simulated d_{max}	1.1	1.6	4.1
Measured d_{max}	0.8	1.3	2.2

For the proposed designs, the read ranges are detected as shown in Table 3.9. The maximum read range values of the simulated Designs 1, 2 and 3 are 1.1 m, 1.6 m and 4.1 m, respectively, while those corresponding to the measured values are 0.8 m, 1.3 m and 2.5 m, respectively. By analyzing the Friis Transmission Formula and the proposed designs, the P_{thR} of the chip (-10 dBm) makes a big impact on the maximum read range, compared to the two-pad chip (Monza R6) with the minimum wake-up power of -20 dBm. In addition, the difference between the simulated and measured results is caused by the silver-plated yarns and the soft substrates. In detail, the silver-plated yarns are different in comparison with the traditional copper line. The radiation ability of the yarns is not totally the same as the simulation results. For design 3, due to the soft masks, the 'circular end caps' has slight shape change in embroidery procedure which implies a more significant difference between the simulated and measured results.

3.2.5 Reliability validation Tests

For textile UHF-RFID tags, reliability is an essential issue due to the features of the textile materials. In this work, considering the uses of surgical masks, the impact of bending and use on the body is expected to be validated. In addition, with regard to the read range results at last section, the Design 3 is selected to be the final design which is tested for bending and skin touching.

Bending Tests

The bending test setup is shown in Figure 3.22 (a). Several moulds with different radius have been used to hold and keep the proposed sample bent. Considering the use of surgical masks, the bending orientation is fixed as shown in Figure 3.22 (b). Note that the bending degree increases with decreasing radius. Figure 3.23 shows the measured antenna impedance curves in different radius. From Figure 3.23, the resistance values at 868 MHz are close to a different radius while the reactance values at 868 MHz increase with decreasing radius. In addition, the reflection coefficient curves as shown in Figure 3.24 have slight resonance frequency shift degrees (all below 20 MHz) and increasing $|S_{11}|$ values at 868 MHz with increasing bending degree. In other words, after bending at certain degrees (radius: 33 mm to the flat), the proposed textile UHF-RFID tag can still work well.

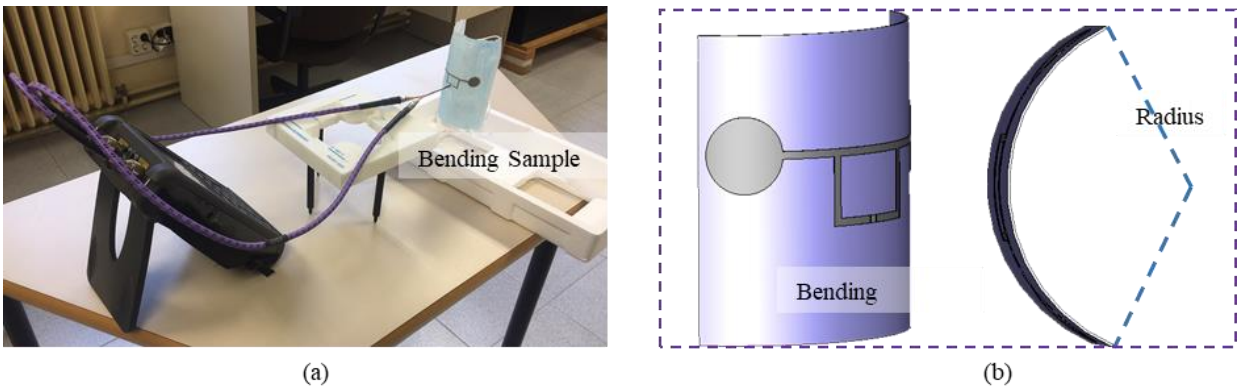

Figure 3.22. Measurement setup for the impedance and reflection coefficients of the embroidered designs. (a) Photograph of measurement setup, (b) Diagram of the bending orientation.

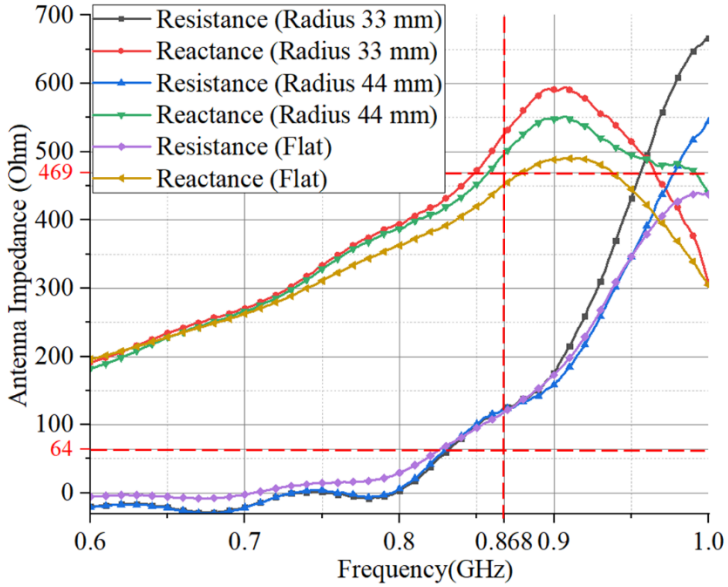

Figure 3.23. Measured impedance in different bending degrees (Dashed lines: required antenna complex impedance 64+i*469 ohm at 868 MHz).

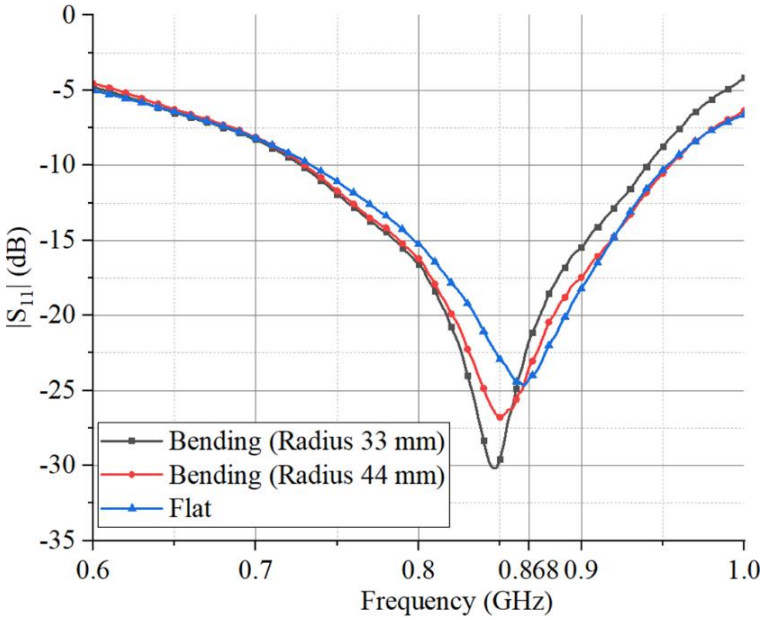

Figure 3.24. Measured reflection coefficients in different bending degrees.

Certainly, read range tests in different bending degrees are still important and the test configuration is shown in Figure 3.21. Considering the real use of the proposed design is on face, the bending radius close to face sizes (33 mm and 44 mm) are chosen. The measured maximum values of the read ranges shown in Table 3.10 are 2.5 m, 2.2 m and 1.7 m at flat, bending radius 33 mm and bending radius 44 mm, respectively. Note that the measured maximum values are obtained by the proposed design facing the reader antenna as shown in Figure 3.20. From the results, increasing bending degrees (radius: flat to 33 mm) cause a decrease in read ranges and the minimum read range in bending is at least 1.7 m.

Table 3.10 Measured maximum read range of the design 3 in bending situation (unit: m)

Type	Flat	Bending (0.044)	Bending (0.033)
Measured d_{max}	2.5	2.2	1.7

Skin Contact Tests

Skin contact test setup is shown in Figure 3.25. The reflection coefficient and read range measurements of the Design 3 are operated when the sample is touched on a hand and worn on the face as shown in Figure 3.25 (a), (b) and (c), respectively. The first application of surgical masks is to be worn on the face,

Figure 3.25. Measurement setup for the impedance, reflection coefficients and read ranges in different skin contact positions. (a) Sample touched on a hand, (b) Sample worn on face, (c) Read range measurement

so the samples tested in air or touched on hands are compared with those worn on face. In general, the skin-contact performance is limited by the resonance frequency shift and reduced radiation efficiency due to the impedance change and power loss in the human body, respectively.

As shown in Figure 3.26, compared with the impedance in air, the impedance on a hand has lower resistance part and reactance part while that on the face has higher both parts. In addition, compared with the curves of the sample in air, the reflection coefficient ($|S_{11}|$) curves as shown in Figure 3.27 on a hand and face show the resonance frequencies are shifted to 956 MHz and 813 MHz, respectively. However, when the samples are on a hand and face, the values at 868 MHz are -13 dB and -13.5 dB, respectively.

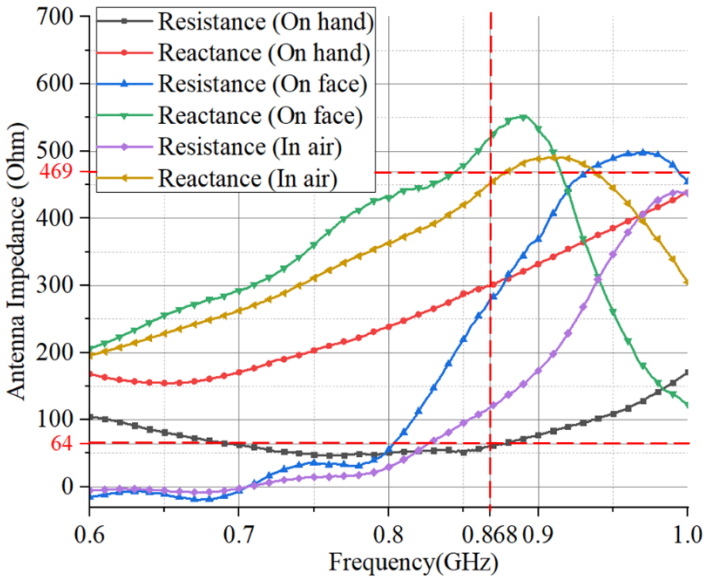

Figure 3.26. Measured impedance in different skin contact positions (Dashed lines: required antenna complex impedance 64+i*469 ohm at 868 MHz).

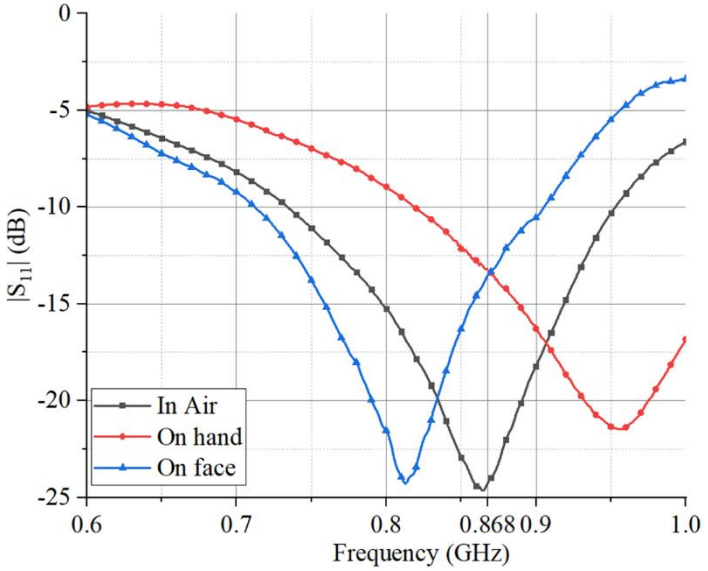

Figure 3.27. Measured reflection coefficients in different skin contact positions.

Read range tests in different situations are necessary and the results are shown in Table 3.11.The measured max values of the read ranges shown in Table 3.11 are 2.5 m, 0.8 m and 1.1 m in air, on hand and on face, respectively. From the results, skin contact causes a decrease in read ranges and the minimum read range (1.1 m) when used on the face proves that Design 3 can be effectively worn.

Table 3.11 Measured maximum read range of the design 3 in different skin contact positions (unit: m)

Type	In air	On a hand	On face
Measured d_{max}	2.5	0.8	1.1

3.2.6 Conclusion

In this section, the progressive designs of textile UHF-RFID antennas on surgical masks are developed and one of them (Design 3) is selected to be validated by reliability tests (bending and skin contact). To explore the possibility and reliability of the function-extensible IC chips for textile UHF-RFID sensors, an IC chip (Rocky 100) with lower sensitivity (-10 dBm) is used in the designs. The simulated and measured resonance curves of the designs all match well (all below -20 dB at 868 MHz) and the radiation performance (realized gain) are improved progressively (maximum values: -10.86 dBi, -7.87 dBi and 1.09 dBi). After comparing the three progressive designs, the best type (Design 3) is selected and its read ranges measured by RFID reader (M6e kit) can reach 2.5 m in air. In addition, the necessary reliability validation measurements (bending and skin contact) are performed. From the results, the resonance frequency shift degrees are slightly different (all below 20 MHz) under different bending degrees (radius: 33 mm to flat) while heavily distinguishing on a hand (88 MHz) or face (55 MHz), but the values of reflection coefficients at 868 MHz all are below -10 dB. The maximum read range can reach 1.1 m wearing the sensor on the face. As a result, the proposed Design 3 has common use as an ID tag for tracking or safe distance alert in the epidemic situation but for the used function-extensible chip, the design can extend many different types of textile sensors for various application scenarios in the future.

3.3 Experimental Comparison of Three Electro-textile Interfaces

***** Ref. D: **C. Luo,** I. Gil and R. Fernández-García, "Experimental Comparison of Three Electro-textile Interfaces for Textile UHF-RFID Tags on Clothes," *Int. J. Electron. Commun.*2022. (Published)

3.3.1 Introduction

As mentioned in the previous chapter, the electro-textile interfaces are still at the stage where no significant breakthrough has been produced. For current textile RFID researches, most of them are developed by welding integrated circuit (IC) chips on a hard or flexible Printed Circuit Board (PCB) or a chipless way. The welding technique for connecting chips to RFID antennas on PCBs is proven and reliable. However, this popular technique is not suitable for most textile RFID devices on clothes due to the high temperature intolerance (< 200°C) of the common knit yarns and fabrics. Even for some wearable polymeric materials such as Polyvinyl Chloride (PVC) fiber, alginate fiber and carbon fiber, the chips on them face the problem of unstable fixation. In a mentioned study, a passive UHF-RFID-based knitted wearable

compression sensor is proposed for monitoring a baby model breathing activity, for which a chip (Monza R6) is welded on a FR4 PCB. Then the board with the chip is inserted into a small pocket knitted in the middle region of the antenna top layer. In the last section, the textile UHF-RFID antenna solution concentration sensor is proposed and the chip is fixed by sewing and glue, which is more flexible for wearable applications. However, many similar designs are foreseen to have difficulties such as chip pads rust due to textile washing and the detachment of the chip-welded board in textile devices.

In this paper, three electro-textile interfaces integrated with the corresponding textile UHF-RFID antennas (by sewing, snap buttons and inserting) are proposed and provide chip-textile connection solutions. Related preparatory work before simulation such as the detailed embroidery method and interface impedance tests is implemented and presented. Based on the accurate impedance of three electro-textile interfaces obtained by the real tests, the simulation of the corresponding antennas is developed and the simulated results are compared with the measured results. Note that the textile UHF-RFID antennas are designed to keep the maximum realized gain values near for performance comparison. Finally, related reliability validation tests including mixed use reliability and use on the body are implemented. The proposed electro-textile interfaces have the potential to be applied into thicker clothes such as winter clothes (not too close to bodies) due to their small sizes and stable performance.

3.3.2 Designs and tests of the three electro-textile interfaces

Structure of the proposed electro-textile interfaces

The PCB boards of the three proposed electro-textile interfaces are shown in Figure 3.28. The models are designed in a PCB with an electronic design automation software and are manufactured. The boards of the three interfaces are made of FR-4 substrate and copper is used for implementing the conductive lines. The FR-4 is a common material for PCB which is based on a class of glass fibre epoxy laminate with dielectric constant (ε_r) of 4.4 and loss tangent (tanD) of 0.02. The type 1 and 2 boards are developed with two parts, the chip weld positions and the connection positions (two copper-plated vias) and the type 3 has different connection structure using copper tips. The type 1's connection method is to sew the board to a textile RFID antenna sensor, the type 2's is by steel-based snap buttons which are very common on clothes, and type 3's is based on inserting the copper tips into the yarn-made antenna sensors. All the connection methods are shown in Figure 3.29. In addition, The PCBs dimensions of the type 1, 2 and 3 are 12.7*6.22*0.8 mm, 16.38*31.12*0.8 mm and 7.76*6.10*0.8 mm, respectively. Moreover, the via radius values of the type 1 and type 2 are 1 mm (R_1) and 4.5 mm (R_2), respectively.

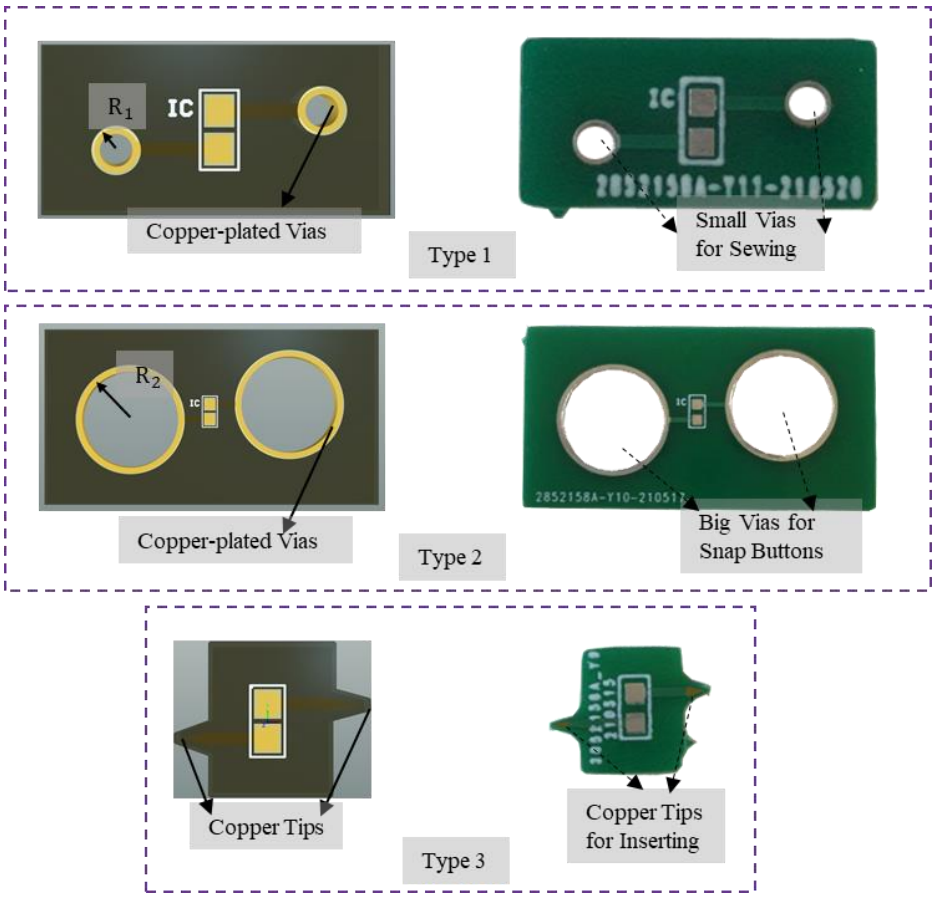

Figure 3.28. PCB boards of the three proposed electro-textile interfaces

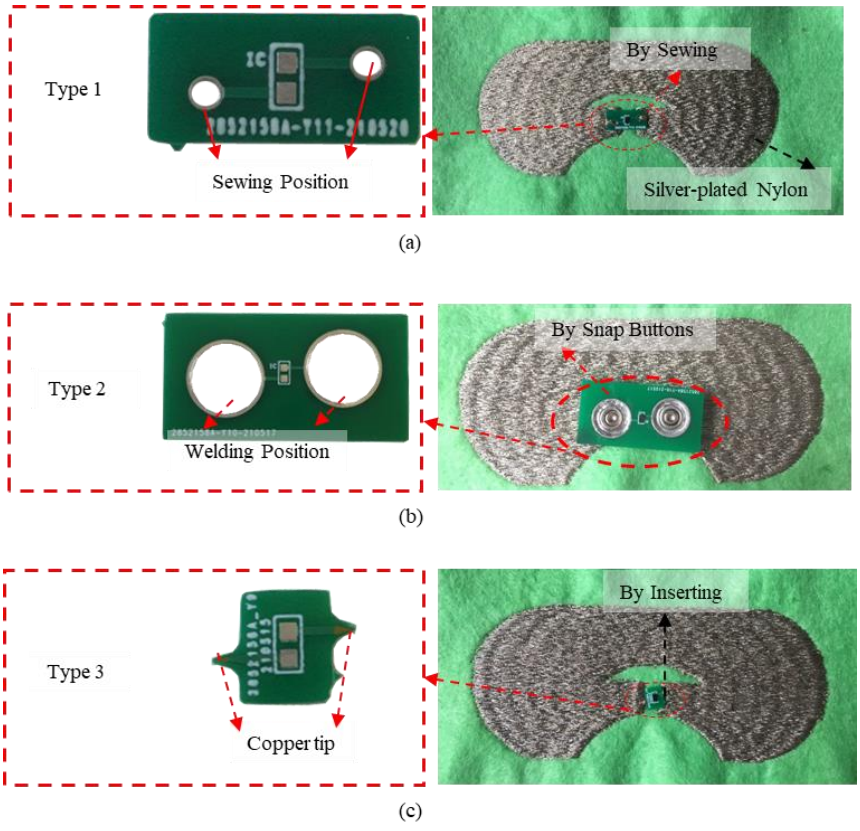

Figure 3.29. Geometry and configuration of the three proposed electro-textile interfaces with the corresponding UHF-RFID antennas. (a) Type 1, (b) Type 2, (c) Type 3.

In this section, the chip from Rock 100 used in last two sections is changed to LXMS21ACNP-184 (impedance: 19-i*284 ohm, wake-up power: -18 dBm) due to the focus on interfaces not the chip extendibility. Note that, all the interfaces have different complex impedance (not 50 ohm) from that of the chip. In addition, despite using the same chips for the three interfaces, they have different complex impedance as feed ports due to the different structures and connection methods. Therefore, the textile UHF-RFID antennas need to be designed based on the corresponding complex impedance.

The details of the textile UHF-RFID antennas are descripted in next sections and in this section, the interface's impedance tests need to be implemented and validated in different situations.

Impedance measurements of the three electro-textile interfaces

The impedance of the three interfaces is different when the chip is welded on the different PCBs and then connected to the textile materials. It is essential to obtain an accurate port impedance before designing antennas. The experimental setup for the complex impedance measurements is shown in Figure 3.30 (a) and (b). As aforementioned, the differential measurement method with the differential mode probes is used. In addition, in order to reduce the impact from the connection, the interface impedance tests are conducted in the case of the three electro-textile interfaces ('With Textile') as shown in Figure 3.30 (c).

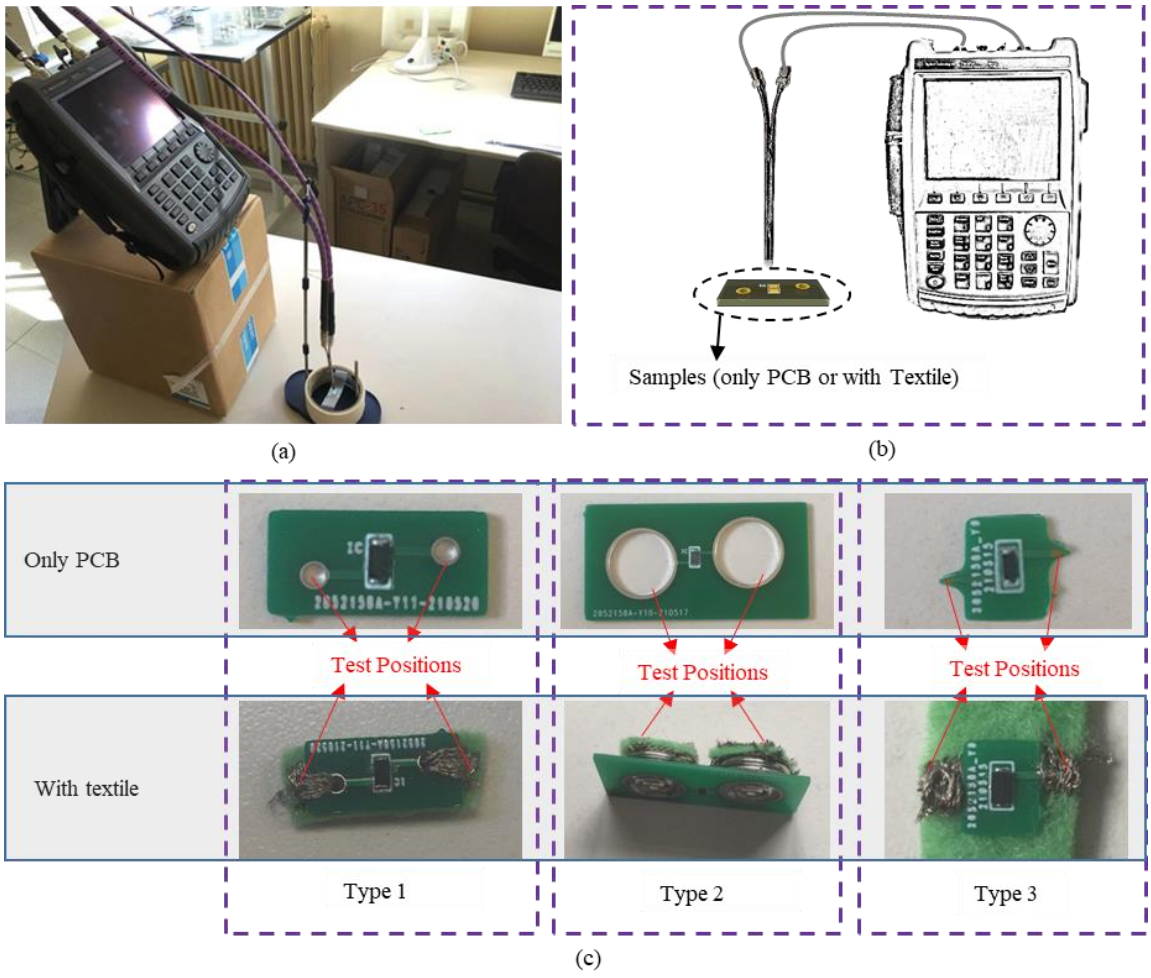

Figure 3.30. Experimental setup for the feed ports impedance. (a) Photograph of the setup, (b) Experimental setup configuration. (c) Tested cases ('Only PCB' and 'With Textile').

After being calculated by Equation 2.1, the measured impedance results of the three feed port types are shown in Figure 3.31, including the resistance part and the reactance part. It is found that for each type, the resistance curves of the 'Only PCB' and 'With textile' are close while the reactance curves of the 'Only PCB' are 20 to 40 bigger than that of the 'With Textile' in the absolute value case. In addition, at 868 MHz, the complex impedance of the feed port types are listed in Table 3.12.

Table 3.12 Complex Impedance of the Types at 868 MHz (Unit: Ohm)

Case	Type 1	Type 2	Type 3
Only PCB	4.34-i*127.43	3.68-i*88.51	3.6-i*148.86
With Textile	5.09-i*107.7	5.06-i*60.27	9.29-i*123.27

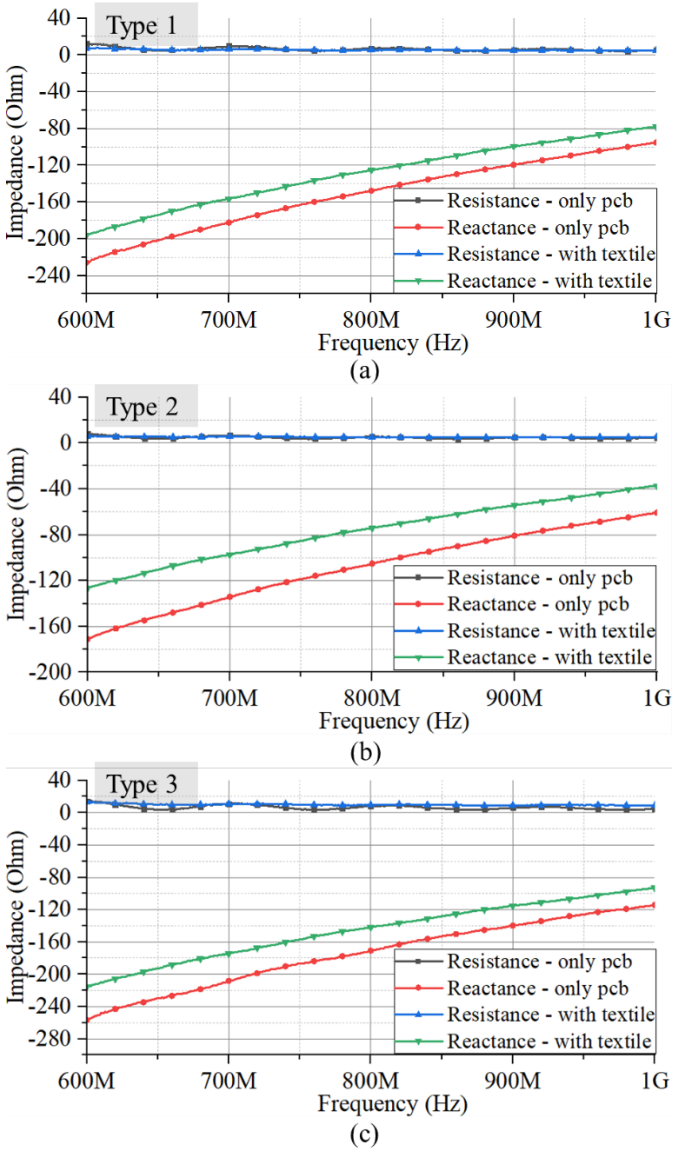

Figure 3.31. Measured impedance for the three feed port types under the two cases ('Only PCB' and 'With Textile'). (a) Type 1, (b) Type 2, (c) Type 3.

3.3.3 Designs and tests of the corresponding textile UHF-RFID antennas

Simulation models of the corresponding textile antennas

After obtaining the measured complex impedance of the three electro-textile interfaces ('with textile'), the corresponding UHF-RFID antennas can be designed based on the measured impedance as feed port impedance. The fundamental model simulated in high-performance 3D EM analysis software is shown in Figure 3.32. Geometry of the fundamental simulated model for the three corresponding UHF-RFID antennas. and the three corresponding textile antennas are developed by adjusting related dimension parameters based on the shown model. The dimension parameters of the three designed antennas are listed in Table 3.13.

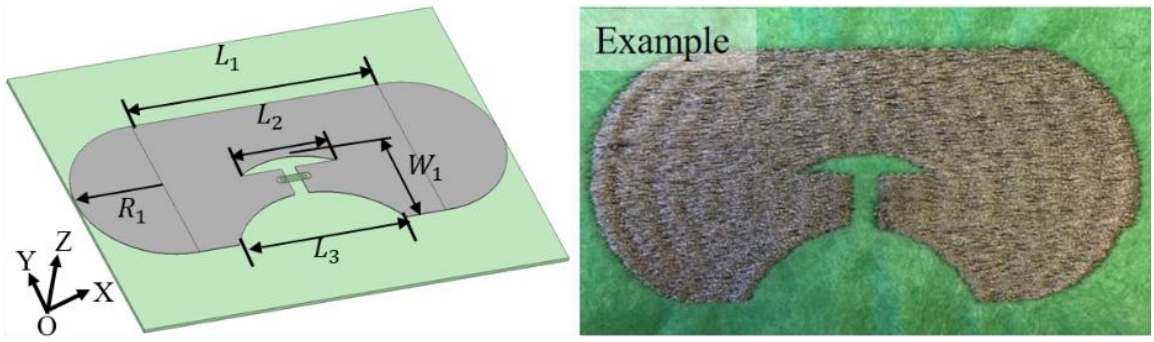

Figure 3.32. Geometry of the fundamental simulated model for the three corresponding UHF-RFID antennas.

Table 3.13 Antenna Dimension Parameters (Unit: mm)

Antenna Designs	L1	L2	L3	W1	R1
Design 1	58	22.6	40	23.4	20
Design 2	74	15	40	22	20
Design 3	58	24.8	40	24	20

The antenna patterns are embroidered by silver-plated Nylon whereas the conductive yarns have 0.2 mm thickness with corresponding bulk conductivity of 11500 siemens/m. The polyester as the substrate has relative dielectric constant, loss tangent and thickness of 1.29 (εr), 0.00188 (tanD) and 0.88 mm, respectively. The ε_r and tanD are a little bit different from the polyester used in previous work because the polyester is remeasured, thus causing difference under different environments. The simulated resistance and reactance of the three corresponding textile antennas are shown Figure 3.33.

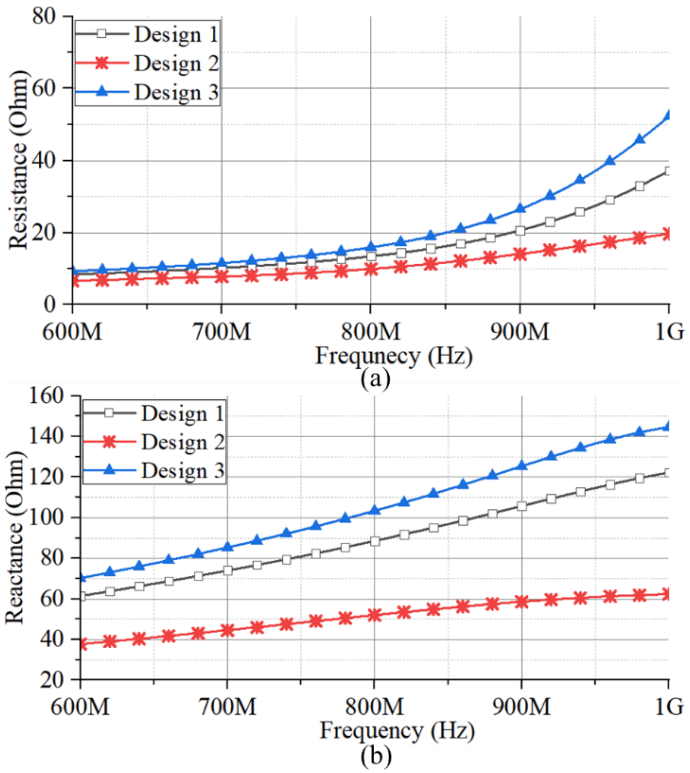

Figure 3.33. Simulated resistance and reactance of the three corresponding textile antennas.

Impedance simulation and measurements of the three textile antennas

As aforementioned, in order to reduce the impact from the connection, the measured complex impedance results of the case 'With Textile' are adopted as conjugate impedance of the antennas for simulation and the simulated designs are described and shown in Figure 3.32. The experimental setup is shown in Figure 3.34 and the antenna impedance results are shown in Figure 3.35, including the simulated and measured curves.

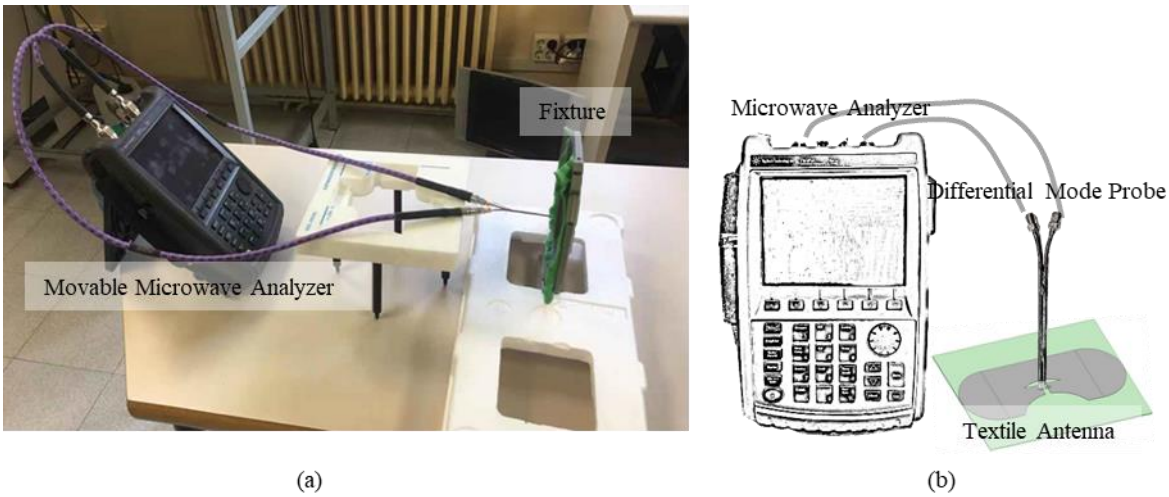

Figure 3.34. Experimental setup for the impedance of the embroidered designs. (a) Photograph of experimental setup, (b) Experimental setup configuration.

By analyzing the three cases, the measured impedance curves are close to the simulated curves. In addition, the simulated and measured results at 868 MHz for each case are listed in Table 3.14. It is found

that the measured antenna impedance values are close to the conjugate impedance values of the corresponding interfaces.

Table 3.14 Complex Impedance of the Antenna Designs at 868 MHz (Unit: Ohm)

Case	Design 1	Design 2	Design 3
Simulated	17.59+i*100	12.52+i*56.77	21.93+i*117.98
Measured	28.86+i*117.8	9.24+i*60.51	23+i*115.42

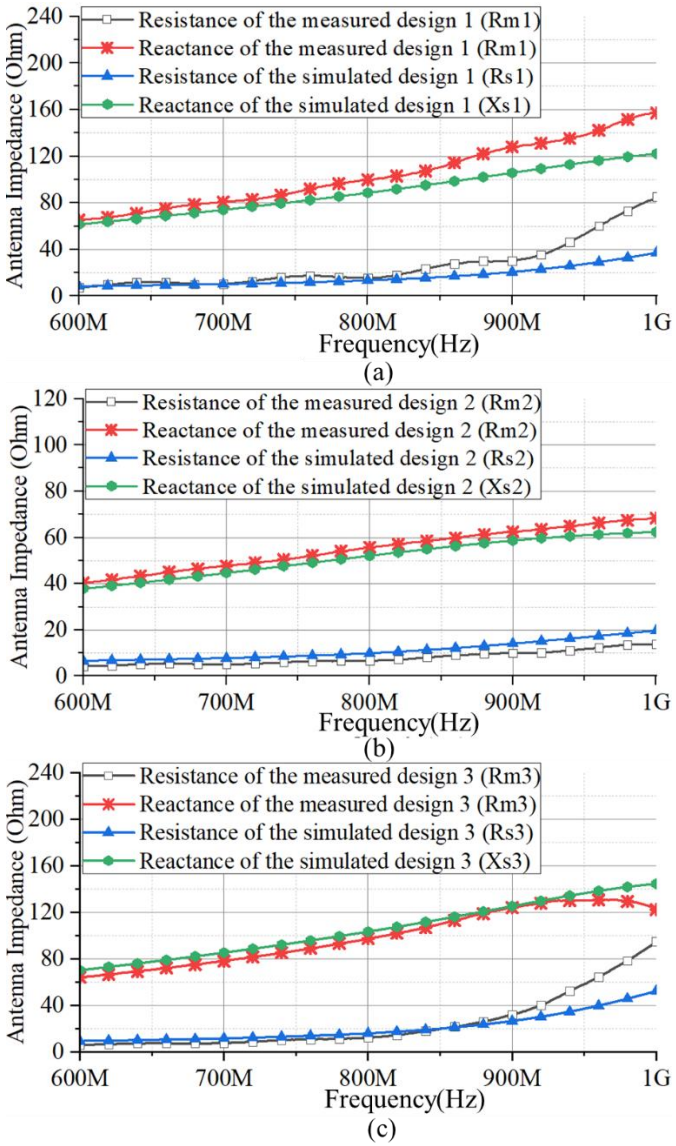

Figure 3.35. Simulated and measured impedance for the three corresponding textile antennas. (a) Design 1, (b) Design 2, (c) Design 3.

Radiation performance comparison

Radiation performance is another important factor affecting the final target of UHF-RFID tags read range. The radiation patterns in the XY, XZ and YZ plane of the three designs are shown in Figure 3.36. The maximum realized gain values of the three designs are close, 1.46 dBi, 1.38 dBi and 1.31 dBi for the

design 1, design 2 and design 3, respectively. In addition, the fundamental structures of the three designs are similar, therefore the radiation patterns are expected to be close as shown in Figure 3.36.

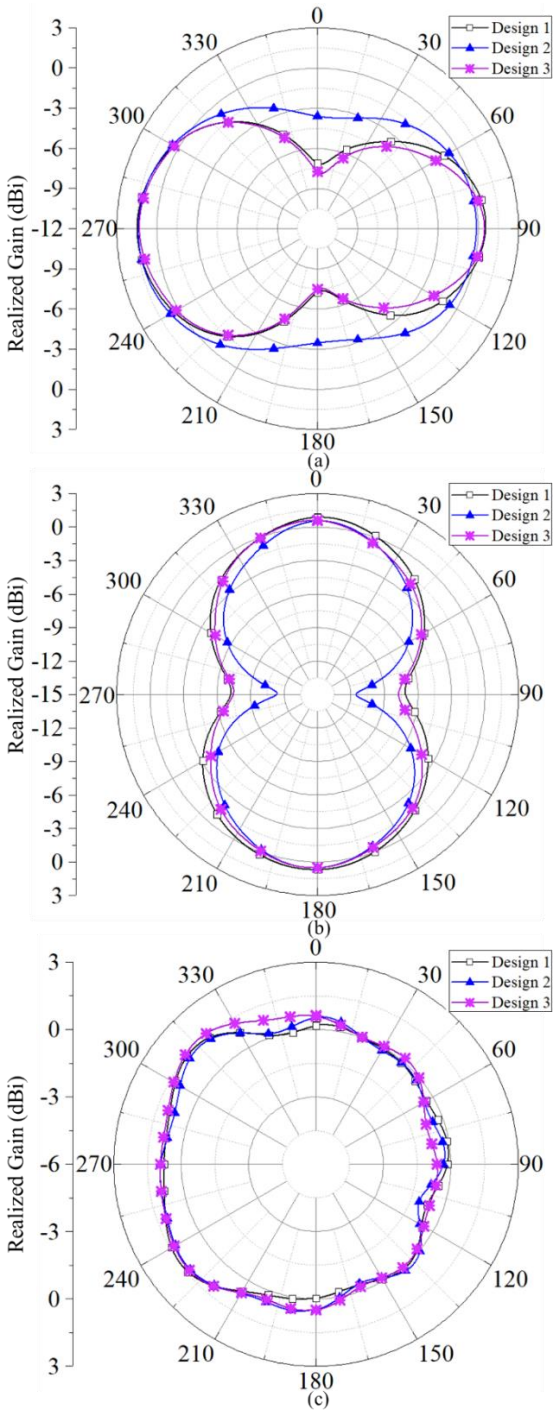

Figure 3.36. Simulated radiation patterns (realized gain) for the three designs. (a)XY plane, (b)XZ plane, (c)YZ plane

Read range tests

For read range tests, the experimental setup is shown in Figure 3.37. In order to avoid moving the design holders frequently, a certain distance between the read antenna and UHF-RFID tags is fixed (0.7 m) and the reader output power is adjusted. The reader antenna (MT-242025/TRH/A/A) can be controlled by the M6E Kit which is connected to a laptop with specified control software. An inquiry signal with data

and clock can be adjusted by the software and sent by the reader antenna. The proposed textile UHF-RFID antennas can send a backscattered signal with data and clock after receiving the inquiry signal. The output power is adjusted until the signal transmission between the read antenna and the tags is disrupted. The maximum value of the read range can be calculated by the threshold power. In addition, the simulated read range can be calculated by the Friis Transmission Formula as follows,

$$d_{max} = \frac{\lambda}{4\pi}\sqrt{\frac{P_t G_t G_{r5} \cdot \tau_5}{P_{thL}}} \qquad 3.6$$

where dmax is the maximum value of the read range, λ is the wavelength at 868 MHz, P_t is the power fed into the reader antenna, G_t is the gain of the reader antenna (7 dBi), G_{r5} is the gain of the proposed antennas, τ_5 is the largest power transmission coefficient (Design 1, 2 and 3: 0.6242, 0.7888 and 0.8149 at 868 MHz, respectively) and P_{thR} is the minimum wake-up power of the chip(-18 dBm). In addition, the cable loss between the reader antenna and the reader is taken into account (0.8 dB).

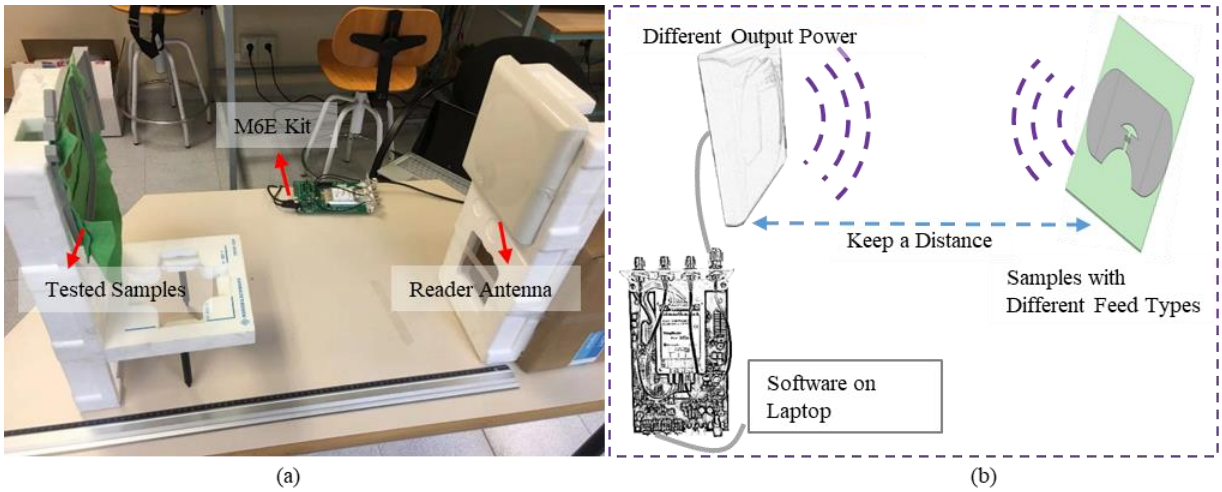

Figure 3.37. Experimental setup for the read ranges of the textile UHF-RFID tags. (a) Photograph of experimental setup, (b) Experimental setup configuration.

Table 3.15 Simulated and Measured Maximum Read Ranges at 868 MHz in Air (Unit: m)

Case	Type 1/Design 1	Type 2/Design 2	Type 3/Design 3
Simulated	5.58	6.74	6.8
Measured 1st	4.52	5.19	5.82
Measured 2nd	4.57	5.25	5.69
Measured 3rd	4.47	5.25	5.76
Average Measured	4.52±0.05	5.22±0.03	5.75±0.07

For the three electro-textile interfaces with the corresponding textile antennas, the simulated and measured maximum read ranges of the type 1, 2 and 3 have been tested several times and the results are listed in Table 3.15. Note that the read range values are recorded when the tags can be read continuously and stably, which is not just an on-off procedure. It is found that when the realized gain and the matching situations of the three types are close, the type 3 presents better performance than the other two in simulation and measurement, respectively. The main reason for the difference between the simulated and measured results is that the real radiation and impedance cannot totally match with the simulated results due to the environmental factors, embroidery error and measuring error.

3.3.4 Reliability validation

Mixed-use feasibility

In the work, 'mixed-use' refers to the interfaces used for other noncorresponding antennas. Generally, for each electro-textile interface, the corresponding UHF-RFID antenna is expected to be redesigned. Considering this case increases costs and design periods, the mixed use feasibility of the different electro-textile interfaces is worth exploring. Therefore, in this section the three electro-textile interfaces are applied to the three different antennas, respectively. There are nine cases, in which the test setup and related measurement method are the same.

Table 3.16 Measured Read Ranges of the Nine Cases in Air (Unit: m)

Case	Design 1	Design 2	Design 3
Type 1	4.5	4.05	3.57
Type 2	3.74	5.22	4.29
Type 3	3.41	4	5.75

As listed in Table 3.16, the matched pairs have the best performance as expected. In addition, it is found that for each interface, the read ranges of the interfaces used on other two designs have tolerable decrease (< 2 m) but are all above 3.41 m. It means the unpaired combination can work normally under specific requirements. Therefore, the mixed use feasibility of the proposed electro-textile interfaces and textile UHF-RFID antennas is validated.

Tests on the body

In this section, the related tests on the body are developed by the three connection methods (sewing by yarns, snap buttons and inserting) and the experimental setup is shown in Figure 3.38. Note that the researcher in the figure wears the winter clothes, which are thicker than normal ones and the tags can be 3 cm to 4 cm from the clothes to the body with air interlayer. In the tests, all the interfaces connect to the three antenna designs, respectively, to explore the performance in the nine cases as aforementioned in the last section.

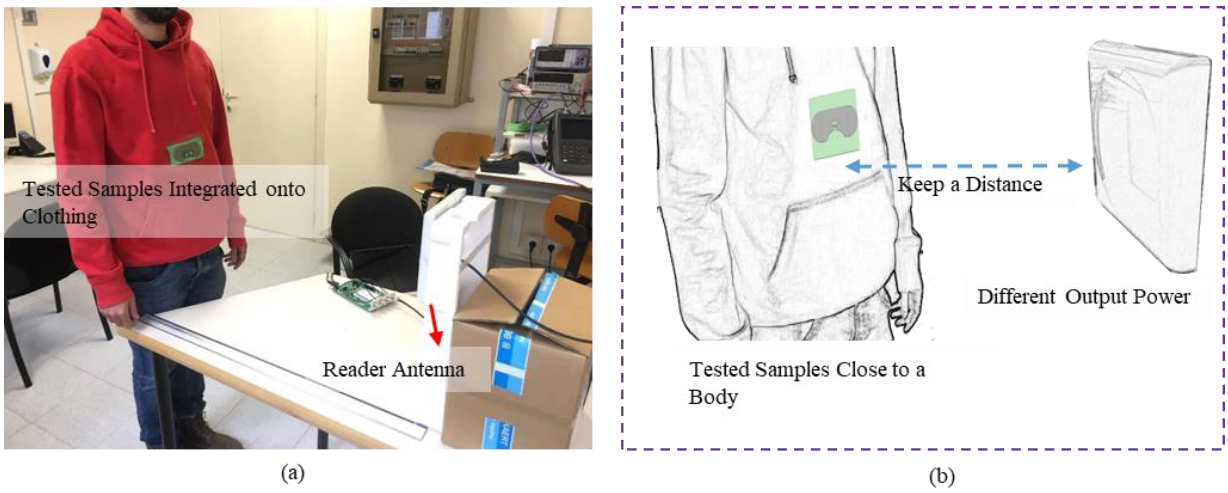

Figure 3.38. Experimental setup for the read ranges of the tags on the body. (a) Photograph of experimental setup, (b) Experimental setup configuration.

The read range results are listed in Table 3.17. As expected, the read ranges for the nine cases on the body are lower than that in air, respectively, due to power loss on the body. However, the worst performance shows a read range of 2.05 m (the type 3 by inserting into the design 1). And all the results prove the on-body use feasibility of the interfaces with the antennas. Certainly, for attractive fashion, the electro-textile interfaces can also be hidden in thinker clothes and the textile antennas can be embroidered with other nonconductive floral patterns. When they are used on clothing, the potential as a RFID sensor such as temperature and humidity sensor can be explored.

Table 3.17 Measured Read Ranges of the Nine Cases on the body (Unit: m)

Case	Design 1	Design 2	Design 3
Type 1	3.68	3.24	2.05
Type 2	3.43	4.57	3.17
Type 3	2.19	3.13	3.35

3.3.5 Conclusion

In this section, three electro-textile interfaces integrated with the corresponding textile UHF-RFID antennas are proposed and evaluated. The simulated and measured impedance curves of the corresponding antennas are all close and the radiation performance (realized gain) are designed to be near (about 1.4 dBi). According to the Friis formula, the simulated and measured read ranges of the interfaces with the corresponding antennas in air are obtained (all above 4.5 m). For reliability validation, the tests for mixed use feasibility and the tests on the body are implemented. The results of mixed use feasibility tests show that the read ranges of each interface used on other two UHF-RFID antennas have tolerable decrease (< 2 m) but are all above 3.41 m. It means the mixed-use feasibility of the proposed electro-textile interfaces and textile UHF-RFID antennas can be proved. In addition, the read ranges of the designs on the body are

all above 2.05 m. Therefore, due to the small sizes of the electro-textile interfaces, stable performance on the body and good reliability, the proposed electro-textile interfaces with the corresponding textile UHF-RFID antennas has potential application in the future medical and daily clothes fields for human presence detection.

3.4 Electro-textile UHF-RFID Compression Sensor

***** Ref. E: **C. Luo,** I. Gil and R. Fernández-García, "Electro-textile UHF-RFID Compression Sensor for Healthcare Applications," *IEEE Sens. J.* 2022 (Under Review)

3.4.1 Introduction

As mentioned in the previous chapter, there are two ways to achieve sensing functions for wireless UHF-RFID devices. One way is that tags can be designed to connect sensors with different functions. For these types of UHF-RFID sensors, chips need to have extendable ports for sensor connection and optional power interface such as ROCKY100 with functional ductility. Another popular way is that tags can be developed to have certain sensing functions as a type of antenna sensor depending on some factors such as different materials of tags and application scenarios. Especially in the textile area, textile materials have different features from common PCBs such as flexibility and hydrophilicity. Some textile UHF-RFID tags are designed as a concentration solution sensor due to good hydrophilicity of the textile substrate as mentioned in the s 1 and a respiration sensor due to certain extensibility of the designs.

Textile UHF-RFID antenna sensors have special feedback modes for obtaining sensing data due to the wireless ability. The typical feedback modes include RSSI (Received Signal Strength Indicator) feedback mode and read range feedback mode. When a UHF-RFID antenna is affected by other factors such as permittivity changing, bending or temperature changing, the RSSI and read range tested by RFID readers for the UHF-RFID antenna are expected to vary in some ways with the related sensing factors.

Moreover, as mentioned in the last section, since standard welding techniques for connecting chips to textile materials are not suitable, the textile designs are foreseen to have difficulties such as chip pads rust due to textile washing and the detachment of the chip-welded board in textile devices. In the last section, three electro-textile interfaces are proposed and the feasibility and reliability on textile UHF-RFID antennas as the important research orientation have been tested. In this section, the UHF-RFID antennas with the novel interfaces are applied for some typical scenarios.

Based on the above discussion, in this section, the mentioned electro-textile UHF-RFID antenna with the corresponding electro-textile interface as a compression sensor is proposed and evaluated for two application scenarios. Typical metallic snap buttons for modern clothes are applied into the interface as shown in the last section. To obtain accurate textile UHF-RFID antenna simulation, the impedance of the interface is obtained by the measurement and compared with the equivalent circuit simulation results. Based on the measured interface impedance, a textile UHF-RFID antenna is designed and its simulated impedance and read ranges are compared with measured results in air. For exploring the electro-textile UHF-RFID tag

as a compression sensor, two application scenarios, bending on a knee and respiration, are tested. The Received Signal Strength Indicator (RSSI) changing ranges are tested for monitoring bending angles on a knee and respiration on a chest. By analysis, the feasibility of the electro-textile UHF-RFID tag as a compression antenna sensor is proved and the proposed electro-textile UHF-RFID antenna sensor has the potential to be applied for future healthcare areas.

3.4.2 Details of the proposed interface and the textile UHF-RFID antenna sensor

In this section, the interface 'type 2' with the snap buttons proposed in the last section is selected for the tests. In order to give more electronic details of the interface, the equivalent circuit for this interface with the snap buttons on textile is modelled, and the simulated and the measured results are compared.

Equivalent circuit simulation and impedance measurement of the interface

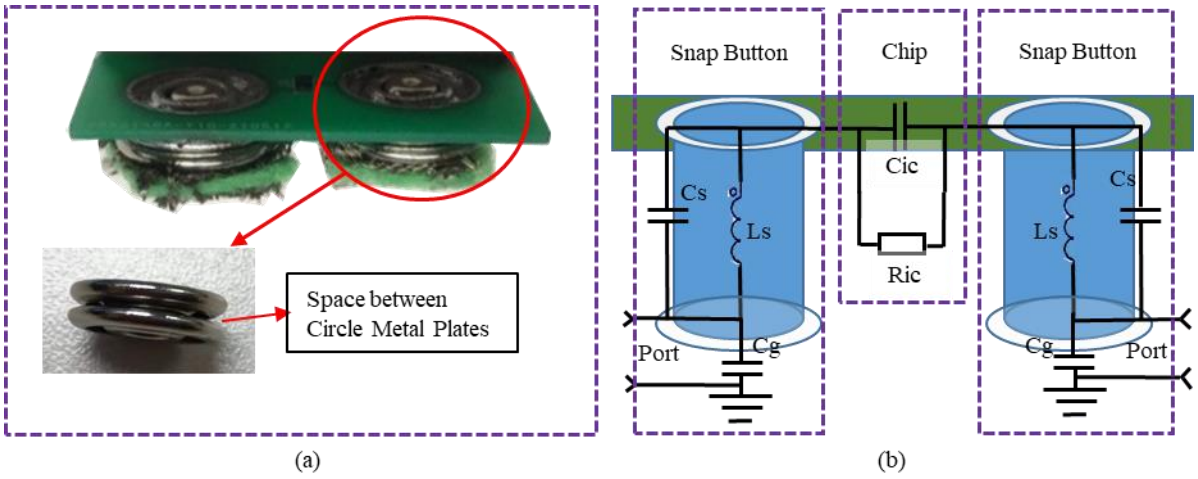

Figure 3.39. Geometry and equivalent circuit of the interface with the chip and the snap buttons. (a) Geometry, (b) equivalent circuit

When the chip is welded on the board, the impedance of the interface is expected to change (different from initial impedance 19-i*284 ohm). Therefore, the accurate impedance of the interface with the chip and snap buttons need to be measured and analyzed for the corresponding textile UHF-RFID antenna sensor simulation as a feed port. The geometry and equivalent circuit of the interface with the chip and the snap buttons are shown in Figure 3.39. Considering that a conventional via can be equivalent to an inductor with a resistor in parallel and a grounded capacitor in cascade, the interface with a similar structure of a via as shown in Figure 3.39 (a) can be simply equivalent to an inductor (L_s) with a grounded capacitor (C_g) in cascade, but due to the circle metal plate of the snap buttons, an additional capacitor (C_s) should be added in parallel with the inductor. In addition, the commercial chip has the same equivalent circuit structure with most capacitive RFID chips, which is a resistor (R_{ic}) and a capacitor (C_{ic}) in parallel. The equivalent circuit is shown in Figure 3.39 (b). Where Ls and Cs represent the inductance and capacitance of the snap button, respectively. Cg models the capaciance between snap button and ground, and Cic and Ric model the IC input impedance.

Therefore, from one port, the equivalent input impedance (Z_e) can be given by,

$$Z_e = (L_s//C_s + R_{ic}//C_{ic} + L_s//C_s + C_g)//C_g \quad 3.7$$

In detail,

$$Z_e(\omega) = \frac{1}{\left(\frac{1}{\frac{2}{\frac{1}{i\omega L_s} + i\omega C_s} + \frac{1}{\frac{1}{R_{ic}} + i\omega C_{ic}} + \frac{1}{i\omega C_g}}\right) + i\omega C_g} \quad 3.8$$

Where ω is the angular frequency. R_{ic} (4.264 kOhm)and C_{ic}(0.64 pF) can be calculated by the complex impedance of the used chip. L_s, C_s and C_g from the snap buttons need to be calculated by the real measured results and the Equation 3.8.

The measurement setup for the interface impedance is shown in Figure 3.40. After obtaining the measured impedance curves of the interface, L_s, C_s and C_g can be calculated by the Equation 3.8 and the results are listed in Table 3.18.

Table 3.18 Values of the equivalent circuit components

Components	L_s	C_s	C_g
Values	12.65 nH	0.43 pF	2.68 pF

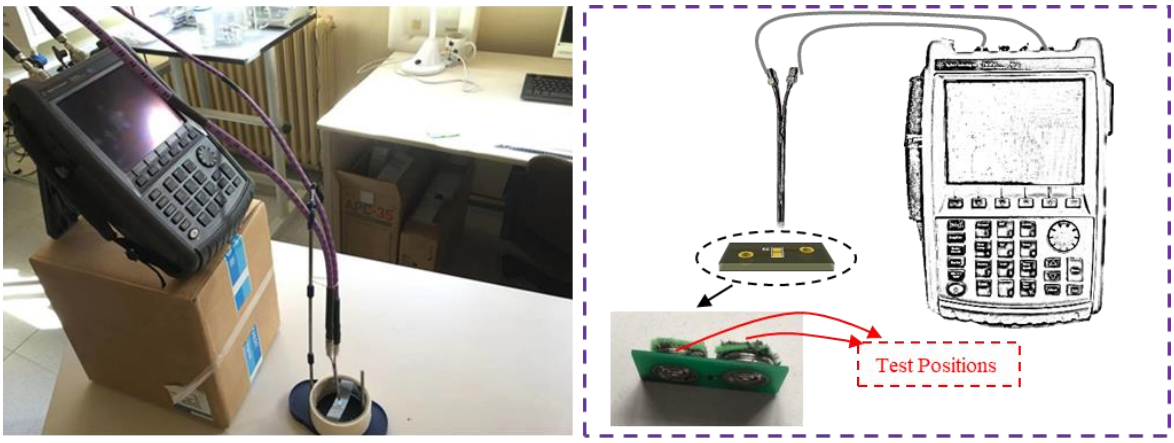

Figure 3.40. Experimental setup for the interface impedance. (a) Photograph of the setup and (b) experimental setup configuration.

The modelled impedance and measured impedance results are shown in Figure 3.41. It is found that the modelled resistance and reactance curves of the interface are close to the measured curves. Therefore, the measured impedance of the interface for the textile UHF-RFID antenna sensor at 868 MHz is 5.06-i*60.27 ohm.

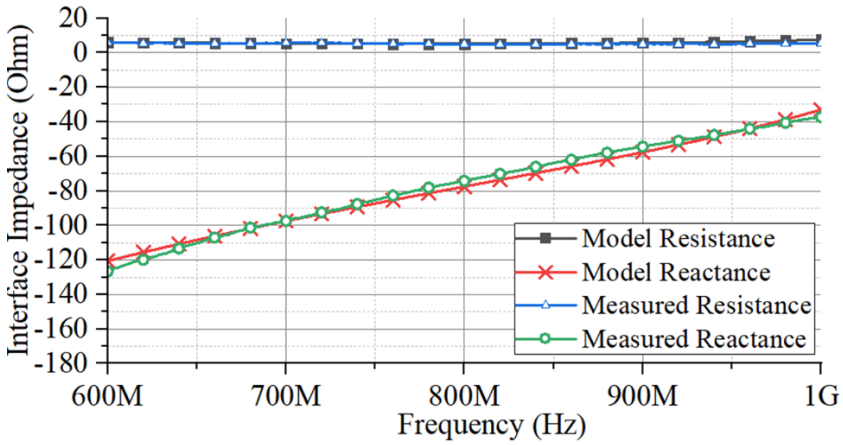

Figure 3.41. Model impedance and measured impedance curves of the interface

3.4.3 Structure of the proposed electro-textile UHF-RFID antenna

Although this proposed electro-textile UHF-RFID antenna is described in the last section, in order to make this section content coherent and easily readable. The 'Design 2' proposed in the last section is selected out and described in detail.

The geometry and configuration of the proposed electro-textile UHF-RFID antenna sensor with the corresponding interface are shown in Figure 3.42. Different from common textile RFID tags with fixed interfaces such as glue-based interfaces, knit-based interfaces and copper-based inserting interfaces, the proposed design adopts typical metallic snap buttons of clothes with a small and detachable PCB as the interface. The proposed design dimension parameters are listed in Table 3.19 and the PCB interface size is 16.38*31.12*0.8 mm. In addition, the type of the UHF-RFID chip is LXMS21ACNP-184, the impedance and the wake-up power of which are 19-i*284 ohm and -18 dBm, respectively. However, note that when the chip is welded on the board, the impedance of the interface is expected to change and the detailed analysis has been carried out in last section

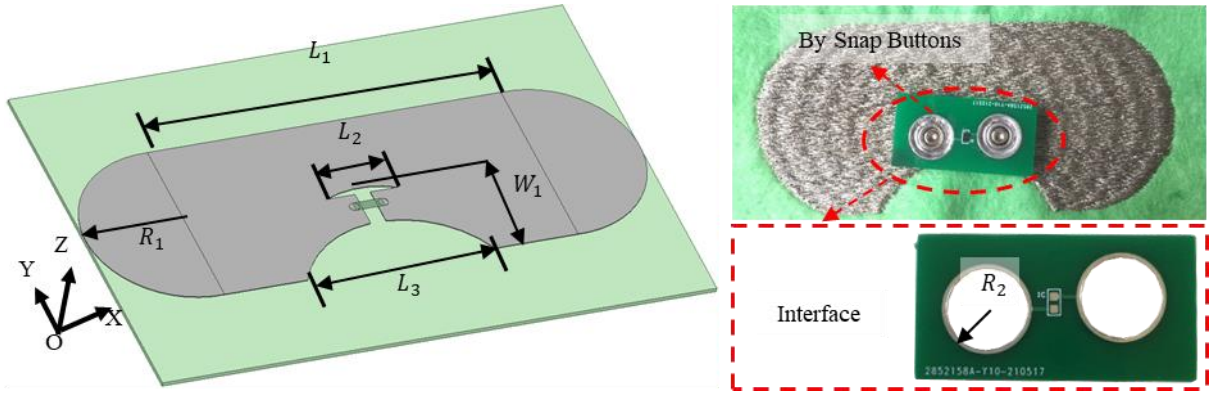

Figure 3.42. Geometry and configuration of the proposed electro-textile UHF-RFID antenna sensor with the corresponding interface

Table 3.19 UHF-RFID sensor dimension parameters (unit: mm)

Design	L1	L2	L3	W1	R1	R2
Values	74	15	40	22	20	4.5

Regarding the used materials, the proposed textile antenna sensor is based on conductive yarns on a polyester substrate. The commercial conductive twisted yarns are made of 99% pure silver-plated Nylon, the conductivity of which is 11500 siemens/m. The relative dielectric constant, loss tangent and thickness of the substrate are 1.29 (εr), 0.00188 (tanD) and 0.88 mm, respectively, measured by a Microwave Frequency Q-Meter. On the other hand, its thickness is 0.88 mm measured by an Electronics Outside Micrometer (132-01-040A) as shown in Figure 2 (b). Moreover, the snap buttons for the interfaces are made of steel.

Impedance simulation and measurement of the textile UHF-RFID design

After obtaining the real impedance of the interfaces at 868 MHz (5.06-i*60.27 ohm), the textile UHF-RFID antenna sensor simulation for the model shown in Figure 3.42 can be carried out by using a full wave 3D electromagnetic (EM) simulation software. Note that the antenna is expected to be designed for a conjugate matching with the interface. The experimental setup for the impedance test of the embroidered designs is shown in Figure 3.34 in the last section and the simulated and measured results are shown in Figure 3.43. It is found that the measured resistance and reactance curves are close to the simulated curves. In detail, the difference between the measured and simulated resistance parts at 868 MHz is 3 ohm and the corresponding to the reactance parts is 4 ohm in absolute value (simulated: 12.52+i*56.77 ohm, measured: 9.24+i*60.51 ohm). Moreover, the interface impedance at 868 MHz (5.06-i*60.27 ohm) is almost conjugate matching with the antenna (9.24+i*60.51 ohm).

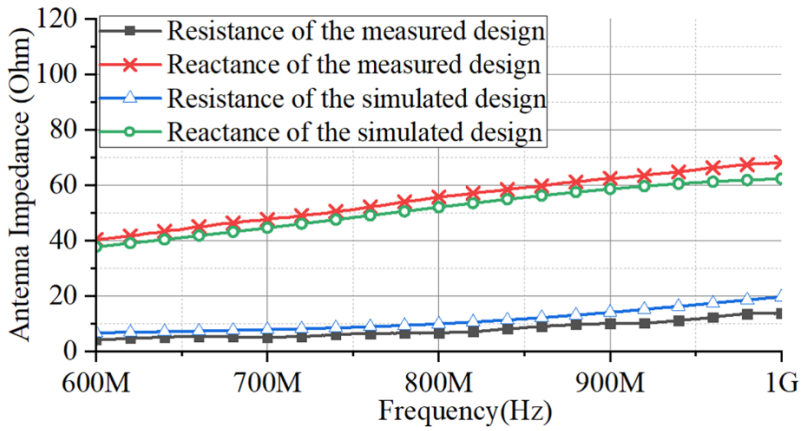

Figure 3.43. Simulated and measured impedance curves of the textile UHF-RFID antenna sensor

Read range tests in air

The experimental read range measurements have been performed in an ordinary room laboratory to reproduce a real environment where some effects such as electromagnetic interference (EMI) or reflective effects can be produced.

The read range test in air for the textile UHF-RFID antenna sensor with the corresponding interface has been done in the last section and the experimental setup is shown in Figure 3.37. The read range evaluation has been done by fixing a constant distance between reader and tag of 0.7m whereas the reader output power is swept down until the tag is not detected.

The reader antenna (MT-242025/TRH/A/A) can be controlled by the M6E Kit which is connected to a laptop with specific control software. An inquiry signal with data and clock can be adjusted by the software and sent by the reader antenna. The proposed textile UHF-RFID antenna sensor can send a backscattered signal with data and clock after receiving the inquiry signal. The output power is adjusted until the signal transmission between the read antenna and the tags is disrupted. The maximum value of the read range can be calculated by the threshold power. In addition, the simulated read range can be calculated by the Equation 3.6 as mentioned in the last section.

In this section, the proposed antenna has a maximum realized gain of 1.38 dBi. The simulated and measured read ranges are listed in Table 3.20. It is found that simulated and measured read ranges are close and the measured read range is up to 5.22 m in air.

Table 3.20 Simulated and measured read ranges at 868 MHz in air (unit: m)

Case	Simulated	Measured
Value	6.74	5.22

3.4.4 Application and discussion

In order to explore the compression ability of the electro-textile UHF-RFID antenna sensor for human beings, two application scenarios; bending on a knee and respiration frequency, are tested. The bending on a knee measurement can be useful when people exercise or have a postoperative recovery process. In this scenario, the electro-textile UHF-RFID antenna sensor on knees can record the knee flexion angles with the corresponding RSSI values. The respiration frequency rate can be applied when breathing of patients or common babies need to be monitored. Moreover, the data can be recorded by portable electronic equipment.

The sensing capability is only due to e-textile antenna; the rigid interface does not have sensing behaviour. However, the rigid PCB is necessary to attach the snap button which guarantees the interconnection under stretching stress and it allows the detachable interface of the IC when washing is required

Bending angles monitor on a knee

For exploring the feasibility in the first application scenario, the experimental setup for a bending angles monitoring on a knee is shown in Figure 3.44. In this test, when the knee is bent, the RFID reader and related software can record the values of the current RSSI as shown in Figure 3.44 (a) and (b). To validate the sensor functionality, a photograph of each measured point has been taken and the knee flexion

angle has been processed through image processing and compared with the proposed sensor as shown in Figure 3.44 (c). Note that the angle of 180º refers to the sensor sample fixed flat on the pants while the angle of 168º refers to the sensor sample fixed on the knee due to the initial shape of the knee. In this case, a distance of 1m between the RFID reader and the RFID tag has been fixed.

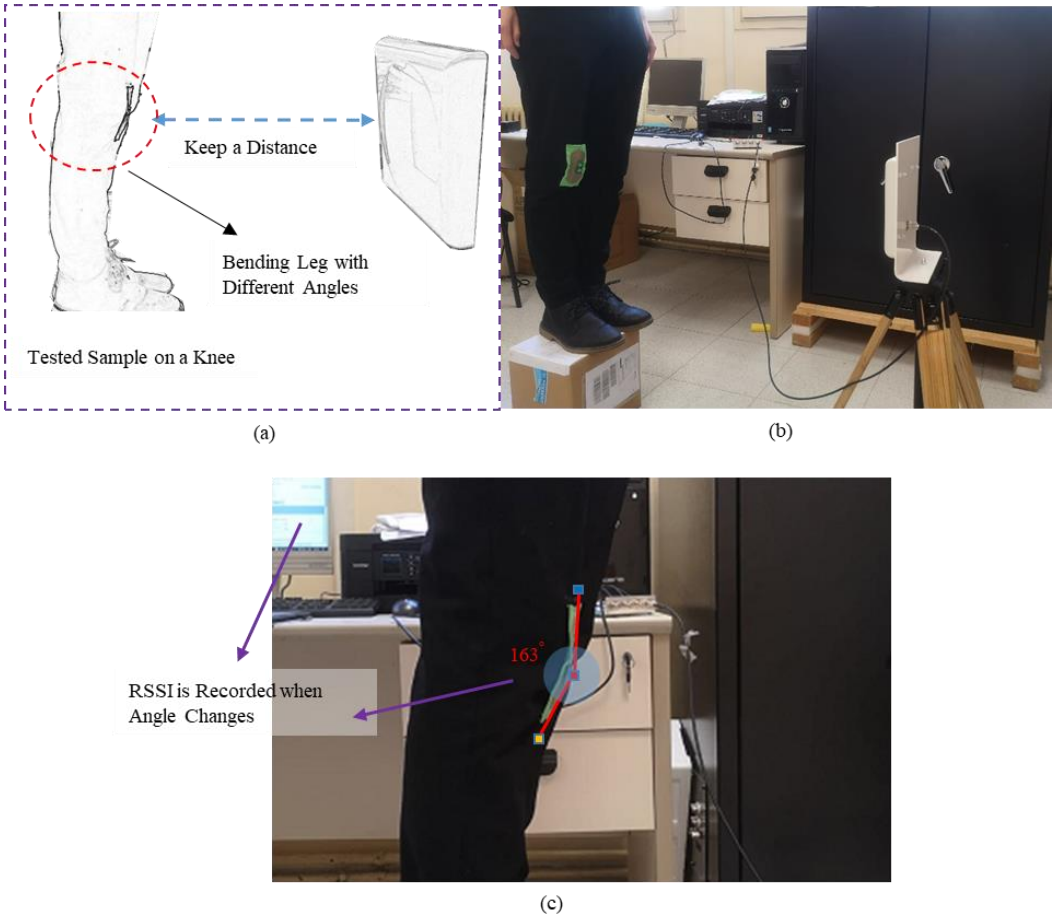

Figure 3.44. Experimental setup for a bending angles monitor on a knee. (a) Experimental setup configuration, (b) photograph of experimental setup, (c) case diagram of angle tests.

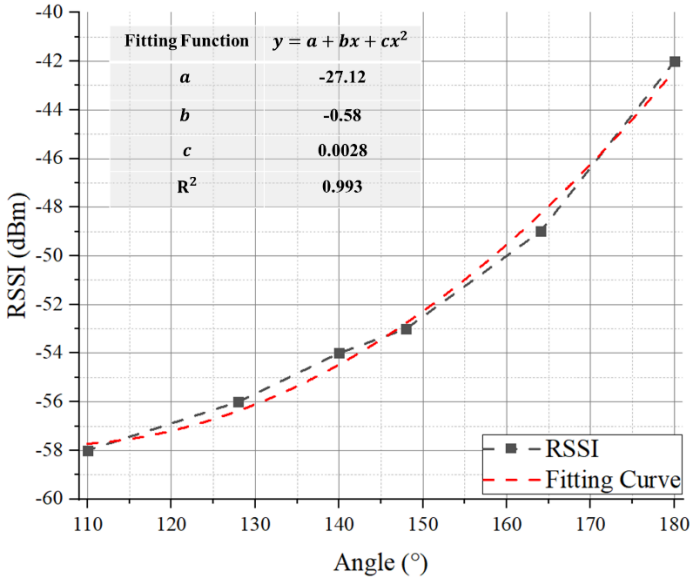

Figure 3.45. Bending angles monitor RSSI values and a fitting curve varying with angles.

The RSSI values and a related fitting curve varying with angles are shown in Figure 3.45. The RSSI-angle fitting curve conforms to a quadratic function model whose coefficients are listed in the Figure 3.45. The RSSI range varies from -42 to -58 dBm when bending angle varies from 180º to 110º, respectively. Moreover, the coefficient of determination (R^2) is 0.993, which means the curve has a good fit to the measured values. From this analysis, the feasibility of the electro-textile UHF-RFID compression sensor as a bending angle monitor on a knee is proved.

Respiration monitor

For exploring the feasibility of the proposed sensor to monitorize the respiration rate, the experimental setup is shown in Figure 3.46. The electro-textile UHF-RFID compression sensor is fixed on a person breathing at a respiration rate of 3 Hz (about 1 breath every 3 seconds). While breathing continues, the RSSI is measured and processed by the RFID reader at a fix distance of 1 m.

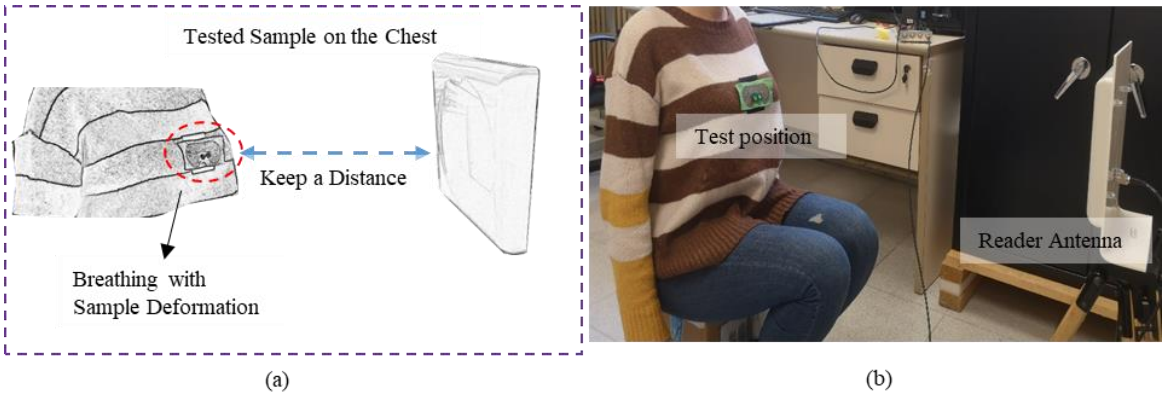

Figure 3.46. Experimental setup for a respiration monitor on a chest (about 1 breath/3 seconds). (a) Experimental setup configuration, (b) photograph of experimental setup.

The measured raw RSSI data and related smoothed RSSI curves are shown in Figure 3.47. The smoothed RSSI curve can be obtained by the Savitzky-Golay fitting way using data analysis and a graphic

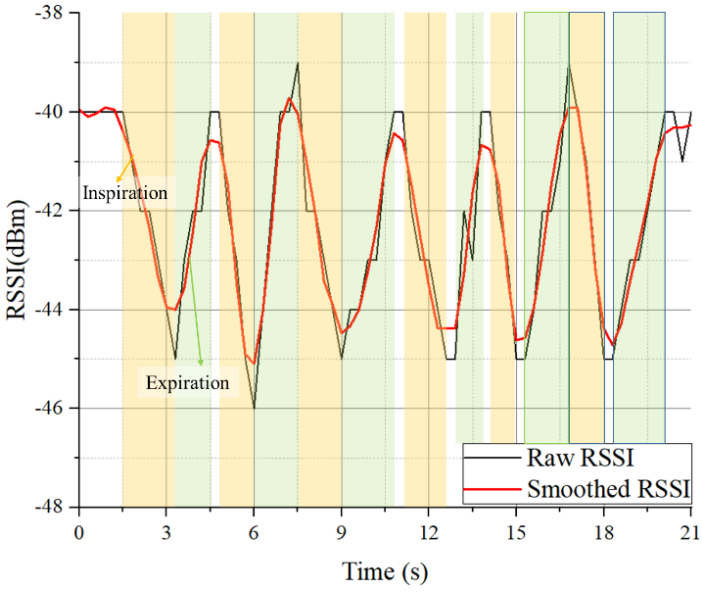

Figure 3.47. Respiration monitor RSSI values and a smoothed curve varying with time (about 1 breath/3 seconds)

software. The measurement results shown the RSSI decreased from -40 dBm to -45 dBm during inspiration phase and increase from -45dbm to -40 dBm during the expiration phase with a respiration rate of 3 Hz, which denotes the feasibility of the proposed electro-textile UHF-RFID compression sensor as a respiration rate sensor

3.4.5 Conclusion

In this section, an electro-textile UHF-RFID compression sensor with the corresponding interface was developed and evaluated for two application scenarios. In order to maximize the read range, the antenna was designed to optimize the matching between IC and antenna. In order to do that, the electro-textile interface based on snap buttons was modelled and experimentally characterized and an experimental read rage of 5.22m was achieved. The RSSI parameter was used as a figure of merit to validate the feasibility of the proposed compression sensor under two different health care applications scenarios. The RSSI showed a variation from -42 dBm to -58 dBm when the RFID tag sensor was located on the knee and a flexion angle from 110º to 180º was applied to the knee, respectively. When the proposed sensor was located in the chest, the RSSI increased and decreased from -45 dBm to -40 dBm during expiration and inspiration phase, respectively. Therefore, the feasibility of the electro-textile UHF-RFID tag as a compression antenna sensor was proved.

Chapter 4

Conclusion and Future Work

4.1 Overall conclusion

In an overall conclusion for contributions to the textile UHF-RFID antenna sensor field in the thesis.

In the first chapter, I put forward my research objectives based on the systematic review of the state of the art of the textile UHF-RFID antennas and sensors. Through the analysis of the state, the three main objectives are proposed including 1) Explore useful textile UHF-RFID antenna sensors with novel functions; 2) Develop some new connection methods for the electro-textile interfaces; 3) Reduce related cost by two methods.

In the second chapter, considering that some essential principles and methods are rarely explained, thus causing misunderstanding and confusion, They are derived in detail. In order to explain the thesis, they include the operating principle of textile UHF-RFID antenna sensors, the impedance measurement method, the conjugate matching principle and electro-textile embroidery methods.

In the third chapter, in order to make a contribution to the researches on novel functions of textile UHF-RFID antenna sensors, the textile UHF-RFID antenna sensor with the two sensing positions (‘radiation parts’ and ‘loop part’) is present. After simulation and real tests, the proposed design used for sensing the sucrose solutions shows good feasibility by comparing the simulated and measured results. Moreover, its two sensing positions have different sensing features and performance. The sensing ‘radiation parts’ shows a stable frequency operation performance but sensing read range is from 1.71 m (dry) to 2.3 m (current measured solutions), while the sensing ‘loop part’ presents a wide sensing read range from 0.4 m (current measured solutions) to 1.71 m (dry) but a lower frequency operation performance. The sensing features give future complete application two choices.

Considering the current global epidemic situation, the progressive designs of textile UHF-RFID antennas on surgical masks are developed and one of them (Design 3) is selected to be validated by reliability tests (bending and skin contact). From the results, the proposed Design 3 can have a common use as an ID tag for tracking or safe distance alert in the epidemic situation but for the used function-extensible chip, the design can extend many different types of textile sensors for various application scenarios in the future.

In order to make a contribution to the researches on the interface methods between textile UHF-RFID antennas and chips, the three electro-textile interfaces integrated with the corresponding textile UHF-RFID antennas are proposed and evaluated. Moreover, it is worth noting that the mixed use feasibility of the proposed electro-textile interfaces and textile UHF-RFID antennas is proved, which can reduce the cost in

the future commercial design procedure. Therefore, due to the small sizes of the electro-textile interfaces, stable performance on the body and good reliability are achieved. The proposed electro-textile interfaces with the corresponding textile UHF-RFID antennas offer a potential application in the future medical and daily clothes fields.

The electro-textile UHF-RFID compression sensor with the corresponding interface is evaluated for two application scenarios. For exploring the electro-textile UHF-RFID tag as the compression sensor, two healthcare application scenarios, bending on a knee and respiration frequency, are tested. The RSSI changing ranges are from -42 dBm to -58 dBm varying with angles as the quadratic function for monitoring bending angles on the knee and from -40 dBm to -45 dBm varying with time for monitoring respiration on the chest. Therefore, the feasibility of the electro-textile UHF-RFID tag as the compression antenna sensor is proved.

Overall, the thesis provides the novel sensing applications, electro-textile interfaces and double sensing functions for cost reduction. All of the work can make a contribution to the current textile UHF-RFID antenna sensor field.

4.2 Future work

Based on all the researches presented in this thesis, it is clear that there is a long way to go for the future work on improving the performance and the futuristic, promising applications and enhancing reliability of the current textile UHF-RFID antenna sensors. Especially for the potential of IOT applications in the ageing society, more attention needs to be paid to develop useful textile UHF-RFID sensors and close research gaps between laboratory researches and real scenario-based textile UHF-RFID sensors.

In detail, there are several ways to dig out the potential of textile UHF-RFID sensors. It is useful to develop new designs and sensing functions of textile UHF-RFID antenna sensors with common or novel textile materials. If the function-extensible chip property can be improved (such as the lower wake-up power), it is worth exploring more about the textile UHF-RFID tags connecting with other textile sensors. And the related novel interfaces between the chips and the textile sensors are potential to be explored and their reliability can be another hot topic.

With regard to the scenario-based applications, textile UHF-RFID sensors have great development potential in many different fields of production and life. Currently, the main application researches focus on the fundamental functions of textile UHF-RFID sensors such as the ID-sensing, strain sensing, humidity sensing, sweat sensing and others. However, advanced functions are not covered. For example, there are exercise-based textile UHF-RFID sweat sensors just for sweat sensing without any elements analysing, on which further researches are worth implementing. Moreover, textile UHF-RFID sensors are more suitable for medical-based applications due to the various medical textiles used for patients or the elderly. Many kinds of medical parameters or body fluids can be detected and analysed by complete textile UHF-RFID sensing systems. The abundant scenarios can create numerous chances for designs and applications of novel textile UHF-RFID sensors in the future.

In addition, reliability is an unavoidable but crucial research direction especially for this kind of flexible and washing-needed component. For example, after fabricating the designs on textile substrates, the performance of UHF-RFID antenna and sensors may decrease such as the resonance frequency shift and performance degradation due to conformal bending or on-body touching. Moreover, environmental factors such as the well-studied humidity and temperature and human activity factors such as washing and sweat corrosion can imply certain impacts on performance. Therefore, the important reliability researches still need to be considered.

References

[1] I. Gil, R. Fernández-García, J.A. Tornero, “Embroidery manufacturing techniques for textile dipole antenna applied to wireless body area network”, *Text. Res. J.*, vol. 89, pp. 573–1581, **2019**.

[2] L. Wang, “Inheritance and Innovation of Embroidery in Modern Design”, *In Proceedings of the 3rd International Conference on Art Studies: Science, Experience, Education*, Moscow, Russia, 4–5 October 2019; pp. 232–234.

[3] S. Merilampi, T. Björninen, L. Sydänheimo, “Passive Uhf Rfid Strain Sensor Tag for Detecting Limb Movement”, *Int. J. Smart Sens. Intell. Syst.*, vol. 5, pp. 315–328, 2012.

[4] S. Merilampi, P. Ruuskanen, T. Björninen, “Printed passive UHF RFID tags as wearable strain sensors”, *In Proceedings of the 2010 3rd International Symposium on Applied Sciences in Biomedical and Communication Technologies (ISABEL 2010)*, Rome, Italy, 7–10 pp. 1–5, November 2010.

[5] C.D.M. Peña, et al, “Ultra slim and small UHF RFID tag design for mounting on curved surfaces”, *AEU - Int. J. Electron. Commun*, vol 128, pp. 153502, 2021.

[6] A. Yang, et al., “Thermal management in nanofiber-based face mask.” Nano letters, vol 17, pp. 3506-3510, 2017.

[7] J. Wang, Q. Li, D. Liu, C. Chen, et al., “High temperature thermal conductive nanocomposite textile by “green” electrospinning,” *Nanoscale*, vol. 10, pp. 16868-16872, 2018.

[8] S. Shao, A. Kiourti, R. J. Burkholder and J. L. Volakis, “Broadband Textile-Based Passive UHF RFID Tag Antenna for Elastic Material,” *IEEE Antennas Wirel. Propag. Lett.*, vol. 14, pp. 1385-1388, 2015.

[9] C. Luo, I. Gil and R. Fernández-García, “Textile UHF-RFID antenna sensor for measurements of sucrose solutions in different levels of concentration,” *Meas. Sci. Technol*, vol. 32, pp. 10, 2021.

[10] Y. Liu, A. Levitt, C. Kara, C. Sahin, G. Dion, and K. R. Dandekar, “An improved design of wearable strain sensor based on knitted RFID technology,” 2*016 IEEE Conference on Antenna Measurements Applications (CAMA)*, pp. 1–4, 2016.

[11] J. Cairó, J. Bonache, F. Paredes and F. Martín, "Interference Sources in Congested Environments and its Effects in UHF-RFID Systems: A Review," IEEE J. Radio Freq. Identif., vol. 2, no. 1, pp. 1-8, 2018.

[12] S. Zuffanelli, P. Aguila, G. Zamora, F. Paredes and J. Bonache, "A high-gain passive UHF-RFID tag with increased read range", Sensors, vol. 16, pp. 1150, 2016

[13] D. Paret, “Standards for RFID at UHF and SHF. In RFID at Ultra and Super High Frequencies Theory and Application”, Wiley: Hoboken NJ, USA, 2009; pp. 369–505.

[14] Y. Kim, K. Lee, Y. Kim and Y.C. Chung, "Wearable UHF RFID tag antenna design using flexible electro-thread and textile", *In Proceedings of the 2007 IEEE Antennas and Propagation Society International Symposium*, Honolulu, HI, USA, 9–15 June 2007; pp. 5487–5490.

[15] R. Nayak, K.N. Chatterjee, G.K. Khurana and A. Khandual, "RFID: Tagging the new ERA", *Man-Made Text. India*, vol. 50, pp. 174–177, 2007.

[16] J. Choi, Y. Kim, L. Lee and Y.C. Chung, "Various wearable embroidery RFID tag antenna using electro-thread", *In Proceedings of the 2008 IEEE Antennas and Propagation Society International Symposium*, San Diego, CA, USA, pp. 1–4, July 2008.

[17] G. Kim, "Design of a UHF RFID fiber tag antenna with electric-thread using a sewing machine", *In Proceedings of the Asia-Pacific Microwave Conference (APMC)*, Macau, China, pp. 1–4, December 2008.

[18] S. Manzari, C. Occhiuzzi and G. Marrocco, "Feasibility of Body-Centric Systems Using Passive Textile RFID Tags", *IEEE Antennas Propagat.* vol. 54, pp. 49–62, 2012.

[19] L. Ukkonen, L. Sydänheimo, and Y. Rahmat-Samii, "Sewed textile RFID tag and sensor antennas for on-body use", *In Proceedings of the 2012 6th European Conference on Antennas and Propagation (EUCAP)*, Prague, Czech Republic, pp. 3450–3454, 2012.

[20] K. Koski, E.S. Lohan and L. Sydänheimo, "Electro-textile UHF RFID patch antennas for positioning and localization applications", *In Proceedings of the 2014 IEEE RFID Technology and Applications Conference (RFID-TA)*, Tampere, Finland, pp. 246–250, 2014.

[21] S. Shao, A. Kiourti and R. Burkholder, "Broadband and flexible textile RFID tags for tires", *In Proceedings of the 2014 IEEE Antennas and Propagation Society International Symposium (APSURSI)*, Memphis, TN, USA, pp. 1507–1507, 2014.

[22] F.Y. Long, "Implementation and wireless readout of passive UHF RFID strain sensor tags based on electro-textile antennas", *In Proceedings of the 2015 9th European Conference on Antennas and Propagation (EuCAP)*, Lisbon, Portugal, pp. 1–5, 2015.

[23] M. Akbari, J. Virkki and L. Sydänheimo, "Toward Graphene-Based Passive UHF RFID Textile Tags: A Reliability Study", *IEEE Trans. Device Mater. Reliab.* vol. 16, pp. 429–431, 2016.

[24] S. Merilampi, H. He and L. Sydänheimo, "The possibilities of passive UHF RFID textile tags as comfortable wearable sweat rate sensors", *In Proceedings of the 2016 Progress in Electromagnetic Research Symposium (PIERS)*, Shanghai, China, pp. 3984–3987, 2016.

[25] D. Shuaib, L. Ukkonen and J. Virkki, "The possibilities of embroidered passive UHF RFID textile tags as wearable mmoisture sensors", *In Proceedings of the 2017 IEEE 5th International Conference on Serious Games and Applications for Health (SeGAH)*, Perth, WA, USA, pp. 1–5, 2017.

[26] X. Chen, H. He and L. Ukkonen, “Embroidered UHF RFID Moisture Sensor Tag on Dishcloth Substrate”, *In Proceedings of the 2018 IEEE International Symposium on Antennas and Propagation USNC/URSI National Radio Science Meeting*, Boston, MA, USA, pp. 2009–2010, 2018.

[27] M. Yu, X. Shang and M. Wang, “Deformation Sensitivity Study of Embroidered UHF RFID Antennas”, *In Proceedings of the 2019 IEEE International Conference on RFID Technology and Applications (RFID-TA)*, Pisa, Italy, pp. 322–326, 2019.

[28] M. A. S. Tajin, C. E. Amanatides, G. Dion and K. R. Dandekar, “Passive UHF RFID-Based Knitted Wearable Compression Sensor”, *IEEE Internet Things J.*, vol. 8, no. 17, pp. 13763-13773, 2021.

[29] L. Zhang, Z. Wang and J.L. Volakis, “Textile antennas and sensors for body-worn applications”, *IEEE Antennas Wirel. Propag. Lett.*, vol. 11, pp. 1690–1693, 2012.

[30] M. Hasani, A. Vena and L. Sydänheimo, “Implementation of a dual-interrogation-mode embroidered RFID-enabled strain sensor”, *IEEE Antennas Wirel. Propag. Lett.* vol. 12, pp. 1272–1275, 2013.

[31] H. He, X. Chen and L. Ukkonen, “Clothing-Integrated Passive RFID Strain Sensor Platform for Body Movement-Based Controlling”, *In Proceedings of the 2019 IEEE International Conference on RFID Technology and Applications (RFID-TA)*, Pisa, Italy, pp. 236–239, 2019.

[32] X. Chen, H. He and Z. Khan, “Textile-Based Batteryless Moisture Sensor”, *IEEE Antennas Wirel. Propag. Lett.*, vol. 19, pp. 298–202, 2019.

[33] D. Patron, “On the Use of Knitted Antennas and Inductively Coupled RFID Tags for Wearable Applications”, *IEEE Trans. Biomed. Circuits. Syst.*, vol.10, pp. 1047-1057, 2016.

[34] W.M. Mongan, I. Rasheed and K. Ved, “On the Use of Radio Frequency Identification for Continuous Biomedical Monitoring”, *In Proceedings of the 2017 IEEE/ACM Second International Conference on Internet-of-Things Design and Implementation (IoTDI)*, Pittsburgh, PA, USA, pp. 197–202, 2017.

[35] M.A. Ennasar, Mrabet.O. El and K. Mohamed, “Design and Characterization of a Broadband Flexible Polyimide RFID Tag Sensor for NaCl and Sugar Detection”, *Prog. Electromagn. Res.*, vol. 94, pp. 273–283, 2019.

[36] A. Moraru, C. Ursachi and E. Helerea, “A New Washable UHF RFID Tag: Design, Fabrication, and Assessment”, *Sensors*, vol. 20, pp. 3451, 2020.

[37] M. Guibert, A. Massicart and X. Chen, “Washing reliability of painted, embroidered, and electro-textile wearable RFID tags”, *In Proceedings of the 2017 Progress in Electromagnetics Research Symposium—Fall (PIERS—FALL)*, Singapore, pp. 828–831, 2017.

[38] D.A. Hardy, Z. Rahemtulla, A. Satharasinghe, A. Shahidi, C. Oliveira, I. Anastasopoulos, M.N. Nashed, M. Kgatuke, A. Komolafe and R. Torah, "Wash Testing of Electronic Yarns", *Materials*, vol.13, pp. 1228, 2020.

[39] V. Gaubert, H. Gidik, N. Bodart and V. Koncar, "Investigating the Impact of Washing Cycles on Silver-Plated Textile Electrodes: A Complete Study", *Sensors*, vol. 20, pp. 1739, 2020.

[40] R.B.V.B. Simorangkir, D. Le and T. Björninen, "Washing Durability of PDMS-Conductive Fabric Composite: Realizing Washable UHF RFID Tags", *IEEE Antennas Wirel. Propag. Lett.*, vol. 18, pp. 2572–2576, 2019.

[41] A. Kazmi, M. Rizwan and L. Sydänheimo, "A reliability study of coating materials for brush-painted washable textile RFID tags", *In Proceedings of the 2016 6th Electronic System-Integration Technology Conference (ESTC)*, Grenoble, France, pp. 1–4, 2016.

[42] A. Kazmi, J. Virkki and T. Björninen, "Performance of silver-based textile UHF passive RFID tags after recurrent washing", *In Proceedings of the 2016 IEEE International Symposium on Antennas and Propagation (APSURSI)*, Fajardo, Puerto Rico, pp. 939–940, 2016.

[43] P. Sharma and E.C. Kan, "Sleep scoring with a UHF RFID tag by near field coherent sensing", *In Proceedings of the 2018 IEEE/MTT-S International Microwave Symposium—IMS, Philadelphia*, PA, USA, pp. 1419–1422, 2018.

[44] X. Chen, A. Liu and Z. Wei, "Experimental study on strain reliability of embroidered passive UHF RFID textile tag antennas and interconnections", *J. Eng. Techno.*, 2017.

[45] Q. Bai, S. Swaisaenyakorn, H.-J. Lee, K.L. Ford, J.C. Batchelor, and R.J. Langley, "Investigation of a Switchable Textile Communication System on the Human Body", *Electronics*, vol. 3, pp. 491–503, 2014.

[46] D. Van Baelen, S. Lemey, J. Verhaevert and H. Rogier, "A Novel Manufacturing Process for Compact, Low-Weight and Flexible Ultra-Wideband Cavity Backed Textile Antennas", *Materials*, vol. 11, pp. 67, 2018.

[47] S. Cheng, S. Wang, W. Guan, H. Xu and P. Li, "3DLRA: An RFID 3D Indoor Localization Method Based on Deep Learning", *Sensors*, vol. 20, pp. 2731, 2020.

[48] M. Chesser, A. Jayatilaka and R. Visvanathan, "Super Low Resolution RF Powered Accelerometers for Alerting on Hospitalized Patient Bed Exits", *In Proceedings of the IEEE International Conference on Pervasive Computing and Communications*, Kyoto, Japan, pp. 1–10, 2019.

[49] B. Puruncajas, Y. Vidal and C. Tutivén, "Vibration-Response-Only Structural Health Monitoring for Offshore Wind Turbine Jacket Foundations via Convolutional Neural Networks", *Sensors*, vol. 20, pp. 3429, 2020.

[50] C.C. Vu and J. Kim, “Highly Sensitive E-Textile Strain Sensors Enhanced by Geometrical Treatment for Human Monitoring”, *Sensors*, vol. 20, pp. 2383, 2020.

[51] G. Zamora, S. Zuffanelli, F. Paredes, F. Martı´n and J. Bonache, "Design and Synthesis Methodology for UHF-RFID Tags Based on the T-Match Network," IEEE Trans Microw. Theory Tech., vol. 61, no. 12, pp. 4090-4098, 2013.

[52] C. Liu, X. Liao, W. Shao, F. Liu, B. Ding, G. Ren, Y. Chu and J. He, “Hot-melt Adhesive Bonding of Polyurethane/Fluorinated Polyurethane/Alkylsilane-Functionalized Graphene Nanofibrous Fabrics with Enhanced Waterproofness”, *Breathability, and Mechanical Properties. Polymers*, vol. 12, pp. 836, 2020.

[53] F. Gaspari and Q. Simone, “Nanostructured Materials for RFID Sensors”, *In Nanomaterials Design for Sensing Applications*, Elsevier: Amsterdam, The Netherlands, pp. 93–128, 2019.

[54] www.urbatex.com/en/tessuto/polyester-fabric/

[55] H. Zhang, “Flexible textile-based strain sensor induced by contacts”, *Meas. Sci. Technol.*, vol. 26 pp. 105102, 2015.

[56] I. Logothetis, D.V. Bayramol and I. Gil, “Evaluating silver-plated nylon (Ag/PA66) e-textiles for bioelectrical impedance analysis (BIA) application”, Meas. Sci. Technol., vol. 31, pp. 075101, 2020.

[57] Y.Y. Fu, Y.L. Chan, M.H. Yang, “Experimental study on the washing durability of electro-textile UHF RFID tags”, *IEEE Antenn. Wirel. Pr.*, vol. 14, pp. 466–469, 2014.

[58] T. Björninen, J. Virkki and L. Sydänheimo, “Ukkonen, L. Impact of recurrent stretching on the performance of electro-textile UHF RFID tags”, *In Proceedings of the 5th Electronics System-integration Technology Conference (ESTC)*, Helsinki, Finland, pp. 251–255, 2014.

[59] T. Björninen, J. Virkki and L. Sydänheimo, “Impact of recurrent washing on the performance of electro-textile UHF RFID tags”, *In Proceedings of the 2014 IEEE RFID Technology and Applications Conference (RFID-TA)*, Tampere, Finland, pp. 251–255, 2014.

[60] J. Virkki, T. Björninen, T. Kellomäki, “Reliability of washable wearable screen printed UHF RFID tags”, *Microelectron. Reliab* , vol. 54, pp. 840–846, 2014.

[61] N.O. Laschuk, I.I. Ebralidze, S. Quaranta, S.T. Kerr, J.G. Egan, S. Gillis, F. Gaspari, A. Latini and O.V. Zenkina, “Rational design of a material for rapid colorimetric Fe2+ detection”, *Mater. Des.*, vol. 107, pp. 18–25, 2016.

[62] N.O. Laschuk, A. Obua, I.I. Ebralidze, H.M. Fruehwald, J. Poisson, J.G. Egan, F. Gaspari, F.Y. Naumkin, E.B. Easton and O.V. Zenkina, “Spacer Conjugation and Surface Support Effects in Monolayer Electrochromic Materials”, *ACS Appl. Electron. Mater.*, vol. 8, pp. 1705–1717, 2019.

[63] S. Quaranta, M. Giorcelli and P. Savi, “Graphene and MWCNT Printed Films: Preparation and RF Electrical Properties Study”, *J. Nanomater.*, vol. 2019, pp. 1–9, 2019.

[64] H. Ujiie, Digital Printing of Textiles; Woodhead Publishing: Sawston, UK, 2006.

[65] C. Cie, Ink Jet Textile Printing; Elsevier: Amsterdam, The Netherlands, 2015.

[66] L. Shan and H. Xiao, “Impedence characterization of RFID tag antennas and application in conformal tag antenna,” *2015 7th Asia-Pacific Conference on Environmental Electromagnetics (CEEM)*, Hangzhou, pp. 140-142, 2015.

[67] H. Zhu, Y. C. A. Ko and T. T. Ye, “Impedance measurement for balanced UHF RFID tag antennas,” *2010 IEEE Radio and Wireless Symposium (RWS)*, New Orleans, LA, pp. 128-131, 2010.

[68] X. Qing, C. K. Goh and Z. N. Chen, “Measurement of UHF RFID tag antenna impedance,” *2009 IEEE International Workshop on Antenna Technology, Santa Monica*, CA, pp. 1-4, 2009.

[69] https://na.support.keysight.com/pxi/help/latest/S3_Cals/Port_Extensions.htm

[70] C.T. Carrasco, C.J. Sieiro, J.M. Lopez-Villegas, N. Vidal, R. Gonzalez-Echevarr´ıa and M.E. Roca, “Mixed-mode impedance and reflection coefficient of two-port devices,” *Prog. Electromagn. Res.*, vol. 130,pp. 411- 428, 2012

[71] C.K. Stoumpos, D.E. Anagnostou and M.T. Chryssomallis, “Experimental characterization of the impedance of balanced UHF RFID tag antennas,” *Microw. Opt. Technol. Lett.* vol. 59(12), pp. 3127-3134, 2017.

[72] L. Wang, “Inheritance and Innovation of Embroidery in Modern Design,” *Proceedings of the 3rd International Conference on Art Studies: Science, Experience, Education*, Moscow, Russia. pp. 4-5. 2019.

[73] M. Catrysse, R. Puers and C. Hertleer, “Towards the integration of textile sensors in a wireless monitoring suit,” *Sens. Actuator A Phys.* vol. 114, pp. 302–311, 2004.

[74] R. Vieroth, C. Kallmayer and R. Aschenbrenner , “A new package for textile integrated RFID tags,” *In Proceedings of the 2009 11th Electronics Packaging Technology Conference*, Singapore, pp. 240–243, 2009.

[75] G.S. Rocha, M.K.L. Silva and I. Cesarino, “Reduced Graphene Oxide-Based Impedimetric Immunosensor for Detection of Enterotoxin A in Milk Samples,” *Materials*, vol. 13, pp. 1751, 2020.

[76] T. Björninen, J. Virkki and L. Sydänheimo, “Manufacturing of antennas for passive UHF RFID tags by direct write dispensing of copper and silver inks on textiles,” *In Proceedings of the 2015 International Conference on Electromagnetics in Advanced Applications (ICEAA)*, Turin, Italy, pp. 589–592, 2015.

[77] P. Lugoda, J.C. Costa, C. Oliveira, L.A. Garcia-Garcia, S.D. Wickramasinghe, A. Pouryazdan, D. Roggen, T. Dias and N. Münzenrieder, "Flexible Temperature Sensor Integration into E-Textiles Using Different Industrial Yarn Fabrication Processes," *Sensors,* vol. 20, pp. 73, 2020.

[78] Z. Gong, Z. Xiang, X. Ouyang, J. Zhang, N. Lau, Zhou, J. and C.C. Chan, "Wearable Fiber Optic Technology Based on Smart Textile: A Review," *Materials*, vol. 12, pp. 3311, 2019.

[79] E. Sazonov, "Wearable Sensors: Fundamentals, Implementation and Applications," Elsevier: Amsterdam, The Netherlands, 2014.

[80] V. Marian, B. Allard and C. Vollaire, "Strategy for microwave energy harvesting from ambient field or a feeding source," *IEEE Trans. Power Electron,*. vol. 27, pp. 4481–4491, 2012.

[81] F. Fuschini, C. Piersanti and F. Paolazzi, "Analytical approach to the backscattering from UHF RFID transponder," *IEEE Antenn. Wirel. Pr.,* vol. 7, pp. 33–35, 2008.

[82] C.H. Loo, K. Elmahgoub, and F. Yang, "Chip impedance matching for UHF RFID tag antenna design," *Prog. Electromagn. Res.*, vol. 81, pp. 359–370, 2008.

[83] C.A. Balanis, "Antenna Theory: Analysis and Design," John Wiley and Sons: Hoboken, NJ, USA, 2016.

[84] I.P. Gravas, Z.D. Zaharis, P.I. Lazaridis, T.V. Yioultsis, N.V. Kantartzis, C.S. Antonopoulos, I.P. Chochliouros and T.D. Xenos, "Optimal Design of Aperiodic Reconfigurable Antenna Array Suitable for Broadcasting Applications," *Electronics.* vol. 9, pp. 818, 2020.

[85] Ž. Korošak, N. Suhadolnik and A. Pleteršek, "The implementation of a low power environmental monitoring and soil moisture measurement system based on UHF RFID," *Sensors.* vol. 19, pp. 5527, 2019.

[86] C. Strangfeld, S. Johann and M. Bartholmai, "Smart RFID Sensors Embedded in Building Structures for Early Damage Detection and Long-Term Monitoring," *Sensors.* vol. 19, pp. 5514, 2019.

[87] M. Rossi, R.M. Liberati, M. Frasca and J. Richardson, "Experimental Implementation of a Low-Cost, Fully-Analog Self-Jamming Canceller for UHF RFID Devices," *Electronics*, vol. 9, pp. 786, 2020.

[88] P. Zradziński, J. Karpowicz, K. Gryz and V. Ramos, "An Evaluation of Electromagnetic Exposure While Using Ultra-High Frequency Radiofrequency Identification (UHF RFID) Guns," *Sensors*, vol. 20, pp. 202, 2020.

[89] M. Wagih, Y. Wei, A. Komolafe, R. Torah and S. Beeby, "Reliable UHF Long-Range Textile-Integrated RFID Tag Based on a Compact Flexible Antenna Filament," *Sensors.* vol. 20, pp. 3435, 2020.

[90] M.T. Islam, T. Alam, I. Yahya and M. Cho, “Flexible radio-frequency identification (RFID) tag antenna for sensor applications,” *Sensors,* vol. 18, pp. 4212, 2018.

[91] X. Chen, B. Li, Y. Qiao and Z. Lu, “Preparing polypyrrole-coated stretchable textile via low-temperature interfacial polymerization for highly sensitive strain sensor,” *Micromachines,* vol. 10, pp. 788, 2019.

[92] B. Abbas, S.K. Khamas, A. Ismail and A. Sali, “Full Embroidery Designed Electro-Textile Wearable Tag Antenna for WBAN Application,” *Sensors,* vol. 19, pp. 2470, 2019.

[93] T. Yang, X. Xiong, M. Petru, X. Tan, H. Kaneko, J. Militký and A. Sakuma, “Theoretical and Experimental Studies on Thermal Properties of Polyester Nonwoven Fibrous Material,” *Materials,* vol. 13, pp. 2882, 2020.

[94] C. Luo, W. Fang, Y. Shen, H. Qiu, W. Shao, Z. Hong, L. Wang, Z. He and Y. En, “Collocated and simultaneous measurements of RF current and voltage on a trace in a noncontact manner,” *IEEE Trans. Microw. Theory. Tech.*, vol. 67, pp. 2406–2415, 2019.

[95] Q. Liu, H. Li, Y.F. Yu, W.S. Zhao and S. Zhang, “A Novel Finger-Controlled Passive RFID Tag Design for Human–Machine Interaction,” *Sensors,* vol. 19, pp. 5125, 2019.

[96] J. Hu, J. Yu, Y. Li, X. Liao, X. Yan and L. Li, “Nano Carbon Black-Based High Performance Wearable Pressure Sensors,” *Nanomaterials,* vol. 10, pp. 664, 2020.

[97] Q. Hu, H. Memon, Y. Qiu, W. Liu, Y. Wei, “A Comprehensive Study on the Mechanical Properties of Different 3D Woven Carbon Fiber-Epoxy Composites,” *Materials,* vol. 13, pp. 2765, 2020.

[98] H.S. Cho, J.H. Yang, J.H. Lee, J.H. Lee, “Evaluation of Joint Motion Sensing Efficiency According to the Implementation Method of SWCNT-Coated Fabric Motion Sensor,” *Sensors,* vol. 20, pp. 284, 2020.

[99] A. Ojstršek, N. Virant, D. Fox, L. Krishnan and A. Cobley, “The Efficacy of Polymer Coatings for the Protection of Electroless Copper Plated Polyester Fabric,” *Polymers,* vol. 12, pp. 1277, 2020.

[100] V. Gaubert, H. Gidik and V. Koncar, “Boxer Underwear Incorporating Textile Moisture Sensor to Prevent Nocturnal Enuresis,” *Sensor,* vol. 20, pp. 3546, 2020.

[101] P.A. García, M. Khoshnam and C. Menon, “Wearable Device to Monitor Back Movements Using an Inductive Textile Sensor.” *Sensors,* vol. 20, pp. 905, 2020.

[102] D.A. Roberson, R.B. Wicker, L.E. Murr, K. Church and E. MacDonald, “Microstructural and process characterization of conductive traces printed from Ag particulate inks,” *Materials,* vol. 4, pp. 963–979, 2011.

[103] Z. Ma and Y. Jiang, “High-density 3D printable chipless RFID tag with structure of passive slot rings,” *Sensors*, vol. 19, pp. 2535, 2019.

[104] S. Liu, Y. Li, S. Xing, L. Liu, G. Zou and P. Zhang, “Structure inheritance in nanoparticle ink direct-writing processes and crack-free nano-copper interconnects printed by a single-run approach.,” *Materials*, vol. 12, pp. 1559, 2019.

Appendix

This appendix part mainly provides the copies of the published articles referred to in this thesis. The order is as below,

Ref. A: **C. Luo,** I. Gil and R. Fernández-García, "Wearable textile UHF-RFID sensors: A systematic review." *Materials*, 2020. (Published)

Ref. B: **C. Luo,** I. Gil and R. Fernández-García, "Textile UHF-RFID antenna sensor for measurements of sucrose solutions in different levels of concentration." *Meas Sci Technol*, 2021. (Published)

Ref. C: **C. Luo,** I. Gil and R. Fernández-García, "Textile UHF-RFID Antenna Embroidered on Surgical Masks for Future Textile Sensing Applications," *IEEE Trans. Antennas Propag.*, 2022. (Published)

Ref. D: **C. Luo,** I. Gil and R. Fernández-García, "Experimental Comparison of Three Electro-textile Interfaces for Textile UHF-RFID Tags on Clothes," *Int. J. Electron. Commun.*2022. (Published)

Ref. E: **C. Luo,** I. Gil and R. Fernández-García, "Electro-textile UHF-RFID Compression Sensor for Healthcare Applications," *IEEE Sens. J.* 2022 (Under Review)

A published conference article for reference in the thesis

C. Luo, I. Gil and R. Fernández-García, "Embroidered Textile Capacitive Sensor for Sucrose Solutions Measurement," 2020 IEEE International Conference on Flexible and Printable Sensors and Systems (FLEPS), 2020. (Published)

materials

MDPI

Article

Wearable Textile UHF-RFID Sensors: A Systematic Review

Chengyang Luo, Ignacio Gil and Raúl Fernández-García *

Department of Electronic Engineering, Universitat Politecnica de Catalunya, 08222 Barcelona, Spain; chengyang.luo@upc.edu (C.L.); ignasi.gil@upc.edu (I.G.)

* Correspondence: raul.fernandez-garcia@upc.edu; Tel.: +34-9373-980-89

Received: 11 June 2020; Accepted: 22 July 2020; Published: 24 July 2020

Abstract: Textile radio-frequency identification operating in ultra-high frequency (UHF-RFID) sensors based on different scenarios are becoming attractive with the forthcoming internet of things (IoT) era and aging society. Compared with conventional UHF-RFID sensors, textile UHF-RFID sensors offer the common textile features, light weight, washability and comfort. Due to the short time and low level of development, researches on the integration of textile UHF-RFID techniques and textile sensing techniques are not flourishing. This paper is motivated by this situation to identify the current research status. In this paper, we provide a systematic review of the fundamentals of textile UHF-RFID sensors techniques, materials, the brief history and the state-of-the-art of the scenario-based development through detailed summary and analysis on the achievements from the starting year of 2004 to the present time. Moreover, according to the analysis, we give a proposal of the future prospects in several aspects, including the new materials and manufacturing processes, machine learning technology, scenario-based applications and unavoidable reliability.

Keywords: textile; ultra-high frequency (UHF); radio frequency identification (RFID); UHF-RFID sensors; scenario-based

1. Introduction

Textile radio-frequency identification operating in ultra-high frequency (UHF-RFID) sensors have been getting more attention since the development of the health-caring field and the calling of the internet of things (IOT) applications because of textiles widely used for everyone and the mature embroidery techniques [1,2]. Moreover, the rapid spread of smart phones, smartbands and other smart devices makes the textile UHF-RFID sensors easier to be connected with individual smart devices by means of RFID modules. Although wearable UHF-RFID sensors on flexible substrates have been focused on for many years, substrate textile materials are still at the early stage due to the short development period since 2004 [3]. Early efforts from textile UHF-RFID techniques were focused on feasibility, reliability and fundamental functions of tags, mainly including identification and tracking for garments in the fabrication process [4]. In recent years since 2012, the research targets of textile UHF-RFID techniques changed from the fundamental researches to tackle scenario-based applications such as exercise tracking [5,6], health-care monitoring [7–9], concentration detection of solutions [10], strain capacity [11] and associated applications. In order to achieve these aims, substantial efforts have been devoted to the development of textile sensors integrated into textile UHF-RFID tags. However, although several of the textile UHF-RFID sensors are tested in real scenarios, successful translation to the commercial market has not been completely deployed and these research samples still require further large-scale validation and reliability studies, performance evaluation under stress conditions and device regulatory approvals for safety.

In addition, exploring methods for performance improving, application diversification and high reliability is also an adjoin research proposition, which lead most aspects of techniques to upgrade and even fuse. For these goals, many kinds of tentative studies have been done, such as the metal-pasted thread as the important conductive medium, the graphene-based conductive medium [12,13], and special synthetic textile materials as substrates. Certainly, the use of novel materials will push the fabrication techniques to make changes. The metal-pasted thread can be embroidered on most kinds of textile substrates by traditional embroidery machines with fundamental techniques whereas graphene-based conductive ink needs to be printed on textile substrates by a screen printing technique with specific printing processes [14].

For all of the researches on textile UHF-RFID sensors, although significant technical progress is gradually getting mature, a gap between in-lab researches and mature commercial applications still exists. In addition, combining current fabrication techniques [15,16], the integration of textile UHF-RFID tag and sensing components is also an important issue worth exploring, which will have an impact on future applications.

In order to understand the current research state-of-the-art of the textile UHF-RFID sensors and related applications, this article is written as a brief review. Section 2 presents the fundamentals of textile UHF-RFID sensors including UHF-RFID sensor techniques and electro-textile techniques. Section 3 presents the materials and related impacts in terms of the theory and formulas. Section 4 presents the review search strategy and paper selection. Section 5 presents the development of textile UHF-RFID sensors including the brief history of the textile UHF-RFID tags and sensors, the state of Scenario-based textile UHF-RFID sensors and the state of researches on the reliability of textile UHF-RFID sensors. Section 6 presents the future perspective and Section 7 summarizes the discussion and highlights the main conclusions.

2. Fundamentals of Textile UHF-RFID Sensor Techniques

From the early 21st century, the standards and theory of RFID have been improving [17] while the cost of RFID integrated circuits decreases gradually. In addition, the RFID operating bandwidth was defined, as shown in Table 1. The RFID tags can be designed for either a low frequency band (120–150 kHz), high frequency band (13.56 MHz), ultra-high frequency band (433 MHz, 865–868 MHz in Europe, 917–922 MHz in China and 902–928 MHz in North America) and microwave band (2.45–5.8 GHz and 3.1–10 GHz) [18]. In these conditions, RFID sensor applications are becoming more and more extensive in many fields such as stuff identification, logistics tracking, health-care monitoring and so on [19]. Especially for the health-care monitoring and diagnosis field, the textile UHF-RFID sensors, which require some considerable features such as noninvasive detection, comfort, convenience and wireless diagnosis, have become a focal research orientation in the scientific community.

Table 1. RFID operating bands.

Band	Range	Regulations	Typical Use
120–150 kHz (LF)	10 cm	Unregulated	Animal identification, factory data collection
13.56 MHz (HF)	10 cm–1 m	ISM band worldwide	Smart cards
433 MHz (UHF)	1–100 m	Short range devices	Defense applications
433 MHz (UHF)	1–100 m	Short range devices	Defense applications
865–868 MHz (Europe) and 902–928 MHz (North America) (UHF)	1–12 m	ISM band	staff identification, logistic tracking
2.45–5.8 GHz (microwave band)	1–2 m	ISM band	802.11 WLAN, Bluetooth standards
3.1–10 GHz (microwave band)	Up to 200 m	Ultra wide band	Active tags

2.1. UHF-RFID Sensor Techniques

There are many researches on common RFID tags and sensors. The main difference between RFID tag designs for the different operating frequency bands is different structures of RFID antennas. Taking a typical dipole antenna as an example, a classical Formula (1) is as follows,

$$\lambda = \frac{c}{f} \tag{1}$$

where c is the speed of light, f is the frequency and λ is the wave length. With respect to the formula, the sizes of the dipole antenna are related to the wave length. When the operating frequency is in ultra-high band, the sizes of the RFID antenna need to be adjusted. The fundamental of a UHF-RFID sensor system is shown in Figure 1. The UHF-RFID sensors mainly consist of the UHF antenna, the application specific integrated circuit (ASIC), a micro controller unit (MCU) and some specific sensors. Note that as the essential element in a UHF-RFID sensing system, the UHF antenna has many kinds of structures such as a modified dipole and a folded dipole, which is included in the UHF-RFID sensors tag to receive the inquiry signals including energy [20] from the UHF-RFID reader, and then transmit the measurement data and tag the identification number through radar backscattering mode [21]. Generally, when a continuous data logging is required and the UHF RFID reader cannot supply the power energy, an extra battery needs to be used as an additional power supply to store the measurement data on an additional memory. Once the UHF-RFID reader is presented, the RFID sensor tag downloads all the storage measurement data on the reader.

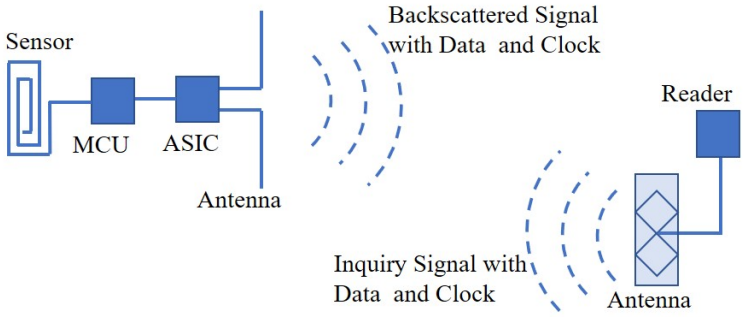

Figure 1. Fundamental of an ultra-high frequency (UHF-RFID) sensor system.

In order to design a suitable UHF antenna for RFID sensors, the size and impedance need to be considered. Different ASICs have different input impedance. Thus to optimize the energy harvesting efficiency, a perfect conjugate matching between the antenna and the ASICs at operating frequency band is required. The complex impedance of the antenna and the ASICs is shown in Formulas (2) and (3), respectively.

$$Z_{ant} = R_{ant} + jX_{ant} \tag{2}$$

$$Z_{IC} = R_{IC} + jX_{IC} \tag{3}$$

where Z_{ant} and Z_{IC} are the impedances of the antenna and the ASICs, respectively, R_{ant} and R_{IC} are the real parts of the antenna and ASICs, respectively, and X_{ant} and X_{IC} are the imaginary parts of the antenna and ASICs, respectively. When the UHF-RFID sensor is working at a required frequency band, the antenna and the ASICs need to keep conjugate matching as follows,

$$Z_{IC} = Z_{IC}^{*} \tag{4}$$

where Z_{IC}^{*} is the complex conjugate of Z_{IC}. Usually the antenna tags are specifically designed taking into account the ASICs input impedance and the RFID tag application environment [22]. As for the

whole performance evaluation, some intuitive parameters are considerable, including return loss (S parameters), gain, resonance frequency, bandwidth, radiation power and read range.

2.2. Electro-Textile Techniques

The fundamental process of two typical electro-textile techniques is illustrated in Figure 2. As shown in Figure 2a, this technique is worth exploring for the combination of electronics and textiles. The conductive yarns are twisted by a proportional metal-plated thread. By this embroidery technique, the conductive yarns can be embroidered on many kinds of common textile substrates by commercial embroidery machines [23]. Generally, the technological process begins from the model design model simulated by means of an electromagnetic software solver to the model importation into embroidery machines and ending with the manufacturing process. Using this technique for UHF-RFID products, the connection of electronic elements such as ASICs and textile structures can be implemented by commercial glue. There are some studies [24–26] on the technique, proving its feasibility for electro-textile RFID or sensors with well ranked performance.

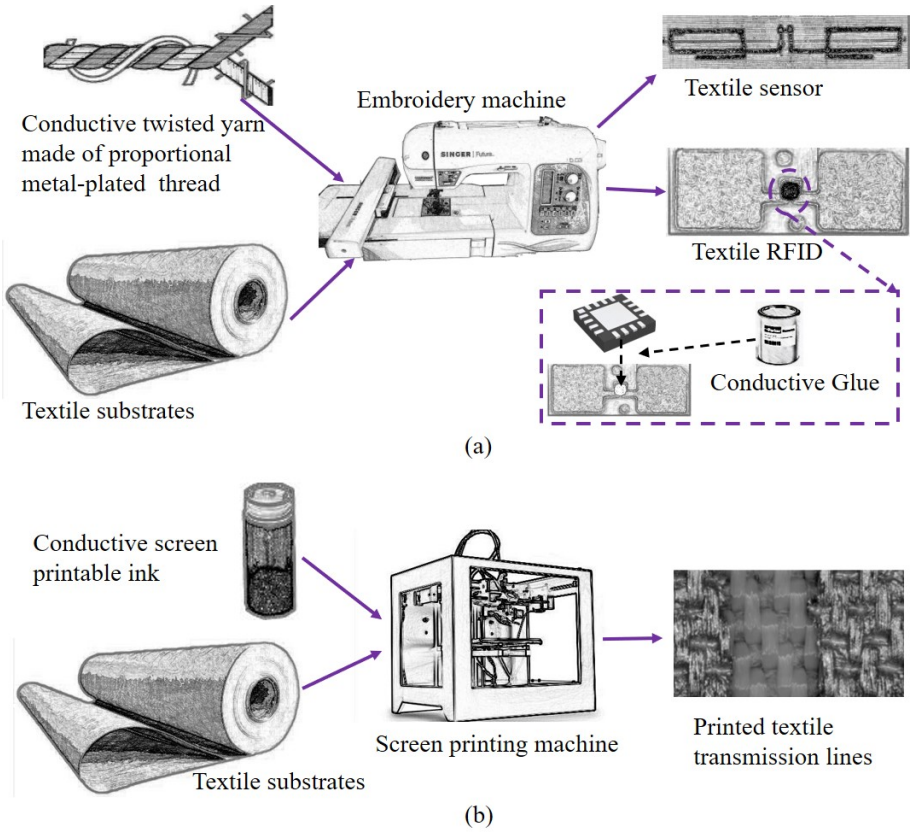

Figure 2. Two typical electro-textile techniques. (**a**) Embroidery technique using conductive yarns, (**b**) screen printing technique using special conductive ink.

Compared with the embroidery technique using conductive yarns, the screen printing technique using special conductive ink, as shown in Figure 2b, is another popular technique for electro-textile applications but more complex due to its technological process [27]. The essential elements are the specially configured conductive ink and the complex screen printing machines. The general conductive ink is a metal-filled paste with a solid content of a certain percentage, for which the curing process under a required temperature by the screen machine is necessarily performed after the ink is pressed. Although the screen printing technique was invented in ancient China, this technique has been systematically developed in the last 20 years and is employed for the design of robust non-bendable chemical sensors [28], electrochromic materials [29], and non-bendable UHF-RFIDs [30].

However, the invention of conductive compositions for textile printing, described by Ujiie in 2006 [31] that was further developed by Cie in 2015 [32] opens the door for utilization of screen printing in flexible electronics.

3. Materials of UHF-RFID Sensors

Compared to common materials such as printed circuit boards (PCB) in UHF-RFID sensor applications, textile materials have quite different physical characteristics, some of which are developed for many novel applications but some pose unavoidable risks. Thus, the investigation of materials of UHF-RFID sensors is necessary for further researches. Especially in recent years, the UHF-RFID sensors based on many textile materials are expected to be applied for human health-caring fields, which need more attention given to safety and reliability.

3.1. Materials of Substrates

Different materials as substrates of UHF-RFID sensors make variable levels of influence on the design due to different physical characteristics such as dielectric constants, loss tangent, texture, etc. For instance, a typical rectangular microstrip antenna without fringing as shown in Figure 3 can be used as an RFID antenna. With respect to the antenna theory [33,34], the resonant frequency (f_{r*}) of the microstrip antenna is a function of its length (L) or width (W). Usually it is given by

$$f_{rL} = \frac{1}{2L\sqrt{\varepsilon_r}\sqrt{\mu_0\varepsilon_0}} = \frac{c}{2L\sqrt{\varepsilon_r}} \qquad (L > W) \tag{5}$$

or

$$f_{rW} = \frac{1}{2W\sqrt{\varepsilon_r}\sqrt{\mu_0\varepsilon_0}} = \frac{c}{2W\sqrt{\varepsilon_r}} \qquad (W > L) \tag{6}$$

where ε_r is the dielectric constant of the substrate, μ_0 is the permeability of vacuum, ε_0 is the permittivity of vacuum and c is the speed of light in free space. Therefore, the resonant frequency is also a function of the dielectric constant ε_r of the substrate. When the resonant frequency is set in an ultra-high frequency band, the different materials certainly influence the size of the model designs.

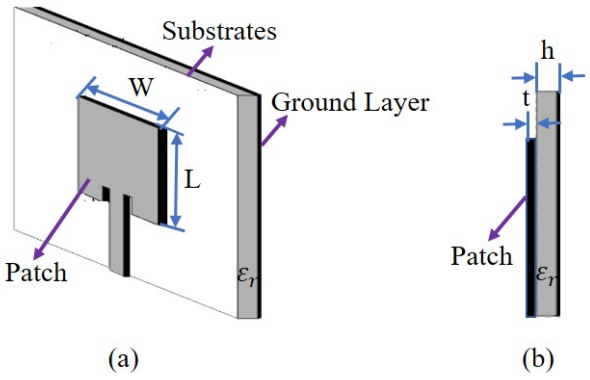

Figure 3. Typical microstrip antenna structure. (**a**) Microstrip antenna. (**b**) Lateral view.

In addition, with regard to loss tangent, some materials with high dielectric constant also have high loss tangent, which increases the energy loss and affects the efficiency of the antenna. As shown in Table 2, some popular materials of UHF-RFID sensors are summarized in terms of the dielectric constant, loss tangent and texture.

The texture is also an important feature that determines the types of application orientation and the main parameters for validating reliability. For example, as shown in Figure 4, there are three typical samples for different materials of the substrates. The material of the substrate, as shown in Figure 4a, is FR4, one type of the rigid PCB, which is different with the polyimide, one type of the

flexible PCB (FPCB), as shown in Figure 4b, and the 50 % cotton and 50% polyester, one type of the mixed textile, as shown in Figure 4c. Note that the FR4 substrate is so rigid that it cannot be bent easily, meanwhile the polyimide substrate needs to be tested in a bending condition. Compared to the FR4 substrate and polyimide substrate, the textile substrate [44] has to face the challenges of not only the bending impact but also the environmental impacts such as humidity and temperature. However, due to the universality of textile materials in human life, the textile UHF-RFID sensors have a good application foundation.

Table 2. Materials of substrates.

Material	Type	Dielectric Constant	Loss Tangent	Texture	Example
FR4	PCB	4.4	0.02	Rigid	[35,36]
Rogers	PCB	2.2	0.0009	Rigid	[37,38]
Polyimide	FPCB	3.5	0.0027	Flexible	[39,40]
Biodegradable paper	FPCB	3.2	0.05	Flexible	[41]
Polyester	textile	3.2	0.003	Flexible	[42,43]

Certainly, the common materials, PCB, can be applied for multi-sensor structures in terms of multi layers, as shown in Figure 4a, which also gives textile UHF-RFID sensors a novel research orientation towards multi-layer structures with flexible and comfortable features.

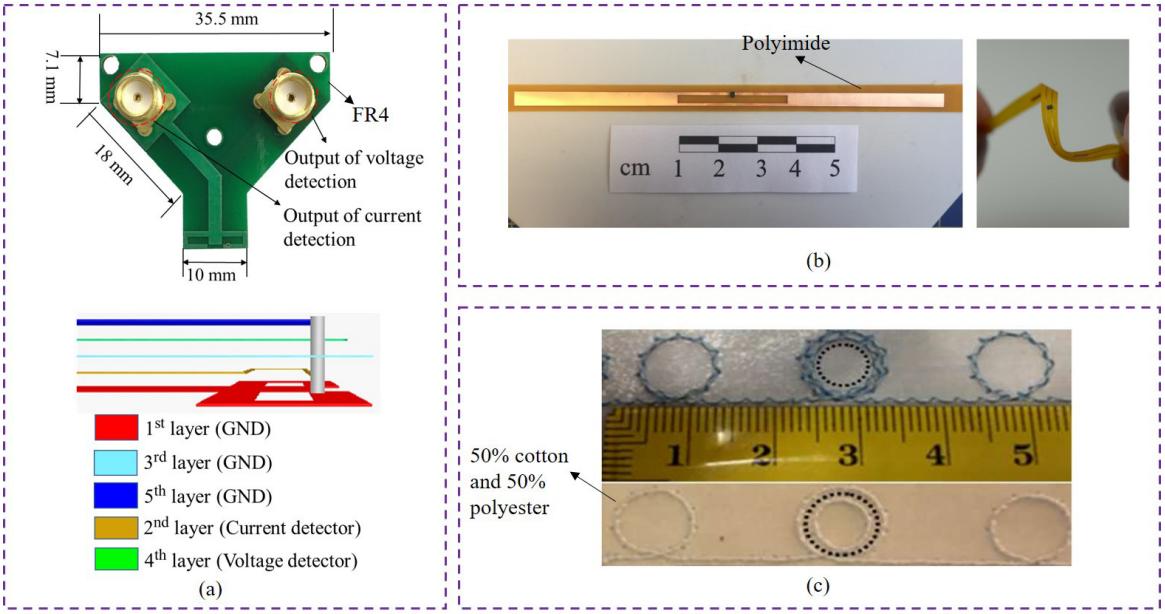

Figure 4. Three typical materials of the substrates. (**a**) Voltage and current sensor with FR4 substrate (adapted from [45]); (**b**) UHF-RFID tag with polyimide substrate (adapted from [40]); (**c**) UHF-RFID tag with 50% cotton and 50% polyester substrate (adapted from [44]).

3.2. Materials of UHF-RFID Antennas and Sensors

As an information and energy transceiver structure, the UHF-RFID antenna is a necessary metallic device for radiating or receiving radio waves in a UHF-RFID sensor. In general, due to the unavoidable lossy nature of the transmission conductors and the reflections losses at several interfaces, there are always conduction-dielectric losses in the real devices. Therefore, the better choice for the conductor is the materials with good conductive ability and the low resistive rate. Currently, metal materials [46], such as copper, aluminum, iron, silver and gold, and synthetic fiber such as graphite fiber [47–49] and glass fiber, are popular in the UHF-RFID antennas and sensors designs. Note that metal materials still

have better conductive ability than that of some synthetic fiber, thus some synthetic fiber is dealt with metal surface [50] or twisted by a proportional metal-plated fiber [51,52]. Certainly, compared with metal materials, synthetic fiber has the greatest strength of designability. Through advanced modal analysis of structures in specific computer programs, proper structure and performance of synthetic materials can be designed.

In addition, due to the development of printed electronics [53], conductive ink with spacial metal elements such as Nano-Ag [54] and Nano-copper [55] is developed and applied for screen-printed UHF-RFID sensor applications. Currently, conductive inks are key enablers for the use of printing techniques in the fabrication of electronic systems.

4. Review Search Strategy and Paper Selection

Full-text articles and conference proceedings were selected from a comprehensive search of PubMed, ScienceDirect, Scopus and IEEE Xplore databases. The search strategy included free text terms and Mesh terms, where suited. These terms were combined using logical Boolean operators. Keywords and their synonyms were combined in each database as follows: (textile OR fabric OR electro-textile) AND (UHF RFID) AND (sensor OR reliability OR feasibility OR sensitivity OR measurement). All results from January 2004 to May 2020 of each database were analyzed and screened to remove duplicates.

The inclusion criteria mainly took into account 5 approaches: (1) The studies that focused on textile UHF-RFID with textile sensing techniques or related reliability researches; (2) the studies that used textile UHF-RFID sensors for certain scenario-based applications; (3) the studies that explored the impact factors on performance for feasibility and reliability of textile UHF-RFID sensors; (4) the papers that are written in English; (5) the selected papers are published in a peer-reviewed journal or presented in a scientific conference.

The exclusion criteria mainly included 2 parts: (1) The papers were not written for reviews or books; (2) the papers only mentioned textile UHF-RFID tags or sensors without reliability researches.

According to the strategy explained above, the selected papers have been classified, as shown in Figure 5. The literature search returned 250 results and the final total of 64 studies fulfilled the inclusion criteria, of which 29.7% focused on basic researches on textile UHF-RFID with textile sensing techniques, 46.9% were related researches on reliability and feasibility and the remaining 23.4% were exploratory researches on scenario-based applications. From the results, the textile UHF-RFID sensors with more research focused on exploring reliability and feasibility and less on real applications are expected to get more attention and have notable potential in the future.

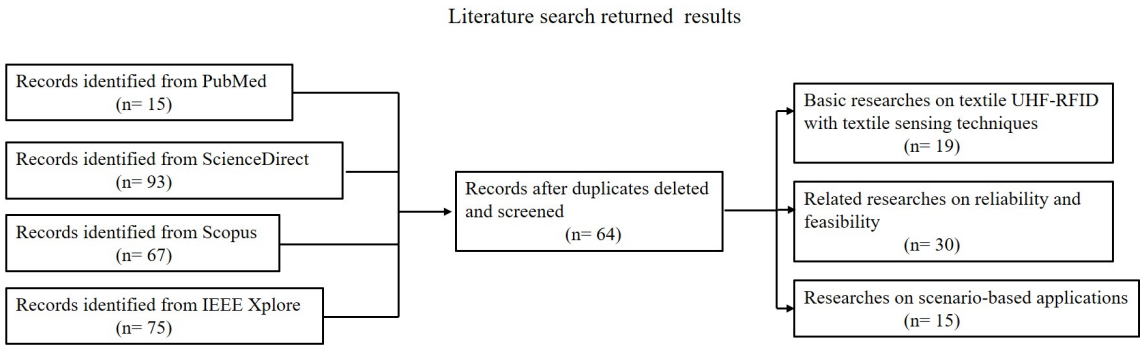

Figure 5. Flow diagram of paper selection.

5. Development of Textile UHF-RFID Sensors

Since the standard EPC Gen2 was first published in 2004, the physical and logical requirements for UHF RFID tags and readers have been defined, which give researchers a basic framework to design a UHF-RFID system integrating many kinds of sensors for different applications. In the beginning, in the

textile industrial field, the UHF-RFID technique was mainly applied for identification purposes for application such as clothing manufacturing, inventory control, warehousing, distribution, logistics and automatic object tracking. Currently, UHF-RFID tags are gradually used for daily living applications with sensing capabilities.

As shown in Figure 6, a brief history of textile UHF-RFID and sensing technologies preceding current UHF-RFID sensors is provided. From 2007 to 2010, the textile UHF-RFID technique was not yet mature and it was mainly focused on feasibility and simple applications with just tags, such as size-optimizing exploration for the textile UHF-RFID antenna in Figure 6a, accessories trace and production process monitor in Figure 6b and exploration for the relation between conductivity and different sewing methods in Figure 6c,d. Then from 2010 to 2015, the textile UHF-RFID technique was gradually applied for simply sensing uses with just the UHF-RFID antennas and ICs, such as the textile UHF-RFID strain sensors for monitoring human bodily functions and movements, as shown in Figure 6e,f, textile UHF-RFID tag for performance exploration in Figure 6g, RSS-based passive UHF-RFID for indoor localization applications in Figure 6h and textile UHF-RFID with broad impedance bandwidth for tire performance monitoring in Figure 6i. Up to now, textile UHF-RFID integrated with textile sensors has been getting more attention, and many novel textile materials on different kinds of sensing fields have been tested. There are some typical applications, such as UHF-RFID strain sensors with copper-coated fabric, as shown in Figure 6j, graphene-based UHF-RFID sensors for moisture monitoring in Figure 6k and sweat sensing in Figure 6l, silver-plated thread UHF-RFID sensors for environment humidity monitoring in Figure 6m,n, accelerometer-based UHF-RFID sensor for patients' activity recognition in Figure 6o, and equally important, reliability exploration in Figure 6p.

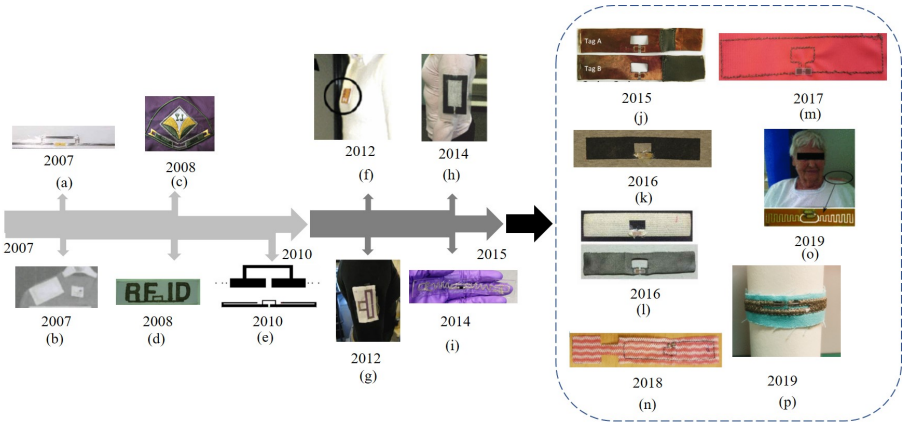

Figure 6. Brief history of textile UHF-RFID and sensing technologies. (**a**) Flexible electro-thread UHF-RFID tag antenna designed using the T-matching method, with a read range of about 2.4 m (adapted from ref. [23]). (**b**) Textile UHF-RFID tag for accessories trace and production process monitor, attached on a garment (adapted from ref. [56]). (**c**) Fabricated 'YJ' symbol type textile UHF-RFID tag for exploring different shapes of embroidery tag antenna (adapted from ref. [57]). (**d**) Fabricated 'RFID' symbol textile UHF-RFID tag for analyzing the changes of conductivity for different sewing methods (adapted from ref. [58]). (**e**) Textile UHF-RFID strain sensor for human bodily functions and movement monitoring, fabricated by screen printing the ink on stretchable PVC and on fabric substrates (adapted from ref. [11]). (**f**) Textile UHF-RFID strain sensor for human movement monitoring and feasibility of effective data interaction (adapted from ref. [59]). (**g**) Textile UHF-RFID tag for performance exploration, mainly validated by the read range (adapted from ref. [60]). (**h**) Textile UHF-RFID tag for positioning and localization through recording and analyzing on-body readability and Received Signal Strength (RSS) in an office environment (adapted from ref. [61]). (**i**) E-fiber UHF-RFID broadband tag for tie health information monitor, fabricated on conductive textiles and embedded into polymer (adapted from ref. [62]). (**j**) Textile UHF-RFID strain sensor for exploring the relation between the antenna elongation and its backscatter strength, based on a stretchable antenna made of conductive fabrics (adapted from ref. [63]). (**k**) Graphene-based UHF-RFID tag on a fabric substrate for exploring feasibility and reliability of the low-cost and eco-friendly graphene tag (adapted from ref. [12]). (**l**) Health-care-based UHF-RFID sweat sensor for sweat rate measurements in exercise, by comparing the silver plated sample and the graphene-printed sample (adapted from ref. [6]). (**m**) Health-care-based textile UHF-RFID moisture sensor for body moisture sensing (adapted from ref. [64]). (**n**) Environment-based textile UHF-RFID moisture sensor for humility detection, with a sensor part and an antenna part (adapted from ref. [65]). (**o**) Health-care-based textile UHF-RFID accelerometer sensor for alerting on hospitalized patient bed exits with a super low resolution (adapted from ref. [9]). (**p**) Textile UHF-RFID tag for exploring the impact from geometrical variations and deformations (adapted from ref. [66]).

5.1. State-of-the-Art of Textile UHF-RFID Sensors Applications

In modern society, electronic devices are always closely relevant to specific application fields. The rule is also suitable for current researches of textile UHF-RFID sensors. The UHF-RFID technique started to be applied in combination with the textile technique and then textile sensors about 15 years ago. However, up to now there have not been enough research achievements applied for current production and living, which also means the huge development prospect is worth paying attention to.

A medical-based UHF-RFID body-worn sensor was fabricated and tested for monitoring fluid accumulation in the lungs, which was integrated as part of the garment on various locations such as front, back and shoulders, as shown in Figure 7a [67]. In this work, textiles made by e-fabrics (conductive polymer fibers) were evaluated with a microstrip transmission line structure, which demonstrates the e-fiber transmission line surface had electrical equivalence to metallic but inflexible surfaces of copper transmission lines. Note that some useful fabrication methods were adopted, such as bundled fibers for improving conductivity and assistant yarn for avoiding abrasion damage of the silver coatings on the e-fiber's polymer core. The important achievement was to use

the same e-fibers to fabricate the medical-based UHF-RFID body-worn sensor for lung monitoring. In addition, textile versions were found to be nearly equivalent to the metal one even after being repetitively flexed, washed, and dried. This work gave a pioneering application for textile sensors for lung monitoring in medical-based fields.

For the flexible feature of textiles, a deformation-monitoring-based UHF-RFID strain sensor was proposed for structural health monitoring applications, as shown in Figure 7b [68]. In this work, a novel dual-interrogation mode was applied for the design of the textile UHF-RFID strain sensor, which provided a large identification coding capacity for the UHF-RFID sensor. The dual-interrogation mode consisted of reading range extraction mode for the threshold-power-required chip-enabled approach and RCS-based (radar cross section) sensing mode for the chipless approach. In fact, the range extraction mode relied on the read range changing with the applied strain, while the RCS-based sensing mode was directly linked to the frequency shift depending on the strain changing. Note that here the strain was related to the electrical length of embroidered UHF-RFID sensor structures. This work proved the feasibility of double modes for the design of textile UHF-RFID strain sensors and it is worth considering in future research, but certainly, some important validation measurements such as bending, environment impacts and washing for the performance and reliability need to be considered.

In another example of the textile UHF-RFID strain sensor, as shown in Figure 7c [69], a notable evaluation for the elongation from an attached object was implemented, compared to the last example in Figure 7b. This textile UHF-RFID strain sensor was based on silver-plated material fabricated by plain knitting and designed into two separate parts, the feeding loop and the radiating antenna. This design makes the radiating antenna part fully stretchable while the IC attached to the feeding loop could be non-stretchable, which avoids the reliability challenges caused by mechanical stresses from clothing-integrated electronics. In this work, this textile UHF-RFID strain sensor was integrated on the shirt, the performance of which was examined on-body by means of backscattered signal power measurements under strain and in unloaded conditions. The results revealed that the strain sensitivity was great and the achievements had the potential for future smart monitoring applications. However, for real applications such as a controller in an embodied game, as mentioned in the paper, some safety and reliability validation measurements were expected to be considered, such as the performance impact after washing or working in a high electromagnetic interference (EMI) area.

These above three current kinds of research actually make use of the flexible feature of textile UHF-RFID sensors, which also lead our way to do related researches on this area. In addition to this feature, it is worth knowing that there are many potential features that push the researches on textile UHF-RFID sensors forward.

There is another example for textile UHF-RFID sensors that are sensitive to humidity. As shown in Figure 7d [65], it is an environment-based textile UHF-RFID moisture sensor fabricated on a very common substrate thin single-use dishcloth, which consisted of a sensor part and UHF-RFID antenna part. In this work, the performance of the textile UHF-RFID moisture sensor was evaluated by 10 drops of water from wet state to dry state and the evaluation parameter was the read range in office conditions after 5, 10, and 15 min. The result showed the small changes of the read range from 4.7 m in the dry state and 5.2 m in the wet state. From the result, this textile UHF-RFID moisture sensor had certain moisture detection ability, however the changes of the read range were small relative to the humility from 10 drops of water and the impact from impurities in water also needed to be considered. Thus, this kind of application research had the potential to be focused on in the future.

Compared with the textile UHF-RFID moisture sensor mentioned in Figure 7d, another example of textile UHF-RFID moisture sensors is shown in Figure 7e [70], which is only a textile UHF-RFID tag with moisture sensor functionality. In this work, textile UHF-RFID sensors could curve automatically and permanently after being dipped into the water due to the special material, polyvinyl alcohol (PVA). Note that in contrast to the example in Figure 7d, the test parameter in this work was the change in the backscattered power percentage, which could be measured and compared in order to detect and record the presence of moisture. The comparative measurements in this work proved the results

reliable, which showed the potential of the textile UHF-RFID sensors to be applied in environment moisture detection.

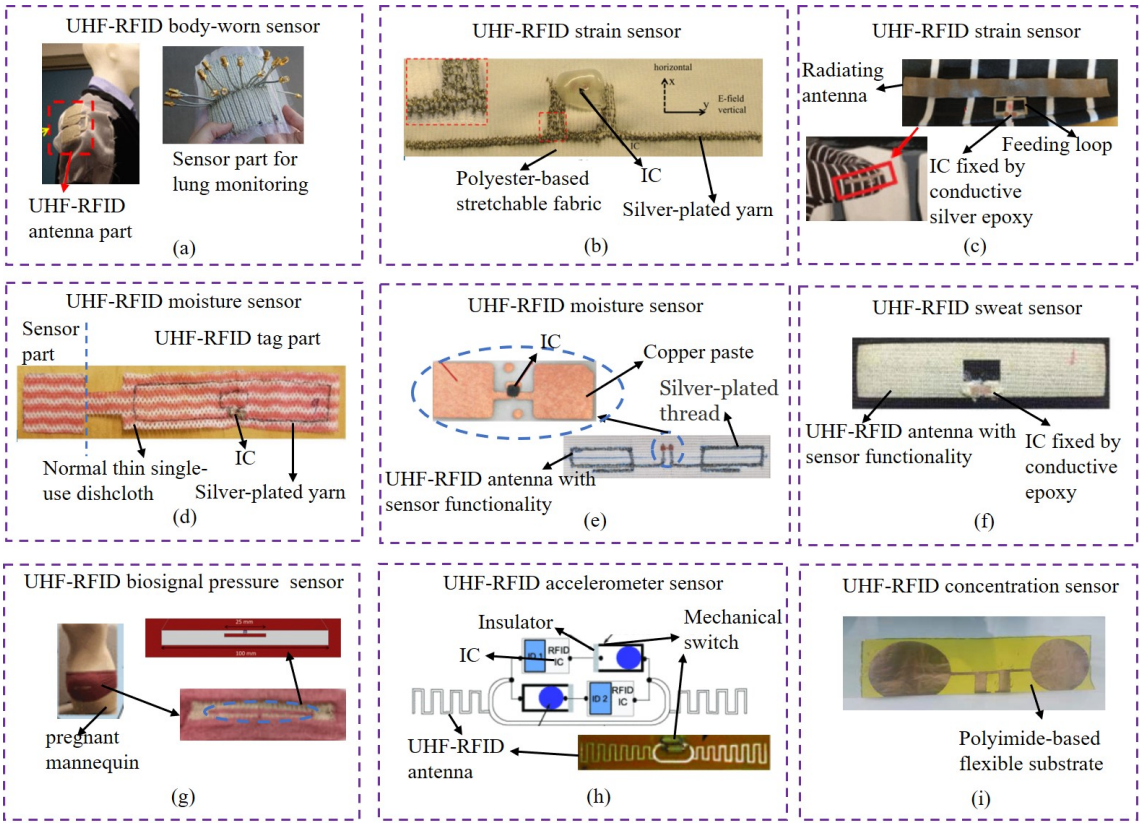

Figure 7. Typical textile UHF-RFID sensor applications. (**a**) Medical-based UHF-RFID body-worn sensor for lung monitoring integrated as part of the garment, with real representation of antenna and sensing array configuration (adapted from ref. [67]); (**b**) deformation-monitoring-based UHF-RFID strain sensor for structural health monitoring applications, with dual-interrogation mode consisting of read range extraction mode and RCS-based sensing mode (adapted from ref. [68]); (**c**) exercise-based textile UHF-RFID strain sensor for movement monitoring attached on a cotton-based shirt, with a non-stretchable feeding loop and a stretchable radiating antenna (adapted from ref. [69]); (**d**) environment-based textile UHF-RFID moisture sensor for humility detection, with a sensor part and an antenna part (adapted from ref. [65]); (**e**) environment-based textile UHF-RFID moisture sensor for environment humility detection, with a humility sensitive UHF-RFID antenna (adapted from ref. [70]); (**f**) health-care-based textile UHF-RFID sweat sensor for sweat rate measurements, with a tag as the sensing part made by screen printing technique (adapted from ref. [6]); (**g**) health-care-based textile UHF-RFID biosignal pressure sensors for infant heart monitoring, integrated with a modular software framework for interrogation, data storage and post-processing [7,8]); (**h**) health-care-based textile UHF-RFID accelerometer sensor for alerting on hospitalized patient bed exits with a superlow resolution (adapted from ref. [9]); (**i**) textile UHF-RFID concentration sensor for concentration detection using a sensing antenna (adapted from ref. [10]).

In the health-care monitoring field, many kinds of common wearable UHF-RFID sensors on flexible substrates, such as the flexible printed circuit board (FPCB), have been proposed and applied for commercial health-care monitoring applications, whereas textile UHF-RFID sensors for this area are still in the early stages and most investigations for health-care application are at the stage of laboratory research. For example, a health-care-based textile UHF-RFID sweat sensor was proposed for sweat rate measurements, as shown in Figure 7f [6]. In this work, the textile UHF-RFID sweat sensor made by screen printing had a noticeable difference in the response of backscattered signal power. The paper explains that the response curves differences are caused by the conductive antenna impedance and

material parameter of the textile substrate changing due to the absorbed sweat. This work indicates the high potential of textile UHF-RFID technology in perspiration sensing, but related sweat components were not analyzed, which were attractive and worth considering.

In another example of the health-care-based textile UHF-RFID biosignal pressure sensors, reliable and secure manner for real-time medical data collection was considered by a software framework, which fills the gap between data safety and textile UHF-RFID sensors for health-care monitoring. As shown in Figure 7g [7,8], the textile UHF-RFID biosignal pressure sensor named bellyband sensor for infant heart monitoring in the paper was applied on a pregnant mannequin driven by proprietary software to simulate various behaviors. In addition, a modular software framework was developed to both interrogate sensor devices and to store that streaming data for live and post-processing. In this work, considering the missed tag reads, two impact factors were found. One was the delay caused by periodic frequency hopping and another one was the greater distance between the tag and the reader. These research achievements are helpful for future applications, but more other impact factors need to be tested such as the comfort and electromagnetic safety for pregnant women and infants.

In addition to textile UHF-RFID sweat sensors for sweat rate measurements and biosignal pressure sensors for infant heart monitoring, another health-care-based textile UHF-RFID accelerometer sensor, as shown in Figure 7h, was proposed for alerting on hospitalized patient bed exits, which could work under a super low resolution. In this work, the sensing device could capture ultra low resolution acceleration data from patients and be analyzed by deep convolutional neural network (CNN) architectures automatically to get the discriminate features. The advances of this work were to combine the textile UHF-RFID accelerometer sensor with neural network approaches, which make the low resolution kinematic sensor possible. This is a mature and useful textile UHF-RFID accelerometer sensor, though the reliability of some components such as the mechanical switch in this sensor device needs to be tested.

The last typical example, as shown in Figure 7i, is a textile UHF-RFID concentration sensor for concentration detection. In this work, the UHF-RFID concentration sensor was printed on a special textile material, which is polyimide flexible substrate, while the sensing antenna was made of copper. The proposed sample is sensitive to the frequency and the concentration of the NaCl solutions and sucrose solutions. Moreover, from the measurement results in the paper, the author proposed that the sensitivity increases with the increase in the percentages of the NaCl and sucrose in water. Although in the work there is no accurate application mentioned, it can give us a research orientation for using total textile UHF-RFID concentration sensors to detect elements in human body fluids.

5.2. State of Researches on Reliability of Textile UHF-RFID Sensors

For each technique and related application from start-ups to mature products, the reliability validation is a crucial and necessary step. Currently, for textile UHF-RFID sensors, related reliability researches are constantly advancing with the development of textile UHF-RFID sensors. The reliability researches mainly focus on the impacts from sensitive features of textile UHF-RFID sensors, such as the washing reliability [71–73], corrosion-resisting reliability, strain and bending reliability.

Washing reliability is an inevitable research point, which needs to be considered and tested before applied for real applications. The main damage factors for textile UHF-RFID sensors from washing are the mechanical and the chemical impacts. Some works prove that taken separately, neither mechanical constraints nor chemicals used have a significant impact on a silver-plated-nylon yarn on short terms (<30 washes) but the coupling of aggressive chemicals and the mechanical rubbings inside the machine can have a dramatic impact [74]. Certainly, different textile materials for the designs have different degrees of ability to resist the impacts from washing cycles, while if washing for enough times, devices damages are unavoidable and have a direct impact on the read range [75]. In order to keep the function of devices, protective coating materials are expected to be printed on the devices [76], however some textile glues as a fit conformal coating could not always provide good protection [77]. All in all,

washing reliability is an important evaluation factor for a good textile UHF-RFID sensor, the impact of which can be reduced by reducing washing cycles or using better protective coating materials.

Corrosion-resisting reliability is another impact factor worth considering for the textile UHF-RFID sensors that are specially applied for sweat and other solution concentration monitoring. The impacts from chemicals for washing are proved small when there are no mechanical rubbings as explained in the last paragraph but complex and corrosive solution and body fluids are proved to have a certain influence on the resistance of textile materials and radiation efficiency of the UHF-RFID antenna in the work [78]. Especially for textile UHF-RFID sweat sensors, due to the complex elements in sweat, the measured data will be interfered with through continuous detection. Currently, painting with conductive paint [72] and developing machine learning technique are some popular methods to reduce this kind of impact.

Strain and bending reliability is also an important factor on performance degradation of textile UHF-RFID sensors although some textile UHF-RFID strain sensors utilize this feature to achieve some health-care monitoring applications [7,8]. However, even for this kind of textile UHF-RFID sensor, the most vulnerable part is the connection of antenna and IC, which can cause total failure of systems when it gets damaged. The sewed and glued interconnections still show strain reliability issues that need to be considered and tested after fabrication [79]. However, when the textile UHF-RFID sensors are applied in harsh conditions, generally a suitable coating would be used to protect the antenna-IC interconnection from mechanical stress. In addition, graphene UHF-RFID on textile substrates is proved to have a remarkable and unique response to high reliability in harsh bending conditions [12], which is another potential choice to solve the problem.

In addition of above three typical reliability problems, many other scenario-based reliability researches need to be explored combining actual situations and applications. Textile UHF-RFID sensors are expected to develop and grow more with the coming of the IoT society and increasing of health-care concerns, meanwhile related safety and reliability of the devices always stay in the spotlight.

6. Future Prospects

Textile UHF-RFID sensors are expected to be deployed more on many kinds of fields such as the garment industry, health-caring service industry, sports equipment industry and so on [80]. Due to short development time, textile UHF-RFID sensors still have a long way to go on improving the performance and the futuristic, promising applications and enhancing reliability. Especially for the calling for varieties of IoT applications and the coming-of-age society, more attention needs to be paid to develop useful textile UHF-RFID sensors and close research gaps between laboratory researches and scenario-based textile UHF-RFID sensors.

In the future, the main research focuses in the laboratory are two aspects, one of which is to develop new designs of textile UHF-RFID tags and sensors with common or novel textile materials and manufacturing process [81], and the other to explore novel application scenarios with certain commercial potential.

New designs with novel textile materials and manufacturing processes are always explored but further research on it is still needed. The novel textile materials such as special conductive yarns integrated with graphene as mentioned in [12] and conductive ink on textile substrates [11], are introduced to improve textile UHF-RFID sensor performance and are expected to reduce their cost. Certainly, if the novel textile materials are applied for new designs, related manufacturing processes are needed such as the advanced screen printing technique especially for conductive ink on textile substrates. Compared with the traditional materials and manufacturing processes, the novel ones are still in development and they will require a notable research orientation.

Machine learning technology for textile UHF-RFID sensors is also a novel research direction [82]. As mentioned in [9], a classical machine learning algorithm is used, which is capable of generating probabilistic models using feature vectors extracted from segments. As a part of machine learning, deep neural networks [83] are useful for feature extraction and classifier building when the

textile UHF-RFID sensors are applied in some complex conditions for numerous data analysis. Currently, internet of things (IoT) is a hot topic, in which machine learning technology plays an important role pushing textile UHF-RFID sensor techniques to revolutionize the traditional applications. Textile UHF-RFID sensor techniques integrated with the machine learning technology are expected to have a big application market in the future IoT era.

With regard to the scenario-based applications, textile UHF-RFID sensors have great development potential in many different fields of productions and life. Currently, the main application researches focus on the fundamental functions of textile UHF-RFID sensors such as the ID-sensing, strain sensing [84], humidity sensing, sweat sensing and others. However, advanced functions are not covered. For example, there are exercise-based textile UHF-RFID sweat sensors just for sweat sensing without any elements analyzing, on which further researches are worth implementing. Moreover, textile UHF-RFID sensors are more suitable for medical-based applications due to the various medical textile used for patients or the elderly. Many kinds of medical parameters or body fluids can be detected and analyzed by complete textile UHF-RFID sensing systems. The abundant scenarios can create numerous chances for designs and applications of novel textile UHF-RFID sensors in the future.

In addition, reliability is an unavoidable but crucial research direction especially for this kind of flexible and washing-needed component [85]. For example, after fabricating the designs on textile substrates, the performance of UHF-RFID antenna and sensors may decrease such as the resonant frequency shift and gain penalty due to conformal bending or on-body touching. Moreover, environmental factors such as the well-studied humidity and temperature and human factors such as washing and sweat corrosion can imply certain impacts on performance. In the future, the concomitant reliability researches still need to be considered.

7. Discussion and Conclusions

Textile UHF-RFID sensors have a very promising prospective for the future society in which many scenario-based applications are needed due to the development of IoT and requirements from aging populations. This review mainly presents the fundamentals and current research state of the textile UHF-RFID sensors and proposes related studies over the lack of further investigation.

According to this review, it can be found that there are many aspects of scenarios, in which current textile UHF-RFID sensors need to be further developed in order to achieve necessary functions with high enough reliability. Apart from fundamental functions that are based on the basic features of textile UHF-RFID tags and sensors, further researches on more complex application such as monitoring and diagnosis of medical parameters should be addressed. In order to achieve these targets, novel materials with advanced manufacturing processes are worth exploring and cross-domain integration with machine learning creates a novel research direction.

In conclusion, the textile UHF-RFID sensor technique as a branch of traditional UHF-RFID sensor techniques offers special advantages such as common use of textile materials in many areas and it is expected to continuously attract research efforts based on different scenarios in the forthcoming IoT era and the aging society.

Author Contributions: All authors jointly planned the content of this paper. C.L. conducted the writing and both R.F.-G. and I.G. gave the review and supervision. All authors have read and agreed to the published version of the manuscript.

Funding: This work was supported by Spanish Government-MINECO under Project TEC2016-79465-R and China Scholarship Council No. 201908440233.

Conflicts of Interest: The authors declare no conflict of interest.

References

1. Gil, I.; Fernández-García, R.; Tornero, J.A. Embroidery manufacturing techniques for textile dipole antenna applied to wireless body area network. *Text. Res. J.* **2019**, *89*, 1573–1581. [CrossRef]
2. Wang, L. Inheritance and Innovation of Embroidery in Modern Design. In Proceedings of the 3rd International Conference on Art Studies: Science, Experience, Education, Moscow, Russia, 4–5 October 2019; pp. 232–234.
3. Catrysse, M.; Puers, R.; Hertleer, C. Towards the integration of textile sensors in a wireless monitoring suit. *Sens. Actuator A Phys.* **2004**, *114*, 302–311. [CrossRef]
4. Vieroth, R.; Kallmayer, C.; Aschenbrenner, R. A new package for textile integrated RFID tags. In Proceedings of the 2009 11th Electronics Packaging Technology Conference, Singapore, 9–11 December 2009; pp. 240–243.
5. Merilampi, S.; Björninen, T.; Sydänheimo, L. Passive Uhf Rfid Strain Sensor Tag for Detecting Limb Movement. *Int. J. Smart Sens. Intell. Syst.* **2012**, *5*, 315–328. [CrossRef]
6. Merilampi, S.; He, H.; Sydänheimo, L. The possibilities of passive UHF RFID textile tags as comfortable wearable sweat rate sensors. In Proceedings of the 2016 Progress in Electromagnetic Research Symposium (PIERS), Shanghai, China, 8–11 August 2016; pp. 3984–3987.
7. Patron, D. On the Use of Knitted Antennas and Inductively Coupled RFID Tags for Wearable Applications. *IEEE Trans. Biomed. Circuits. Syst.* **2016**, *10*, 1047–1057. [CrossRef] [PubMed]
8. Mongan, W.M.; Rasheed, I.; Ved, K. On the Use of Radio Frequency Identification for Continuous Biomedical Monitoring. In Proceedings of the 2017 IEEE/ACM Second International Conference on Internet-of-Things Design and Implementation (IoTDI), Pittsburgh, PA, USA, 18–21 April 2017; pp. 197–202.
9. Chesser, M.; Jayatilaka, A.; Visvanathan, R. Super Low Resolution RF Powered Accelerometers for Alerting on Hospitalized Patient Bed Exits. In Proceedings of the IEEE International Conference on Pervasive Computing and Communications, Kyoto, Japan, 11–15 March 2019; pp. 1–10.
10. Ennasar, M.A.; El, Mrabet, O.; Mohamed, K. Design and Characterization of a Broadband Flexible Polyimide RFID Tag Sensor for NaCl and Sugar Detection. *Prog. Electromagn. Res.* **2019**, *94*, 273–283. [CrossRef]
11. Merilampi, S.; Ruuskanen, P.; Björninen, T. Printed passive UHF RFID tags as wearable strain sensors. In Proceedings of the 2010 3rd International Symposium on Applied Sciences in Biomedical and Communication Technologies (ISABEL 2010), Rome, Italy, 7–10 November 2010; pp. 1–5.
12. Akbari, M.; Virkki, J.; Sydänheimo, L. Toward Graphene-Based Passive UHF RFID Textile Tags: A Reliability Study. *IEEE Trans. Device Mater. Reliab.* **2016**, *16*, 429–431. [CrossRef]
13. Rocha, G.S.; Silva, M.K.L.; Cesarino, I. Reduced Graphene Oxide-Based Impedimetric Immunosensor for Detection of Enterotoxin A in Milk Samples. *Materials* **2020**, *13*, 1751. [CrossRef]
14. Björninen, T.; Virkki, J.; Sydänheimo, L. Manufacturing of antennas for passive UHF RFID tags by direct write dispensing of copper and silver inks on textiles. In Proceedings of the 2015 International Conference on Electromagnetics in Advanced Applications (ICEAA), Turin, Italy, 7–11 September 2015; pp. 589–592.
15. Lugoda, P.; Costa, J.C.; Oliveira, C.; Garcia-Garcia, L.A.; Wickramasinghe, S.D.; Pouryazdan, A.; Roggen, D.; Dias, T.; Münzenrieder, N. Flexible Temperature Sensor Integration into E-Textiles Using Different Industrial Yarn Fabrication Processes. *Sensors* **2020**, *20*, 73. [CrossRef]
16. Gong, Z.; Xiang, Z.; Ouyang, X.; Zhang, J.; Lau, N.; Zhou, J.; Chan, C.C. Wearable Fiber Optic Technology Based on Smart Textile: A Review. *Materials* **2019**, *12*, 3311. [CrossRef]
17. Paret, D. Standards for RFID at UHF and SHF. In *RFID at Ultra and Super High Frequencies Theory and Application*; Wiley: Hoboken, NJ, USA, 2009; pp. 369–505.
18. Gaspari, F.; Simone, Q. Nanostructured Materials for RFID Sensors. In *Nanomaterials Design for Sensing Applications*; Elsevier: Amsterdam, The Netherlands, 2019; pp. 93–128.
19. Sazonov, E. *Wearable Sensors: Fundamentals, Implementation and Applications*; Elsevier: Amsterdam, The Netherlands, 2014.
20. Marian, V.; Allard, B.; Vollaire, C. Strategy for microwave energy harvesting from ambient field or a feeding source. *IEEE Trans. Power Electron.* **2012**, *27*, 4481–4491. [CrossRef]
21. Fuschini, F.; Piersanti, C.; Paolazzi, F. Analytical approach to the backscattering from UHF RFID transponder. *IEEE Antenn. Wirel. Pr.* **2008**, *7*, 33–35. [CrossRef]
22. Loo, C.H.; Elmahgoub, K.; Yang, F. Chip impedance matching for UHF RFID tag antenna design. *Prog. Electromagn. Res.* **2008**, *81*, 359–370. [CrossRef]

23. Kim, Y.; Lee, K.; Kim, Y.; Chung, Y.C. Wearable UHF RFID tag antenna design using flexible electro-thread and textile. In Proceedings of the 2007 IEEE Antennas and Propagation Society International Symposium, Honolulu, HI, USA, 9–15 June 2007; pp. 5487–5490.
24. Fu, Y.Y.; Chan, Y.L.; Yang, M.H. Experimental study on the washing durability of electro-textile UHF RFID tags. *IEEE Antenn. Wirel. Pr.* **2014**, *14*, 466–469. [CrossRef]
25. Björninen, T.; Virkki, J.; Sydänheimo, L.; Ukkonen, L. Impact of recurrent stretching on the performance of electro-textile UHF RFID tags. In Proceedings of the 5th Electronics System-integration Technology Conference (ESTC), Helsinki, Finland, 16–18 September 2014; pp. 251–255.
26. Björninen, T.; Virkki, J.; Sydänheimo, L. Impact of recurrent washing on the performance of electro-textile UHF RFID tags. In Proceedings of the 2014 IEEE RFID Technology and Applications Conference (RFID-TA), Tampere, Finland, 8–9 September 2014; pp. 251–255.
27. Virkki, J.; Björninen, T.; Kellomäki, T. Reliability of washable wearable screen printed UHF RFID tags. *Microelectron. Reliab.* **2014**, *54*, 840–846. [CrossRef]
28. Laschuk, N.O.; Ebralidze, I.I.; Quaranta, S.; Kerr, S.T.; Egan, J.G.; Gillis, S.; Gaspari, F.; Latini, A.; Zenkina, O.V. Rational design of a material for rapid colorimetric Fe^{2+} detection. *Mater. Des.* **2016**, *107*, 18–25. [CrossRef]
29. Laschuk, N.O.; Obua, A.; Ebralidze, I.I.; Fruehwald, H.M.; Poisson, J.; Egan, J.G.; Gaspari, F.; Naumkin, F.Y.; Easton, E.B.; Zenkina, O.V. Spacer Conjugation and Surface Support Effects in Monolayer Electrochromic Materials. *ACS Appl. Electron. Mater.* **2019**, *8*, 1705–1717. [CrossRef]
30. Quaranta, S.; Giorcelli, M.; Savi, P. Graphene and MWCNT Printed Films: Preparation and RF Electrical Properties Study. *J. Nanomater.* **2019**, *2019*, 1–9. [CrossRef]
31. Ujiie, H. *Digital Printing of Textiles*; Woodhead Publishing: Sawston, UK, 2006.
32. Cie, C. *Ink Jet Textile Printing*; Elsevier: Amsterdam, The Netherlands, 2015.
33. Balanis, C.A. *Antenna Theory: Analysis and Design*; John Wiley and Sons: Hoboken, NJ, USA, 2016.
34. Gravas, I.P.; Zaharis, Z.D.; Lazaridis, P.I.; Yioultsis, T.V.; Kantartzis, N.V.; Antonopoulos, C.S.; Chochliouros, I.P.; Xenos, T.D. Optimal Design of Aperiodic Reconfigurable Antenna Array Suitable for Broadcasting Applications. *Electronics* **2020**, *9*, 818. [CrossRef]
35. Korošak, Ž.; Suhadolnik, N.; Pleteršek, A. The implementation of a low power environmental monitoring and soil moisture measurement system based on UHF RFID. *Sensors* **2019**, *19*, 5527. [CrossRef]
36. Strangfeld, C.; Johann, S.; Bartholmai, M. Smart RFID Sensors Embedded in Building Structures for Early Damage Detection and Long-Term Monitoring. *Sensors* **2019**, *19*, 5514. [CrossRef]
37. Rossi, M.; Liberati, R.M.; Frasca, M.; Richardson, J. Experimental Implementation of a Low-Cost, Fully-Analog Self-Jamming Canceller for UHF RFID Devices. *Electronics* **2020**, *9*, 786. [CrossRef]
38. Zradziński, P.; Karpowicz, J.; Gryz, K.; Ramos, V. An Evaluation of Electromagnetic Exposure While Using Ultra-High Frequency Radiofrequency Identification (UHF RFID) Guns. *Sensors* **2020**, *20*, 202. [CrossRef] [PubMed]
39. El Khamlichi, M.; Alvarez Melcon, A.; El Mrabet, O.; Ennasar, M.A.; Hinojosa, J. Flexible UHF RFID Tag for Blood Tubes Monitoring. *Sensors* **2019**, *19*, 4903. [CrossRef] [PubMed]
40. Wagih, M.; Wei, Y.; Komolafe, A.; Torah, R.; Beeby, S. Reliable UHF Long-Range Textile-Integrated RFID Tag Based on a Compact Flexible Antenna Filament. *Sensors* **2020**, *20*, 3435. [CrossRef] [PubMed]
41. Islam, M.T.; Alam, T.; Yahya, I.; Cho, M. Flexible radio-frequency identification (RFID) tag antenna for sensor applications. *Sensors* **2018**, *18*, 4212. [CrossRef] [PubMed]
42. Chen, X.; Li, B.; Qiao, Y.; Lu, Z. Preparing polypyrrole-coated stretchable textile via low-temperature interfacial polymerization for highly sensitive strain sensor. *Micromachines* **2019**, *10*, 788. [CrossRef]
43. Abbas, B.; Khamas, S.K.; Ismail, A.; Sali, A. Full Embroidery Designed Electro-Textile Wearable Tag Antenna for WBAN Application. *Sensors* **2019**, *19*, 2470. [CrossRef]
44. Yang, T.; Xiong, X.; Petrů, M.; Tan, X.; Kaneko, H.; Militký, J.; Sakuma, A. Theoretical and Experimental Studies on Thermal Properties of Polyester Nonwoven Fibrous Material. *Materials* **2020**, *13*, 2882. [CrossRef]
45. Luo, C.; Fang, W.; Shen, Y.; Qiu, H.; Shao, W.; Hong, Z.; Wang, L.; He, Z.; En, Y. Collocated and simultaneous measurements of RF current and voltage on a trace in a noncontact manner. *IEEE Trans. Microw. Theory. Tech.* **2019**, *67*, 2406–2415. [CrossRef]
46. Liu, Q.; Li, H.; Yu, Y.F.; Zhao, W.S.; Zhang, S. A Novel Finger-Controlled Passive RFID Tag Design for Human–Machine Interaction. *Sensors* **2019**, *19*, 5125. [CrossRef]

47. Hu, J.; Yu, J.; Li, Y.; Liao, X.; Yan, X.; Li, L. Nano Carbon Black-Based High Performance Wearable Pressure Sensors. *Nanomaterials* **2020**, *10*, 664. [CrossRef] [PubMed]
48. Hu, Q.; Memon, H.; Qiu, Y.; Liu, W.; Wei, Y. A Comprehensive Study on the Mechanical Properties of Different 3D Woven Carbon Fiber-Epoxy Composites. *Materials* **2020**, *13*, 2765. [CrossRef] [PubMed]
49. Cho, H.S.; Yang, J.H.; Lee, J.H.; Lee, J.H. Evaluation of Joint Motion Sensing Efficiency According to the Implementation Method of SWCNT-Coated Fabric Motion Sensor. *Sensors* **2020**, *20*, 284. [CrossRef]
50. Ojstršek, A.; Virant, N.; Fox, D.; Krishnan, L.; Cobley, A. The Efficacy of Polymer Coatings for the Protection of Electroless Copper Plated Polyester Fabric. *Polymers* **2020**, *12*, 1277. [CrossRef] [PubMed]
51. Gaubert, V.; Gidik, H.; Koncar, V. Boxer Underwear Incorporating Textile Moisture Sensor to Prevent Nocturnal Enuresis. *Sensor* **2020**, *20*, 3546. [CrossRef] [PubMed]
52. García P.A.; Khoshnam, M.; Menon, C. Wearable Device to Monitor Back Movements Using an Inductive Textile Sensor. *Sensors* **2020**, *20*, 905. [CrossRef] [PubMed]
53. Roberson, D.A.; Wicker, R.B.; Murr, L.E.; Church, K.; MacDonald, E. Microstructural and process characterization of conductive traces printed from Ag particulate inks. *Materials* **2011**, *4*, 963–979. [CrossRef]
54. Ma, Z.; Jiang, Y. High-density 3D printable chipless RFID tag with structure of passive slot rings. *Sensors* **2019**, *19*, 2535. [CrossRef]
55. Liu, S.; Li, Y.; Xing, S.; Liu, L.; Zou, G.; Zhang, P. Structure inheritance in nanoparticle ink direct-writing processes and crack-free nano-copper interconnects printed by a single-run approach. *Materials* **2019**, *12*, 1559. [CrossRef]
56. Nayak, R.; Chatterjee, K.N.; Khurana, G.K.; Khandual, A. RFID: Tagging the new ERA. *Man-Made Text. India* **2007**, *50*, 174–177.
57. Choi, J.; Kim, Y.; Lee, L.; Chung, Y.C. Various wearable embroidery RFID tag antenna using electro-thread. In Proceedings of the 2008 IEEE Antennas and Propagation Society International Symposium, San Diego, CA, USA, 5–11 July 2008; pp. 1–4.
58. Kim G. Design of a UHF RFID fiber tag antenna with electric-thread using a sewing machine. In Proceedings of the Asia-Pacific Microwave Conference (APMC), Macau, China, 16–20 December 2008; pp. 1–4.
59. Manzari, S.; Occhiuzzi, C.; Marrocco, G. Feasibility of Body-Centric Systems Using Passive Textile RFID Tags. *IEEE Antennas Propagat. Mag.* **2012**, *54*, 49–62. [CrossRef]
60. Ukkonen, L.; Sydänheimo, L.; Rahmat-Samii, Y. Sewed textile RFID tag and sensor antennas for on-body use. In Proceedings of the 2012 6th European Conference on Antennas and Propagation (EUCAP), Prague, Czech Republic, 26–30 March 2012; pp. 3450–3454.
61. Koski, K.; Lohan, E.S.; Sydänheimo, L. Electro-textile UHF RFID patch antennas for positioning and localization applications. In Proceedings of the 2014 IEEE RFID Technology and Applications Conference (RFID-TA), Tampere, Finland, 8–9 September 2014; pp. 246–250.
62. Shao, S.; Kiourti, A.; Burkholder, R. Broadband and flexible textile RFID tags for tires. In Proceedings of the 2014 IEEE Antennas and Propagation Society International Symposium (APSURSI), Memphis, TN, USA, 6–11 July 2014; pp. 1507.
63. Long F.Y. Implementation and wireless readout of passive UHF RFID strain sensor tags based on electro-textile antennas. In Proceedings of the 2015 9th European Conference on Antennas and Propagation (EuCAP), Lisbon, Portugal, 13–17 April 2015; pp. 1–5.
64. Shuaib, D.; Ukkonen, L.; Virkki, J. The possibilities of embroidered passive UHF RFID textile tags as wearable moisture sensors. In Proceedings of the 2017 IEEE 5th International Conference on Serious Games and Applications for Health (SeGAH), Perth, WA, USA, 2–4 April 2017; pp. 1–5.
65. Chen, X.; He, H.; Ukkonen, L. Embroidered UHF RFID Moisture Sensor Tag on Dishcloth Substrate. In Proceedings of the 2018 IEEE International Symposium on Antennas and Propagation USNC/URSI National Radio Science Meeting, Boston, MA, USA, 8–13 July 2018; pp. 2009–2010.
66. Yu, M.; Shang, X.; Wang, M. Deformation Sensitivity Study of Embroidered UHF RFID Antennas. In Proceedings of the 2019 IEEE International Conference on RFID Technology and Applications (RFID-TA), Pisa, Italy, 25–27 September 2019; pp. 322–326.
67. Zhang, L.; Wang, Z.; Volakis, J.L. Textile antennas and sensors for body-worn applications. *IEEE Antennas Wirel. Propag. Lett.* **2012**, *11*, 1690–1693. [CrossRef]
68. Hasani, M.; Vena, A.; Sydänheimo, L. Implementation of a dual-interrogation-mode embroidered RFID-enabled strain sensor. *IEEE Antennas Wirel. Propag. Lett.* **2013**, *12*, 1272–1275. [CrossRef]

69. He, H.; Chen, X.; Ukkonen, L. Clothing-Integrated Passive RFID Strain Sensor Platform for Body Movement-Based Controlling. In Proceedings of the 2019 IEEE International Conference on RFID Technology and Applications (RFID-TA), Pisa, Italy, 25–27 September 2019; pp. 236–239.
70. Chen, X.; He, H.; Khan, Z. Textile-Based Batteryless Moisture Sensor. *IEEE Antennas Wirel. Propag. Lett.* **2019**, *19*, 198–202. [CrossRef]
71. Moraru, A.; Ursachi, C.; Helerea, E. A New Washable UHF RFID Tag: Design, Fabrication, and Assessment. *Sensors* **2020**, *20*, 3451. [CrossRef]
72. Guibert, M.; Massicart, A.; Chen, X. Washing reliability of painted, embroidered, and electro-textile wearable RFID tags. In Proceedings of the 2017 Progress in Electromagnetics Research Symposium—Fall (PIERS—FALL), Singapore, 19–22 November 2017; pp. 828–831.
73. Hardy, D.A.; Rahemtulla, Z.; Satharasinghe, A.; Shahidi, A.; Oliveira, C.; Anastasopoulos, I.; Nashed, M.N.; Kgatuke, M.; Komolafe, A.; Torah, R.; et al. Wash Testing of Electronic Yarn. *Materials* **2020**, *13*, 1228. [CrossRef] [PubMed]
74. Gaubert, V.; Gidik, H.; Bodart, N.; Koncar, V. Investigating the Impact of Washing Cycles on Silver-Plated Textile Electrodes: A Complete Study. *Sensors* **2020**, *20*, 1739. [CrossRef] [PubMed]
75. Simorangkir, R.B.V.B.; Le, D.; Björninen, T. Washing Durability of PDMS-Conductive Fabric Composite: Realizing Washable UHF RFID Tags. *IEEE Antennas Wirel. Propag. Lett.* **2019**, *18*, 2572–2576. [CrossRef]
76. Kazmi, A.; Rizwan, M.; Sydänheimo, L. A reliability study of coating materials for brush-painted washable textile RFID tags. In Proceedings of the 2016 6th Electronic System-Integration Technology Conference (ESTC), Grenoble, France, 13–15 September 2016; pp. 1–4.
77. Kazmi, A.; Virkki, J.; Björninen, T. Performance of silver-based textile UHF passive RFID tags after recurrent washing. In Proceedings of the 2016 IEEE International Symposium on Antennas and Propagation (APSURSI), Fajardo, Puerto Rico, 26 June–1 July 2016; pp. 939–940.
78. Sharma, P.; Kan, E.C. Sleep scoring with a UHF RFID tag by near field coherent sensing. In Proceedings of the 2018 IEEE/MTT-S International Microwave Symposium—IMS, Philadelphia, PA, USA, 10–15 June 2018; pp. 1419–1422.
79. Chen, X.; Liu, A.; Wei, Z. Experimental study on strain reliability of embroidered passive UHF RFID textile tag antennas and interconnections. *J. Eng. Technol.* **2017**, *2017*, 8493405. [CrossRef]
80. Bai, Q.; Swaisaenyakorn, S.; Lee, H.-J.; Ford, K.L.; Batchelor, J.C.; Langley, R.J. Investigation of a Switchable Textile Communication System on the Human Body. *Electronics* **2014**, *3*, 491–503. [CrossRef]
81. Van Baelen, D.; Lemey, S.; Verhaevert, J.; Rogier, H. A Novel Manufacturing Process for Compact, Low-Weight and Flexible Ultra-Wideband Cavity Backed Textile Antennas. *Materials* **2018**, *11*, 67. [CrossRef] [PubMed]
82. Cheng, S.; Wang, S.; Guan, W.; Xu, H.; Li, P. 3DLRA: An RFID 3D Indoor Localization Method Based on Deep Learning. *Sensors* **2020**, *20*, 2731. [CrossRef] [PubMed]
83. Puruncajas, B.; Vidal, Y.; Tutivén, C. Vibration-Response-Only Structural Health Monitoring for Offshore Wind Turbine Jacket Foundations via Convolutional Neural Networks. *Sensors* **2020**, *20*, 3429. [CrossRef]
84. Vu, C.C.; Kim, J. Highly Sensitive E-Textile Strain Sensors Enhanced by Geometrical Treatment for Human Monitoring. *Sensors* **2020**, *20*, 2383. [CrossRef] [PubMed]
85. Liu, C.; Liao, X.; Shao, W.; Liu, F.; Ding, B.; Ren, G.; Chu, Y.; He, J. Hot-melt Adhesive Bonding of Polyurethane/Fluorinated Polyurethane/Alkylsilane-Functionalized Graphene Nanofibrous Fabrics with Enhanced Waterproofness, Breathability, and Mechanical Properties. *Polymers* **2020**, *12*, 836. [CrossRef]

IOP Publishing Measurement Science and Technology
Meas. Sci. Technol. **32** (2021) 105112 (9pp) https://doi.org/10.1088/1361-6501/ac0ca7

Textile UHF-RFID antenna sensor for measurements of sucrose solutions in different levels of concentration

Chengyang Luo* , **Ignacio Gil** and **Raúl Fernández-García***

Department of Electronic Engineering, Universitat Politecnica de Catalunya, Barcelona 08222, Spain

E-mail: chengyang.luo@upc.edu and raul.fernandez-garcia@upc.edu

Received 27 April 2021, revised 7 June 2021
Accepted for publication 18 June 2021
Published 2 July 2021

Abstract

With the trend of textile antennas development, ultra high frequency (UHF, 865–868 MHz) radio frequency identification (RFID) devices using textile materials are expected to be developed in many areas for replacing or simplifying some complex RFID devices on a PCB. In this paper, we present a textile UHF-RFID tag with two sensing positions ('radiation parts' and 'loop part') for exploring the feasibility of sucrose solutions measurements and the relationship between variables of the proposed design and the sucrose solutions. The simulated and measured resonance curves of the designs both match well (—20 dB in the simulation and – 15.8 dB in the measurement at 868 MHz) and the read range measured by the RFID reader (M6e kit) is 1.71 m in air. Before the tests by the solutions on the proposed designs, a test board is developed as a preparation work for confirming the relative dielectric constants of the sensing substrate area in the real measurements. Compare the results of the simulation and the real tests, the proposed design shows good feasibility by comparing the simulated and measured results in confirmed relative dielectric constants. Moreover, its two sensing positions have different sensing features. The sensing 'radiation parts' position shows a stable frequency operation performance but sensing range is from 1.71 m (dry) to 2.3 m, while the sensing 'loop part' position has a wide sensing range from 0.4 m to 1.71 m (dry) but a lower frequency operation performance.

Keywords: textile, radio frequency identification (RFID), ultra high (UHF) frequency, sucrose solution, concentration, read range, relative dielectric constant

(Some figures may appear in colour only in the online journal)

Textile UHF-RFID Antenna Embroidered on Surgical Masks for Future Textile Sensing Applications

Chengyang Luo, *Member, IEEE,* Ignacio Gil, and Raúl Fernández-García

***Abstract*—Ultra High Frequency (UHF, 865-868 MHz) Radio Frequency Identification (RFID) devices are expected to be implemented in many health-caring areas. In this paper, we present three progressive designs of textile UHF-RFID antennas on surgical masks using a function-extensible integrated circuit (IC) chip (Rocky 100). The simulated and measured resonance curves of the designs all match well ($|S_{11}| <$ -20 dB at 868 MHz) and the maximum realized gain are improved progressively in order to overcome the difficulty of the chip low sensitivity and increase the maximum read range. The best type (Design 3) is selected and its read range measured by the RFID reader (M6e kit) can reach 2.5 m in air. In addition, several reliability validation measurements are performed, such as bending and skin contact, and maximum read range can reach 1.1 m considering the on-body worn worst case. The proposed Design 3 allows common use as a tag for tracking or safe distance alert under an epidemic situation. Alternatively, for the used function-extensible chip, the design can be applied to many different types of sensors for various application scenarios.**

***Index Terms*—Textile, Ultra High Frequency Radio Frequency Identification (UHF-RFID), textile antenna, conductive yarns, surgical masks, bending, skin contact, backscattering, read range, Rocky 100, M6e kit**

I. Introduction

In modern society, Radio Frequency Identification (RFID) technology is essential in diverse applications [1] [2] [3] such as the goods classification, industrial process monitoring [4], transportation [5], localization and stuff management [6]. Most of them are developed on a hard or flexible Printed Circuit Board (PCB) with popular circuit (IC) chips such as EM4237SLIC, SL3S5002N0FUD and Monza R6. In addition, some tags can be designed to connect sensors with different functions [7]. For these types of RFID sensors, IC chips need to have extendable ports for sensors connection and optional power interface. Compared with the common Ultra High Frequency (UHF, 865-868 MHz) RFID tags and sensors on PCB, the majority of textile UHF-RFID tags and sensors are embroidered by conductive yarns on textile substrates [2] [8], which is different with the copper on PCB. On the one hand, the textile tags can be developed on common clothes which are more comfortable and lighter than those based on PCB inserted into clothes. On the other hand, the conductive yarns and textile substrates are sensitive to the environmental factors such as humidity [9], temperature, bending and washing [10] [11]. As a result, before addressing the electromagnetic simulation design, the parameters of the materials such as permittivity, loss tangent and thickness need to be confirmed. After the designs are embroidered, related reliability tests need to be operated.

Some textile RFID tags and sensors are designed with two-pad IC chips which are small and more sensitive to wake up. However, these types of chips with two pads and low wake-up power are especially used as ID textile tags [14]. The related sensing functions can be only explored by the features of textile materials, which limits the sensing applications. For example, the textile antenna (Bellyband antenna) [16] designed with the IC chip Murata Magicstrap LMXS31ACNA-011 is used as a tag with a strain sensing function. In addition, there is no other interface for extensional sensing functions and on-body read range is only 0.6 m [18]. As a result, exploring the possibility and reliability of the function-extensible IC chips is also a novel research orientation.

Moreover, for the special features of textile materials [12], related UHF-RFID tags and sensors for health-caring monitoring [13] [14] and diagnosis [15] are of growing concern in recent years. Most of them are used in health-caring applications such as breath monitoring for pregnant women or babies [16], move tracking for patients [19] and temperature monitoring. However, for the future aging society and Internet of Things (IOT) development, novel applications for health-caring areas based on textile UHF-RFID sensing technology are expected to be explored and related challenges such as the function-extensible IC chips used on textile materials need to be overcome.

In this paper, considering a general epidemic situation in which the surgical masks are frequently used for human beings protection, we develop three progressive designs of textile UHF-RFID antennas on surgical masks and the used IC chip (Rocky 100) is extensible for different sensors. Related preparatory work before simulation such as the permittivity, loss tangent, thickness measurements and detailed embroidery method is implemented and presented. We explain the progress of the three designs through comparison between their simulated resonance and radiation performance. For the measurements of the impedance and read range, we compare the results to the electromagnetic simulations to validate their performance. Finally, we apply the selected sample to

Manuscript received Month DD, YYYY; revised Month DD, YYYY; accepted Month DD, YYYY. This work was supported in part by Spanish Government-MINECO under Project TEC2016-79465-R, and China Scholarship Council under Grant No.201908440233. Corresponding authors: Raúl Fernández-García.

The authors are with Department of Electronic Engineering, Universitat Politecnica de Catalunya, Barcelona 08222, Spain (e-mail: raul.fernandez-garcia@upc.edu; chengyang.luo@upc.edu).

validate the reliability by the tests under bending and skin-contact situations. The basic use of the designs is the user identification, Nevertheless, due to the function extensibility of the chips, various textile sensors can be included under specific scenarios.

II. Design and Related Work

A. Progressive textile UHF-RFID designs

The textile UHF-RFID antennas are designed on surgical masks and the configuration of the proposed progressive designs are shown in Fig.1. Considering the used chip (Rocky 100) with a capacitive impedance of 64-i*469 ohm, the proposed antennas are expected to be designed with an inductive behavior. Note that for UHF-RFID chips with complex impedance, the corresponding antenna design way is different from conventional antenna design experience (such as W11<<L11 for a conventional folded dipole) with a feed port of 50 ohm. Therefore, a loop structure for matching as shown in Fig. 1 (a) has been selected as a design strategy. Then through an electromagnetic field analysis as illustrated in next section and typical 'T-match' structure analysis [17], the progressive structures, Design 2 and 3 are developed as shown in Fig. 1 (b) and (c), respectively. As a consequence, the Design 3 is derived from the simple 'T-match' structure with 'circular end caps' for increasing the radiation property (directivity and realized gain). The size parameters are detailed in Table I. All of the designs are embroidered using conductive yarns as antennas and surgical masks as substrates. The textile material of the antennas is a commercial conductive twisted yarn (Shieldex 117/17 dtex 2-ply) made of 99% pure silver-plated Nylon (bulk conductivity: 11500 siemens/m). Moreover, as shown in Fig. 1 (c), the UHF-RFID chip (Rocky 100) is sewed by Nylon yarn which is not conductive and fixed by a type of glue (G-15). The substrate is a type of common surgical masks made of staple fibres (short) and long fibres (continuous long).

Due to the non-rigid geometry of the surgical mask and its electrical parameters such as permittivity (ε_r) and loss tangent ($tan\theta$), the surgical mask has an effect on the UHF-RFID antenna performance. In addition, ε_r and $tan\theta$ are two essential parameters for simulation and in order to obtain more accurate values, the two parameters of the masks (ε_r: 1.1439 and $tan\theta$: 0.0001265) are measured by a split post dielectric resonator with a Microwave Frequency Q-Meter as shown in Fig. 2. On the other hand, its thickness ($Thic_r$ = 0.62 mm) can be measured by the Electronics Outside Micrometer (132-01-040A) which has 0 - 25 mm read range and 0.001 mm resolution of digit.

TABLE I
Size Parameters of the Designs (Unit: mm)

$Type$	L_{11}	W_{11}	T_{11}		
$Design\ 1$	34	21	2		
$Type$	L_{21}	L_{22}	W_{21}	T_{21}	
$Design\ 2$	33	22	20	2	
$Type$	L_{31}	L_{32}	W_{31}	T_{31}	R_{31}
$Design\ 3$	27	20	20	2	10

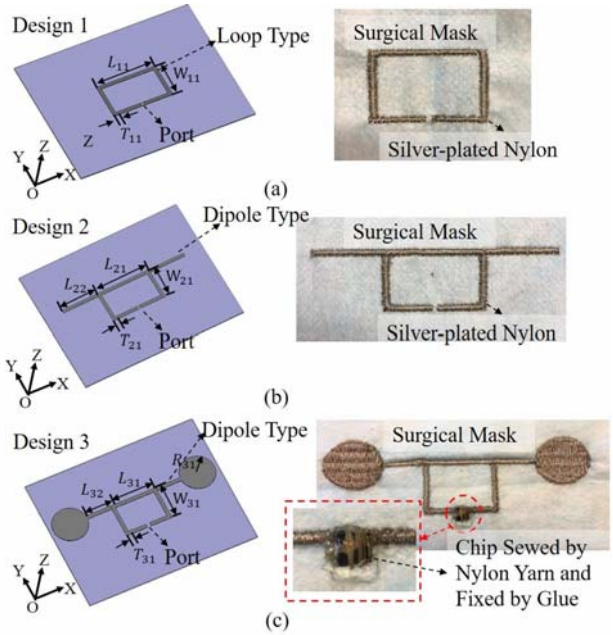

Fig. 1. Configuration of the proposed progressive designs. (a)loop type, (b) dipole type with balanced 'arms', (c) dipole type with balanced 'circular end caps'.

In addition, note that the UHF-RFID chip (Rocky 100) is selected for the work, which is different from the chips used in most textile/knitted wearable UHF-RFID tags. The Rocky 100 chip is normally used for UHF-RFID sensors on PCB. In other words, this chip has several pads (16 pads) which can be used for sensors connection in active/passive situations for many different sensing applications. Compared with some popular chips such as Monza R6 with two pads, the Rocky 100 has a lower sensitivity (minimum wake-up power) of -10 dBm, while Monza R6 has higher sensitivity of about -20 dBm. As a result, the UHF-RFID antenna needs to be designed for higher gain and good conjugate impedance match with the chip.

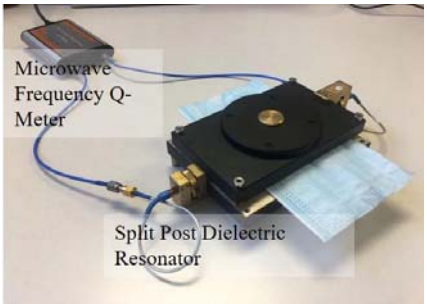

Fig. 2. Substrate permittivity and loss tangent measurements.

B. Method for Impedance Measurements

For balanced antennas, a popular method for impedance measurements is to combine the function (port extension) of the Microwave Analyzer (N9916A) with the common-earth cables as shown in Fig. 3. This method was validated in some

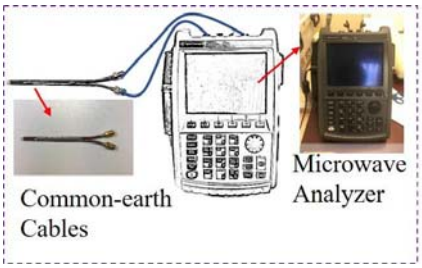

Fig. 3. Calibration setup with the common-earth cables for impedance measurements method.

works [20] [21] [22]. Concerning to the procedure, first of all, the Microwave Analyzer with two professional cables needs to be calibrated by a standard calibration kit. Secondly, after connecting the professional cables to the common-earth cables, the function (port extension) of the Microwave Analyzer needs to be adjusted in order to move the calibration plane from the ends of the professional cables to the ends of the common-earth cables. And then, the traces in smith chart of the two ports should roughly converge to the open circuit position in Microwave Analyzer.. Next, the two tips of the common-earth cables are connected to the proposed textile UHF-RFID antennas and the S parameters in 50 ohms can be obtained. Note that the measured S parameters using the common-earth cables are earth-referenced and need to be transferred for the differential reflection coefficient (ρ) of the antennas. Finally, Z parameters of the tested antennas and the differential reflection coefficient (ρ) in the complex conjugate impedance of the chip can be calculated using the equations 1 and 2 as follows,

$$Z_{ant} = \frac{2Z_0(1 - S_{11}S_{22} + S_{12}S_{21} - S_{12} - S_{21})}{(1 - S_{11})(1 - S_{22}) - S_{12}S_{21}} \quad (1)$$

Where Z_0 is 50 ohms, S_{11}, S_{12}, S_{21} and S_{22} are the measured S parameters, Z_{ant} is the Z parameters of the tested antennas. And,

$$\rho = \frac{Z_{ant} - Z^*_{chip}}{Z_{ant} + Z^*_{chip}} \quad (2)$$

Where Z^*_{chip} is the conjugate impedance(64+i*469) of the chip and ρ is the differential reflection coefficient (also called S_{11}) in the complex conjugate impedance of the chip.

III. Simulation and Analysis

Considering that the complex impedance of the used chip (Rocky 100) is 64-i*469 ohm, the impedance of the designed antenna should be close to 64+i*469 ohm. Note that the chip has higher resistance and reactance than that of some two-pad UHF-RFID chips such as the Monza R6 with the complex impedance of 12-i*120 ohm. In some antenna designs, resistance and reactance curves for antennas present fast-changing slopes and larger tangent, which means that the resistance and reactance values change sensitively. Hence in order to reduce the effects on frequency bandwidth of antenna designs, it is more important that the designed antenna can have a good conjugate impedance match with the chip [23] [24], which implies that the designed antennas need to have complex impedance with the conjugate impedance of the chip as close as possible. In addition, the differential reflection coefficient (ρ) of the work band should be lower than -10 dB.

In addition, as mentioned in previous section, although the function-extensible feature of the chip (Rocky 100) is attractive, its lower sensitivity still needs to be considered. Therefore, the UHF-RFID antenna needs to be designed to achieve a realized gain as high as possible (at least higher than -3 dBi). For the proposed three designs, one of the targets is to improve the gain but reduce the impact on the conjugate impedance match. As a results, the Design 1, 2 and 3 are optimized progressively. After being optimized, the three designs are shown in Fig.1 and the final size parameters are shown in Table I.

A. Resonance Analysis

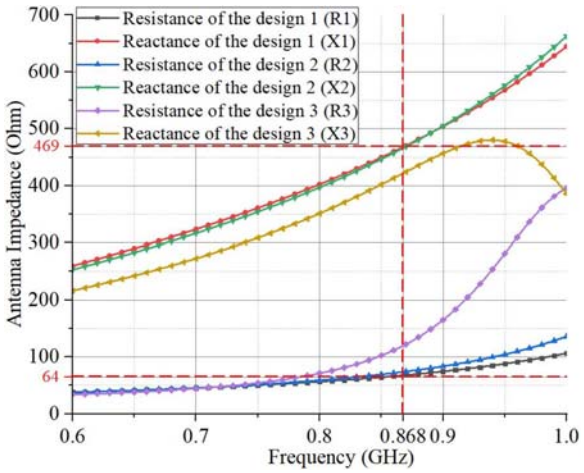

Fig. 4. Simulated impedance for the three progressive designs (Dashed lines: required antenna complex impedance 64+i*469 ohm at 868 MHz).

Fig. 4 shows the simulated impedance for the three progressive designs, including the resistance and reactance curves. The three designs behave inductively at the resonance frequency (868 MHz), in which the closer two to the feed impedance are the Design 1 and 2 with impedance of 67+i*468 ohm and 74+i*466 ohm, respectively. The Design 2 can be developed by a size-optimized Design 1 with balanced 'arms'. By adding the circular end caps to the Design 2 and optimizing the size parameters, Design 3 has impedance of 119+i*421 ohm. Although the impedance match seems to degrade from Design 1 to 3, the reflection coefficients of the three designs as shown in Fig. 5 are still within acceptable limits. In addition, the 'arms' and the 'circular end caps' are expected to increase the antenna gain.

In detail, the S parameters (reflection coefficients) of the three designs as shown in Fig. 5 are all under the -10 dB at 868 MHz. At resonance point (868 MHz), the Design 1, 2 and 3 have reflection coefficients of -48 dB, -39 dB and -22 dB, respectively. The Design 1 and 2 present a bandwidth of at least 400 MHz (Design 1: 560 MHz and Design 2: 515 MHz), while Design 3 have a bandwidth of 370 MHz. In addition, transmission coefficients (τ) for the Design 1, 2 and 3 can be

calculated as 0.9992, 0.9945 and 0.8519, respectively. Due to the basic features of general textile materials, environmental factors often make influence on the resonance frequency of the textile UHF-RFID antennas. As a result, the bigger bandwidth can improve reliability when the resonance frequency shifts within a certain range.

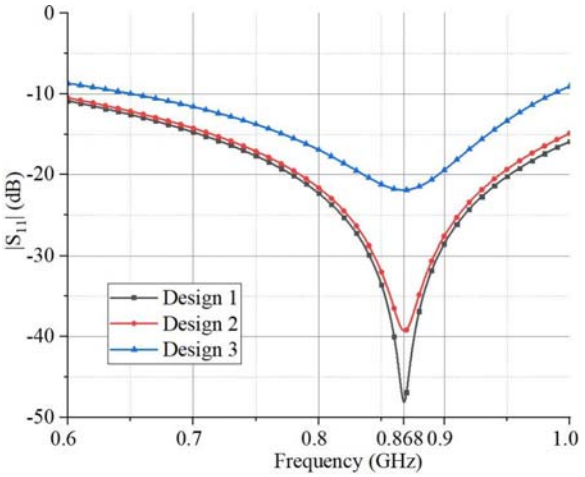

Fig. 5. Simulated reflection coefficients for the three progressive designs.

B. Radiation Performance Comparison

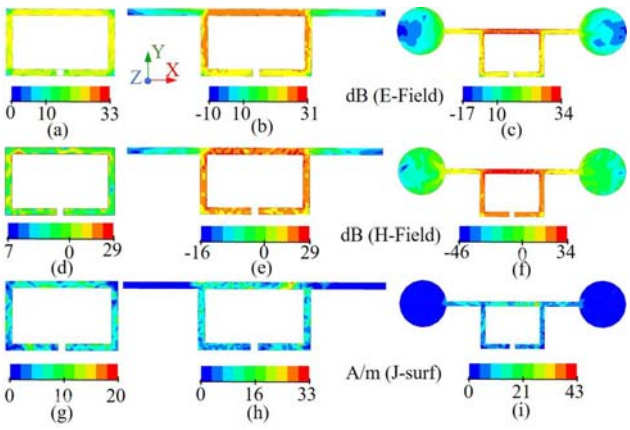

Fig. 6. Electromagnetic fields and current distribution at 868 MHz. Design1: (a), (d) and (g). Design 2: (b), (e) and (h). Design 3: (c), (f) and (i).

The electric field, magnetic field and current distribution at 868 MHz are shown in Fig. 6. It is found that from the Design 1 to the design 3, the electric fields and magnetic fields are raised and their distribution ranges are extended gradually after adding the 'arms' and 'circular end caps'and adjusting loop and 'arms' sizes. In addition, it is found that after adding arms and changing loop size, the overall fields and currents of the Design 1, 2 and 3 get stronger. From the aforementioned features, adjusting the loop and 'arms' can obtain required the frequency and changing the size of the 'circular end caps' can affect the radiation performance. Fig. 7 shows the radiation patterns in the xoy cut for the three designs. The structure of the Design 1 is only a loop which means the radiation ability is weak. For increasing the radiation ability (realized gain), the 'arms' can be added into the structure as the Design 2 which also make an impact on the impedance. From the current distribution as shown in Fig. 6, the realized gain of the Design 3 is expected to be higher than that of the previous designs. As shown in Fig. 7, the peak realized gain values of the three designs are -10.86 dBi, -7.87 dBi and 1.09 dBi, respectively. In addition, from the H-plane (yoz cut) as shown in Fig. 7 (b), the proposed Design 3 has a dipole-like radiation pattern as expected.

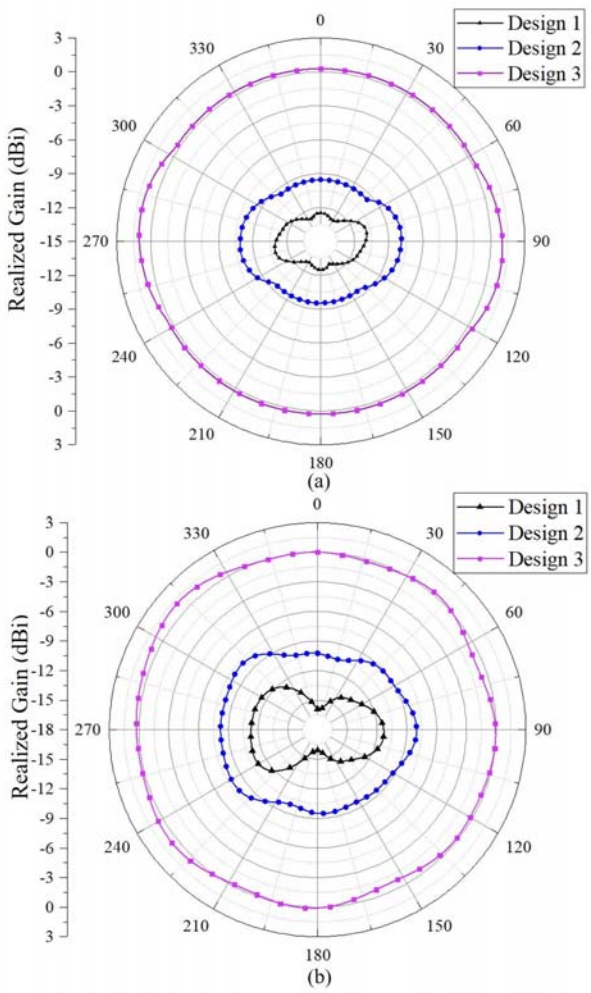

Fig. 7. Simulated normalized radiation patterns ~~(normalized realized gain)~~ for the three progressive designs (a) xoy cut, (b) yoz cut.

IV. Manufacture and Test

A. Embroidery Method

To embroider the patterns on the substrate (surgical masks), a professional embroidery machine (Singer Futura XL-550) is used. For the embroidery procedure as shown in Fig. 8, some details need attention. First of all, after obtaining appropriate designs in simulation software (ADS momentum, CST and HFSS), the simulated models need to be exported to a type of formats which can be converted with same size into the related embroidery software. Secondly, the knit pattern size and boundaries of the designs affected slightly by embroidery

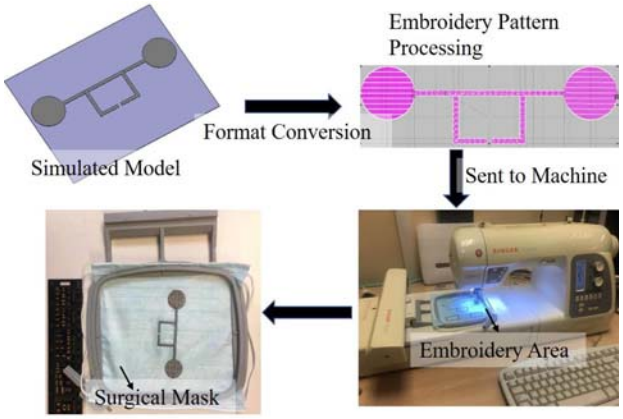

Fig. 8. Embroidery procedure.

modes in the embroidery software (EasyDesign EX4.0) need to be adjusted carefully, which is a factor affecting real conductivity of the conductive yarns. For the proposed designs, the 'satin fill' mode in the embroidery software is adopted. Finally, in the manufacturing process, the proposed yarn is utilized in both sides of the substrate as the conductive yarn and support yarn for reducing the influence from other dielectric yarns as support yarn.

B. Impedance Tests

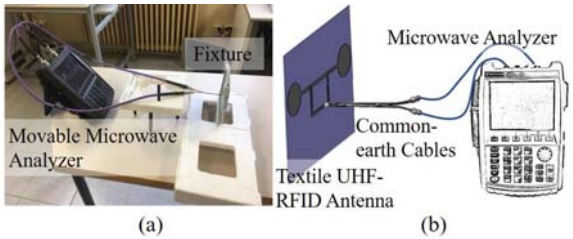

Fig. 9. Measurement setup for the impedance and reflection coefficients of the embroidered designs. (a) Photograph of measurement setup, (b) Measurement setup configuration.

For the measurements of the impedance and reflection coefficients of the embroidered designs, the experimental setup is shown in Fig. 9. As mentioned in section II, the common-earth cables are added at the end of the two ports and the related differential measurement method is used. Fig. 10 shows the antenna impedance of the proposed simulated and measured Design 3, including the resistance part and the reactance part. It is found that the resistance parts are higher than 64 ohm and reactance parts are lower than 469 ohm. Certainly, analyzing all of the results, the measured curves are close to the simulated curves.

From equation 2, the reflection coefficient (S parameter) can be calculated as shown in Fig. 11. It is found that the $|S_{11}|$ of the measured Design 3 is -24 dB which is better than the simulated results at 868 MHz. Note that the Design 3 have slight difference of the resonance frequency shift degrees between the simulated and measured results (below 10 MHz).

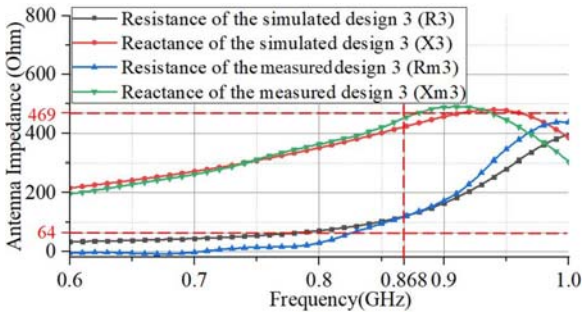

Fig. 10. Simulated and measured impedance for the embroidered Design 3 (Dashed lines: required antenna complex impedance 64+i*469 ohm at 868 MHz).

In addition, the Design 3 have narrower bandwidths of about than that of the simulated designs.

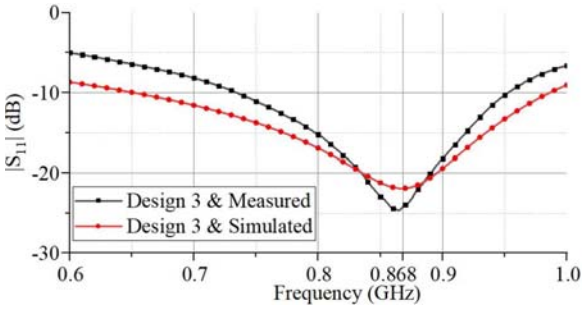

Fig. 11. Simulated and measured reflection coefficients for the embroidered Design 3.

C. Read Range Tests

Considering the real use conditions of the proposed textile UHF-RFID tag on surgical masks such as in the hospital channels and rooms, the read range measurement setup is shown in Fig. 12. The reader antenna (MT-242025/TRH/A/A) can be controlled by the M6E Kit which is connected to a laptop with control software. An inquiry signal with data and clock can be adjusted by the software and sent by the reader antenna. The proposed textile UHF-RFID antennas can send a backscattered signal with data and clock after receiving the inquiry signal. Note that backscattering coupling is a common mode in UHF RFID and Radar areas. In detail, when an electromagnetic wave encounters a space target, part of its energy is absorbed by the target, while the other part is scattered in various directions at different intensities. A portion of the scattered energy is reflected back to the transmitting antenna. [25]

When moving the proposed designs to a certain distance d as shown in Fig. 12 (b), the signal transmission is expected to be interrupted. This threshold distance is the maximum value of the read range.

To avoid moving the designs holders frequently, a certain distance is fixed (1 m) and then adjust the reader power to obtain the read range. In addition, the simulated read range can be calculated by the Friis Transmission Formula as follows,

$$d_{max} = \frac{\lambda}{4\pi}\sqrt{\frac{P_t G_t G_r \cdot \tau}{P_{th}}} \quad (3)$$

where d_{max} is the maximum value of the read range, λ is the wave length at 868 MHz, P_t is the power fed into the reader antenna, G_t is the gain of the reader antenna (7 dBi), G_r is the gain of the proposed antennas, τ is the largest power transmission coefficient and P_{th} is the minimum wake-up power of the chip (-10 dBm). In addition, the cable between the reader antenna and the reader have a loss of 0.8 dB.

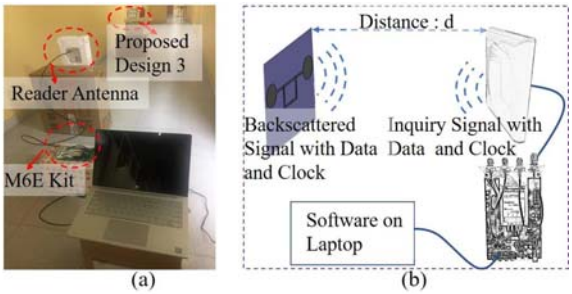

Fig. 12. Measurement setup for the read ranges of the embroidered designs. (a) Photograph of measurement setup, (b) Measurement setup configuration.

For the proposed designs, the read ranges are detected as shown in Table II. The maximum read range values of the simulated Design 1, 2 and 3 are 1.1 m, 1.6 m and 4.1 m, respectively, while that of the measured are 0.8 m, 1.3 m and 2.5 m, respectively. By analyzing the Friis Transmission Formula 3 and the proposed designs, the P_{th} of the chip (-10 dBm) makes a big impact on the maximum read range, compared to the two-pad chip (Monza R6) with the minimum wake-up power of -20 dBm. In addition, the difference between the simulated and measured results is caused by the silver-plated yarns and the soft substrates. In details, the silver-plated yarns are different with traditional copper line. The radiation ability of the yarns cannot be totally same with simulation results. For design 3, due to the soft masks, the 'circular end caps' has slight shape change in embroidery procedure which make a bigger difference between the simulated and measured results.

TABLE II
SIMULATED AND MEASURED MAXIMUM READ RANGE OF THE DESIGNS (UNIT: M)

Type	*Design* 1	*Design* 2	*Design* 3
Simulated d_{max}	1.1	1.6	4.1
Measured d_{max}	0.8	1.3	2.5

V. RELIABILITY VALIDATION

For textile UHF-RFID tags, reliability is an essential issue due to the features of the textile materials. In this work, considering the uses of surgical masks, the impact of bending and use on body is expected to be validated. In addition, with regard to the read range results at last section, the Design 3 is selected to be the final design which is tested for bending and skin touching.

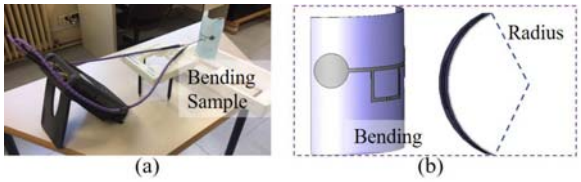

Fig. 13. Measurement setup for the impedance and reflection coefficients of the embroidered designs. (a) Photograph of measurement setup, (b) Diagram of the bending orientation.

A. Bending

The bending test setup is shown in Fig. 13 (a). Several molds with different radius have been used for hold and keep the proposed sample bent. Considering the use of surgical masks, the bending orientation is fixed as shown in Fig. 13 (b). Note that the bending degree increases with decreasing radius. Fig. 14 shows the measured antenna impedance curves in different radius. From Fig. 14, the resistance values at 868 MHz are close with different radius while the reactance values at 868 MHz increase with decreasing radius. In addition, the reflection coefficient curves as shown in Fig. 15 have slight resonance frequency shift degrees (all below 20 MHz) and increasing $|S_{11}|$ values at 868 MHz with increasing bending degree. In other words, after bending in certain degrees (radius: 33 mm to the flat), the proposed textile UHF-RFID tag can still work well.

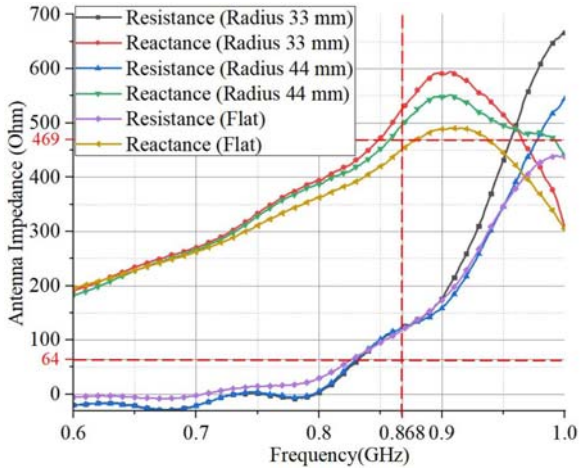

Fig. 14. Measured impedance in different bending degrees (Dashed lines: required antenna complex impedance 64+i*469 ohm at 868 MHz).

Certainly, read range tests in different bending degrees are still important and the test configuration is shown in Fig. 12. Considering the real use of the proposed design is on face, the bending radius close to face sizes (33 mm and 44 mm) are chosen. The measured max values of the read ranges shown in Table III are 2.5 m, 2.2 m and 1.7 m at flat, bending radius 33 mm and bending radius 44 mm, respectively. Note that the measured max values are obtained by the proposed design facing to the reader antenna as shown in Fig. 11. From the results, increasing bending degrees (radius: flat to 33 mm) cause a decrease in read ranges and the minimum read range in bending is at least 1.7 m.

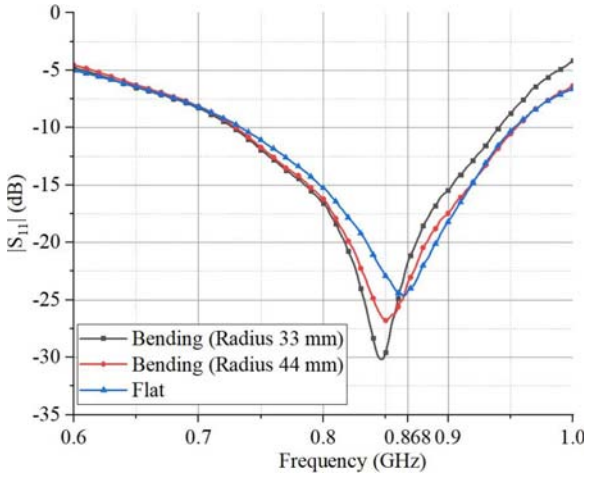

Fig. 15. Measured reflection coefficients in different bending degrees.

TABLE III
MEASURED MAXIMUM READ RANGE OF THE DESIGN 3 IN BENDING SITUATION (UNIT: M)

$Type$	$Flat$	$Bending(0.044)$	$Bending(0.033)$
$Measured\ d_{max}$	2.5	2.2	1.7

B. Skin Contact

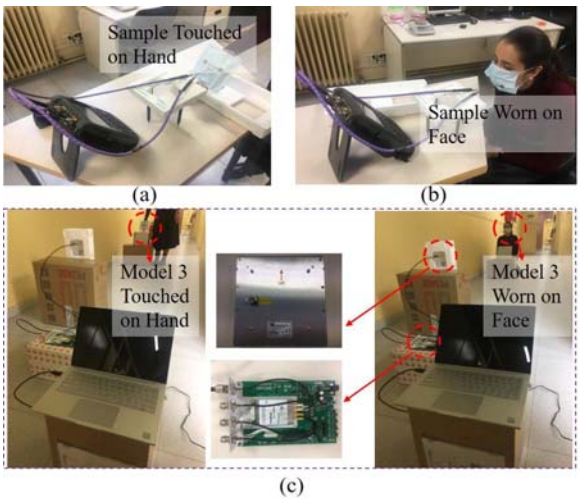

Fig. 16. Measurement setup for the impedance, reflection coefficients and read ranges in different skin contact positions. (a) Sample touched on a hand, (b) Sample worn on face, (c) Read range measurement

Skin contact test setup is shown in Fig. 16. The reflection coefficient and read range measurements of the Design 3 are operated when the sample is touched on a hand and worn on face as shown in Fig. 16(a) (b) and (c), respectively. The first application of surgical masks is to be worn on face, so the samples tested in air or touched on hands are compared with that worn on face. In general, the skin-contact performance is limited by the resonance frequency shift and reduced radiation efficiency due to the impedance change and power loss in the human body, respectively.

As shown in Fig. 17, compared with the impedance in air, the impedance on a hand has lower resistance part and reactance part while that on face has higher both parts. In addition, compared with the curves of the sample in air, the reflection coefficient ($|S_{11}|$) curves as shown in Fig. 18 on a hand and face show the resonance frequencies are shifted to 956 MHz and 813 MHz, respectively. However, when the sample are on a hand and face, the values at 868 MHz are -13 dB and -13.5 dB, respectively.

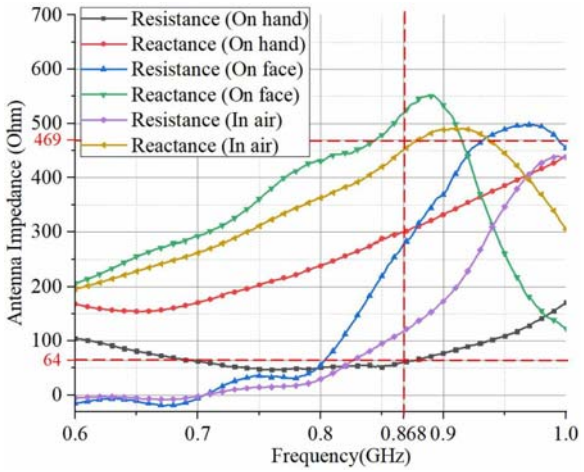

Fig. 17. Measured impedance in different skin contact positions (Dashed lines: required antenna complex impedance 64+i*469 ohm at 868 MHz).

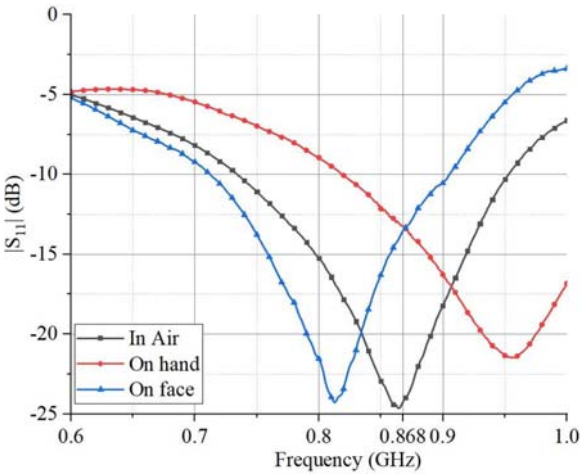

Fig. 18. Measured reflection coefficients in different skin contact positions.

TABLE IV
MEASURED MAXIMUM READ RANGE OF THE DESIGN 3 IN DIFFERENT SKIN CONTACT POSITIONS(UNIT: M)

$Type$	$InAir$	$On\ a\ Hand$	$On\ face$
$Measured\ d_{max}$	2.5	0.8	1.1

Read range tests in different situations are necessary and the results are shown in Table IV.The measured max values of the read ranges shown in Table IV are 2.5 m, 0.8 m and 1.1 m in air, on hand and on face, respectively. From the results, skin contact causes a decrease in read ranges and the minimum read range (1.1 m) when used on face proves that Design 3 can be effectively worn.

VI. Conclusion

To conclude, the progressive designs of textile UHF-RFID antennas on surgical masks are developed and one of them (Design 3) is selected to be validated by reliability tests (bending and skin contact). To explore the possibility and reliability of the function-extensible IC chips for textile UHF-RFID sensors, an IC chip (Rocky 100) with lower sensitivity (-10 dBm) than that of the popular chip (Monza R6, -20 dBm) is used in the designs. The simulated and measured resonance curves of the designs all match well (all below -20 dB at 868 MHz) and the radiation performance (realized gain) are improved progressively (maximum values: -10.86 dBi, -7.87 dBi and 1.09 dBi). After comparing the three progressive designs, the best type (Design 3) is selected and its read ranges measured by RFID reader (M6e kit) can reach 2.5 m in air. In addition, the necessary reliability validation measurements (bending and skin contact) are performed. From the results, the resonance frequency shift degrees are slightly different (all below 20 MHz) under different bending degrees (radius: 33 mm to flat) while heavily distinguishing on a hand (88 MHz) or face (55 MHz), but the values of reflection coefficients at 868 MHz all are below -10 dB. The maximum read range can reach 1.1 m on face. As a result, the proposed Design 3 has common use as an ID tag for tracking or safe distance alert in the epidemic situation but for the used function-extensible chip, the design can extend many different types of textile sensors for various application scenarios in the future.

References

[1] C. Occhiuzzi, C. Paggi and G. Marrocco, "Passive RFID Strain-Sensor Based on Meander-Line Antennas," *IEEE Trans. Antennas Propag.*, vol. 59, no. 12, pp. 4836-4840, Dec. 2011.

[2] C.Y. Luo, I. Gil and R. Fernández-García, "Wearable Textile UHF-RFID Sensors: A Systematic Review," *Materials*, vol. 13, no. 15, pp. 3292, 2020.

[3] M. Yang, Wen. Zhang, L. Li, L. Han, X. Chen, R. Yang and Q. Zeng, "A Resistance-Type Sensor Based on Chipless RFID," *IEEE Trans. Antennas Propag.*, vol. 65, no. 7, pp. 3319-3325, Jul. 2017.

[4] Y. Shafiq, J. S. Gibson, H. Kim, C. P. Ambulo, T. H. Ware and S. V. Georgakopoulos, "A Reusable Battery-Free RFID Temperature Sensor,"*IEEE Trans. Antennas Propag.*, vol. 67, no. 10, pp. 6612-6626, Oct. 2019.

[5] Y. Wang, A. J. Pretorius and A. M. Abbosh, "Low-Profile Antenna With Elevated Toroid-Shaped Radiation for On-Road Reader of RFID-Enabled Vehicle Registration Plate," *IEEE Trans. Antennas Propag.*, vol. 64, no. 4, pp. 1520-1525, Apr. 2016.

[6] Z. Ali, E. Perre, N. Barbot and R. Siragusa, "Authentication Using Metallic Inkjet-Printed Chipless RFID Tags," *IEEE Trans. Antennas Propag.*, vol. 68, no. 5, pp. 4137-4142, May. 2020.

[7] K. Kapucu and C. Dehollain, "A passive UHF RFID system with a low-power capacitive sensor interface," in *2014 IEEE RFID Technology and Applications Conference (RFID-TA)*, Tampere, 2014,pp. 301-305.

[8] K. Koski, L. Sydänheimo, Y. Rahmat-Samii and L. Ukkonen, "Fundamental Characteristics of Electro-Textiles in Wearable UHF RFID Patch Antennas for Body-Centric Sensing Systems," *IEEE Trans. Antennas Propag.*, vol. 62, no. 12, pp. 6454-6462, Dec. 2014.

[9] H. He, X. Chen, Z. Khan, L. Sydänheimo, L. Ukkonen,J. Li, H. Nishikawa and J. Virkki, "Textile-based Passive Sensor for Air Humidity," in *2020 IEEE 8th Electronics System-Integration Technology Conference (ESTC)*, Tønsberg, Vestfold, Norway, 2020, pp. 1-3.

[10] Y.Y. Fu, Y. Chan, M. Yang, Y. Chan and J. Virkki, "Experimental Study on the Washing Durability of Electro-Textile UHF RFID Tags," *IEEE Antennas Wirel. Propag. Lett.*, vol. 14, pp. 466-469, Nov. 2014.

[11] R.B.V.B. Simorangkir, D. Le, T. Björninen, A. S. M. Sayem, M. Zhadobov and R. Sauleau, "Washing Durability of PDMS-Conductive Fabric Composite: Realizing Washable UHF RFID Tags," *IEEE Antennas Wirel. Propag. Lett.*, vol. 18, no. 12, pp. 2572-2576, Dec. 2019

[12] S. Shao, A. Kiourti, R. J. Burkholder and J. L. Volakis, "Broadband Textile-Based Passive UHF RFID Tag Antenna for Elastic Material," *IEEE Antennas Wirel. Propag. Lett.*, vol. 14, pp. 1385-1388, Feb. 2015.

[13] D.P. Rose, M. E. Ratterman, D. K. Griffin, L. Hou, N. Kelley-Loughnane, R. R. Naik, J. A. Hagen, I. Papautsky and J. C. Heikenfeld, "Adhesive RFID Sensor Patch for Monitoring of Sweat Electrolytes," *IEEE. Trans. Biomed. Eng.*, vol. 62, no. 6, pp. 1457-1465, Jun. 2015.

[14] D. Patron, W. Mongan, T. P. Kurzweg, A. Fontecchio, G. Dion, E. K. Anday and K. R. Dandekar, "On the Use of Knitted Antennas and Inductively Coupled RFID Tags for Wearable Applications," *IEEE Trans. Biomed. Circuits Syst.* , vol. 10, no. 6, pp. 1047-1057, Dec. 2016.

[15] M. A. S. Tajin, A. S. Levitt, Y. Liu, C. E. Amanatides, C. L. Schauer,G. Dion, and K. R. Dandekar, "On the effect of sweat on sheet resistance of knitted conductive yarns in wearable antenna design," *IEEE Antennas Wirel. Propag. Lett.*, vol. 19, no. 4, pp. 542–546, Feb. 2020.

[16] Y. Liu, A. Levitt, C. Kara, C. Sahin, G. Dion, and K. R. Dandekar,"An improved design of wearable strain sensor based on knitted RFID technology," in *2016 IEEE Conference on Antenna Measurements Applications (CAMA)*, 2016, pp. 1–4.

[17] C. A. Balanis, Antenna Theory Analysis And Design, 3rd ed., John Wiley and Sons, 2005, pp.523–533.

[18] M. A. S. Tajin, O. Bshara, Y. Liu, A. Levitt, G. Dion, and K. R. Dandekar, "Efficiency measurement of the flexible on-body antenna at varying levels of stretch in a reverberation chamber," *IET Microw. Antennas Propag.*, Jul. 2019.

[19] M. Chesser, A. Jayatilaka, R. Visvanathan, C. Fumeaux, A. Sample and D. C. Ranasinghe, "Super Low Resolution RF Powered Accelerometers for Alerting on Hospitalized Patient Bed Exits," in *2019 IEEE International Conference on Pervasive Computing and Communications (PerCom)*, Kyoto, Japan, 2019, pp. 1-10

[20] L. Shan and H. Xiao, "Impedence characterization of RFID tag antennas and application in conformal tag antenna," in *2015 7th Asia-Pacific Conference on Environmental Electromagnetics (CEEM)*, Hangzhou, 2015, pp. 140-142

[21] H. Zhu, Y. C. A. Ko and T. T. Ye, "Impedance measurement for balanced UHF RFID tag antennas," in *2010 IEEE Radio and Wireless Symposium (RWS)*, New Orleans, LA, 2010, pp. 128-131

[22] X. Qing, C. K. Goh and Z. N. Chen, "Measurement of UHF RFID tag antenna impedance," in *2009 IEEE International Workshop on Antenna Technology*, Santa Monica, CA, 2009, pp. 1-4

[23] M. Svanda and M. Polivka, "Matching Technique for an On-Body Low-Profile Coupled-Patches UHF RFID Tag and for Sensor Antennas," *IEEE Trans. Antennas Propag.*, vol. 63, no. 5, pp. 2295-2301, May. 2015.

[24] K. Rasilainen, J. Ilvonen and V. Viikari, "Antenna Matching at Harmonic Frequencies to Complex Load Impedance," *IEEE Antennas Wirel. Propag. Lett.*, vol. 14, pp. 535-538, Nov. 2015.

[25] M. A. Richards, Fundamentals of Radar Signal Processing, 2nd ed., McGraw-Hill Education, 2005, pp.523–533.

Chengyang Luo was born in Hubei, China, in 1995. He received the B. Eng. degree in integrated circuit design and integration system from Xidian University, Xi'an, China, in 2017. From 2019 to now, he is studying for the Electronics Engineering Ph.D. degree in Universitat Politecnica de Catalunya, Barcelona, Spain.

In 2017, he joined the China Electronic Product Reliability and Environmental Testing Research Institute (CEPREI), Guangzhou, China, where he served as a research assistant of the Science and Technology on Reliability Physics and Application of Electronic Component Laboratory, Guangzhou, China. In 2019, he obtained the national CSC-UPC Scholarship for the Ph.D. degree in Universitat Politecnica de Catalunya, Barcelona, Spain. His current research interests include textile UHF-RFID tags and sensing techniques, smart devices and noncontact voltage, current and power measurement techniques.

Ignacio Gil was born in 1978 in Barcelona, Spain. He received degrees in physics and electronics engineering in 2000 and 2003, and then his PhD in 2007 from the Universitat Autònoma de Barcelona, Spain. From 2003 to 2008 he was assistant professor in electronics and a researcher with the RF-Microwave Group in the Electronic Engineering Department, Universitat Autonòma de Barcelona, Spain. From 2006 to 2008 he worked for EPSON Europe Electronics GmbH where he developed high-performance integrated RF CMOS circuits, transceivers and system design. In 2008 he joined the Electronic Engineering Department, Universitat Politècnica de Catalunya (UPC), Spain, as lecturer and researcher. Since 2011 he is associate professor at UPC. Since 2012 he is also a collaborator at Universitat Oberta de Catalunya (UOC), Spain. He has been involved in 12 research projects (3 as principal researcher) in different research activities including passive and active RF and microwave devices and circuits, metamaterials, EMC and smart textile electronics. From 2012-2014 he served as Chairman of the Spanish IEEE EMC Chapter. In 2017 he was academic visitor at Loughborough University (UK) in the Wireless Communications Research Group. Since 2019 he is Deputy Director of International Relations at ESEIAAT (UPC). Dr. Gil is co-author of more than 150 scientific publications and 17 patents. He has been awarded the Duran Farell de Investigación Tecnológica (2006) and the patent award from SEIKO EPSON Corporation (2010). Dr. Gil has been visiting professor in different Universities: New Jersey Institute of Technology (USA), Limerick University (Ireland), Loughborough University (UK), Shaoxing University (China) and Polytechnic University of Tirana (Albania).

Raul Fernandez Garcia received the B.Eng. degree in telecommunications and M.Eng degree in electronics from the Universitat Politecnica de Catalunya, Barcelona, in 1997 and 1999, respectively. In 2007 he received the Ph.D. degree from the Universitat Autonoma de Barcelona. From 1998 to 2001, he worked for Sony Spain, as Radiofrequency Engineer, where he developed analog and digital TV tuners. From 2001 to 2007, he was part-time Assistant Professor in electronics with the Department of Electronics Engineering, Universitat Autonoma de Barcelona. Funded by the European Marie Curie Program, he worked on devices and circuits reliability at IMEC (Belgium) between 2005 and 2006. From 2008 to 2011, he was full-time Assistant Professor in the Department of Electronics Engineering, Universitat Politecnica de Catalunya. At present he is Associate Professor at the same department. Dr. Fernandez-Garcia is author or a co-author of more than 110 papers in international journals and conferences and he has been involved in 18 research projects (6 as principal researcher) in different research activities including reliability, electromagnetic compatibility and electronic textile. He was the recipient of Best Paper Awards at IPFA 2007. His current scientific interest is focused on wearable sensor development for sport and health applications.

Int. J. Electron. Commun. (AEÜ) 146 (2022) 154137

Contents lists available at ScienceDirect

International Journal of Electronics and Communications

journal homepage: www.elsevier.com/locate/aeue

Experimental comparison of three electro-textile interfaces for textile UHF-RFID tags on clothes

Chengyang Luo, Ignacio Gil, Raúl Fernández-García

Department of Electronic Engineering, Universitat Politecnica de Catalunya, Carrer de Colom 1, Terrassa, 08222 Barcelona, Spain

ARTICLE INFO

Keywords:
Electro-textile
Interface
UHF-RFID
Antenna
Mix use
On body

ABSTRACT

Textile Ultra High Frequency (UHF, 865–868 MHz) Radio Frequency Identification (RFID) devices meet difficulties from connection of solid chips and textile antennas. In this work, three electro-textile interfaces integrated with the corresponding textile UHF-RFID antennas as the solutions are proposed and compared. The simulated and measured impedance curves of the corresponding antennas are all close and the radiation performance (realized gain) are designed to be near (about 1.4 dBi). According to the Friis formula, the simulated and measured read ranges of the interfaces with the corresponding antennas in air are obtained (all above 4.5 m). For reliability validation, mixed use feasibility tests are implemented and the results show the read ranges of each interface used on other two designs have tolerable read range decrease (< 2 m but all above 3.41 m).In addition, the read ranges of the designs on body are all above 2.05 m. Due to the small sizes of the interfaces, stable performance on body and good reliability, the proposed interfaces solutions are proved feasible.

1. Introduction

With Radio Frequency Identification (RFID) technology development, many commercial devices are applied in diverse scenarios [1–3] such as health-caring monitoring [4], goods tracking [5,6], classification, localization and stuff management [7]. Most of them are developed by welding integrated circuit (IC) chips on a hard or flexible Printed Circuit Board (PCB) [8] or a chipless way [9,10]. The welding technique for connecting chips to RFID antennas on PCBs is proven and reliable. However, this popular technique is not suitable for most textile RFID devices on clothes due to the high temperature intolerance (< 200°C) of the common knit yarns and fabrics [11–13]. Even for some wearable polymeric materials such as Polyvinyl Chlorid (PVC) fiber, alginate fiber and carbon fiber, the chips on them face the problem of unstable fixation.

To avoid this connection problem, some works are exploring free welding methods such as fixing with glue [14], non-conducting yarns or copper plates [15,18]. In a study [15], a passive UHF-RFID-based knitted wearable compression sensor is proposed for monitoring a baby breathing activity, for which a chip (Monza R6) is welded on a FR4 PCB. Then the board with the chip is inserted into a small pocket knitted in the middle region of the antenna top layer. In another work [14], a textile UHF-RFID antenna solution concentration sensor is proposed and the chip is fixed by sewing and glue, which is more flexible for wearable applications. However, many similar designs are foreseen to have difficulties such as chip pads rust due to textile washing and the detachment of the chip-welded board in textile devices.

In this paper, three electro-textile interfaces integrated with the corresponding textile UHF-RFID antennas (by sewing, snap buttons and inserting) are proposed and compared to provide chip-textile connection solutions. Related preparatory work before simulation such as the detailed embroidery method and interface impedance tests is implemented and presented. Based on the accurate impedance of three electro-textile interfaces obtained by the real tests, the simulation of the corresponding antennas is developed and the simulated results are compared with the measured results. Note that the textile UHF-RFID antennas are designed to keep the maximum realized gain values near for next performance comparison. Finally, related reliability validation tests including mixed use reliability and use on body are implemented. The proposed electro-textile interfaces have the potential to be applied into thicker clothes such as winter clothes (not too close to bodies) due to their small sizes and stable performance.

2. Design and Related Details

2.1. Structure of the Proposed Electro-textile Interfaces

The geometry and configuration of the three proposed electro-textile interfaces with the corresponding textile UHF-RFID antennas are shown in Fig. 1. Considering the common problem about the difficulty of the chips and textile interconnection, the three interfaces (type1 to 3) are proposed and analyzed for the textile UHF-RFID antennas and the UHF-RFID chip (LXMS21ACNP-184, impedance: 19-i*284 ohm, wake-up power: −18 dBm)[16,17] on the small PCBs. The three connection

https://doi.org/10.1016/j.aeue.2022.154137
Received 22 October 2021; Accepted 25 January 2022
Available online 1 February 2022

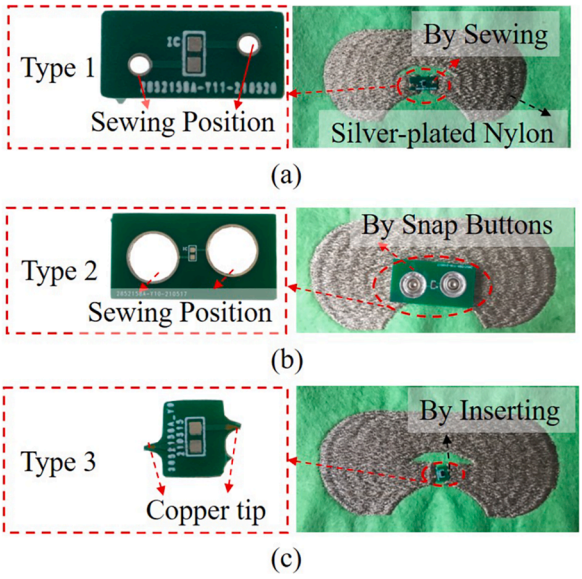

Fig. 1. Geometry and configuration of the three proposed electro-textile interfaces with the corresponding UHF-RFID antennas. (a) Type 1, (b) Type 2, (c) Type 3.

ways as shown in Fig. 1 are by sewing, snap buttons and inserting, respectively. Note that, all the interfaces have different complex impedance (not 50 ohm) from that of the chip. In addition, despite of using the same chips for the three interfaces, they have different complex impedance as feed ports due to the different structures and connection methods. Therefore, the textile UHF-RFID antennas are designed based on the corresponding complex impedance. The PCBs dimensions of the type 1, 2 and 3 are 12.7*6.22*0.8 mm, 16.38*31.12*0.8 mm and 7.76*6.10*0.8 mm, respectively. Moreover, the hole diameters of the type 1 and type 2 are 2 mm and 9 mm, respectively.

The proposed textile UHF-RFID antennas are embroidered using conductive yarns as on a polyester fibers substrate. A commercial conductive twisted yarn made of 99% pure silver-plated Nylon is used as the textile material of the antenna, the bulk conductivity of which is 11500 siemens/m with 0.2 mm thickness obtained by the previous works[14,15]. Moreover, the polyester is selected as the substrate, the relative dielectric constant, loss tangent and thickness of which are 1.29 (ε_r) 0.00188 (tanD) and 0.88 mm, respectively. In addition, the sewing yarns for the 'Type 1' are adopted the same as the conductive yarns of the antennas whereas the snap buttons for the 'Type 2' are made of steel.

2.2. Impedance Characterization

2.2.1. Impedance Measurement Method

For balanced structures, a popular method validated in some works [14,19–21] for impedance measurements is to combine the function (port extension[22]) of the Microwave Analyzer (N9916A) with the differential mode probes as shown in Fig. 2. The probes are made from two semi-rigid cables with ground shields soldered together. Concerning to the procedure, first of all, the Microwave Analyzer with two coaxial cables needs to be calibrated by a standard calibration kit. Secondly, after connecting the coaxial cables to the differential mode probes, the function (port extension [22]) of the Microwave Analyzer needs to be adjusted in order to move the calibration plane from the ends of the coaxial cables to the ends of the differential mode probes. Meanwhile, the traces in Smith chart of the two ports should roughly converge to the open circuit position in the Microwave Analyzer. Next, the two tips of the differential mode probes are connected to the proposed textile UHF-RFID antennas or the feed port PCBs and the Z parameters in 50 ohms can be obtained. Note that the measured Z parameters using the differential mode probes are earth-referenced and need to be transferred for the differential reflection coefficient (ρ) of the balanced samples [23,24]. Finally, Z parameters of the tested samples in the complex conjugate impedance of the chip can be calculated using the Eqs. 1 as follows,

$$Z_{ant} = \frac{2Z_0(1 - S_{11}S_{22} + S_{12}S_{21} - S_{12} - S_{21})}{(1 - S_{11})(1 - S_{22}) - S_{12}S_{21}} \tag{1}$$

Where Z_0 is 50 ohms, S_{11}, S_{12}, S_{21} and S_{22} are the measured S parameters, Z_{ant} is the Z parameter of the balanced samples.

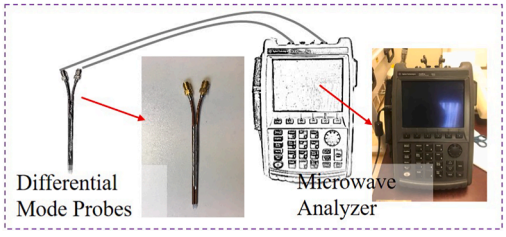

Fig. 2. Calibration setup with the differential mode probes for impedance measurements method.

2.2.2. Impedance Measurements of the Three Electro-textile Interfaces

The impedance of the three interfaces is different when the chip is welded on the different PCBs and then connected to the textile materials. It is essential to obtain the accurate port impedance before designing antennas. The experimental setup for the complex impedance measurements is shown in Fig. 3 (a) and (b). As aforementioned, the differential measurement method with the differential mode probes is used. In addition, in order to reduce the impact from the connection, the interface impedance tests are conducted in the case of the three electro-textile interfaces ('With Textile') as shown in Fig. 3 (c).

After being calculated by Eq. 1, the measured impedance results of the three interfaces are shown in Fig. 4, including the resistance part and the reactance part. It is found that the resistance curves of the three types has a difference of less than 5 ohm difference in the absolute value case while their reactance curves have obvious differences (about 20 to 60 ohm in the absolute value case). In addition, at 868 MHz, the complex impedance of the interfaces are listed in Table 1.

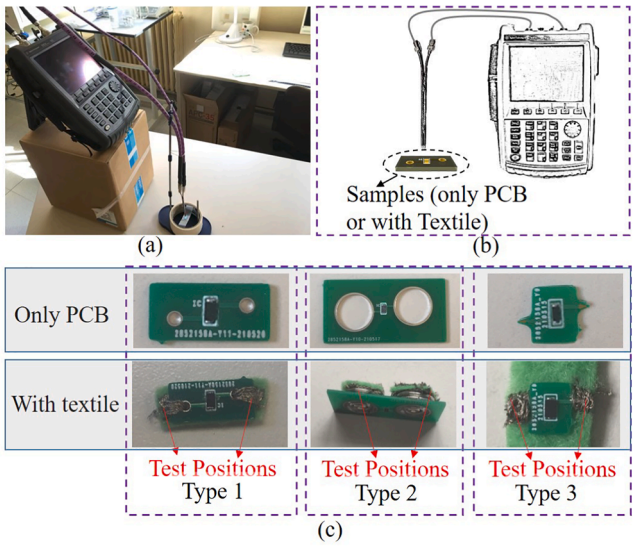

Fig. 3. Experimental setup for the interfaces impedance. (a) Photograph of the setup, (b) Experimental setup configuration. (c) Tested cases ('Only PCB' and 'With Textile').

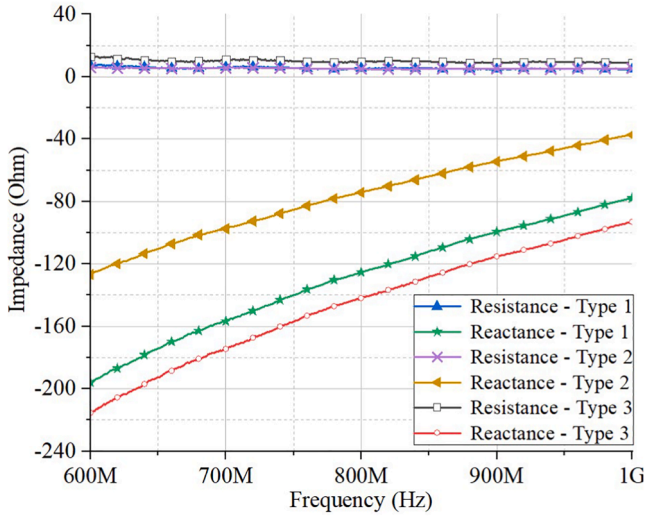

Fig. 4. Measured impedance for the three electro-textile interfaces ('With Textile').

Table 1
Complex Impedance of the Interfaces at 868 MHz(Unit: Ohm).

Case	*Type*1	*Type*2	*Type*3
WithTextile	5.09-i*107.7	5.06-i*60.27	9.29-i*123.27

2.3. Simulation and Measurements

2.3.1. Simulation models of the corresponding textile antennas

After obtaining the measured complex impedance of the three electro-textile interfaces ('with textile'), the corresponding UHF-RFID antennas can be designed based on the measured impedance as feed port impedance. The fundamental model simulated in high-performance 3D EM analysis software (CST) is shown in Fig. 5 and the three corresponding textile antennas are developed by adjusting related dimension parameters based on the shown model. The dimension parameters of the three designed antennas are listed in the Table 2. the antenna patterns are embroidered by silver-plated Nylon whereas the conductive yarns have 0.2 mm thickness with corresponding bulk conductivity of 11500 siemens/m. The polyester as the substrate has relative dielectric constant, loss tangent and thickness of 1.29 (ε_r)), 0.00188 (tanD) and 0.88 mm, respectively. The simulated resistance and reactance of the three corresponding textile antennas are shown Fig. 6

2.3.2. Antenna Manufacturing Method

To embroider the patterns on the substrate (polyester), a commercial embroidery machine (Singer Futura XL-550) is used. The embroidery procedure is detailed in Fig. 7. First of all, after obtaining appropriate designs in 3D full electromagnetic simulations, the layout models need to be exported to a type of formats which can be converted with same size into the related embroidery software. Secondly, the knit pattern size and boundaries of the designs affected slightly by embroidery modes in

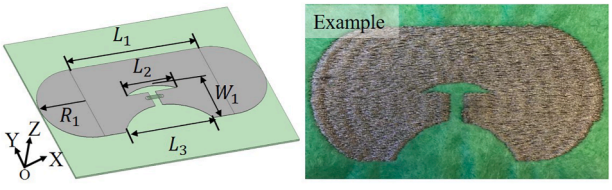

Fig. 5. Geometry of the fundamental simulated model for the three corresponding UHF-RFID antennas.

Table 2
Antenna Dimension Parameters (Unit: mm).

AntennaDesigns	L_1	L_2	L_3	W_1	R_1
*Design*1	58	22.6	40	23.4	20
*Design*2	74	15	40	22	20
*Design*3	58	24.8	40	24	20

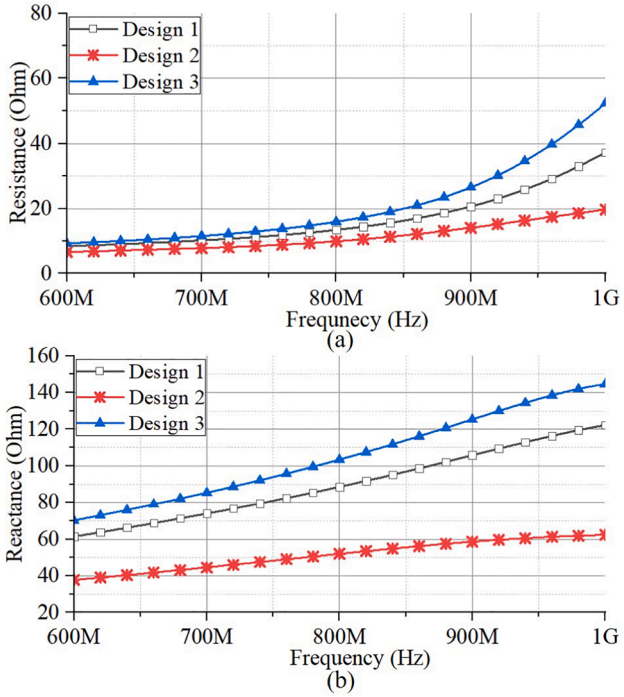

Fig. 6. Simulated resistance and reactance of the three corresponding textile antennas.

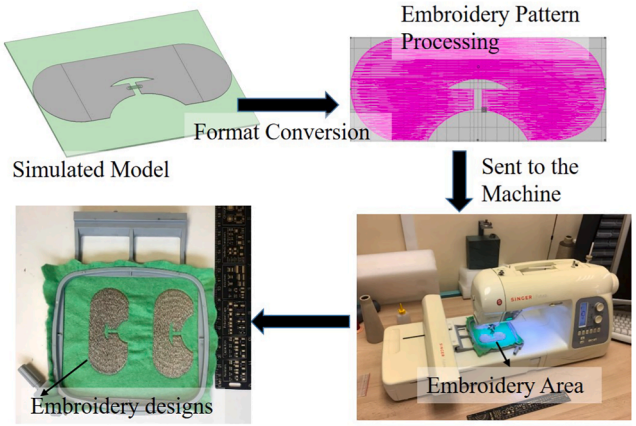

Fig. 7. Embroidery procedure.

the embroidery software (EasyDesign EX4.0) need to be adjusted carefully. For the proposed designs, the 'satin fill' mode in the embroidery software is adopted. Finally, in the manufacturing process, the proposed yarns are utilized in both sides of the substrate as the conductive yarns and support yarns.

2.3.3. Impedance Simulation and Measurements of the Three Textile Antennas

As aforementioned, in order to reduce the impact from the

connection, the measured complex impedance results of the case 'With Textile' are adopted as conjugate impedance of the antennas [25,26] for simulation and the simulated designs are described and shown in Fig. 5. The experimental setup is shown in Fig. 8 and the antenna impedance results are shown in Fig. 9, including the simulated and measured curves.

By analyzing the three cases, the measured impedance curves are close to the simulated curves. In addition, the simulated and measured results at 868 MHz for each case are listed in Table 3. It is found that the measured antenna impedance values are close to the conjugate impedance values of the corresponding interfaces.

2.3.4. Radiation Performance Comparison

Radiation performance is the another important factor affecting the final target of UHF-RFID tags read range. The radiation patterns in the xoy cut of the three designs are shown in Fig. 10. The maximum realized gain values of the three designs are close, 1.46 dBi, 1.38 dBi and 1.31 dBi for the design 1, design 2 and design 3, respectively.

2.3.5. Read Range Tests

For read range tests, the experimental setup is shown in Fig. 11. In order to avoid moving the designs holders frequently, a certain distance between the read antenna and UHF-RFID tags is fixed (0.7 m) and the reader output power is adjusted. The reader antenna (MT-242025/TRH/A/A) can be controlled by the M6E Kit which is connected to a laptop with specified control software. A inquiry signal with data and clock can be adjusted by the software and sent by the reader antenna. The proposed textile UHF-RFID antennas can send a backscattered signal with data and clock after receiving the inquiry signal. The output power is adjusted until the signal transmission between the read antenna and the tags is disrupted. The maximum value of the read range can be calculated by the threshold power. In addition, the simulated read range can be calculated by the Friis Transmission Formula [27] as follows,

$$d_{max} = \frac{\lambda}{4\pi}\sqrt{\frac{P_t G_t G_r \cdot \tau}{P_{th}}} \tag{2}$$

where d_{max} is the maximum value of the read range, λ is the wavelength at 868 MHz, P_t is the power fed into the reader antenna, G_t is the gain of the reader antenna (7 dBi), G_r is the gain of the proposed antennas, τ is the largest power transmission coefficient (Design 1, 2 and 3: 0.6242, 0.7888 and 0.8149 at 868 MHz, respectively) and P_{th} is the minimum wake-up power of the chip(-18 dBm). In addition, the cable loss between the reader antenna and the reader is taking into account (0.8 dB).

For the three electro-textile interfaces with the corresponding textile antennas, the simulated and measured maximum read ranges of the type 1, 2 and 3 have been tested several times and the results are listed in Table 4. Note that the read range values are recorded when the tags can be read continuously and stably, which is not just an on–off procedure. It is found that when the realized gain and the matching situations of the three types are close, the type 3 has the better performance than the other two in simulation and measurement, respectively. The main

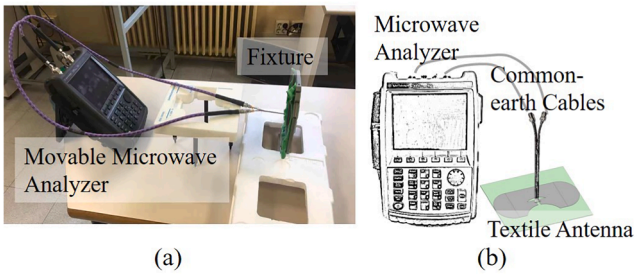

Fig. 8. Experimental setup for the impedance of the embroidered designs. (a) Photograph of experimental setup, (b) Experimental setup configuration.

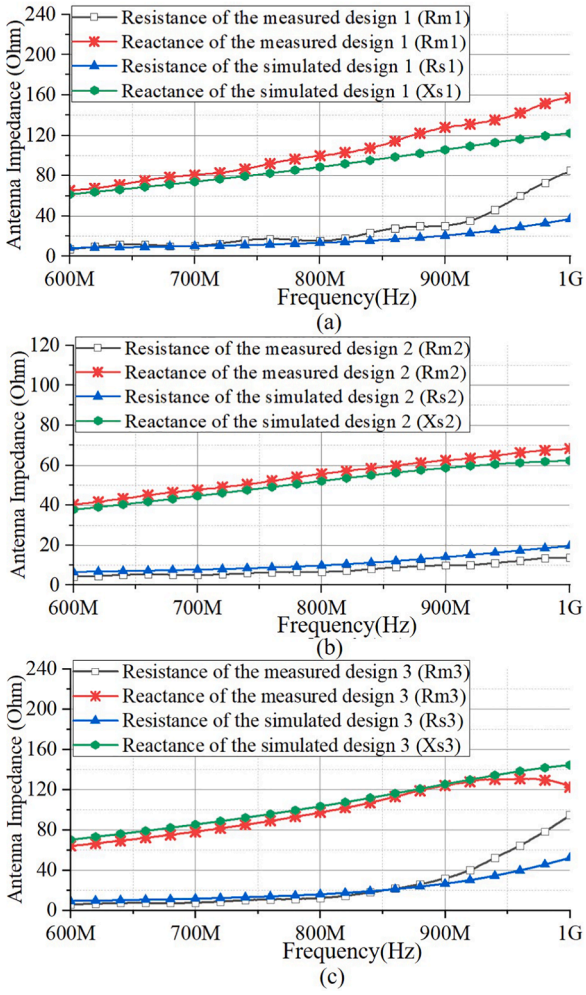

Fig. 9. Simulated and measured impedance for the three corresponding textile antennas. (a) Design 1, (b) Design 2, (c) Design 3.

Table 3
Complex Impedance of the Antenna Designs at 868 MHz(Unit: Ohm).

Case	*Design*1	*Design*2	*Design*3
Simulated	17.59 + i*100	12.52 + i*56.77	21.93 + i*117.98
Measured	28.86 + i*117.8	9.24 + i*60.51	23 + i*115.42

reason for the difference between the simulated and measured results is that the real radiation and impedance cannot totally match with the simulated results due to the environmental factors, embroidery error and measuring error.

2.4. Reliability Validation

2.4.1. Mixed Use Feasibility

In the work, 'mixed use' refers to the interfaces used for other non-corresponding antennas. Generally, for each electro-textile interface, the corresponding UHF-RFID antenna is expected to be redesigned. Considering this case increases costs and design periods, the mixed use feasibility of the different electro-textile interfaces is worth exploring. Therefore, in this section the three electro-textile interfaces are applied to the three different antennas, respectively. There are nine cases, in which the test setup and related measurement method are same.

As listed in Table 5, the matched pairs have the best performance as expected. In addition, it is found that for each interface, the read ranges of the interfaces used on other two designs have tolerable decrease (< 2

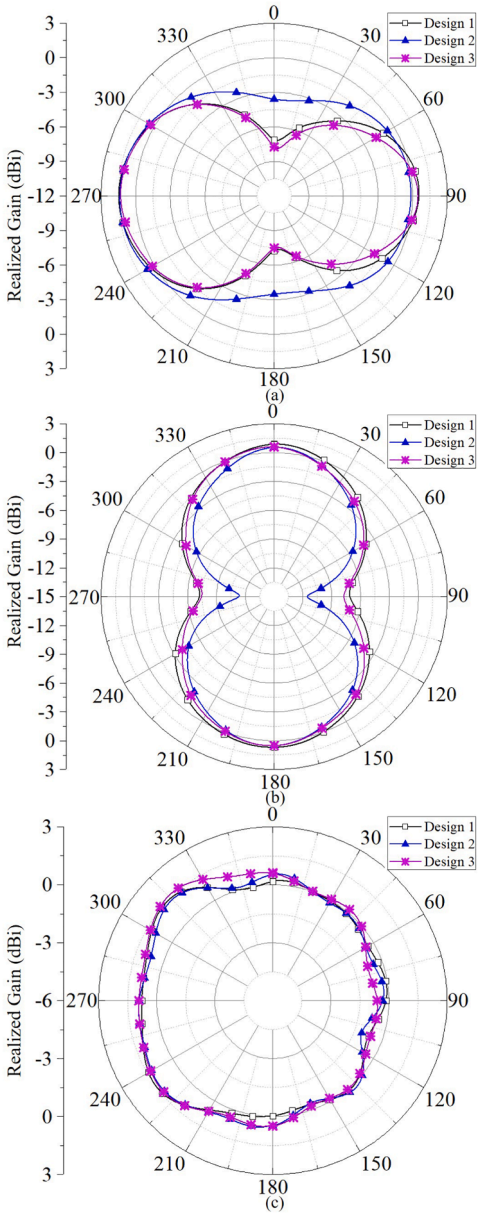

Fig. 10. Simulated radiation patterns (realized gain) for the three designs. (a) XY plane, (b) XZ plane, (c) YZ plane.

m) but are all above 3.41 m. It means the unpaired combination can work normally under specific requirements. Therefore, the mixed use feasibility of the proposed electro-textile interfaces and textile UHF-RFID antennas is validated.

2.4.2. Tests On Body

In this section, the related tests on body are developed by the three connection methods (sewing by yarns, snap buttons and inserting) and the experimental setup is shown in Fig. 12. Note that the researcher in the figure wears the winter clothes, which are thicker than normal ones and the tags can be 3 cm 4 cm from the clothes to the body with air interlayer. In the tests, all the interfaces connect to the three antenna designs, respectively, to explore the performance in the nine cases as aforementioned in last section.

The read range results are listed in Table 6. As expected, the read ranges for the nine cases on body are lower than that in air, respectively, due to power loss on body. However, the worst performance shows a read range of 2.05 m (the type 3 by inserting into the design 1). And all the results prove the on-body use feasibility of the interfaces with the antennas. Certainly, for attractive fashion, the electro-textile interfaces can also be hidden in thinker clothes and the textile antennas can be embroidered with other nonconductive floral patterns. When they are used on clothing, the potential as a RFID sensor such as temperature and humility sensor can be explored.

3. Conclusion

To conclude, three electro-textile interfaces integrated with the corresponding textile UHF-RFID antennas are proposed and evaluated in this work. The simulated and measured impedance curves of the cor-

Table 4
Simulated and Measured Maximum Read Ranges at 868 MHz in Air (Unit: m).

Case	*Type1/Design1*	*Type2/Design2*	*Type3/Design3*
Simulated	5.58	6.74	6.8
Measured1st	4.52	5.19	5.82
Measured2nd	4.57	5.25	5.69
Measured3rd	4.47	5.25	5.76
AverageMeasured	4.52±0.05	5.22±0.03	5.75±0.07

Table 5
Measured Read Ranges of the Nine Cases in Air (Unit: m).

Case	*Design1*	*Design2*	*Design3*
Type1	**4.5**	4.05	3.57
Type2	3.74	**5.22**	4.29
Type3	3.41	4	**5.75**

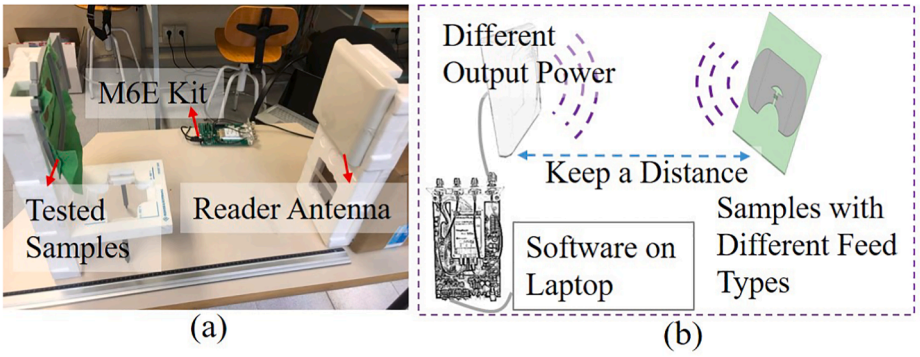

Fig. 11. Experimental setup for the read ranges of the textile UHF-RFID tags. (a) Photograph of experimental setup, (b) Experimental setup configuration.

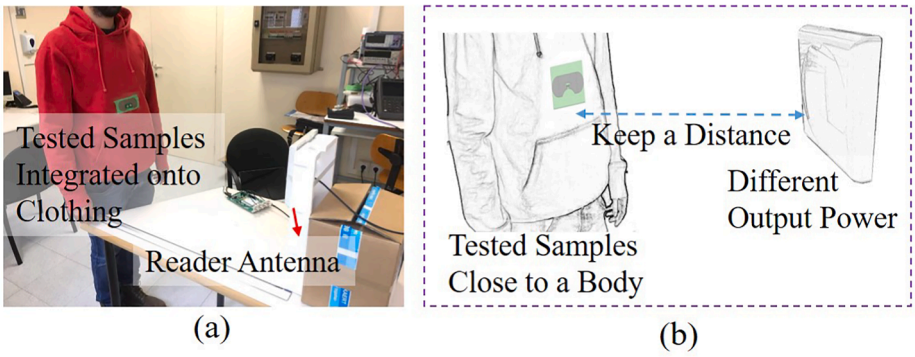

Fig. 12. Experimental setup for the read ranges of the tags on body. (a) Photograph of experimental setup, (b) Experimental setup configuration.

Table 6
Measured Read Ranges of the Nine Cases on Body (Unit: m).

Case	*Design1*	*Design2*	*Design3*
Type1	**3.68**	3.24	2.05
Type2	3.43	**4.57**	3.17
Type3	2.19	3.13	**3.35**

responding antennas are all close and the radiation performance (realized gain) are designed to be near (about 1.4 dBi). According to the Friis formula, the simulated and measured read ranges of the interfaces with the corresponding antennas in air are obtained (all above 4.5 m). For reliability validation, the tests for mixed use feasibility and the tests on body are implemented. The results of mixed use feasibility tests show that the read ranges of the each interface used on other two UHF-RFID antennas have tolerable decrease (< 2 m) but are all above 3.41 m. It means the mixed use feasibility of the proposed electro-textile interfaces and textile UHF-RFID antennas can be proved. In addition, the read ranges of the designs on body are all above 2.05 m. Therefore, due to the small sizes of the electro-textile interfaces, stable performance on body and good reliability, the proposed electro-textile interfaces with the corresponding textile UHF-RFID antennas has potential application in the future medical and daily clothes fields.

Declaration of Competing Interest

The authors declare that they have no known competing financial interests or personal relationships that could have appeared to influence the work reported in this paper.

References

[1] Arun H. Advancements in the use of carbon nanotubes for antenna realization. AEU - Int J Electron Commun 2021;136:153753.
[2] Occhiuzzi C, Paggi C, Marrocco G. Passive RFID Strain-Sensor Based on Meander-Line Antennas. IEEE Trans Antennas Propag 2011;59(12):4836–40.
[3] Luo CY, Gil I, Fernández-García R. Wearable Textile UHF-RFID Sensors: A Systematic Review. Materials 2020;13(15):3292.
[4] Prather JC, Meng Y, Bolt Ml, Horton T, Adams Mark. Wireless head impact monitoring system utilizing eye movement as a surrogate for brain movement. AEU - Int J Electron Commun 2019;vol. 105. p. 54-61.
[5] Shafiq Y, Gibson JS, Kim H, Ambulo CP, Ware TH, Georgakopoulos SV. A Reusable Battery-Free RFID Temperature Sensor. IEEE Trans Antennas Propag 2019;67(10):6612–26.
[6] Wang Y, Pretorius AJ, Abbosh AM. Low-Profile Antenna With Elevated Toroid-Shaped Radiation for On-Road Reader of RFID-Enabled Vehicle Registration Plate. IEEE Trans Antennas Propag 2016;64(4):1520–5.
[7] Ali Z, et al. Authentication Using Metallic Inkjet-Printed Chipless RFID Tags. IEEE Trans Antennas Propag 2020;68(5):4137–42.
[8] Peña CDM, et al. Ultra slim and small UHF RFID tag design for mounting on curved surfaces. AEU - Int J Electron Commun 2021;128:153502.
[9] Zarif AH. A compact half butterfly chipless RFID tag based on image theory with DER analysis. AEU - Int J Electron Commun 2020;127:153486.
[10] Yang M, et al. A Resistance-Type Sensor Based on Chipless RFID. IEEE Trans Antennas Propag 2017;65(7):3319–25.
[11] Yang A, et al. Thermal management in nanofiber-based face mask. Nano Lett 2017;17:3506–10.
[12] Wang J, Li Q, Liu D, Chen C, et al. High temperature thermal conductive nanocomposite textile by "green electrospinning. Nanoscale 2018;10:16868–72.
[13] Shao S, Kiourti A, Burkholder RJ, Volakis JL. Broadband Textile-Based Passive UHF RFID Tag Antenna for Elastic Material. IEEE Antennas Wirel Propag Lett 2015;14:1385–8.
[14] Luo C, Gil I, Fernández-García R. Textile UHF-RFID antenna sensor for measurements of sucrose solutions in different levels of concentration. Meas Sci Technol 2021;vol. 32, pp. 10.
[15] Tajin M, Amanatides C, Dion G, Dandekar K. Passive UHF RFID-Based Knitted Wearable Compression Sensor. IEEE Internet Things J 2021;8(17):13763–73.
[16] https://www.nxp.com/docs/en/data-sheet/SL3S10X4.pdf.
[17] https://www.mouser.com/datasheet/2/281/UHF_RFID_Tag_LXMS21ACNP-184_datasheet_Rev1_1_18113-1877823.pdf.
[18] Liu Y, Levitt A, Kara C, Sahin C, Dion G, Dandekar KR. "An improved design of wearable strain sensor based on knitted RFID technology. In: 2016 IEEE Conference on Antenna Measurements Applications (CAMA); 2016. p. 1–4.
[19] Shan L, Xiao H. Impedence characterization of RFID tag antennas and application in conformal tag antenna. In: 2015 7th Asia-Pacific Conference on Environmental Electromagnetics (CEEM), Hangzhou; 2015. p. 140-2.
[20] Zhu H, Ko YCA, Ye TT. Impedance measurement for balanced UHF RFID tag antennas. In: 2010 IEEE Radio and Wireless Symposium (RWS), New Orleans, LA; 2010. p. 128-131.
[21] Qing X, Goh CK, Chen ZN. Measurement of UHF RFID tag antenna impedance. In: 2009 IEEE International Workshop on Antenna Technology, Santa Monica, CA; 2009. p. 1-4.
[22] https://na.support.keysight.com/pxi/help/latest/S3_Cals/Port_Extensions.htm.
[23] Carrasco CT, Sieiro CJ, Lopez-Villegas JM, Vidal N, Gonzalez-Echevarría R, Roca ME. Mixed-mode impedance and reflection coefficient of two-port devices. Prog Electromagn Res 2012;130:411–28.
[24] Stoumpos CK, Anagnostou DE, Chryssomallis MT. Experimental characterization of the impedance of balanced UHF RFID tag antennas. Microw Opt Technol Lett 2017;59(12):3127–34.
[25] Svanda M, Polivka M. Matching Technique for an On-Body Low-Profile Coupled-Patches UHF RFID Tag and for Sensor Antennas. IEEE Trans Antennas Propag 2015;63(5):2295–301.
[26] Rasilainen K, Ilvonen J, Viikari V. Antenna Matching at Harmonic Frequencies to Complex Load Impedance. IEEE Antennas Wirel Propag Lett 2015;14:535–8.
[27] Kulkarni S, Baghel A, Nayak S. Graded refractive index metamaterial for enhanced far-field wireless power transfer efficiency in S-band. AEU - Int J Electron Commun 2021;138:153859.

Electro-textile UHF-RFID Compression Sensor for Health-caring Applications

Chengyang Luo, *Member, IEEE*, Ignacio Gil and Raúl Fernández-García

***Abstract*— Electro-textile Ultra High Frequency (UHF, 865-868 MHz) Radio Frequency Identification (RFID) devices have great potential to be explored as sensors due to the features of fabric materials. In this work, an electro-textile UHF-RFID compression sensor base on T-match structure with a corresponding interface are developed and evaluated for two application scenarios. For accurate textile UHF-RFID antenna design and maximize the read range, the impedance of the electro-textile based on snap buttons is modelled and characterized an a measured read range of 5.22m is experimentally obtained. If the distance of the RFID reader and RFID sensor remain constant at 1 m. The experimental results show that RSSI range change from -42 dBm to -58 dBm as a quadratic function in terms of the knee angle bending and from -45 dBm to -40 dBm during expiration and inspiration phase when the sensor is located on the chest, which validated the usefulness of the proposed sensor.**

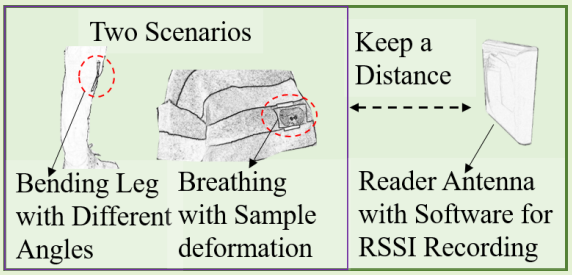

***Index Terms*— Antenna sensor, electro-textile, bending angles, conductive yarn, compression sensor, equivalent circuit, interface, Received Signal Strength Indicator (RSSI), respiration, Ultra High Frequency (UHF), RFID**

I. Introduction

With Radio Frequency Identification (RFID) technology development, many commercial devices are applied in diverse scenarios [1] [2] [3] such as health-caring monitoring [4], goods tracking [5] [6], classification, localization [7] and stuff management [8]. Especially in health-caring monitoring scenarios, the wireless RFID devices are expected to play a role as respiration sensors [9] [10], skin temperature sensors [5] [15] [16] and strain sensors [17] [18]. Generally, the operation frequency selection and structure designs of RFID sensors depend on the required sensing functions. With regard to the working frequency selection, Ultra High Frequency (UHF) RFID devices are getting more attention due to their lower cost, long-distance transmission and fast-easy identification. There are two ways to achieve sensing functions for wireless UHF-RFID devices. One way is that tags can be designed to connect sensors with different functions [19]. For these types of UHF-RFID sensors, chips need to have extendable ports for sensors connection (such as the ROCKY100) [19]. Another way is to use the antenna as a sensor.

The development of textile UHF-RFID tags are getting more attention due to several useful features such as flexibility and hydrophilicity. Some textile UHF-RFID tags are designed as a concentration solution sensor due to their good hydrophilicity [20].

Texitle UHF-RFID antenna sensors combine the ability of wirelessly sensing data with flexible and weareable substrates. The typical measurement methods is based on the received signal strength indicator (RSSI) parameter [10] [20]. When the UHF-RFID antenna is affected by external factors such as permittivity changing, bending or temperatura variation, the RSSI and read range are expected to vary in some ways with the related sensing factors. The standard welding techniques for connecting chips to textile materials are not suitable. Some works are exploring free welding methods such as fixing with glue [20], non-conducting yarns or copper plates [9] [10]. However, the textile designs are foreseen to have difficulties such as chip pads rust due to textile washing and the detachment of the chip-welded board in textile devices.

There are some solutions for the electro-textile interfaces used in RFID devices. In [11] polydimethylsiloxane (PDMS) pads are reported. In [12] several snap buttons are used for the connection of a RFID-sensor module and a textile PIFA antenna. However, the impact from the connection of the male and female snap buttons is ignored, which is proved important according to [13] [14]. The snap button was compared with other electro-textile interfaces by the authors in previous publication [14]. The snap button was the best option to guarantee the interconnection under stretching stress. However, in order to guarantee a good matching, the snap button electrical behaviour should be considered. One of the novelties of this paper is the introduction of an equivalent circuit model of the snap button.

Manuscript received Month DD, YYYY; revised Month DD, YYYY; accepted Month DD, YYYY. This work was supported in part by Spanish Government-MINECO under Project TEC2016-79465-R and China Scholarship Council under Grant No.201908440233.

The authors are with Department of Electronic Engineering, Universitat Politecnica de Catalunya, Barcelona 08222, Spain (e-mail: raul.fernandez-garcia@upc.edu).

In this paper, an electro-textile UHF-RFID compression sensor with the corresponding electro-textile interface are developed and evaluated for two application scenarios. Snap buttons for modern clothes are applied into the interface. To obtain accurate textile UHF-RFID antenna performance, the impedance of the interface is modelled, simulated and experimentally validated. Based on the interface impedance results, a textile UHF-RFID antenna is designed and tested by means of read ranges in free space. The proposed antenna is used as a compression sensor under two application scenarios: bending on a knee and respiration using the RSSI parameter as a figure of merit. The aim of the work is to evaluate the e-textile RFID tag as healthcare sensor.

II. Textile UHF-RFID Tag Design

A. Structure of the Proposed Electro-textile Design

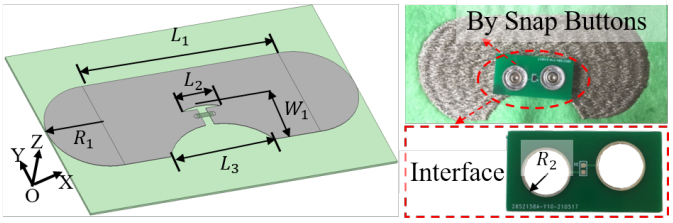

Fig. 1. Geometry and configuration of the proposed electro-textile UHF-RFID sensor with the corresponding interface

The geometry and configuration of the proposed electro-textile UHF-RFID sensor with the corresponding interface are shown in Fig.1. The RFID antenna design is inspired by a typical 'T-match' structure including the male snap button as an electro-textile interface between textile and detachable printed circuit board (PCB) which includes the IC. The proper feed port size for the male snap button is calculated. The geometry dimensions of the textile have been adapted to the human knee and chest shape to improve the sensing performance. Note, that the sensing area corresponds to the textile material, whereas the rigid PCB do not affect the sensing behaviour.

The proposed design dimension parameters are listed in Table I and the PCB interface size is 16.38 x 31.12 x 0.8 mm. The UHF-RFID chip is LXMS21ACNP-184, with input impedance of 19-j284 ohm and wake-up power of -18 dBm. When the chip is welded on the board, the impedance of the interface is expected to change and the detailed analysis is carried out in next section.

TABLE I
UHF-RFID Sensor Dimension Parameters (Unit: mm)

Design	L_1	L_2	L_3	W_1	R_1	R_2
Values	74	15	40	22	20	4.5

The proposed textile antenna sensor is based on embroidered conductive yarns on a polyester substrate (thickness 0.88 mm.) The commercial conductive twisted yarns are made of 99% pure silver-plated Nylon, the conductivity of which is 11500 siemens/m. The relative dielectric constant, loss tangent and thickness of the substrate are 1.29 (ε_r), 0.00188 (tanD) and 0.88 mm, respectively, measured by a Microwave Frequency Q-Meter as shown in Figure 2 (a). The thickness is measured by an Electronics Outside Micrometer (132-01-040A) as shown in Figure 2 (b). The snap buttons for the interfaces are made of steel.

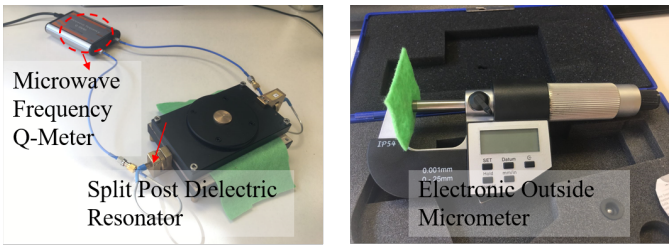

(a) (b)

Fig. 2. Substrate parameters measurements. (a) Permittivity and loss tangent measurements, (b) Thickness measurement.

B. Impedance Measurement Method

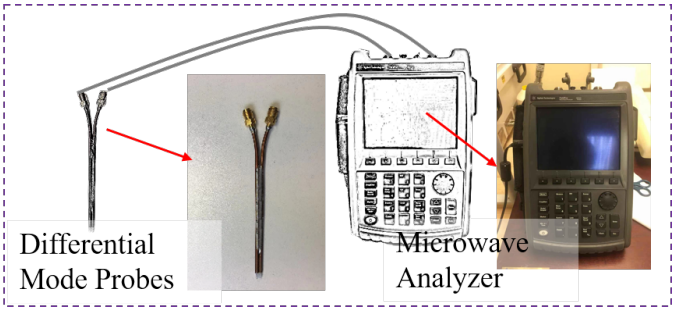

Fig. 3. Calibration setup with the differential mode probes for impedance measurements method

For balanced structures, the impedance characterization consists of differential mode measurement combined with port extension of the Microwave Analyzer as shown in Fig. 3 and it was previously used in [20] [22] [23] [24].

The probes are made from two semi-rigid cables with ground shields soldered together. Concerning to the procedure, first of all, the Microwave Analyzer with two coaxial cables needs to be calibrated by a standard calibration kit. Secondly, after connecting the coaxial cables to the probes, the function (port extension [25]) of the Microwave Analyzer needs to be adjusted in order to move the calibration plane from the ends of the coaxial cables to the ends of the probes. The traces in Smith chart of the two ports should roughly converge to the open circuit position in Microwave Analyzer. Next, the two tips of the differential mode probes are connected to the proposed textile UHF-RFID antennas or the feed port PCBs and the Z parameters in 50 ohms can be obtained. Note that the measured Z parameters using the differential mode probes are earth-referenced and need to be transferred for the differential reflection coefficient (ρ) of the balanced samples [26] [27]. Finally, Z parameters of the tested samples can be calculated using the equations 1 as follows,

$$Z_{ant} = \frac{2Z_0(1 - S_{11}S_{22} + S_{12}S_{21} - S_{12} - S_{21})}{(1 - S_{11})(1 - S_{22}) - S_{12}S_{21}} \quad (1)$$

Where Z_0 is 50 ohms, S_{11}, S_{12}, S_{21} and S_{22} are the measured S parameters, Z_{ant} is the Z parameter of the balanced samples.

C. Embroidery Procedure

The electrical and mechanical characteristics of an embroidered design are highly dependent on the embroidery setting such as the stitch pattern, stitch density and number of embroidered layers. A commercial embroidery machine (Singer Futura XL-550) is used to embroider the patterns on the substrate (polyester). For the proposed design, the 'satin fill' mode in the embroidery software (EasyDesign EX4.0) is adopted, the stitch density is adjusted to 80% of the default value and in the manufacturing process, the proposed yarns are utilized in both sides of the substrate as the conductive yarns and support yarns.

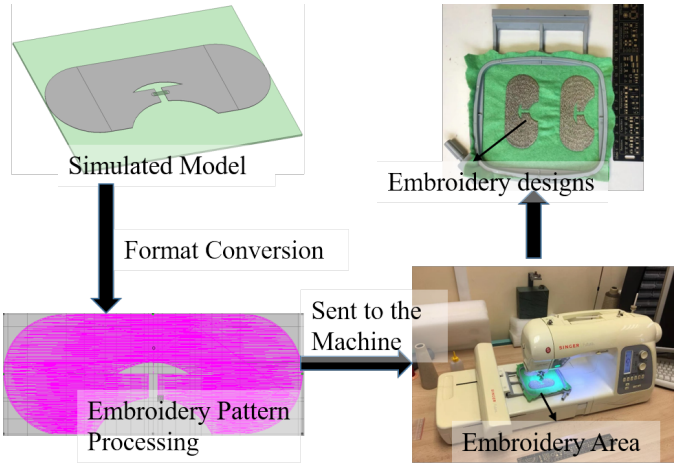

Fig. 4. Embroidery procedure.

The embroidery procedure is detailed in Figure 4. And the detailed steps are listed as below,

1.First, the geometric dimension of the design is obtained from the 3D full electromagnetic simulations.

2. Second, the antenna geometry is converted to an embroidered pattern. The software needs to be adjusted carefully to guarantee that the size and boundaries of the designs are not affected by the embroidery patterns.

3. Third, the stitch pattern and the density should be adjusted and kept constant.

Note that, in order to reduce the electrical conductivity of the embroidered substrate, both, top and bottom yarns are conductive.

D. RSSI Sensing Principle

RSSI determines the strength of a wireless signal received by a device, which is affected by many factors in the environment according to the Equation 2

$$RSSI = P_t + G_t + G_r - L_c - L_{fs}(dB) \quad (2)$$

Where P_t is the power from the transmitting antennas, G_t is the gain of the UHF RFID Reader, G_r is the gain of the UHF RFID tag, L_c is the power loss of the conductive lines and L_{fs} is the power loss in free space, Equation 3).

$$L_{fs} = 32.5 + 20\lg f(MHz) + 20\lg D(km) \quad (3)$$

Where f is the wave frequency in MHz and D is the transmission distance in km.

When the antenna gain of the UHF RFID tag is affected by factors such as bending and/or stretching and the rest of the parameters remains constants, the RSSI is modified and it can be used as a sensing parameter. Therefore, the UHF RFID textile tag can be used as a sensor.

III. Simulation and Measurement

A. Equivalent Circuit Simulation and Impedance Measurement of the Interface

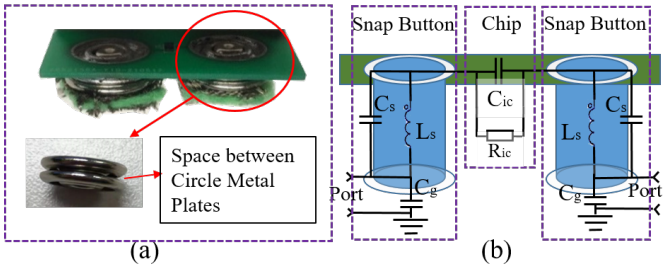

Fig. 5. Geometry and equivalent circuit of the interface with the chip and the snap buttons. (a)Geometry, (b)equivalent circuit

When the chip is welded on the board, the impedance of the interface is expected to change (different from initial impedance 19-j284 ohm). Therefore, the accurate impedance of the interface with the chip and snap buttons need to be measured and analyzed for the textile UHF-RFID antenna sensor simulation as a feed port. The geometry and equivalent circuit of the interface with the chip and the snap buttons are shown in Fig. 5. A conventional via can be equivalent to an inductor with a resistor in parallel and a grounded capacitor in cascade [28].

The equivalent circuit of the interface with the chip and the snap buttons is shown in Fig. 5 (b). Where Ls and Cs represent the inductance and capacitance of snap button, respectively. Cg models the capaciante between snap button and ground, and Cic and Ric model the IC input impedance.

Therefore, from one port, the equivalent input impedance (Z_e) can be given by,

$$Z_e = (L_s//C_s + R_{ic}//C_{ic} + L_s//C_s + C_g)//C_g \quad (4)$$

in detail,

$$Z_e(\omega) = \frac{1}{\left(\frac{2}{\frac{1}{j\omega L_s} + j\omega C_s} + \frac{1}{\frac{1}{R_{ic}} + j\omega C_{ic}} + \frac{1}{j\omega C_g}\right)} + j\omega C_g \quad (5)$$

Where ω is the angular frequency. R_{ic} (4.264 kOhm) and C_{ic} (0.64 pF) are the complex impedance of the used chip. L_s, C_s

and C_g need to be estimated by means of measured results and the Equation 5.

The measurement setup for the interface impedance is shown in Fig. 6. After obtaining the measured impedance curves of the interface, L_s, C_s and C_g can be calculated by the Equation 5 and the results are listed in Table II.

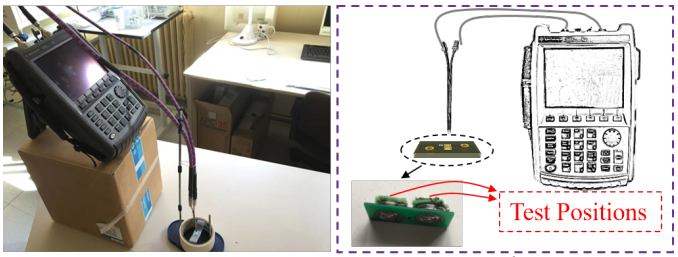

Fig. 6. Experimental setup for the interface impedance. (a) Photograph of the setup and (b) experimental setup configuration.

TABLE II
VALUES OF THE EQUIVALENT CIRCUIT COMPONENTS

Components	L_s	C_s	C_g
Values	12.65 nH	0.43 pF	2.68 pF

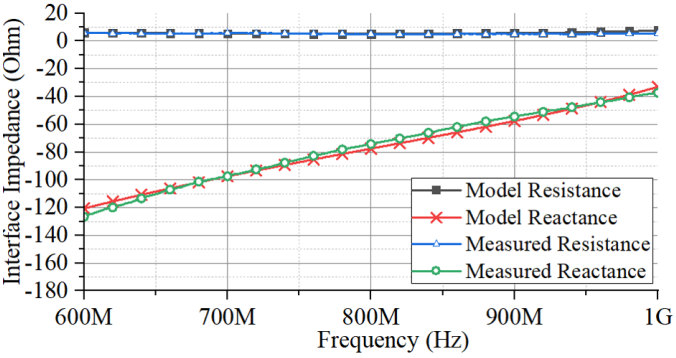

Fig. 7. Modelled impedance and measured impedance curves of the interface

The modelled and measured impedance results are shown in Fig. 7. It is found that the modelled resistance and reactance curves of the interface are close to the measured curves. Therefore, the measured impedance of the interface for the textile UHF-RFID antenna sensor is 5.06-j60.27 ohm.

B. Impedance Simulation and Measurement of the Textile UHF-RFID Design

After obtaining the real impedance of the interfaces at 868 MHz (5.06-j60.27 ohm), the textile UHF-RFID antenna sensor simulation for the model shown in Fig. 1 can be carried out by using a full wave 3D electromagnetic (EM) simulation software. Note that the antenna is expected to be designed for a conjugate matching with the interface. The experimental setup for the impedance test of the embroidered designs is shown in Fig. 8 and the simulated and measured results are shown in Fig. 9. It is found that the measured resistance

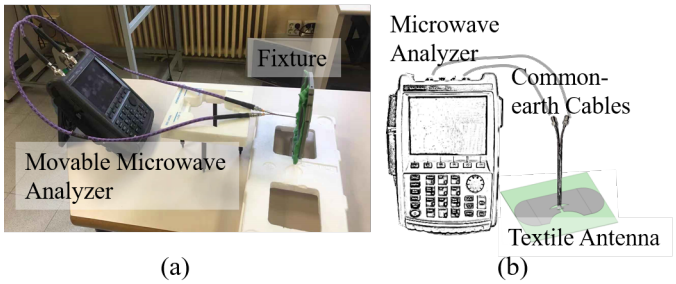

Fig. 8. Experimental setup for the impedance of the embroidered designs. (a) Photograph of experimental setup, (b) Experimental setup configuration.

and reactance curves are close to the simulated curves. In detail, the difference between the measured and simulated resistance parts at 868 MHz is 3 ohm and the corresponding to the reactance parts is 4 ohm in absolute value (simulated: 12.52+j56.77 ohm, measured: 9.24+j60.51 ohm). Moreover, the interface impedance at 868 MHz (5.06-j60.27 ohm) is almost conjugate matching with the antenna (9.24+j60.51 ohm).

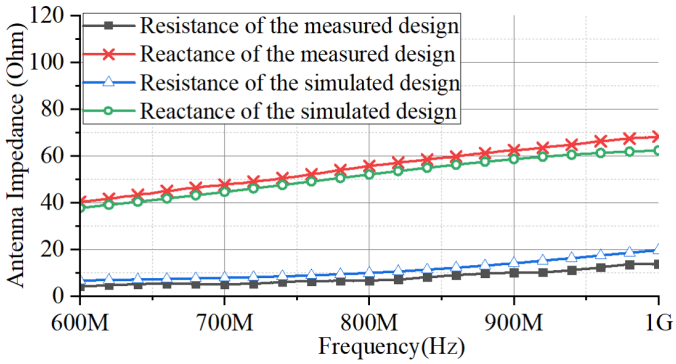

Fig. 9. Simulated and measured impedance curves of the textile UHF-RFID antenna sensor

C. Read Range Tests in Air

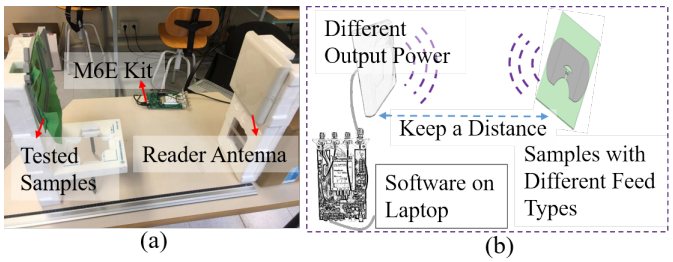

Fig. 10. Experimental setup for the read ranges of the textile UHF-RFID antenna sensor. (a) Photograph of experimental setup, (b) Experimental setup configuration.

The experimental read range measurements have been performed in an ordinary room laboratory to reproduce a real environment where some effects such as electromagnetic interference (EMI) or reflective effects can be produced.

The read range setup test is shown in Fig. 10. The read range evaluation has been done by fixing a constant distance between reader and tag of 0.7m whereas the reader output power is swept down until the tag is not detected.

The reader antenna (MT-242025/TRH/A/A) can be controlled by the M6E Kit which is connected to a laptop with specific control software.The maximum value of the read range can be calculated by the threshold power and the read range is obteined by the Friis Transmission Formula [29] as follows,

$$d_{max} = \frac{\lambda}{4\pi}\sqrt{\frac{P_t G_t G_r \cdot \tau}{P_{th}}} \tag{6}$$

where d_{max} is the maximum value of the read range, λ is the wavelength at 868 MHz, P_t is the power fed into the reader antenna, G_t is the gain of the reader antenna (7 dBi), G_r is the gain of the proposed UHF-RFID antenna, τ is the largest power transmission coefficient and P_{th} is the minimum wake-up power of the chip(-18 dBm). In addition, the cable loss between the reader antenna and the reader is considered (0.8 dB). Note that the P_t, G_t, G_r and P_{th} are expressed in international system units.

The proposed antenna has a maximum realized gain of 1.38 dBi. The simulated and measured read ranges are listed in the Table III. It is found that simulated and measured read ranges are close and the measured read range is up to 5.22 m in air.

TABLE III
SIMULATED AND MEASURED READ RANGES AT 868 MHZ IN AIR (UNIT: M)

Case	*Simulated*	*Measured*
Value	6.74	5.22

IV. APPLICATION AND DISCUSSION

In order to explore the compression ability of the electro-textile UHF-RFID antenna sensor for human beings, two application scenarios; bending on a knee and respiration frequency, are tested. The bending on a knee measurement can be useful when people exercise or have a postoperative recovery process. In this scenario, the electro-textile UHF-RFID antenna sensor on knees can record the knee flexion angles with the corresponding RSSI values. The respiration frequency rate can be applied when breathing of patients or common babies need to be monitored. Moreover, the data can be recorded by portable electronic equipments.

The sensing capability is only due to e-textile antenna; the rigid interface does not have sensing behaviour. However, the rigid PCB is necessary to attach the snap button which guarantees the interconnection under stretching stress and it allows the detachable interface of the IC when washing is required.

A. Bending Angles Monitor on a Knee

For exploring the feasibility in the first application scenario, the experimental setup for a bending angles monitoring on a knee is shown in Fig. 11. In this test, when the knee is bended, the RFID reader and related software can record the values of

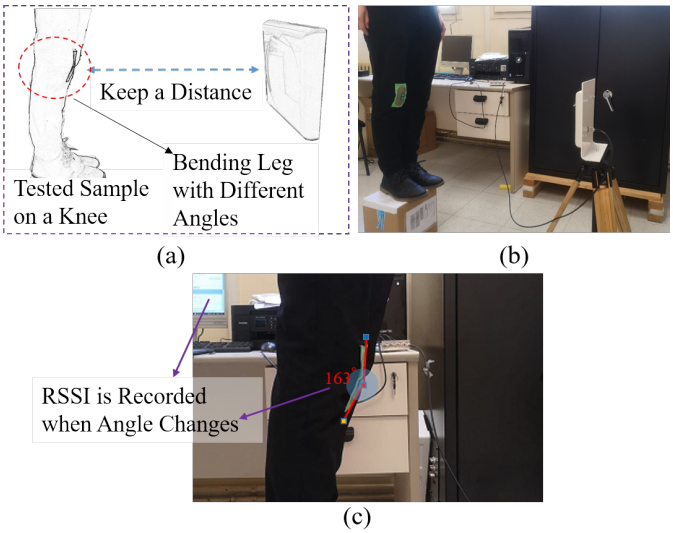

Fig. 11. Experimental setup for a bending angles monitor on a knee. (a) Experimental setup configuration, (b) photograph of experimental setup, (c) case diagram of angle tests.

the current RSSI as shown in Figs. 11 (a) and (b). To validate the sensor functionality, a photograph of each measured point has been taken and the knee flexion angle has been processed through image processing and compared with the proposed sensor as shown in Fig. 11 (c). Note that the angle of 180° refers to the sensor sample fixed flat on the pants while the angle of 168° refers to the sensor sample fixed on the knee due to the initial shape of the knee. In this case, a distance of 1m between the RFID reader and the RFID tag has been fixed.

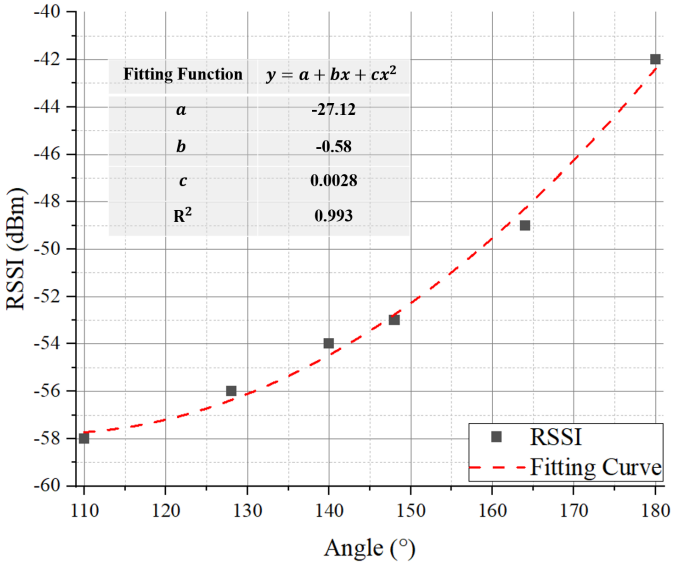

Fig. 12. Bending angles monitor RSSI values and a fitting curve varying with angles.

The RSSI values and a related fitting curve varying with angles are shown in Fig. 12. The RSSI-angle fitting curve conforms to a quadratic function model whose coefficients are listed in the Fig. 12. The RSSI range varies from -

42 to -58 dBm when bending angle varies from 180º to 110º, respectively. The fitting coefficient (R_2) is 0.993, which means the curve has a good fit to the measured values. From this analysis, the feasibility of the electro-textile UHF-RFID compression sensor as a bending knee angles monitor is proved.

B. Respiration Monitor

For exploring the feasibility of the proposed sensor to monitorize the respiration rate, the experimental setup is shown in Fig. 13. The electro-textile UHF-RFID compression sensor is fixed on a person breathing at respiration rate of 3 Hz (about 1 breath every 3 seconds). While breathing continues, the RSSI is measured and processed by the RFID reader at a fix distance of 1 m.

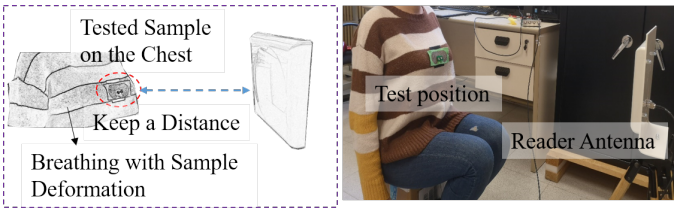

Fig. 13. Experimental setup for a respiration monitor on a chest (about 1 breath/3 seconds). (a) Experimental setup configuration, (b) photograph of experimental setup.

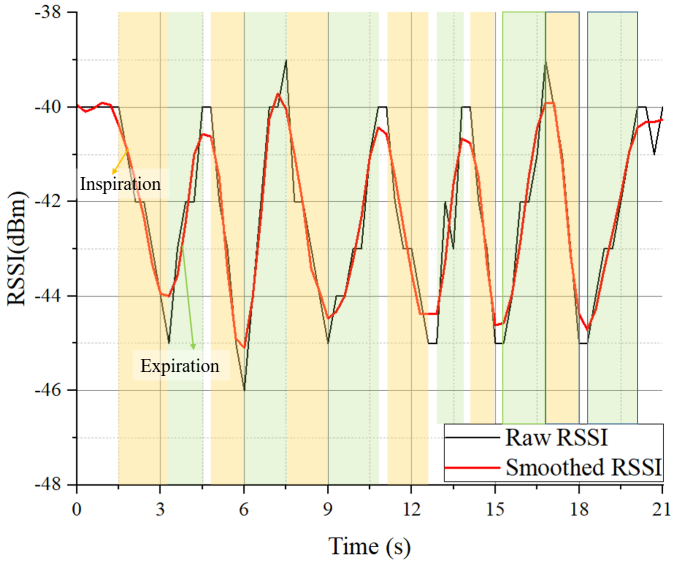

Fig. 14. Respiration monitor RSSI values and a smoothed curve varying with time (about 1 breath/3 seconds)

The measured raw RSSI data and related smoothed RSSI curves are shown in Fig. 14. The smoothed RSSI curve can be obtained by the Savitzky-Golay fitting way using data analysis and a graphic software. The measurement results shown the RSSI decreased from -40 dBm to -45 dBm during inspiration phase and increase from -45dbm to -40 dBm during the expiration phase with a respiration rate of 3 Hz, which denotes the feasibility of the proposed electro-textile UHF-RFID compression sensor as a respiration rate sensor.

V. Conclusion

In this paper, an electro-textile UHF-RFID compression sensor with the corresponding interface was developed and evaluated for two application scenarios. In order to maximize the read range, the antenna was designed to optimize the matching between IC and antenna. In order to do that, the electro-textile interface based on snap buttons was modelled and experimentally characterized and an experimental read rage of 5.22m was achieved. The RSSI parameter was used as a figure of merit to validate the feasibility of the proposed compression sensor under two different health care applications scenarios. The RSSI showed a variation from -42 dBm to -58 dBm when the RFID tag sensor was located on the knee and a flexion angle from 110º to 180º was applied to the knee, respectively. When the proposed sensor was located in the chest, the RSSI increased and decreased from -45 dBm to -40 dBm during expiration and inspiration phase, respectively. Therefore, the feasibility of the electro-textile UHF-RFID tag as a compression antenna sensor was proved.

References

[1] H. Arun, "Advancements in the use of carbon nanotubes for antenna realization," *AEU - Int. J. Electron. Commun*, vol 136, pp.153753, 2021.
[2] C. Occhiuzzi, C. Paggi and G. Marrocco, "Passive RFID Strain-Sensor Based on Meander-Line Antennas," *IEEE Trans. Antennas Propag.*, vol. 59, no. 12, pp. 4836–4840, Dec. 2011.
[3] C.Y. Luo, I. Gil and R. Fernández-García, "Wearable Textile UHF-RFID Sensors: A Systematic Review," *Materials*, vol. 13, no. 15, pp. 3292, 2020.
[4] J.C. Prather, Y. Meng, M.l Bolt, T. Horton and M. Adams, "Wireless head impact monitoring system utilizing eye movement as a surrogate for brain movement," *AEU - Int. J. Electron. Commun*, vol. 105, pp. 54–61, 2019.
[5] Y. Shafiq, J. S. Gibson, H. Kim, C. P. Ambulo, T. H. Ware and S. V. Georgakopoulos, "A Reusable Battery-Free RFID Temperature Sensor,"*IEEE Trans. Antennas Propag.*, vol. 67, no. 10, pp. 6612–6626, Oct. 2019.
[6] Y. Wang, A. J. Pretorius and A. M. Abbosh, "Low-Profile Antenna With Elevated Toroid-Shaped Radiation for On-Road Reader of RFID-Enabled Vehicle Registration Plate," *IEEE Trans. Antennas Propag.*, vol. 64, no. 4, pp. 1520–1525, April 2016.
[7] C. Luo, I. Gil and R. Fernández-García, "Textile UHF-RFID Antenna Embroidered on Surgical Masks for Future Textile Sensing Applications," *IEEE Trans. Antennas Propag.*, pp 1-8, 2022.
[8] Z. Ali, et al., "Authentication Using Metallic Inkjet-Printed Chipless RFID Tags," *IEEE Trans. Antennas Propag.*, vol. 68, no. 5, pp. 4137–4142, May 2020.
[9] Y. Liu, A. Levitt, C. Kara, C. Sahin, G. Dion, and K. R. Dandekar,"An improved design of wearable strain sensor based on knitted RFID technology," *2016 IEEE Conference on Antenna Measurements Applications (CAMA)*, pp. 1—4, 2016
[10] M. Tajin, C. Amanatides, G. Dion and K. Dandekar, "Passive UHF RFID-Based Knitted Wearable Compression Sensor," *IEEE Internet Things J.*, vol. 8, no. 17, pp. 13763–13773, 2021
[11] R.B.V.B. Simorangkir, D.Le, T.Björninen, A.S.M.Sayem, M.Zhadobov and R.Sauleau, "Washing Durability of PDMS-Conductive Fabric Composite: Realizing Washable UHF RFID Tags," *IEEE Antennas Wirel. Propag. Lett.*, vol. 18, no. 12, pp. 2572-2576, Dec. 2019.
[12] Q.H. Dang, S.J. Chen, D.C. Ranasinghe and C. Fumeaux, "Modular Integration of a Passive RFID Sensor With Wearable Textile Antennas for Patient Monitoring," *IEEE Trans Compon. Packaging. Manuf. Technol.*, vol. 10, no. 12, pp. 1979-1988, Dec. 2020.
[13] S.J. Chen, D.C. Ranasinghe and C. Fumeaux, "A Robust Snap-On Button Solution for Reconfigurable Wearable Textile Antennas," *IEEE Trans. Antennas Propag.*, vol. 66, no. 9, pp. 4541-4551, Sept. 2018.
[14] C.Y. Luo, I. Gil and R. Fernández-García, "Experimental comparison of three electro-textile interfaces for textile UHF-RFID tags on clothes," *Int. J. Electron. Commun.*, vol. 146, pp. 154137, 2022.

[15] A. Vaz, et al., "Full Passive UHF Tag With a Temperature Sensor Suitable for Human Body Temperature Monitoring," *IEEE Trans. Circuits Syst. II Express Briefs*, vol. 57, no. 2, pp. 95–99, 2010.
[16] W. Zhu, et al., "Passive Digital Sensing Method and Its Implementation on Passive RFID Temperature Sensors," *IEEE Sens. J.*, vol. 21, no. 4, pp. 4793–4800, 2021.
[17] X. Chen, L. Ukkonen and T. Björninen, "Passive E-Textile UHF RFID-Based Wireless Strain Sensors With Integrated References," *IEEE Sens. J.*, vol. 16, no. 22, pp. 7835–7836, 2016.
[18] G. Chakaravarthi, K.P. Logakannan, J. Philip, J. Rengaswamy, V. Ramachandran and K. Arunachalam, "Reusable Passive Wireless RFID Sensor for Strain Measurement on Metals," *IEEE Sens. J.*,, vol. 18, no. 12, pp. 5143–5150, 2018.
[19] A. Vena, B. Sorli, B. Saggin, R. Garcia and J. Podlecki, "Passive UHF RFID Sensor to Monitor Fragile Objects during Transportation," *2019 IEEE International Conference on RFID Technology and Applications (RFID-TA)*, 2019, pp. 415-420.
[20] C. Luo,1, I. Gil and R. Fernández-García, "Textile UHF-RFID antenna sensor for measurements of sucrose solutions in different levels of concentration," *Meas. Sci. Technol*, vol. 32, pp. 10, 2021.
[21] C. Luo et al., "Collocated and Simultaneous Measurements of RF Current and Voltage on a Trace in a Noncontact Manner," *IEEE Trans Microw. Theory Tech.*, vol. 67, no. 6, pp. 2406–2415, 2019.
[22] L. Shan and H. Xiao, "Impedence characterization of RFID tag antennas and application in conformal tag antenna," *2015 7th Asia-Pacific Conference on Environmental Electromagnetics (CEEM)*, Hangzhou, 2015, pp. 140–142.
[23] H. Zhu, Y. C. A. Ko and T. T. Ye, "Impedance measurement for balanced UHF RFID tag antennas," 2010 IEEE Radio and Wireless Symposium (RWS), New Orleans, LA, 2010, pp. 128–131
[24] X. Qing, C. K. Goh and Z. N. Chen, "Measurement of UHF RFID tag antenna impedance," *2009 IEEE International Workshop on Antenna Technology*, Santa Monica, CA, 2009, pp. 1–4
[25] na.support.keysight.com/pxi/help/latest/S3_Cals/Port_Extensions.htm
[26] C.T. Carrasco, C.J. Sieiro, J.M. Lopez-Villegas, N. Vidal, R. Gonzalez-Echevarría and M.E. Roca, "Mixed-mode impedance and reflection coefficient of two-port devices," *Prog. Electromagn. Res.*, vol. 130,pp. 411-428, 2012
[27] C.K. Stoumpos, D.E. Anagnostou and M.T. Chryssomallis, "Experimental characterization of the impedance of balanced UHF RFID tag antennas," *Microw. Opt. Technol. Lett.* vol. 59(12), pp. 3127-3134, 2017
[28] H.H.M. Ghouz and E.B. El-Sharawy, "An accurate equivalent circuit model of flip chip and via interconnects," *IEEE Trans Microw. Theory Tech.*, vol. 44, no. 12, pp. 2543–2554, 1996.
[29] S. Kulkarni, A. Baghel, S. Nayak, "Graded refractive index metamaterial for enhanced far-field wireless power transfer efficiency in S-band," *AEU - Int. J. Electron. Commun*, vol 138, pp.153859, 2021

Chengyang Luo was born in Hubei, China, in 1995. He received the B. Eng. degree in integrated circuit design and integration system from Xidian University, Xi'an, China, in 2017. From 2019 to now, he is studying for the Electronics Engineering Ph.D. degree in Universitat Politecnica de Catalunya, Barcelona, Spain.

In 2017, he joined the China Electronic Product Reliability and Environmental Testing Research Institute (CEPREI), Guangzhou, China, where he served as a research assistant of the Science and Technology on Reliability Physics and Application of Electronic Component Laboratory, Guangzhou, China. In 2019, he obtained the national CSC-UPC Scholarship for the Ph.D. degree in Universitat Politecnica de Catalunya, Barcelona, Spain. His current research interests include textile UHF-RFID tags and sensing techniques, smart devices and noncontact voltage, current and power measurement techniques.

Ignacio Gil was born in 1978 in Barcelona, Spain. He received degrees in physics and electronics engineering in 2000 and 2003, and then his PhD in 2007 from the Universitat Autònoma de Barcelona, Spain. From 2003 to 2008 he was assistant professor in electronics and a researcher with the RF-Microwave Group in the Electronic Engineering Department, Universitat Autonòma de Barcelona, Spain. From 2006 to 2008 he worked for EPSON Europe Electronics GmbH where he developed high-performance integrated RF CMOS circuits, transceivers and system design. In 2008 he joined the Electronic Engineering Department, Universitat Politècnica de Catalunya (UPC), Spain, as lecturer and researcher. Since 2011 he is associate professor at UPC. Since 2012 he is also a collaborator at Universitat Oberta de Catalunya (UOC), Spain. He has been involved in 12 research projects (3 as principal researcher) in different research activities including passive and active RF and microwave devices and circuits, metamaterials, EMC and smart textile electronics. From 2012-2014 he served as Chairman of the Spanish IEEE EMC Chapter. In 2017 he was academic visitor at Loughborough University (UK) in the Wireless Communications Research Group. Since 2019 he is Deputy Director of International Relations at ESEIAAT (UPC). Dr. Gil is co-author of more than 150 scientific publications and 17 patents. He has been awarded the Duran Farell de Investigación Tecnológica (2006) and the patent award from SEIKO EPSON Corporation (2010). Dr. Gil has been visiting professor in different Universities: New Jersey Institute of Technology (USA), Limerick University (Ireland), Loughborough University (UK), Shaoxing University (China) and Polytechnic University of Tirana (Albania).

Raul Fernandez Garcia received the B.Eng. degree in telecommunications and M.Eng degree in electronics from the Universitat Politecnica de Catalunya, Barcelona, in 1997 and 1999, respectively. In 2007 he received the Ph.D. degree from the Universitat Autonoma de Barcelona. From 1998 to 2001, he worked for Sony Spain, as Radiofrequency Engineer, where he developed analog and digital TV tuners. From 2001 to 2007, he was part-time Assistant Professor in electronics with the Department of Electronics Engineering, Universitat Autonoma de Barcelona. Funded by the European Marie Curie Program, he worked on devices and circuits reliability at IMEC (Belgium) between 2005 and 2006. From 2008 to 2011, he was full-time Assistant Professor in the Department of Electronics Engineering, Universitat Politecnica de Catalunya. At present he is Associate Professor at the same department. Dr. Fernandez-Garcia is author or a co-author of more than 110 papers in international journals and conferences and he has been involved in 18 research projects (6 as principal researcher) in different research activities including reliability, electromagnetic compatibility and electronic textile. He was the recipient of Best Paper Awards at IPFA 2007. His current scientific interest is focused on wearable sensor development for sport and health applications.

Embroidered Textile Capacitive Sensor for Sucrose Solutions Measurement

Chengyang Luo, Raúl Fernández-García, Ignacio Gil
Department of Electronic Engineering, Universitat Politècnica de Catalunya, Barcelona, Spain
Email: Chengyang.luo@upc.edu

***Abstract*—With the trend of textile sensors, embroidered sensors for body fluids measurements are getting attention. In this paper, an embroidered textile sensor with a capacitive spiral structure is proposed and used to measure the capacitance when being poured by sucrose solutions with different levels of concentration at different frequencies. Since the coefficient of determination (R^2) near 0.997 from 250 Hz to 500 Hz shows the curves fitting well, the feasibility of the capacitance varying with different levels of concentration (0 - 250 mg/dl) in a linear curve at certain frequency range (250 - 500 Hz) is confirmed.**

***Index Terms*—Embroidered textile sensor; capacitive spiral structure; sucrose solutions; yarn; polyester.**

I. Introduction

Wearable sensors for health-caring monitoring and diagnosis are of growing concern in recent years. Some wearable sensors have been utilized for some disease-warning, physical fitness monitoring or emergency-rescuing applications, such as contact lens[1][2] with electrochemistry sensors for glucose monitoring in tears, an epidermal patch [3] with chemical-electrophysiological hybrid biosensor configuration for monitoring of sweat lactate levels and heart rate, and an instrumented mouthguard capable [4] with wearable salivary uric acid biosensing platform for the response or uric acid levels monitoring. These sensors are complexly designed on special substrates to measure and monitor some kinds of body fluids in special situations where some sensor platforms need to be put into eyes or mouth of human beings. In order to relieve discomfort and fully utilize advantages of modern clothes, wearable textile materials are worth choosing to design sensors for body fluids monitoring due to the fast development of embroidery technologies [5] and flexible electronic components and technologies [6]. With regard to the reliability for textile wearable sensors on different textile substrates, our group proved that certain textile sensors can keep its functions and performance in standard conditions after several washing [7]. Moreover, textile wearable sensors can reduce the manufacturing time and cost due to embroidery technique processing and low-cost yarns and textile substrates.

currently, some embroidered textile sensors correspond to textile piezoresistive sensors and inductive sensors designed for some health-caring, environment-monitoring or artificial intelligence applications. The applications mainly include physiological recordings by electrocardiogram and thoracic impedance measurements [8], trunk movements tracking using a zigzag pattern sensor [9], and skin temperature monitoring using an armband with a sensing yarn [10]. However, there are less embroidered textile sensors for body fluids measurements compared with the aforementioned cases and some internal biosensors with advanced integrated circuit technologies. In this paper, an embroidered textile sensor with a capacitive spiral structure is designed and utilized to measure the capacitance when being poured by sucrose solutions with different levels of concentration at different frequencies.

The paper is structured as follows, the manufactured materials and designed methods for the proposed sensor, measurements setup and test methods are illustrated and described in Section II. The experimental results, analysis and discussion are shown in Section III. The conclusion is made in Section IV.

II. Materials and Methods

A. Capacitive Spiral Sensor

The proposed textile sensor based on a capacitive spiral structure is embroidered on a polyester woven fabric as shown in Fig. 1. A practical sample is shown in Fig. 1(a), and the designed model with some structure details is shown in Fig. 1(b). The textile sensor is considered to be compact and certain capacitive characteristics in a limited space, the spiral structure becomes a one of choices which refers to the common plate capacitors and electrolytic capacitors. The textile material of this sensor is a commercial conductive twisted yarn (Shieldex 117/17 dtex 2-ply) made of 99% pure silver-plated Nylon. This kind of conductive yarn is chosen since sensors with the silver-plated yarn had better ranked performance in terms of sensitivity, linearity, and steady state for wearable applications[11]. With regard to the substrate material for the sensor, it is a good choice to use polyester woven fabric due to the high popularity in clothing and good dielectric performance.

In addition, permittivity (ε_{rp} = 1.5) and loss tangent ($tan\theta$ = 0.0189) of the polyester woven fabric have an effect on the sensor performance. Thus the two factors are measured by a split post dielectric resonator with a Microwave Frequency Q-Meter as shown in Fig. 2(a). To embroider the pattern of the sensor on the polyester woven fabric substrate, a professional embroidery machine (Singer Futura XL-550) is used as shown

978-1-7281-5278-3/20/$31.00 ©2020 IEEE

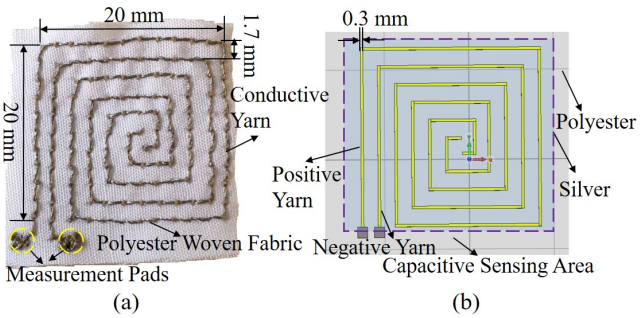

Fig. 1. (a) Embroidered capacitive sensor (b) Designed model with some structure details

in Fig. 2(b). In the manufacturing process, the proposed yarn are utilized in both sides of the substrate as the conductive yarn and support yarn.

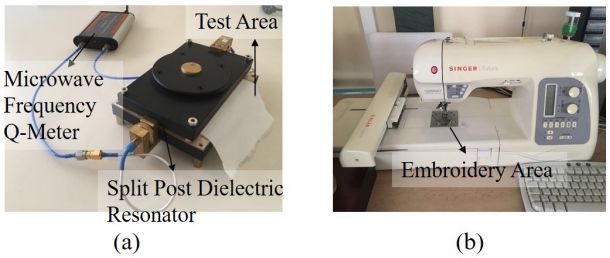

Fig. 2. (a) Microwave frequency Q-Meter for permittivity measurements (b) Embroidery machine

B. Measurement Methods and Setup

The proposed sensor is a type of electrolytic capacitive sensors whose capacitance is sensitive to different materials of the substrate and the distances between the positive and negative yarns. The two conductive yarns both are embroidered by a single yarn as the positive electrode and negative electrode. When the sucrose solutions are poured on the sensor, the substrate (polyester) will absorb the solutions which make the dielectric properties of the substrate changing. When the distance between the positive and negative yarns is fixed after embroidering, the capacitance will change due to the impact of the solutions with different levels of concentration onto the effective dielectric constant of the sensor.

As shown in Fig. 3, the pads of the positive and negative yarns are connected to the LCR Meter (Rhode & Schwarz HM8118) with a couple of flips and the sucrose solutions with different levels of concentration from 0 mg/dl to 250 mg/dl are poured onto the surface on the sensor, respectively. Note that the pure water was used as the solvent to avoid effects from impurities. For each solution, the capacitance values of the sensor are measured at frequencies from 20 Hz to 200 kHz in order to determine the frequency where the capacitance varies with different levels of concentration in a linear curve.

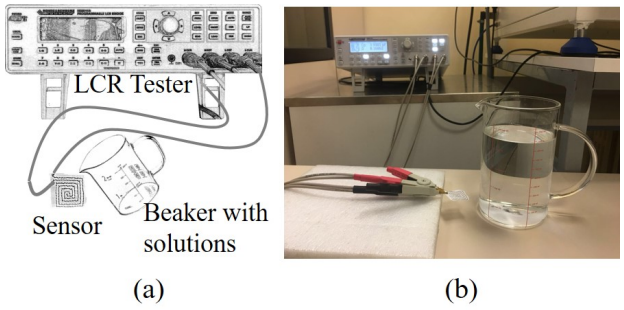

Fig. 3. Measurement setup for capacitance values of the sensor with the solutions with different levels of concentration. (a) Measurement setup configuration. (b) Photograph of measurement setup.

III. Results and Discussion

A. Results

The experimental capacitive frequency response for the sucrose solutions with the concentration from 0 mg/dl to 250 mg/dl has been tested and three levels (0 mg/dl, 100mg/dl and 250mg/dl)of them are shown in Fig. 4. From this figure, it can be observed that the capacitance is affected by the frequencies and the levels of concentration. The measured capacitance decreases gradually before the frequency of 1kHz and slowly after it in all cases, meanwhile, the capacitance also decreases with rise in concentration. The trends of the curves can be simply analyzed using the operation principle of electrolytic capacitor [12]. with regard to some studies [13], in qualitative terms, due to the interaction between the sucrose solution and the textiles, the parasitic capacitances exist. However, when the frequency rise, the impacts of parasitic capacitances decrease which cause the overall capacitance gradually decline as the frequency increases.

Moreover, the fact that the capacitance also decreases with rise in concentration can be simply analyzed according to the ideal formula corresponding to a capacitor as follows,

$$C = \frac{\varepsilon_0 \varepsilon_r S}{d} \tag{1}$$

where ε_0 is the permittivity of free space, ε_r is the relative permittivity of the material between the positive and negative yarns, d is the distance between the two yarns and C is the capacitance of the sensor.

Note that the formula 1 is just used to analyze the trends of the curves but in real measurements there are some impact factors from environments and errors that need to be considered. For the fixed sensor, the S, d and ε_0 can be considered as constant, thus the ε_r is the main factor to affect the capacitance. From formula 1, when the sucrose solutions are poured onto the embroidered sensor, the value of ε_r will change with different levels of concentration. In addition, with regard to the studies [14][15], the relative permittivity ε_r of sucrose solutions is expected to decrease as the concentration increases.

Figs. 5 (a), (b), (c) and (d) provide the measured capacitance curves of the sensor tested in terms of the sucrose solutions

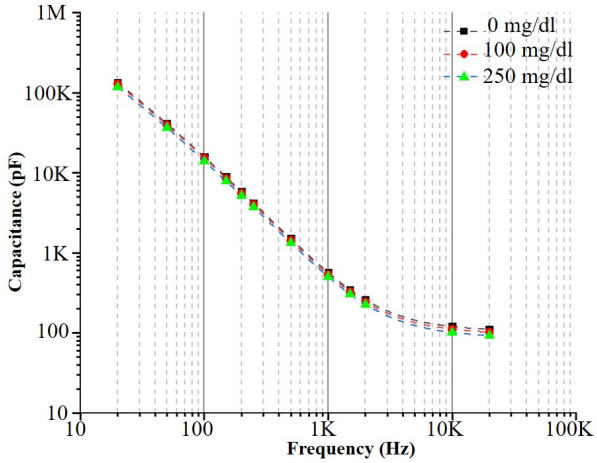

Fig. 4. Capacitance of the sensor tested at different frequencies in the sucrose solutions with concentration of 0 mg/dl, 100mg/dl and 250mg/dl.

with concentration values from 0 mg/dl to 250 mg/dl at 20Hz, 250Hz, 500Hz and 20kHz, respectively. In general, the concentration of an unknown sucrose solutions can be calculated by the regular Xc-concentration curve. However, it is difficult to analyse the concentration when the sensor works in an irregular way at lower frequency point such as 20Hz in Fig. 5(a) or higher frequency point such as 20kHz in Fig. 5(d). From Figs. 5(b) and (c), a linear function (y=a+bx) is utilized to fit the data and the coefficient of determination (R^2) shows the curves fitting well. Thus the typical working frequency range can be confirmed from 250Hz to 500Hz. In this frequency range, the capacitive sensor can work in the sucrose solutions with a certain linear trend.

B. Discussion

From the results, the feasibility of the embroidered capacitive sensor for sucrose solutions is confirmed and the sensor can work to measure the capacitcance with solutions in a linear way at the certain frequency range. Since currently there are less researches on body fluids measurement using embroidery sensors, this work is a first step for this kind of measurements. Next step of the work is to test the similar body fluids measurement and solve some reliability problems.

IV. Conclusion

To conclude, an embroidered textile sensor with a capacitive spiral structure is proposed to contribute to the embroidery sensors research about body fluids measurements. In this work, the proposed sensor is embroidered by polyester woven fabric as the substrate and silver-plated Nylon as the conductive and support yarn. The sensor is used to measure the capacitance when being poured by sucrose solutions with different levels of concentration in different frequencies in order to confirm the feasibility of the concentration measurements in a linear way for this sensor. Through analysing the results, the capacitance varying with different levels of concentration in a linear curve

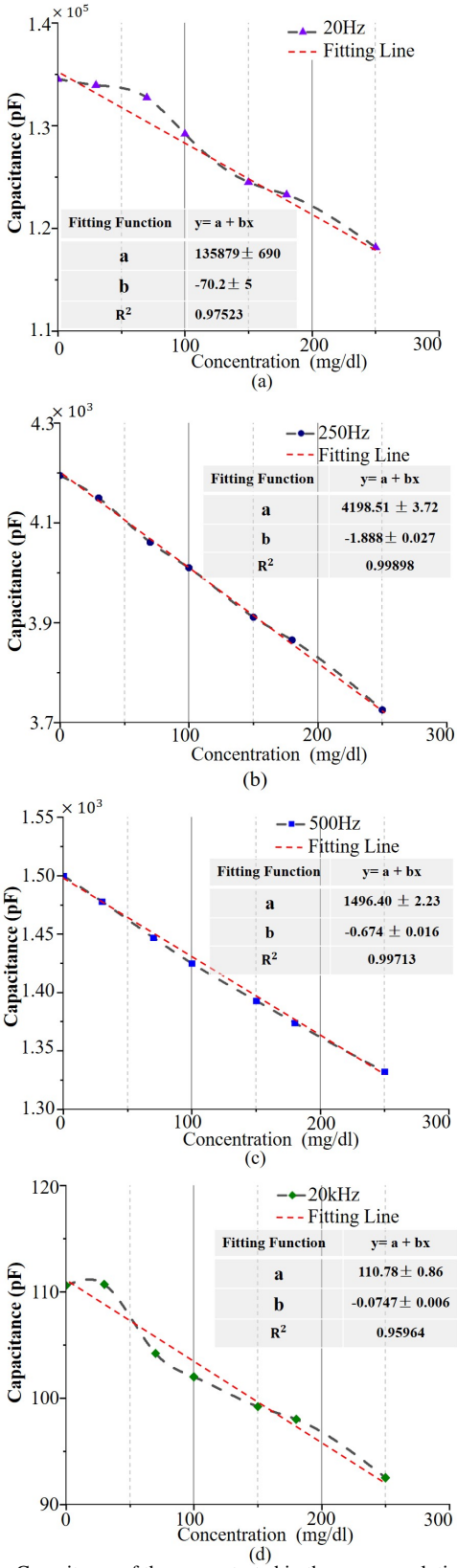

Fig. 5. Capacitance of the sensor tested in the sucrose solutions with different levels of concentration at different frequencies. (a) 20Hz. (b) 250Hz. (c) 500Hz. (d) 20kHz.

can be measured at certain frequency range from 250Hz to 500Hz.

ACKNOWLEDGMENT

This work was supported by Spanish Government-MINECO under Project TEC2016-79465-R and China Scholarship Council.

REFERENCES

[1] M. Senior, "Novartis signs up for Google smart lens," *Nat. Biotechnol*,vol. 32, no. 856, Sept. 2014.

[2] K. Joohee, et al, "Wearable smart sensor systems integrated on soft contact lenses for wireless ocular diagnostics," *Nat. Commun*, vol. 8, no. 1, pp. 1-8, 2017.

[3] S. Imani, A.J. Bandodkar and et al, "A wearable chemical–electrophysiological hybrid biosensing system for real-time health and fitness monitoring," *Nat. Commun*, vol. 7, no. 1, pp. 1-7, 2016.

[4] J. Kim, S. Imani and et al, "Wearable salivary uric acid mouthguard biosensor with integrated wireless electronics," *Biosens. Bioelectron*, vol. 74, pp. 1061–1068, 2015.

[5] O.O. Ojuroye, R. N. Torah, S. Beeby, "Modified PDMS packaging of sensory e-textile circuit microsystems for improved robustness with washing", *Microsyst. Technol*, pp. 1-18, 2019.

[6] O.O. Ojuroye, R. N. Torah, A. O. Komolafe and S. P. Beeby, "Embedded Capacitive Proximity and Touch Sensing Flexible Circuit System for Electronic Textile and Wearable Systems," *IEEE Sens. J.*, vol. 19, no. 16, pp. 6975-6985, 15 Aug.15, 2019.

[7] M. Martinez-Estrada, B. Moradi, R. Fernandez-Garcia and I. Gil, "Impact of manufacturing variability and washing on embroidery textile sensors," *Sensors*, vol. 18, no. 11, pp. 3824, 2018.

[8] K. Arquilla, A.K. Webb and A.P. Anderson, "Textile Electrocardiogram (ECG) Electrodes for Wearable Health Monitoring," *Sensors*, vol. 20, no. 4, pp. 1013, 2020.

[9] P. Garcia, M. Khoshnam and C. Menon, "Wearable Device to Monitor Back Movements Using an Inductive Textile Sensor," *Sensors*, vol. 20, no. 3, pp. 905, 2020.

[10] P. Lugoda, J.C. Costa, C. Oliveira, L.A. Garcia-Garcia and et al, "Flexible Temperature Sensor Integration into E-Textiles Using Different Industrial Yarn Fabrication Processes," *Sensors*, vol. 20, no. 1, pp. 73, 2020.

[11] A. Liang, R. Stewart and N. Bryan-Kinns, "Analysis of sensitivity, linearity, hysteresis, responsiveness, and fatigue of textile knit stretch sensors," *Sensors*, vol. 19, no. 16, pp. 3618, Aug. 2019.

[12] C.J. Kaiser, "The capacitor handbook," *Springer Science and Business Media*, pp 51-65, 1993.

[13] A.M. Imam, D.M. Divan, R.G. Harley and T. G. Habetler, "Real-Time Condition Monitoring of the Electrolytic Capacitors for Power Electronics Applications," *APEC 07*, Anaheim, CA, USA, pp. 1057-1061, 2007.

[14] C.G. Malmberg and A.A. Maryott, "Dielectric Constants of Aqueous Solutions of Dextrose and Sucrose," *J. Res. Natl. Bur. Stand.*, Vol. 45, no. 4, pp. 299-303, 1950.

[15] M.A. Ennasar, O.E. Mrabet, K. Mohamed, and M. Essaaidi, "Design and Characterization of a Broadband Flexible Polyimide RFID Tag Sensor for NaCl and Sugar Detection," *Prog. Electromagn. Res. C*, Vol. 94, pp. 273-283, 2019.